

NOTE TO USERS

This reproduction is the best copy available.

UMI[®]

*Investigating the Ionization State and Structure / Function Relationship
of Ionizable Residues in Escherichia coli
Chorismate Mutase – Prephenate Dehydrogenase
and the
Catalytic Trimer of Aspartate Transcarbamylase*

John Manioudakis

A Thesis

In

The Department

of

Chemistry and Biochemistry

*Presented in Partial Fulfillment of the Requirements
for the Degree of Doctor of Philosophy at
Concordia University
Montreal, Quebec, Canada*

December 2008

© John Manioudakis, 2008



Library and Archives
Canada

Published Heritage
Branch

395 Wellington Street
Ottawa ON K1A 0N4
Canada

Bibliothèque et
Archives Canada

Direction du
Patrimoine de l'édition

395, rue Wellington
Ottawa ON K1A 0N4
Canada

Your file *Votre référence*
ISBN: 978-0-494-63358-8
Our file *Notre référence*
ISBN: 978-0-494-63358-8

NOTICE:

The author has granted a non-exclusive license allowing Library and Archives Canada to reproduce, publish, archive, preserve, conserve, communicate to the public by telecommunication or on the Internet, loan, distribute and sell theses worldwide, for commercial or non-commercial purposes, in microform, paper, electronic and/or any other formats.

The author retains copyright ownership and moral rights in this thesis. Neither the thesis nor substantial extracts from it may be printed or otherwise reproduced without the author's permission.

In compliance with the Canadian Privacy Act some supporting forms may have been removed from this thesis.

While these forms may be included in the document page count, their removal does not represent any loss of content from the thesis.

AVIS:

L'auteur a accordé une licence non exclusive permettant à la Bibliothèque et Archives Canada de reproduire, publier, archiver, sauvegarder, conserver, transmettre au public par télécommunication ou par l'Internet, prêter, distribuer et vendre des thèses partout dans le monde, à des fins commerciales ou autres, sur support microforme, papier, électronique et/ou autres formats.

L'auteur conserve la propriété du droit d'auteur et des droits moraux qui protègent cette thèse. Ni la thèse ni des extraits substantiels de celle-ci ne doivent être imprimés ou autrement reproduits sans son autorisation.

Conformément à la loi canadienne sur la protection de la vie privée, quelques formulaires secondaires ont été enlevés de cette thèse.

Bien que ces formulaires aient inclus dans la pagination, il n'y aura aucun contenu manquant.

■❖■
Canada

ABSTRACT

Investigating the Ionization State and Structure / Function Relationship of Ionizable Residues in *E. coli* Chorismate Mutase – Prephenate Dehydrogenase and the Catalytic Trimer of Aspartate Transcarbamylase

John Manioudakis, Ph. D.

Modern mass spectrometry has gained tremendous attention in the field of enzymology, in particular as a tool for dissecting enzyme mechanism. In this thesis we use mass spectrometry in combination with chemical modification to help define the roles and ionization states of active site residues that are important for enzyme activity. Enzymes of particular interest are chorismate mutase-prephenate dehydrogenase (CM-PD), a bifunctional enzyme from *Escherichia coli* that catalyzes two consecutive steps in tyrosine biosynthesis, and the catalytic trimer of *E. coli* aspartate transcarbamylase (ATCase), which catalyzes the first committed step in the biosynthesis of pyrimidines. All three enzymes are of industrial or medical value as targets for the design of inhibitors that can act as either anti-neoplastic agents, antimicrobial agents or herbicides.

Three cysteine residues are found within each monomer of the dimeric CM-PD. Site-directed mutagenesis and kinetic analysis of variants of Cys95, Cys169 and Cys215 indicated that only Cys215 is important for both CM and PD activities. Chemical modification with cysteine-specific reagents, iodoacetamide and Ellman's Reagent, resulted in the loss of both activities but only Cys215 is protected against alkylation by ligands of the reaction and therefore near or in the active site. Time-dependent chemical

modification followed by peptide mapping indicated that Cys95 is the most reactive and/or accessible cysteine followed by Cys215 and Cys169. The results are discussed in terms of a structural model of the *E. coli* PD domain; Cys215 is near His245, which appears to help orient the catalytic base of the dehydrogenase reaction, His197.

In *E. coli*, mutase activity is associated with the N-terminal domain of CM-PD. pH rate profiles of the mutase reaction show that there are two residues whose ionization states are important for catalysis and/or substrate binding. Studies examining the rates of chemical modification of the enzyme with a lysine-specific reagent and the stoichiometry of modification indicate that only one lysine residue per monomer, Lys37, is particularly reactive. Peptide mapping was used to determine the pK_a of the ϵ -amino group of Lys37 to be 7.5. Chemical modifications, kinetic and binding studies on Lys37Gln, an inactive variant, show that Lys37 is critical for CM activity. We propose that Lys37 participates in catalysis by protonating the ether oxygen of chorismate in the reaction's transition state.

ATCase is composed of 3 regulatory dimers and 2 catalytic trimers. Treatment with mercurial reagents dissociates the regulatory subunits (RSU) from the catalytic subunits (CSU) without compromising their functions. An improved purification scheme is outlined for the different subunits. Biophysical studies on an inactive CSU variant, Ser52Cys, indicated that the substitution resulted in a more thermally stable enzyme. Chemical modification by cysteine-specific reagents and mass spectrometric analysis indicated that Cys52 is very reactive/accessible and possesses a pK_a of ~ 5.6 . The unusual characteristics of the Ser52Cys variant are attributed to the markedly depressed pK_a of Cys52. The biophysical reasons for the ionization state of Cys52 are discussed in terms of the crystal structure of the unliganded *E. coli* CSU.

Acknowledgements

First, I would like to thank my thesis supervisor, Dr. Joanne Turnbull, for her guidance, encouragement, patience and support throughout my Ph.D. studies. Her insights, expertise and dedication to research are admirable and inspiring.

I warmly thank the members of my research committee, Dr. Ann English and Dr. Paul Joyce, for their help and suggestions during my Ph.D. studies.

I want to thank my father George and my brother Kosta for their love, neverending support and encouragement, and without whom my Ph.D. and my life would have no meaning...

I want to thank all the members of the Turnbull's lab encountered during these years (Kevork Mekhssian, Raphael Aponte, Said Hassounah, Wenjuan Hou, Peter K.Q. "The Illustrious", Elizabeth Andrews, Francis, Natasha, etc...).

A special thanks to Julie Bonvin (ma pepette), with whom I spent over a quarter of my life cooped up in a lab... We stuck together through thick and thin, through low and high times, laughed together, cried together, and became very close throughout the years. Without her, my Ph.D. experience would be incomplete...

Special thanks to my best friend Jimmy Nassios for his neverending support, help, patience and understanding and for always being there whenever I need him. Thank you for being the bestest friend a guy could have....shamona!

I want to give a special thanks to my best friends from the “dark side” Ligris and Phil, for being awesome friends and not forgetting me when I was forgetting myself... You guys always take care of me and made Thursdays and Saturdays unforgettable... and yes!... It IS time to get paid!!!

I would also like to thank my family, Ann, Christina and Corey, Liv, Christos, my godson Thomas and my nieces Emma and baby Alexandra for their love, encouragement and support throughout my Ph.D. studies and for always being there when I need them.

I would also like to give a special thank you to Dr. Angelo E. Bourkas without whom completion of this thesis would not be possible.

And last but not least, I want to give a heartfelt thank you to my cats Sifi and Manoli, who kept me company every single night and whose silliness allowed me to keep whatever sanity I have left...

In loving memory of my Mother,

Who gave her all for us but never got a chance to see the fruits of her labor...

To my Father and Brother

“Some men see things as they are and ask why. Others dream things that never were and ask why not.”

George B. Shaw (1856 – 1950)

“We choose to go to the moon. We choose to go to the moon in this decade and do the other things, not because they are easy, but because they are hard, because that goal will serve to organize and measure the best of our energies and skills, because that challenge is one that we are willing to accept, one we are unwilling to postpone, and one which we intend to win, and the others, too.”

John F. Kennedy (1917 - 1963)

Table of Contents

List of Figures.....	xiv
List of Tables.....	xix
List of Abbreviations.....	xx
CHAPTER 1.....	1
1.1. BIFUNCTIONAL CHORISMATE MUTASE-PREPHENATE DEHYDROGENASE (CM-PD) in <i>E. Coli</i>.....	3
1.1.1. Biosynthesis of Aromatic Amino Acids	3
1.1.2. The Pathway to Tyrosine and Phenylalanine Biosynthesis in <i>E. coli</i>	5
1.1.3. The Bifunctional <i>E. coli</i> Enzyme, CM-PD: The Structural Relationship Between the Two Activities.....	10
1.1.4. Chorismate Mutase	11
1.1.5. Prephenate Dehydrogenase.....	19
1.1.6. Allosteric Regulation	23
1.1.7. Role of Cysteines in CM-PDT and CM-PD of <i>E. coli</i>	25
1.2. ASPARTATE TRANSCARBAMYLASE (ATCase) in <i>E. coli</i>.....	27
1.2.1. Chemical Modification of Cysteine and Lysine Residues of Proteins	38
1.2.2. Enzyme Reaction with DTNB (Ellman's reagent).....	40
1.2.3. Enzyme Reaction with Iodoacetamide.....	41
1.2.4. Enzyme Reaction with Trinitrobenzene Sulfonic Acid (TNBS)	42
1.3. SCOPE AND ORGANIZATION OF THIS THESIS.....	43
CHAPTER 2.....	45
2.1. INTRODUCTION.....	46

2.2. MATERIALS AND METHODS	48
2.2.1. Chemicals.....	48
2.2.2. Source of Recombinant WT and Variant CM-PD of <i>E. coli</i>	49
2.2.3. Expression and Purification of WT and Variant Forms of <i>E. coli</i> CM-PD ..	50
2.2.4. SDS—Polyacrylamide Gel Electrophoresis	51
2.2.5. Protein Concentration Determination	53
2.2.6. Determination of Enzyme Activity	53
2.2.7. Kinetic Parameter Determination	54
2.2.8. ESI-MS of Native and Variant CM-PD.....	55
2.2.9. Chemical Modification of Native Enzymes.....	56
2.2.10. Probing Cysteine Accessibility/Reactivity by Modification with IAM and CIAM Monitored by MALDI-ToF Mass Spectrometry	57
2.2.11. Ligand Protection Experiments.....	58
2.2.12. DTNB Inactivation and Reactivation by Cyanolysis.....	58
2.2.13. Determination of Cysteine pK_a Values in Native WT, Cys95Ala and Cys215Ala CM-PD Variants by ESI-MS	59
2.3. RESULTS	61
2.3.1. Expression and Purification of WT and Variant Forms of <i>E. coli</i> CM-PD ..	61
2.3.2. Chemical Modification of Native Enzymes.....	66
2.3.3. Inactivation of CM-PD Activities by DTNB and Reactivation by Cyanolysis	72
2.3.4. Probing Cysteine Accessibility/Reactivity by Modification with IAM and Detection by MALDI.....	75
2.3.5. Determination of Cysteine pK_a Values in Native WT, Cys95Ala and Cys215Ala CM-PD Variants by ESI-MS	82
2.4. DISCUSSION.....	86

CHAPTER 3	100
3.1. INTRODUCTION	101
3.2. EXPERIMENTAL PROCEDURES	103
3.2.1. Materials	103
3.2.2. Source of Recombinant WT and Variant CM-PD of <i>E. coli</i>	103
3.2.3. Expression and Purification of WT and Variant Forms of <i>E. coli</i> CM-PD	103
3.2.4. Sample Preparation of CM-PD	104
3.2.5. SDS—Polyacrylamide Gel Electrophoresis	104
3.2.6. Protein Concentration Determination	105
3.2.7. Determination of Enzyme Activity	105
3.2.8. Kinetic Parameter Determination	105
3.2.9. ESI-MS of Native WT and Variant CM-PD.....	105
3.2.10. Time-Dependent Chemical modification of WT CM-PD with TNBS at Neutral pH.....	106
3.2.10.1. WT CM-PD Mutase Inactivation by TNBS.....	106
3.2.10.2. Quantitation of Stoichiometry of Trinitrophenylation.....	106
3.2.11. pH-Dependent Mutase Inactivation of WT CM-PD by Chemical modification Using TNBS	107
3.2.12. pH-Dependency of WT CM-PD Mutase Activity	107
3.2.13. <i>In-silico</i> Digestion of WT CM-PD with Endopeptidase GluC	109
3.2.14. <i>In-vitro</i> Digestion of WT CM-PD with Endopeptidase GluC	109
3.2.15. Peptide Sequencing by ESI-MS/MS.....	110
3.2.16. Determination of Dissociation Constants for the Transition State Analogue by Fluorescence	110
3.2.17. Substrate Protection from Chemical Modification	111

3.2.18. Determination of Lys37 pK_a by Titration With TNBS.....	112
3.3. RESULTS	115
3.3.1. Purification and Purity Assessment of WT and Lys37Gln Variant CM-PD	115
3.3.2. <i>In-silico</i> Digestion of WT CM-PD With Endopeptidase GluC	120
3.3.3. Time-Dependent Chemical modification of WT CM-PD with TNBS at Neutral pH.....	122
3.3.4. <i>In-vitro</i> Digestion of WT CM-PD With Endopeptidase GluC	128
3.3.5. pH-Dependent Mutase Inactivation of WT CM-PD by Chemical Modification Using TNBS.....	134
3.3.6. pH-Dependence of the Mutase Reaction	138
3.3.7. Determination of Dissociation Constant of Mutase Transition State Analogue WT and Lys37Gln CM-PD by Fluorescence Spectroscopy	140
3.3.8. Substrate Protection from Chemical Modification	143
3.3.9. Determination of Lys37 pK_a by Titration with TNBS.....	148
3.3.10. Determination of Lys37 pK_a in WT CM-PD by Titration with TNBS.....	153
3.4. DISCUSSION	155
Chapter 4	167
4.1. INTRODUCTION.....	168
4.2. EXPERIMENTAL PROCEDURES	170
4.2.1. Materials	170
4.2.2. Expression and Purification of WT ATCase CSU.....	171
4.2.3. Expression and Purification of Ser52Cys ATCase CSU	173
4.2.4. Determination of Protein Concentration.....	173
4.2.5. Polyacrylamide Gel Electrophoresis of Proteins	173

4.2.6. Electrospray Ionization Mass Spectrometry (ESI-MS)	174
4.2.7. ICP-MS for Detection of Mercury in CSU Sample	174
4.2.8. Sample Preparation of Ammonium Sulphate Precipitated ATCase CSUs.	175
4.2.9. WT ATCase CSU Multiple Sequence Alignments.....	176
4.2.10. Far-UV Circular Dichroism Spectroscopy for Assessment of Secondary Structure.....	177
4.2.11. Fluorescence Spectroscopy for Assessment of Tertiary Structure	177
4.2.12. Thermal Denaturation of WT and Ser52Cys CSU Secondary Structure Monitored by Circular Dichroism.....	178
4.2.13. Chemical Modification of WT and Ser52Cys CSU by Cysteine-Specific Modifying Reagents.....	178
4.2.13.1. Sample Preparation Prior to Chemical Modification.....	178
4.2.13.2. Chemical Modification Using Ellman's reagent (DTNB)	179
4.2.13.3. Time-Dependent Chemical Modification Using Iodoacetamide (IAM) and Chloroacetamide (CIAM).....	180
4.2.14. <i>In-silico</i> Digestion of WT and Ser52Cys ATCase CSU With Endopeptidase GluC.....	181
4.2.15. Digestion of WT and Ser52Cys ATCase CSU With Endopeptidase GluC	181
4.2.16. Peptide Sequencing by ESI-MS/MS.....	182
4.2.17. Determination of Cys52 pK_a by Titration With Chloroacetamide.....	182
4.3. RESULTS	184
4.3.1. Purification and Purity Assessment of WT and Ser52Cys CSU.....	184
4.3.2. Sample Preparation of Ammonium Sulfate Precipitated ATCase CSUs....	191
4.3.3. WT CSU Multiple Sequence Alignments.....	196
4.3.4. Secondary and Tertiary Structure Assessment of WT and Ser52Cys CSU	198

4.3.5. Thermal Stability of WT and Ser52Cys CSU Secondary Structure Monitored by Circular Dichroism.....	201
4.3.6. Chemical Modification of WT and Ser52Cys CSU by Cysteine-Specific Modifying Reagents.....	203
4.3.6.1. Chemical Modification Using Ellman’s Reagent (DTNB).....	203
4.3.6.2. Time-Dependent Chemical Modification Using Iodoacetamide (IAM) and Chloroacetamide (CIAM).....	207
4.3.7. <i>In-silico</i> Digestion of WT and Ser52Cys CSU With Endopeptidase GluC	219
4.3.8. <i>In-vitro</i> Digestion of WT and Ser52Cys CSU With Endopeptidase GluC.	222
4.3.9. Determination of Cys52 pK_a by Titration with Chloroacetamide	229
4.3.10. Determination of Cys52 pK_a in Ser52Cys CSU by Titration With CIAM	237
4.4. DISCUSSION	239

List of Figures

Figure 1.1: The shikimate pathway	4
Figure 1.2: Aromatic amino acid biosynthesis in <i>E. coli</i> via the “common pathway”	6
Figure 1.3: Tryptophan biosynthesis	9
Figure 1.4: Uncatalyzed rearrangement of chorismate.....	13
Figure 1.5: Ribbon diagram representations of the AroQ and AroH folds	15
Figure 1.6: Schematic diagram of the crystal structure of the active site of yeast chorismate mutase and <i>E. coli</i> “mini-mutase” complexed with endo-oxabicyclic diacid	17
Figure 1.7: pH profile of V and V/K for the reaction catalyzed by <i>E. coli</i> CM.....	19
Figure 1.8: A possible mechanism of the PD reaction involving ionizable amino acid residues at the active site.....	22
Figure 1.9: Carbamylation reaction catalyzed by ATCase.....	28
Figure 1.10: The de novo pathway for biosynthesis of pyrimidine nucleotides	30
Figure 1.11: Subunit arrangement in ATCase holoenzyme	31
Figure 1.12: Domain structures of the catalytic and regulatory chains.....	34
Figure 1.13: Schematic representation of WT ATCase CSU active site residues interacting with PALA	37
Figure 1.14: Reaction of cysteine thiol with DTNB (Ellman’s reagent)	40
Figure 1.15: Reaction of cysteine thiol with iodoacetamide	41
Figure 1.16: Reaction of lysine ϵ -amino with TNBS	42
Figure 2.1: SDS-PAGE analysis of native <i>E. coli</i> CM-PD variants.....	62
Figure 2.2: ESI-MS spectrum of native <i>E. coli</i> WT CM-PD	63

Figure 2.3: Chemical modification of WT CM-PD and variants with 10 mM IAM.....	68
Figure 2.4: Chemical modification and ligand protection of WT CM-PD and variants using Ellman's reagent.....	70
Figure 2.5: Inactivation of CM-PD variants by DTNB and Reactivation by Cyanolysis	73
Figure 2.6: Time dependent chemical modification of WT CM-PD with 10 mM IAM and 10 mM CIAM.....	77
Figure 2.7: Representative ESI-MS spectra of the pH-dependent alkylation of WT CM-PD with IAM.....	83
Figure 2.8: Plot of peak intensity ratios of (adduct / (adduct + native)) for WT, Cys95Ala and Cys215Ala CM-PD	85
Figure 2.9: Spacefill representation of the modeled E. coli WT CM-PD PD domain illustrating the accessibility of the cysteine residues	97
Figure 2.10: Modeled PD active site of E. coli CM-PD.....	98
Figure 2.11: Modeled PD domain of E. coli WT CM-PD and key amino acids	99
Figure 3.1: SDS-PAGE Analysis of ion-exchange and AMP-affinity purification of Lys37Gln CM-PD.....	118
Figure 3.2: Correlation of TNBS adduct formation with mutase inactivation at neutral pH.....	124
Figure 3.3: Deconvoluted ESI-MS spectra following the time-dependent modification of WT CM-PD with TNBS	126
Figure 3.4: ESI-MS spectrum of the WT CM-PD digestion profile with endopeptidase GluC in bicarbonate buffer	129
Figure 3.5: In-vitro digest of WT CM-PD with endopeptidase GluC in bicarbonate buffer.....	131
Figure 3.6: ESI-MS/MS spectrum of peptide sequencing data for alkylated P(36-48)	133
Figure 3.7: Stoichiometric chemical modification of WT CM-PD with TNBS at various pH values	135
Figure 3.8: Titration of trinitrophenylated residue by reaction of WT CM-PD with TNBS for 40 minutes at different pH values	137

Figure 3.9: Variation of log V and log V/K with pH for the chorismate mutase reaction catalyzed by WT CM-PD.....	139
Figure 3.10: Fluorescence emission spectra of WT and Lys37Gln CM-PD in the presence of increasing amounts of endo	141
Figure 3.11: Changes in fluorescence intensity of WT and Lys37Gln variant CM-PD upon binding of endo	142
Figure 3.12: Mass spectrometric analysis of ligand protection experiments for WT and Lys37Gln CM-PD.....	145
Figure 3.13: ESI-MS Spectra of the GluC-digested WT CM-PD after pH-dependent modification with TNBS.....	149
Figure 3.14: Titration of Lys37 in P(36-48) of WT CM-PD by reaction with TNBS for 10 minutes at different pH values	154
Figure 3.15: Schematic representation of the mutase active site in the E. coli CM-PD model.....	160
Figure 3.16: Possible mechanism for the chorismate mutase mechanism	165
Figure 3.17: Illustration of mutase active site in the monomer model of E. coli CM-PD	166
Figure 4.1: SDS-PAGE analysis of the nickel affinity purification of Ser52Cys CSU	186
Figure 4.2: Deconvoluted electrospray ionization mass spectra of untreated CSU	189
Figure 4.3: Deconvoluted electrospray ionization mass spectra of treated CSU	193
Figure 4.4: Multiple sequence alignments for E. coli WT CSU	197
Figure 4.5: Far-UV CD spectra analysis of WT and Ser52Cys CSU.....	199
Figure 4.6: Fluorescence spectroscopy of WT and Ser52Cys ATCase CSU.....	200
Figure 4.7: Thermal denaturation curves for WT and Ser52Cys CSUs monitored by circular dichroism	202
Figure 4.8: Chemical Modification of WT (A) and Ser52Cys (B) CSU With Ellman's Reagent	205

Figure 4.9: Deconvoluted electrospray ionization mass spectra displaying time-course modification of Ser52Cys CSU with 10 mM IAM.....	209
Figure 4.10: Deconvoluted electrospray ionization mass spectra following the time-dependent modification of Ser52Cys CSU with CIAM.....	213
Figure 4.11: Deconvoluted electrospray ionization mass spectra displaying time-course modification of WT CSU with 10 mM CIAM.....	217
Figure 4.12: ESI-MS spectrum of WT CSU digestion profile with endopeptidase GluC in bicarbonate buffer	223
Figure 4.13: ESI-MS spectrum of Ser52Cys CSU digestion profile with endopeptidase GluC in bicarbonate buffer	224
Figure 4.14: In-vitro digest of WT and Ser52Cys CSU with endopeptidase GluC in bicarbonate buffer	226
Figure 4.15: ESI-MS/MS spectrum of peptide sequencing data for alkylated P(51-60)	228
Figure 4.16: Deconvoluted electrospray ionization mass spectra of the pH-dependent modification of Ser52Cys CSU with 10 mM CIAM	231
Figure 4.17: Titration of Cys52 residue by reaction of Ser52Cys catalytic trimer with CIAM for 40 minutes at different pH values	238
Figure 4.18: Schematic representation of the surface accessibility of Cys47 and Ser(Cys)52 in WT CSU	244
Figure 4.19: Schematic representation of the location of Ser(Cys)52 on helix 52-66 Within WT CSU	248

List of Tables

Table 2.1: Summary of kinetic parameters for WT and variant mutase-dehydrogenases measured at pH 7.2 and 30°C	64
Table 2.2: Tabulation of results from figure 2.6.....	74
Table 2.3: Tabulation of pK _a values of Cys95 and Cys215 in CM-PD variants.....	85
Table 3.1: Purification table for WT (A) and Lys37Gln (B) CM-PD.....	117
Table 3.2: Kinetic data for WT and Lys37Gln CM-PD measured at pH 7.2 and 30°C.....	119
Table 3.3: <i>In-silico</i> digest of WT CM-PD with endopeptidase GluC in bicarbonate buffer.....	121
Table 3.4: <i>In-vitro</i> digest of WT CM-PD with endopeptidase GluC in bicarbonate buffer.....	130
Table 4.1: <i>In-silico</i> digest of WT CSU with endopeptidase GluC in bicarbonate buffer.....	220
Table 4.2: <i>In-silico</i> digest of Ser52Cys CSU with endopeptidase GluC in bicarbonate buffer.....	221
Table 4.3: <i>In-vitro</i> digest of WT and Ser52Cys CSU with endopeptidase GluC in bicarbonate buffer.....	225

List of abbreviations

Å	Angstroms
ACN	acetonitrile
AD	arogenate dehydrogenase
amu	atomic mass units
ANS	1-anilino-8-naphthalene sulfonic acid
°C	degree Celsius
CD	circular dichroism
CIAM	chloroacetamide
CM	chorismate mutase
CM-PD	chorismate mutase–prephenate dehydrogenase
CM-PDT	chorismate mutase–prephenate dehydratase
Da	Dalton
DEPC	diethylpyrocarbonate
DMSO	dimethyl sulfoxide
DNA	deoxyribonucleic acid
DSC	differential scanning calorimetry
DTNB	5, 5'-dithiobis-(2-nitrobenzoic acid) or Ellman's reagent
DTT	dithiothreitol
EDTA	ethylenediaminetetraacetic acid
<i>Endo</i>	<i>endo</i> -oxabicyclic diacid
ESI	electrospray ionization

F.I.	fluorescence intensity
Gdn-HCl	guanidinium hydrochloride
HCCA	α -cyano-4-hydroxycinnamic acid
HEPES	4-(2-hydroxyethyl)-1-piperazineethanesulfonic acid
HPLC	high performance liquid chromatography
HPP	(4-hydroxyphenyl)pyruvate
HPPionate	4-hydroxyphenyl propionate
IMAC	immobilized metal affinity chromatography
IAM	iodoacetamide
IPTG	isopropyl- β -D-thiogalactopyranoside
IR	infrared
LB	Luria broth
MALDI	matrix assisted laser desorption ionization
MeOH	methanol
MES	2-morpholinoethanesulfonic
MS	mass spectrometry
MW	molecular weight
MWCO	molecular weight cut-off
m/z	mass to charge ratio
NAD ⁺	oxidized form of nicotinamide adenine dinucleotide
NADH	reduced form of nicotinamide adenine dinucleotide
NAD(P) ⁺	oxidized form of nicotinamide adenine dinucleotide (phosphate)
NAD(P)H	reduced form of nicotinamide adenine dinucleotide (phosphate)

NATA	N-Acetyl-L-tryptophanamide
NAYA	N-acetyl-L-tyrosinamide
NEM	N-ethylmorpholine
NMR	nuclear magnetic resonance
NTA	nitrolotriacetic acid
PAGE	polyacrylamide gel electrophoresis
PCR	polymerase chain reaction
PD	prephenate dehydrogenase
PMSF	phenylmethanesulfonyl fluoride
TCEP	tri(2-carboxyethyl)phosphine hydrochloride
rpm	revolutions per minute
SDS	sodium dodecylsulfate
TFA	trifluoroacetic acid
TNBS	2,4,6-trinitrobenzenesulfonic acid
Tris	tris(hydroxymethyl)aminomethane
U	units
UV	ultraviolet
3CB	three-component buffer (0.1 M MES, 51 mM N-ethylmorpholine, 51 mM diethanolamine, 1 mM EDTA and 1 mM DTT at pH 7.2)

CHAPTER 1

General Introduction

Amino acids possess a pivotal role in the biochemistry of living organisms, both as building blocks of proteins as well as intermediates in metabolism (1).

Proteins accomplish multiple tasks such as catalysis of all (or most) reactions in living cells as well as control of virtually all cellular processes. Protein amino acid sequences are dictated by the sequence of deoxyribonucleotide bases in the genes that encode them. This predetermined sequence of 20 amino acids conveys a vast array of physico-chemical properties to proteins, which defines their three dimensional structure, their structural stability as well as their biological activity (2).

Humans do not possess the enzymes necessary for the biosynthesis of all amino acids. Only 10 of the 20 amino acids can be synthesized in the human body and are hence termed non-essential. The remaining 10 amino acids must be obtained via the dietary regime and are thus designated as being essential. Tyrosine, which is one of the three aromatic amino acids, is produced via the hydroxylation of phenylalanine, an essential amino acid (3).

In contrast, bacteria, plants and microorganisms are able to biosynthesize all the amino acids.

1.1 BIFUNCTIONAL CHORISMATE MUTASE-PREPHENATE DEHYDROGENASE (CM-PD) in *E. coli*

1.1.1 Biosynthesis of Aromatic Amino Acids

The biosynthesis of the aromatic amino acids phenylalanine, tyrosine and tryptophan in plants, *E. coli* and other microorganisms is funneled through the shikimate pathway (Figure 1.1) (4-6), which links the metabolism of carbohydrates to the biosynthesis of aromatic amino acids. A series of seven metabolic steps, starting from the condensation of phosphoenolpyruvate and erythrose 4-phosphate, yields chorismate, which is located at a key branch point in this pathway. Chorismate then serves as a precursor for the biosynthesis of phenylalanine, tyrosine and tryptophan via the “common pathway”, as well as a number of aromatic compounds such as vitamin K, ubiquinone, folate and enterobactin (6-8). These aromatic amino acids may then be used as building blocks for protein synthesis or as substrates for enzymes in downstream pathways.

In microorganisms, the shikimate pathway is regulated by both feedback inhibition and repression of the first enzyme. Among the enzymes responsible for the biosynthesis of aromatic amino acids, several are present as isozymes, multifunctional proteins or multienzyme complexes. This diversity allows for regulation at both the gene and protein level. In higher plants, no physiological feedback inhibitor has been identified, which suggests that the regulation of this pathway may be exclusively at the genetic level (6).

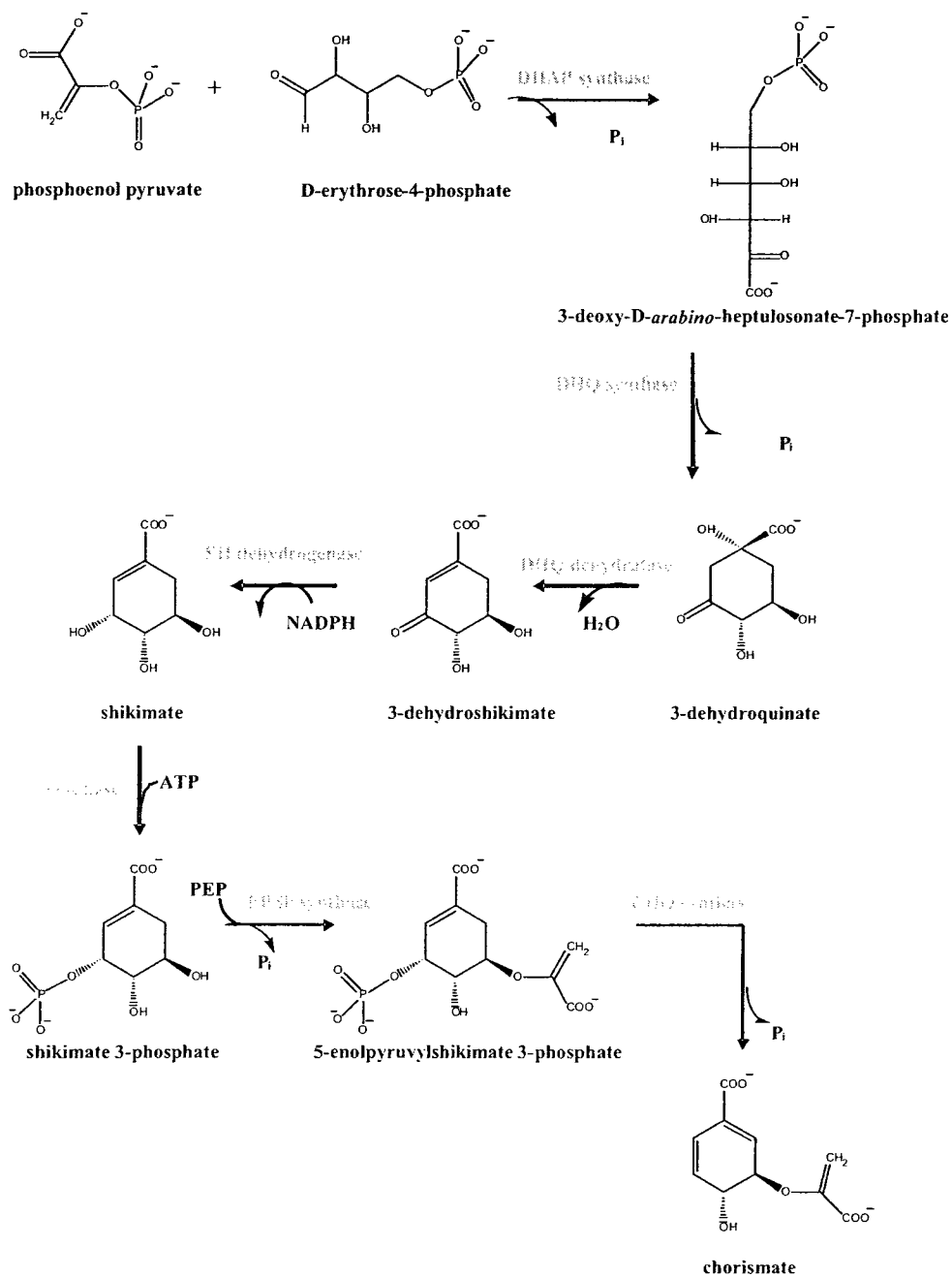


Figure 1.1: The shikimate pathway

The shikimate pathway consists of seven enzyme-catalyzed steps. Metabolite symbols: DHAP, 3-deoxy-D-arabino-heptulosonate 7-phosphate; DHQ, 3-dehydroquinatate; SH, shikimate; EPSP, 5-enolpyruvylshikimate 3-phosphate and CHO, chorismate.

Many of the genes responsible for the biosynthesis of aromatic amino acids are organized in operons, which are controlled by regulatory proteins encoded by the *tyrR*, *trpR* and *pheR* genes (9, 10). The proteins resulting from these genes associate with the appropriate amino acid co-repressor, which results in the formation of complexes that bind at the operator loci. Additional regulation is achieved through attenuation at the level of charged tRNA(s) (11). The main form of regulation however is accomplished through feedback inhibition of the enzymes present at the beginning of the branch point in the shikimate pathway by the end products phenylalanine, tyrosine and tryptophan.

1.1.2 The Pathway to Tyrosine and Phenylalanine Biosynthesis in *E. coli*

The end of the pathway for the biosynthesis of tyrosine in *E. coli* involves two sequential reactions catalyzed by the enzyme chorismate mutase-prephenate dehydrogenase (CM-PD) (12, 13). CM (EC 5.4.99.5) catalyzes the Claisen rearrangement of chorismate to prephenate, while PD (EC 1.3.1.12) oxidatively decarboxylates prephenate to (4-hydroxyphenyl)pyruvate (HPP) and CO₂ in the presence of NAD⁺ (Figure 1.2). An aromatic aminotransferase subsequently converts HPP to L-tyrosine (13). CM-PD activity is regulated by the end-product of its pathway, L-tyrosine (13). However, prephenate dehydrogenase activity is reported to be inhibited to a greater extent than the mutase reaction (14). Moreover, NAD⁺ enhances tyrosine inhibition of both mutase and dehydrogenase activities by increasing the enzyme's affinity for the modulator (15, 16).

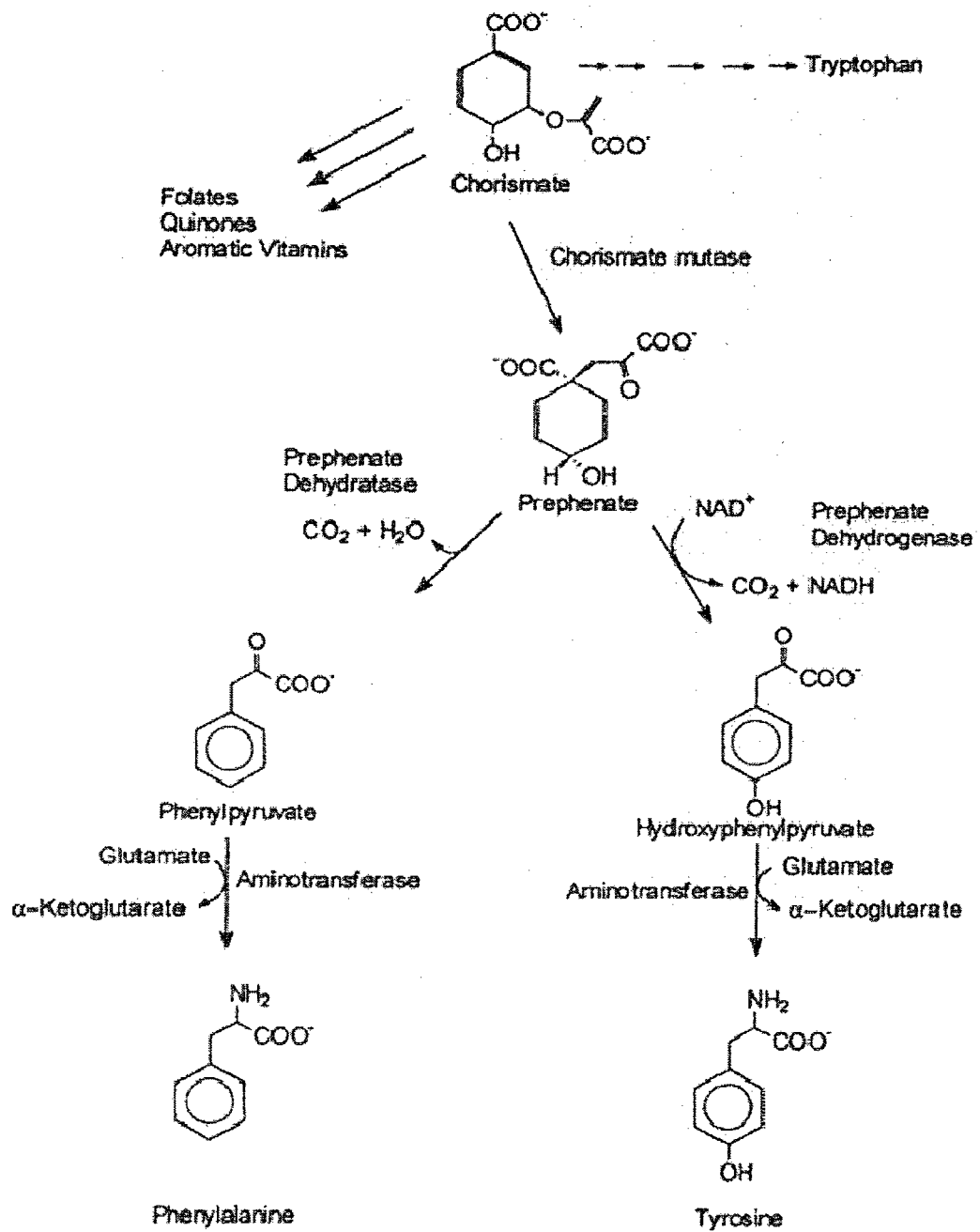


Figure 1.2: Aromatic amino acid biosynthesis in *E. coli* via the “common pathway”

Figure adapted from D. Christendat (17).

The biosynthesis of phenylalanine from chorismate in *E. coli* also involves a bifunctional enzyme, namely chorismate mutase-prephenate dehydratase (CM-PDT). CM converts chorismate to prephenate, while PDT catalyzes the dehydration and decarboxylation of prephenate to yield phenylpyruvate. Phenylpyruvate undergoes transamination to form phenylalanine (Figure 1.2). The end-product phenylalanine inhibits both mutase and dehydratase activities (18), with the dehydratase activity being affected significantly more than the mutase (19).

The biosynthesis of tryptophan also stems from chorismate but requires six extra steps from a separate pathway illustrated in Figure 1.3. The first two and last two reactions are catalyzed by enzyme complexes, namely the anthranilate synthase-phosphoribosyl transferase complex and the tryptophan synthase complex, respectively.

Interestingly, both the shikimate and the “common” pathways are not present in mammals, which makes the enzymes associated with these pathways attractive targets for the design of inhibitors which may serve as herbicides, fungicides and antimicrobial agents (20, 21). Glyphosate, the active ingredient in Roundup®, is the best known herbicide stemming from this pathway, and functions as an inhibitor of 5-enolpyruvyl shikimate 3-phosphate synthase (22). Additionally, these enzymes are well recognized in bioengineering as targets for aromatic amino acid and secondary metabolite production (23). The use of metabolic engineering to produce aromatic amino acids (and their synthetic intermediates) has gained considerable attention due to their commercial value in the food, pharmaceutical and agricultural industries. For example, phenylalanine is used for the production of the low-calorie sweetener aspartame, marketed as NutraSweet® (24). Additionally, the Trp biosynthetic pathway has been exploited in

E. coli for the production of aromatic compounds such as bio-indigo (25, 26) and shikimic acid (27) as well as animal feed. Tyrosine has historically been supplied by chemical synthesis and protein hydrolysis since only small volume applications were required. The recognition of the importance of tyrosine as a precursor in the synthesis of melanin (28), anti-Parkinson's drugs such as L-dopa (29, 30) and 3,4-dihydroxyphenyl-L-alanine (27) and biodegradable polymers (31) has engaged scientists to explore strategies for the manipulation of its biosynthetic route (32, 33), rendering its production more environmentally-friendly. The need for these aromatic compounds as well as the associated financial implications emphasize the importance of understanding the catalytic mechanism and modes of regulation of aromatic amino acid producing enzymes in a number of organisms.

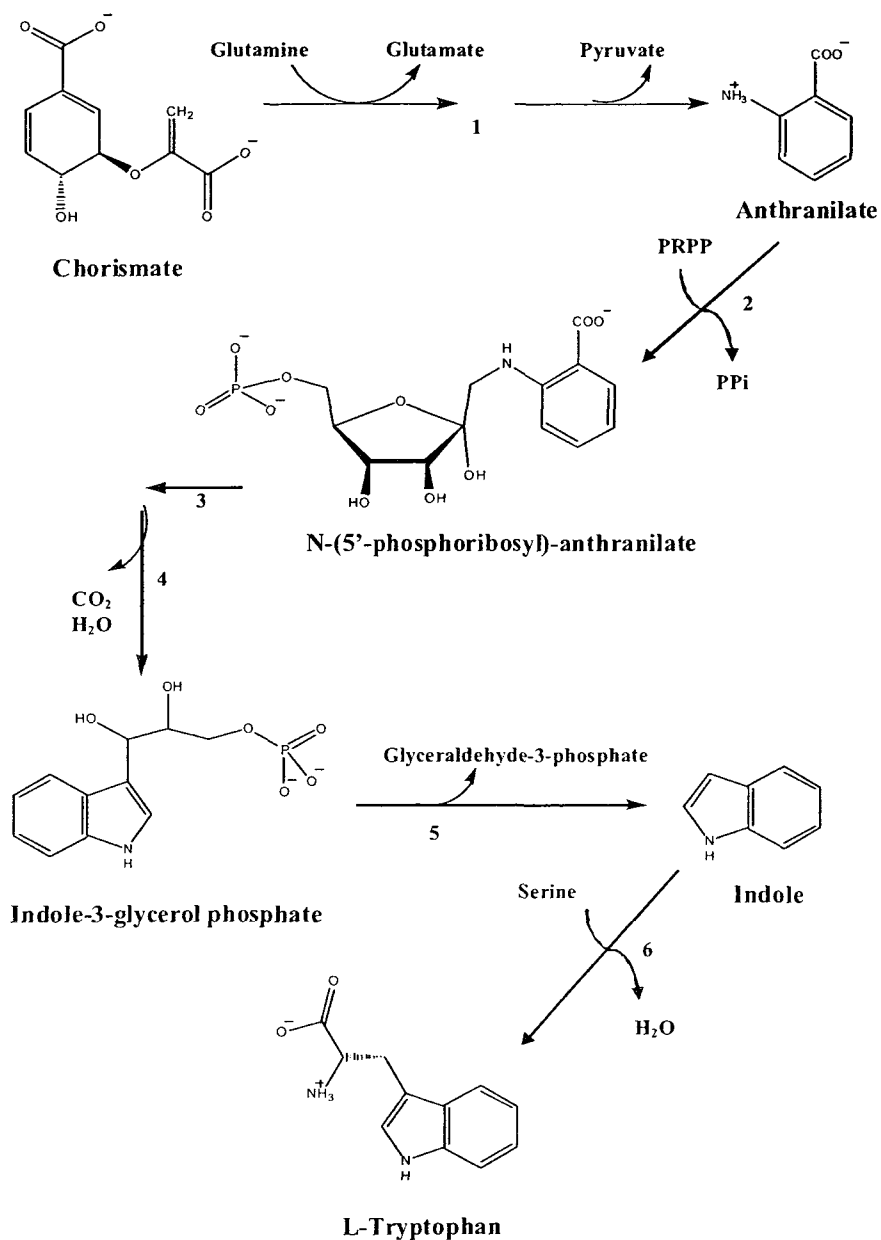


Figure 1.3: Tryptophan biosynthesis

The pathway consists of six enzyme-catalyzed steps. **1**, anthranilate synthase, **2**, anthranilate phosphoribosyltransferase, **3**, phosphoribosylanthranilate isomerase, **4**, indole-3-glycerol-phosphate synthase, **5-6**, tryptophan synthase enzyme complex. PRPP: 5-phosphoribosyl- α -pyrophosphate

1.1.3 The Bifunctional *E. coli* Enzyme, CM-PD: The Structural Relationship Between the Two Activities

E. coli CM-PD is a bifunctional homodimeric enzyme with a molecular weight of 42 kDa per monomer (14, 34). The structural organization of the active sites, in which both reactions are catalyzed however, has not been firmly established since no crystal structure is available for this bifunctional enzyme. Amino acid sequence alignments of the primary sequence of *E. coli* CM-PD with that of *E. coli* CM-PDT suggest that the first 100 amino acid residues of the polypeptide chain of the former are responsible for the mutase activity, while the remaining 273 residues constitute the dehydrogenase domain (35). Since the product of the first reaction, prephenate, is a substrate for the second reaction, there has been much interest concerning the spatial geometry of the active site(s) in which the two reactions occur.

Evidence suggesting two distinct active sites or of specific residues involved in catalyzing each of the two reactions stems from observations that the two activities exhibit strikingly different pH rate profiles (14, 16, 36) and are inhibited to different degrees by both L-tyrosine (14, 16) and a family of dicarboxylic acid-containing compounds (malonic acid derivatives) (14). The most compelling evidence however, comes from the synthesis and characterization of *endo*-oxabicyclic diacid, a putative transition state analogue of the mutase reaction, which exhibited selective inhibition of the mutase reaction without affecting dehydrogenase activity (14). Additionally *trans*-2,3-pleiadanedicarboxylic acid has been recently synthesized, which specifically inhibits PD without affecting mutase activity (37). The idea of distinct active sites has been supported through recent site-directed mutagenesis studies reported by Turnbull *et al.*

(38, 39), where a His197Gln substitution eliminated dehydrogenase activity (39) while Arg294Gln affected prephenate binding (38). Both substitutions did not affect the mutase reaction. Similarly a substitution in the mutase portion (Lys37Gln) has no effect on dehydrogenase activity (38).

Computer simulation studies in conjunction with channeling experiments using radiolabelled substrate demonstrated that some of the prephenate formed from chorismate is converted directly to HPP (40), thus providing evidence suggesting that if there are two active sites, they are in very close proximity to each other and are structurally interrelated. Inhibition studies employing malonic acids were reported by Christopherson (41), which provided additional kinetic evidence that the two sites overlap. Lastly, protein variants produced by site-directed mutagenesis of residues in the dehydrogenase domain (His189Asn, Lys178Arg, and Arg286Ala) have been characterized which clearly affect both CM and PD activities (38, 39). Ganem and coworkers (42) have also reported that the CM-PD domains are structurally dependent on each other; expressing each domain separately destabilizes the enzymes.

1.1.4 Chorismate Mutase

Chorismate mutase catalyzes the only pericyclic Claisen rearrangement reaction reported in nature (43). The rearrangement of chorismate to prephenate is possible in the absence of enzyme, however the rate of the reaction is accelerated by over a million-fold when catalyzed by chorismate mutase (44, 45). Proton NMR studies have indicated that 10 to 20% of chorismate, with its hydroxyl and enolpyruvyl group in the diaxial conformer, exists in equilibrium with the more stable diequatorial form (46). Both the

catalyzed and uncatalyzed rearrangement of chorismate occurs by an intramolecular mechanism, which is believed to proceed via a transition state following the selection of chorismate's less stable diaxial form (45-49) (Figure 1.4).

The non-enzymatic reaction occurs via the diaxial conformer of chorismate. In aqueous solution, the enolpyruvyl group of the diaxial conformer of chorismate is stabilized by hydrogen bonding to water molecules thus facilitating bond breakage between C₅ and the oxygen of chorismate. Similar to the uncatalyzed rearrangement, chorismate mutase also selectively discriminates against the diequatorial conformer of chorismate (46). The structural features required for catalysis have been determined by the synthesis and characterization of numerous chorismate analogues (50, 51). Neither the 5,6-olefinic nor the 4-hydroxyl are necessary, but CM requires the allyl vinyl ether and the two carboxylate groups for binding chorismate to the active site (52). Kinetic studies suggest that the mutase reaction catalyzed by bifunctional CM-PD of *E. coli* is mediated by enzymic acids and bases (36, 38), which have been proposed to either protonate the ether oxygen (O₇) or heterolytically cleave the ether bond. It has been proposed that the rearrangement is facilitated by the protonation of the ether oxygen (O₇) by an enzymic acid, in conjunction with the attack on the C₁ by an electron pair on the methylene group of the enol pyruvyl side chain (14). In contrast, the monofunctional mutase from *B. subtilis* specifically binds the diaxial conformer of chorismate, which then spontaneously undergoes Claisen rearrangement to prephenate (53, 54).

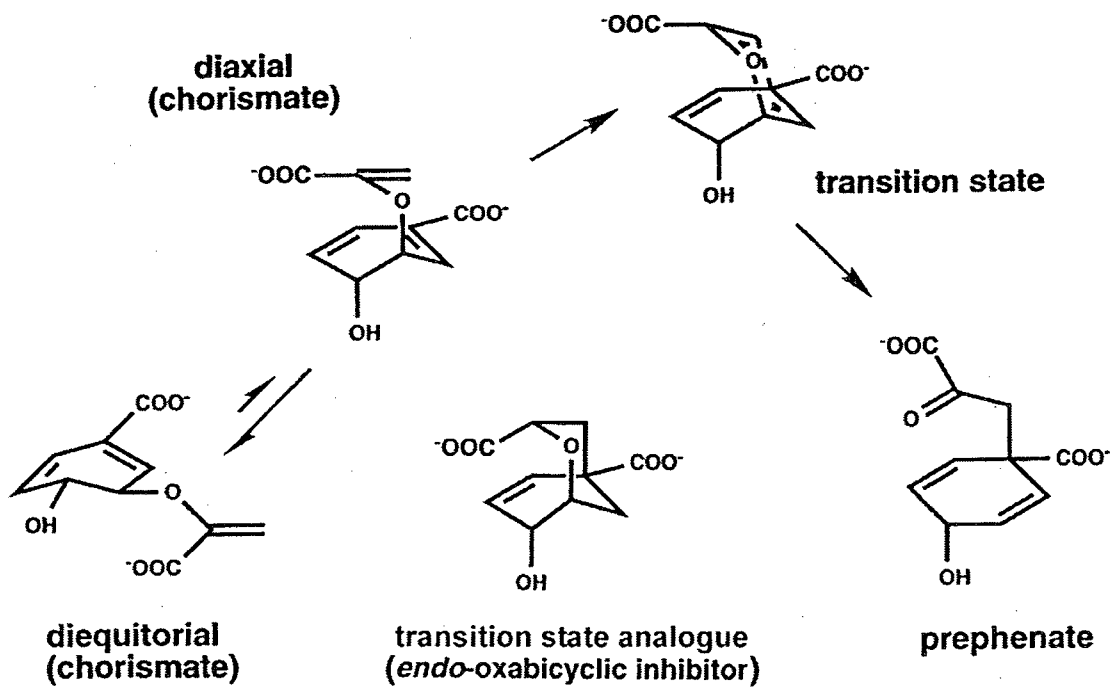


Figure 1.4: Uncatalyzed rearrangement of chorismate.

Adapted from Christendat *et al.* (39)

Several chorismate analogues have been synthesized to delineate the structural features required for catalysis (50). An *endo*-oxabicyclic diacid inhibitor (51), with its bridged ether oxygen and *endo* conformation of the bridged carboxylate, appears to mimic the bicyclic structure of the transition state most effectively; the analogue binds about 300 times more tightly to the *E. coli* enzyme than chorismate (14) and has been shown to selectively inhibit mutase activity without affecting dehydrogenase activity (36).

Several natural monofunctional CMs have been crystallized such as those of *Bacillus subtilis* (46), *Saccharomyces cerevisiae* (55), *Thermus thermophilus* (56), *Clostridium thermocellum* (57), *Mycobacterium tuberculosis* (58), as well as the engineered mutase domain of the bifunctional *E. coli* CM-PDT (59), “mini-mutase”, many of which are complexed with the mutase transition-state analogue. CMs generally belong to one of two structurally distinct classes denoted AroH and AroQ (Figure 1.5). The less abundant AroH class comprises mainly trimeric α/β proteins with shared active sites at the subunit interfaces. In contrast, the protein scaffold of the more abundant AroQ class, (which is adopted by the *E. coli* “mini-mutase” (59), is mainly α -helical and dimeric. The dimeric yeast CM is larger and more elaborate than *E. coli* CM, and contains a regulatory domain where allosteric effectors can bind (55). Finally, *M. tuberculosis* CM is part of the AroQ protein family but exhibits a novel fold topology (58) and has only one active site entirely contained within each polypeptide (58). Interestingly, alignment of the primary sequences of all five mutases shows little similarity and their crystal structures reveal that they adopt unique folds, however, the electronic environment and the geometry of the active site appears well conserved

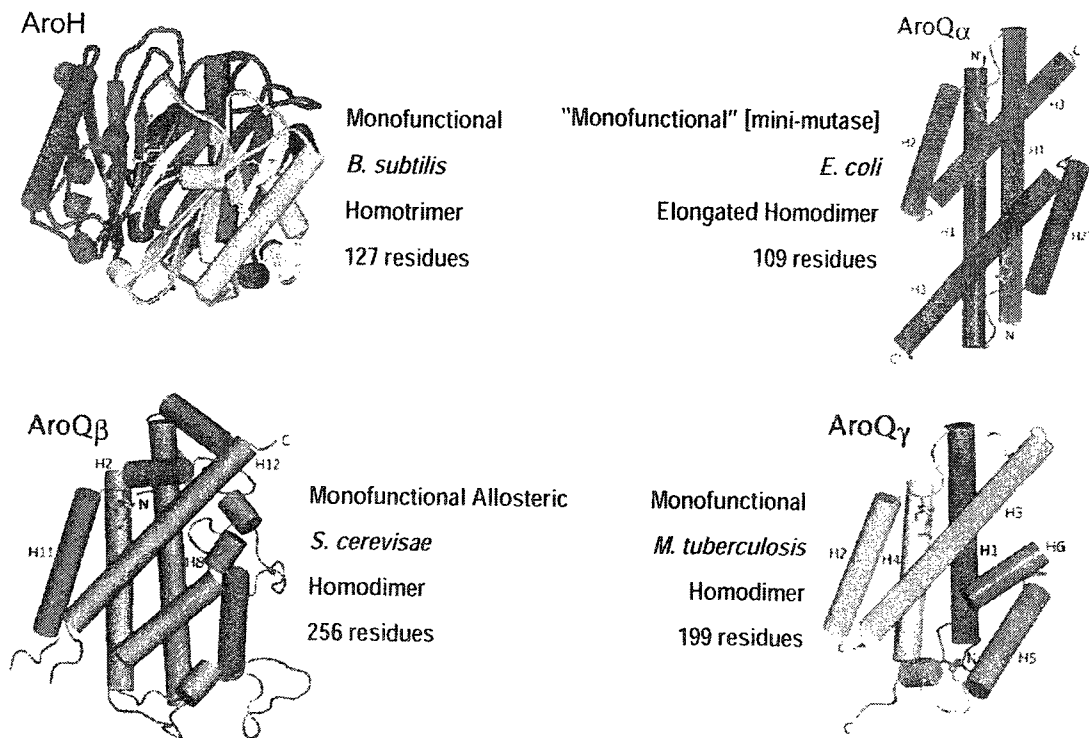


Figure 1.5: Ribbon diagram representations of the AroQ and AroH folds

The AroH class is organized as a trimeric α/β -barrel fold; *B. subtilis* and *C. thermocellum* CMs are representative of this class. The AroQ class is completely helical and includes CMs from *E. coli* and *S. cerevisiae*

The mutase domains of CM-PD and CM-PDT are homologous; hence the structure of the CM portion of CM-PDT has provided valuable insights as to the residues that may participate in the mutase reaction catalyzed by CM-PD. In Figure 1.6, Lys39 of the “mini-mutase” forms an electrostatic bond with the C₁₁ carboxylate group and a hydrogen bond with O₇. By homology, this suggests that Lys37 of CM-PD is important in stabilizing the intermediates in the mutase reaction. Specifically, either it may lock the chorismate into the diaxial conformation, facilitating the formation of the transition state, in which the bridge atoms are in the chair-like conformation or protonate the ether oxygen of chorismate in the TS to promote the rearrangement (14). Site-directed mutagenesis performed on CM-PD and the mini-mutase (39, 60, 61) has shown that the cationic residue Lys37 (Lys39 in the mini-mutase) is indeed crucial for CM activity. Substitution of this Lys residue by Ala or Gln completely abolishes mutase activity without causing a significant effect on dehydrogenase activity in CM-PD (38). The structures of CM complexed with *endo*-oxabicyclic acid for the *B. subtilis* (62), *S. cerevisiae* (43) and the *E. coli* “mini-mutase” enzyme have provided the template for the design of extensive mutagenesis experiments, through site-directed approaches (60, 61) and directed evolution (63). These results, in combination with structural data, bring to light the importance of the active site groups Lys37 and Gln88 in the stabilization of the ether oxygen and of Lys39 and Arg11' in positioning the C₁₁ carboxylate group in the highly charged region of the active site (Figure 1.6).

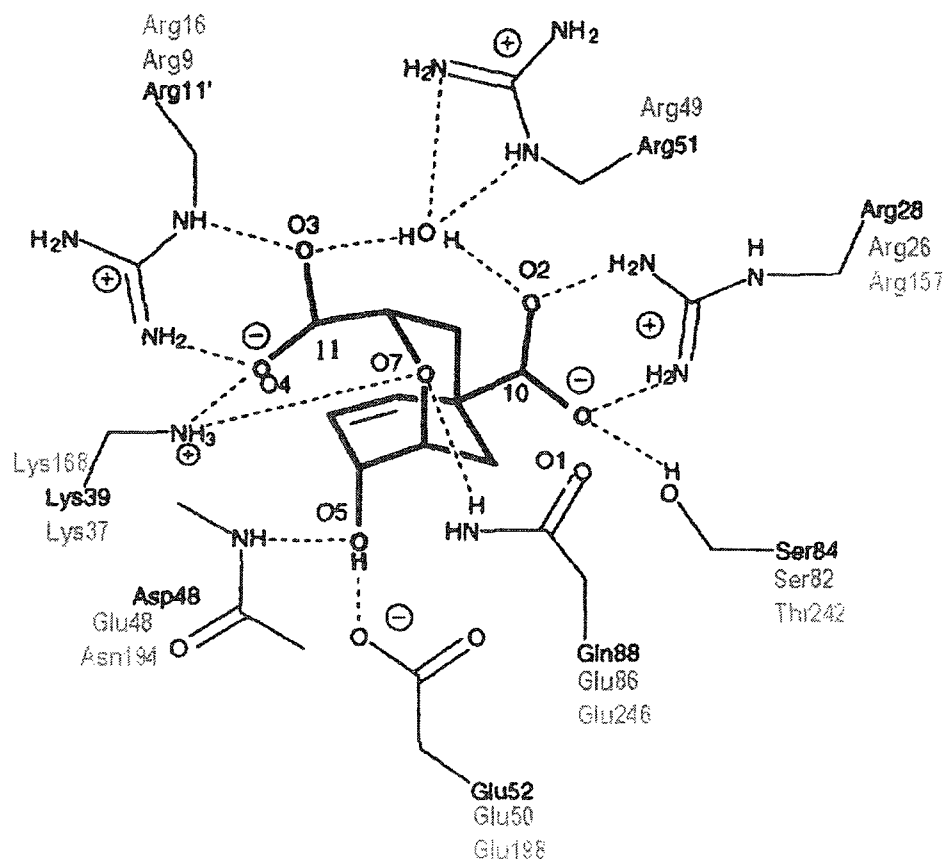


Figure 1.6: Schematic diagram of the crystal structure of the active site of yeast chorismate mutase and *E. coli* “mini-mutase” complexed with *endo*-oxabicyclic diacid

Residues from *E. coli* “mini-mutase” (black) and *S. cerevisiae* (green) were determined by X-ray crystallography while those from *E. coli* CM-PD (red) were elucidated through sequence alignments.

Additional evidence suggesting that a cationic residue, possibly Lys37, is involved in chorismate binding arises from the pH dependence of $(V/K)_{\text{chorismate}}$. Residues titrating in this pH profile are associated with the free enzyme and/or substrate and are hence essential for substrate binding and/or catalysis. Early work by Turnbull *et al.* (36) showed that the pH dependence of $(V/K)_{\text{chorismate}}$ is a bell-shaped curve and indicated the involvement of three ionizable groups (Figure 1.7). The slope of the acid and alkaline limbs of +1 and -2, respectively suggest that two groups had to be protonated and one deprotonated for activity. One of these protonated residues may be Lys37. Additional pH-dependent activity profiles described for a variant of the mini-mutase (Gln88Glu) and for wild-type CM from yeast (contains Glu at position 246) indicated the importance of a protonated side chain at this position.

There have been a number of mechanisms proposed for the CM reactions that have been derived from experimental and/or computational chemistry studies (64), such as acid/base catalysis, nucleophile-assisted dissociative (48) and transition state stabilization (or conformational trapping); the catalytic mechanism of the CM-catalyzed reaction continues to be under intense study.

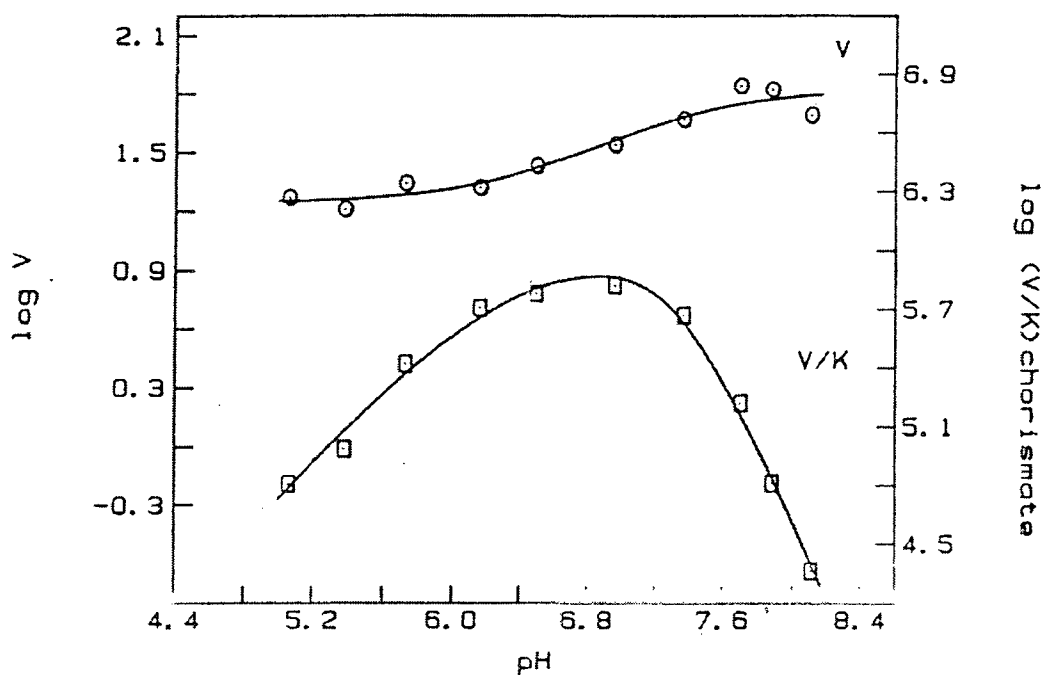


Figure 1.7: pH profile of V and V/K for the reaction catalyzed by *E. coli* CM

This figure was adapted from Turnbull *et al.* (36).

1.1.5 Prephenate Dehydrogenase

Prephenate dehydrogenase catalyzes the oxidative decarboxylation of prephenate in the presence of the cofactor NAD^+ to yield HPP and CO_2 . This reaction is essentially irreversible, driven by the aromaticity of HPP. The non-enzymatic reaction has not been observed, however, under acidic condition, prephenate can rapidly undergo decarboxylation to give phenylpyruvate. The acid-assisted decarboxylation occurs *via* a stepwise mechanism, where protonation of the hydroxyl group of the prephenate leads to the formation of a resonance stabilized carbonium ion with subsequent decarboxylation.

On the contrary, in the enzyme-catalyzed reaction, decarboxylation and hydride transfer are concomitant (65). This mechanism was suggested by isotope effect studies performed by Hermes *et al.* (65) in the presence of prephenate and prephenate analogues. Using the substrate analogue deoxoprephenate, deuterated at C₄, they observed an isotope effect for the hydride transfer to NAD⁺ (65). Furthermore, using the natural abundance of ¹³C in the substrate, they observed a carbon isotope effect for the cleavage of the C-C bond between the cyclohexadiene ring and the ring carboxylate. Interestingly, the carbon isotope effect obtained with the deuterium *versus* the hydrogen at position C₄ was smaller than with the natural ¹³C indicating that both the deuterium and the ¹³C isotope effects are in the same transition state; that is, deuterium has made the ¹³C-sensitive step more rate-limiting by slowing it down (65).

Initial velocity, product and dead-end inhibition studies have established that the kinetic mechanism of the *E. coli* PD reaction follows a sequential mechanism (34). Furthermore, product and dead-end inhibition studies have established that PD conforms to a rapid-equilibrium, random kinetic mechanism with two dead end complexes, enzyme-NADH-prephenate and enzyme-NAD⁺-hydroxyphenylpyruvate (66). Isotope trapping with the enzyme-NAD⁺ complex suggested that catalysis is the rate-limiting step since only a small proportion of the enzyme was trapped as [¹⁴C]NADH (66). A similar reaction mechanism has been reported for CM-PD from *A. aerogenes* (15).

The pH dependence of the log *V* of the PD-catalyzed reaction showed that a single ionizing group was titrating (p*K*_a 6.5) thus suggesting that this group had to be deprotonated for maximum activity (36). In contrast, the log(*V*/*K*)_{prephenate} pH profile displayed, in addition to the deprotonated group, a second ionizing group with a p*K*_a

value of about 8.4 which must be protonated for the reaction to occur. This group was not observed in the V profile and since prephenate does not possess a group titrating in this region, they proposed that this enzyme residue was involved in prephenate binding (36). Similar results for the $(V/K)_{\text{prephenate}}$ profile were obtained by Hermes *et al.* (65). Moreover, their results from temperature and solvent perturbation studies (65) suggest that the catalytic group is likely a histidine.

Based on the results of pH profiles (36, 65), isotope effects (48, 67), chemical modification of the enzyme with diethylpyrocarbonate (DEPC) (38), peptide mapping (38), and site-directed mutagenesis (39, 68), a model for the catalytic mechanism has been put forward (Figure 1.8). It has been proposed that prephenate and NAD^+ bind to distinct subsites in the PD domain. An enzymic hydrogen bond acceptor (His197, $\text{p}K_{\text{a}}$ 6.7) is believed to polarize the 4-hydroxyl group of prephenate, lowering the activation barrier to facilitate decarboxylation and hydride transfer of prephenate to NAD^+ (68). Replacement of the histidine by an asparagine reduced the dehydrogenase activity by five orders of magnitude (39). The two chemical steps occur simultaneously, driven by the aromaticity of the product and also possibly because the ring carboxylate is near and/or in a hydrophobic pocket promoting decarboxylation (39). Unfortunately, attempts to identify the group titrating in the pH-rate profile with a $\text{p}K_{\text{a}}$ value of about 8.4 involved in the binding of prephenate have failed.

Furthermore, Arg294 was identified to be critical for the binding of prephenate as suggested by the 120-fold increase in K_{m} for prephenate observed when Arg294 was substituted by a glutamine (68). These inhibition studies led to the proposal that Arg294 interacts electrostatically with the ring carboxylate of prephenate (Figure 1.8). Several

substrate analogues, all lacking the ring carboxylate group at C₁ relative to prephenate, exhibited similar dissociation constants with the Arg294Gln variant with wild-type enzyme. Multiple sequence alignments of prephenate dehydrogenases from a number of organisms shows these residues are conserved.

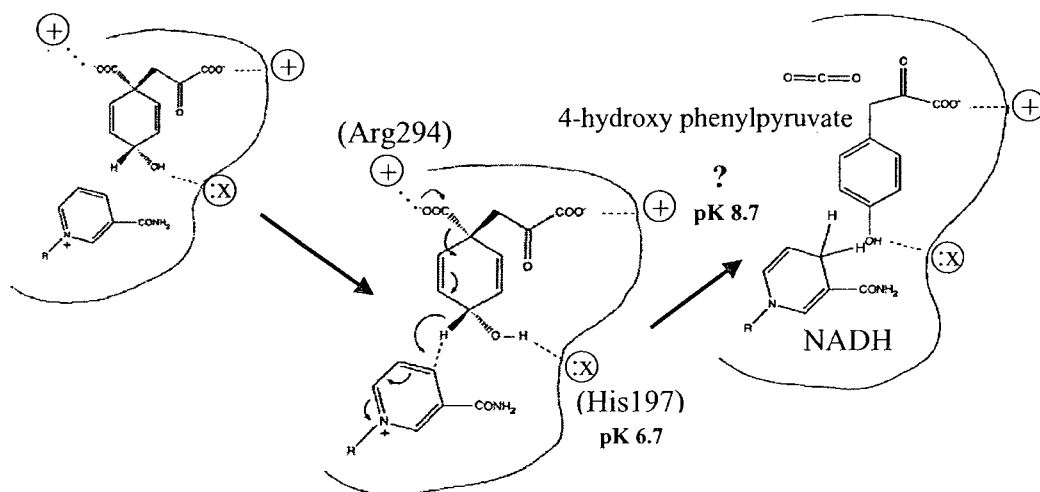


Figure 1.8: A possible mechanism of the PD reaction involving ionizable amino acid residues at the active site

Unknown group (?) interacts with side chain carboxylate. Adapted from Christendat and Turnbull (68).

The recently solved three-dimensional crystal structure for the monofunctional prephenate dehydrogenase from the hyperthermophile *Aquifex aeolicus* clearly shows that the residues corresponding to His197 and Arg294 in *E. coli* (His147 and Arg250, respectively) play a role in catalysis and/or substrate binding (69). The imidazole ring of His147 (equivalent to His197 in *E. coli*) is within hydrogen bonding distance of the hydroxyl group of prephenate. Interestingly, in the enzyme-NAD⁺ crystal structure, the electron density map around Arg250 was poorly ordered indicating considerable side chain flexibility (69) but in the presence of the product HPP (which does not possess the ring carboxylate), Arg250 was shown to interact with the side chain carboxylate of the product (submitted *JBC*).

1.1.6 Allosteric Regulation

Allosteric enzymes are widely distributed in living organisms and their interactions are important in many biological processes. Allosteric regulation is thought to directly control protein function *via* conformational changes to a given protein structure, induced by the binding of an effector at a site other than the orthosteric site. The changes are transmitted through the bulk of the protein to the catalytic site and hence modulate the rate of the reaction with the substrate. Consequently, the rate vs. substrate concentration plot displays a sigmoidal rather than hyperbolic dependence.

Most allosteric enzymes are oligomeric and are often found at key branch points in metabolic pathways. Two notable models have been proposed, notably the Monod, Wyman and Changeux concerted model (70) (MWC model) and the Koshland, Némethy and Filmer (71) (KNF model) sequential model. In the MWC model, allosteric control in

proteins displays cooperative functional behavior along with feedback inhibition (70). An equilibrium exists whereby all of the protein subunits exist in low activity or high activity states and the relative amounts of the protein in its different forms depend on the degree of saturation with the substrate. This facilitated the understanding of kinetic results obtained with hemoglobin, aspartate transcarbamylase (ATCase), threonine deaminase and many other well known enzymes. In contrast, the KNF model for cooperative behavior, proposes that a conformational change in one subunit does not necessarily induce a change in other subunits. Each subunit is allowed to change its tertiary structure on substrate binding permitting alteration of the chemical activities of its nearest neighbors. In both theories, the enzyme subunits exist in a tense (less active) or relaxed conformation (more active).

Tyrosine, the end product of the pathway, inhibits both dehydrogenase and mutase activities (72) and recent crystallographic studies on PDs from *H. influenzae* (unpublished) and *A. aeolicus* (JBC submitted) suggest that it does so by binding to the same active site to which prephenate binds. However, the mechanism of the inhibition is still under debate. To explain the sigmoidal kinetics produced in the presence of L-Tyr and prephenate, several mechanisms have been proposed. Analytical ultracentrifugation experiments provided evidence that tyrosine inhibits enzyme activity by promoting the formation of an inactive tetramer from the active dimer (16). In contrast, sucrose density experiments showed no evidence for a quaternary structural change upon inhibition (72, 73). Furthermore, it has been suggested through analysis of kinetic models that there are tertiary structural changes in the enzyme propagated through the subunits that promote the formation of the inactive conformation of CM-PD (74). Work by Lütke-Eversloh and

Stephanopoulos (75) has identified residues at the C-terminus of the enzyme that are distant from the proposed active site, that are important for L-Tyr inhibition. In contrast, the Turnbull lab has identified active site residues that play a role in L-Tyr binding (unpublished).

1.1.7 Role of Cysteines in CM-PDT and CM-PD of *E. coli*

Sulfhydryl groups of cysteine residues of peptides and proteins are generally the most reactive of all amino acid side-chain moieties under normal physiological conditions. They may be readily alkylated, acylated, arylated, and oxidized, and will form complexes with many heavy-metal ions (76). Sulfhydryl groups are important to both the structure and function of many proteins. In the protonated form they are capable of providing weak hydrogen-bonding in relatively water-free environments, such as those which occur within the protein or at the active sites. But it is their ability to dissociate to the strongly nucleophilic anion at moderately alkaline pH that renders these groups very reactive towards a variety of reagents (76, 77).

E. coli CM-PD is composed of 373 amino acids, three of which are cysteines at positions 95, 169 and 215. Cys95 is found in the mutase portion of the enzyme whereas Cys169 and Cys215 are located in the dehydrogenase domain. Previous studies using a combination of chemical modification, peptide mapping and kinetic analysis have indicated that Cys215 is important for maintaining the structural integrity of both the dehydrogenase and mutase active sites (14, 35). In contrast, studies using similar techniques revealed that the homologous residue in CM-PDT (Cys216) is critical for prephenate binding but plays no role in the mutase reaction (35, 78, 79). Site-directed

mutagenesis has also pinpointed Cys374 as an important residue in the binding of phenylalanine to PDT (80). Furthermore, the monofunctional chorismate mutase from *B. subtilis* contains a Cys residue (Cys75) at the active site, which has been shown by X-ray diffraction studies to interact with the TS analog (81).

1.2 ASPARTATE TRANSCARBAMYLASE (ATCase) IN *E. coli*

Aspartate transcarbamylase (ATCase) (EC 2.1.3.2) catalyzes the first committed step in pyrimidine biosynthesis, namely the carbamylation of L-aspartate from carbamyl phosphate to yield carbamyl aspartate with the concomitant release of inorganic phosphate (Figure 1.9). The ATCase mechanism implicates a precatalytic conformational change of the enzyme-carbamyl phosphate-L-Asp ternary complex to its activated form, which facilitates the deprotonation of the α -amino group of L-Asp by an active site base. The carbonyl carbon of carbamyl phosphate then undergoes nucleophilic attack by the α -amino group of L-Asp, resulting in the formation of a tetrahedral intermediate. A subsequent intramolecular proton transfer between the positively charged amino group of L-Asp and one of the negatively charged phosphate oxygens leads to the collapse of the tetrahedral intermediate to form carbamylaspartate and inorganic phosphate (82, 83). Carbamylaspartate is then funneled down the pyrimidine biosynthetic pathway for the synthesis of CTP and dCTP (Figure 1.10). These nucleotides are subsequently used for the biosynthesis of RNA and DNA, respectively.

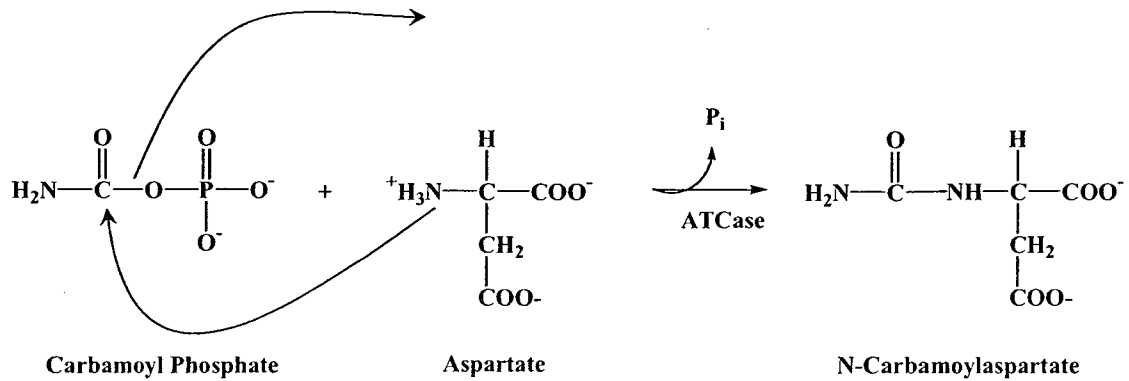


Figure 1.9: Carbamylation reaction catalyzed by ATCase

ATCase in bacteria is present as a monofunctional enzyme, whereas in higher organisms it is present within a multifunctional enzyme consisting of carbamyl-phosphate synthetase 2, aspartate transcarbamylase and dihydroorotase. ATCase from *E. coli* is the most extensively studied allosterically regulated enzyme. In addition to catalyzing an enzymatic reaction in the organism, it is also present at the beginning of a key metabolic pathway, which also confers additional regulatory responsibilities (82) (Figure 1.10).

Enzymes of such importance are generally fairly large and contain multiple subunits (82). The subunit structure of ATCase was elucidated in two separate crystallographic investigations by Weber (84) and Lipscomb (85). The holoenzyme is a heterododecamer with a molecular weight of approximately 300 kDa. It consists of six copies of each of two distinct polypeptides, which are classified as regulatory (R) and catalytic (C), stemming from the nature of their function. Within the C_6R_6 complex, the catalytic chains are arranged as two catalytic trimers, denoted CSU, whereas the regulatory chains are arranged as three regulatory dimers, denoted RSU. The 17 kDa

regulatory polypeptide is composed of 158 amino acids, while the 33 kDa catalytic polypeptide is composed of 310 amino acids. The overall tertiary structure of the holoenzyme is arranged in such a way as to possess D_3 symmetry, that is, it has a 3-fold rotational axis, which is perpendicular to three equivalent 2-fold rotational axes that are 60 degrees apart (86) (Figure 1.11).

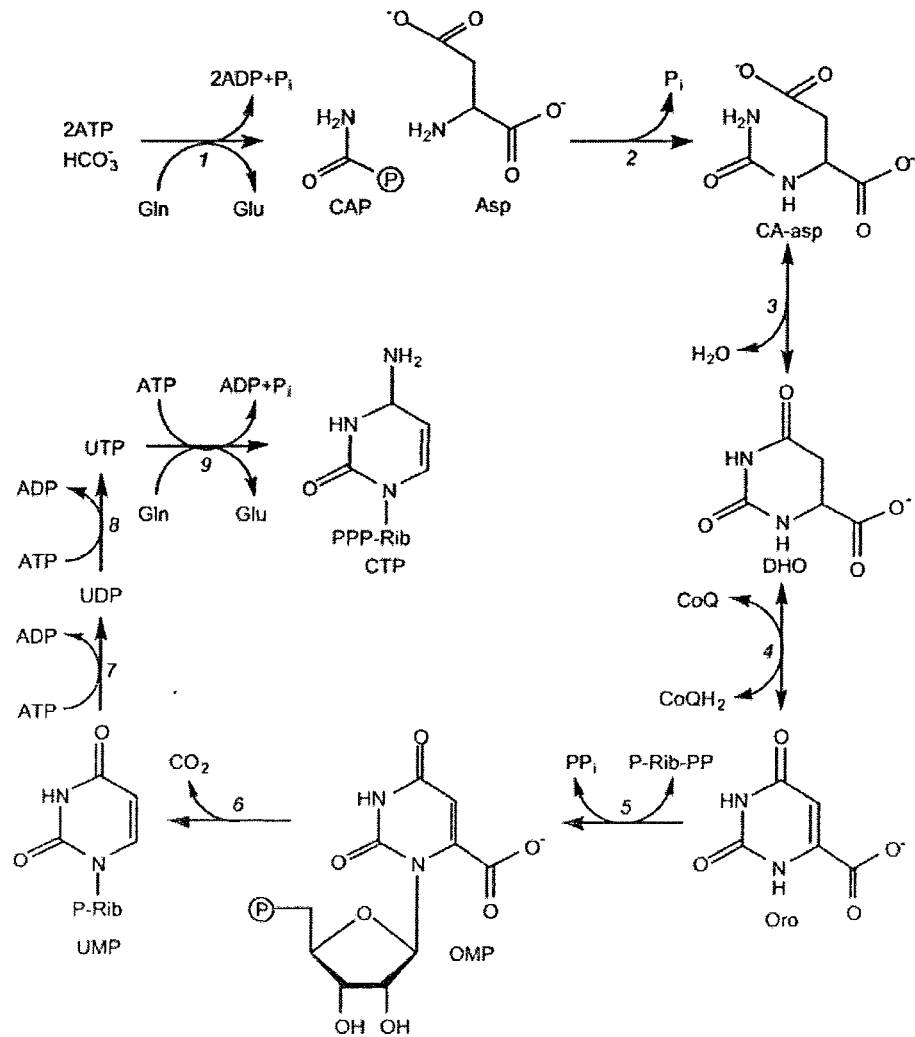


Figure 1.10: The *de novo* pathway for biosynthesis of pyrimidine nucleotides

The enzymes are: 1, carbamyl phosphate synthetase (CPSase); 2, aspartate transcarbamylase (ATCase); 3, dihydroorotase (DHOase); 4, dihydroorotate dehydrogenase (DHODHase); 5, orotate phosphoribosyltransferase (OPRTase); 6, OMP decarboxylase (ODCase); 7, UMP kinase; 8, nucleoside diphosphokinase; 9, CTP synthase (CTPSase).

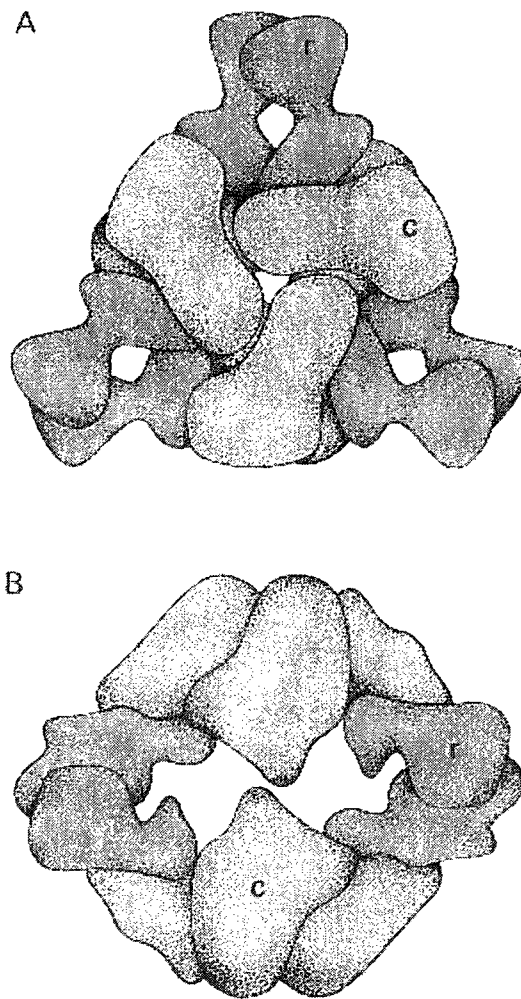


Figure 1.11: Subunit arrangement in ATCase holoenzyme

The RSUs are shown in pink (r) and the CSUs are shown in blue (c). A) View down the three-fold symmetry axis. (B) Perpendicular view. Picture adapted from Krause *et al.* (87).

Each type of subunit is composed of two separate domains (Figure 1.12); the catalytic chain consists of an aspartate and a carbamyl phosphate binding domain, whereas the regulatory chain consists of an allosteric effector and a Zn^{+2} binding domain (88). The holoenzyme can be separated into its regulatory and catalytic components upon treatment with neohydrin (a mercurial agent) with negligible effects on the intrinsic properties of the isolated subunits; the RSU can still bind the allosteric regulators but possesses no catalytic activity, whereas the CSU is catalytically more active but cannot be allosterically regulated as in the holoenzyme (89, 90).

ATCase possesses an extremely complex kinetic behavior exhibiting positive cooperativity (homotropic effect) for either of the substrates (91, 92). Furthermore, kinetic studies have been performed in order to determine the heterotropic effects of nucleotides on the activity of ATCase (91); CTP, the end product of the reaction, functioning as an allosteric inhibitor whereas ATP is an allosteric activator. Moreover, UTP alone does not appear to affect ATCase activity except in the presence of CTP, in which case, enzyme inhibition is increased (93).

Allosteric interactions are known to be crucial in the regulation of enzyme activity (70). Kinetic studies using a engineered holoenzyme composed of a 70-amino acid zinc-binding polypeptide from the regulatory chain with intact WT and variant CSUs have shown that the homotropic properties of this enzyme are dependent on the presence of both polypeptides within the quaternary structure of the enzyme (94).

A C-terminal zinc domain on the regulatory polypeptide contains a structural Zn^{+2} ion coordinated by four cysteines 109, 114, 138 and 141 which also mediate R-C interactions. This ion is required for structured assembly but does not participate in

. The Zn^{+2} domain hence possesses a pivotal role in the association of the RSU to the CSU and treatment with neohydrin causes the holoenzyme to dissociate into its catalytic and regulatory subunits (95). Moreover, treatment of the holoenzyme with mercurial reagents also results in altered allosteric properties for ATCase; its activity is significantly increased but CTP's inhibitory capabilities are abolished; these results clearly suggest distinct sites of binding for the allosteric regulators and the substrates (96).

Much effort has been devoted towards understanding the nature of the tertiary and quaternary structural changes upon binding of substrates and allosteric effectors. According to the Monod Wyman Changeux model, ATCase has two conformational states: a more active R state and a less active T state. The substrates, as well as the bisubstrate analogue B-(Phosphonacetyl)-L-aspartate (PALA), cause complex changes in its quaternary structure resulting in an increase in its hydrodynamic volume, which favors the R state of the holoenzyme (97). Newell *et al.* (98) established by equilibrium dialysis experiments using 3H -labeled PALA, that the dissociation constant of PALA is 110 nM for the ATCase holoenzyme and 95 nM for isolated catalytic subunits. At low concentrations, PALA binding promotes a closure of the hinge between the C chain domains by 8° , while the region between the allosteric and Zn domains expands. On the quaternary structural level, the holoenzyme undergoes a shift of 11 Å along and a rotation of 7° about the threefold axis and a 15° rotation of the regulatory chains about the three twofold axes. Binding of ATP and CTP, cause only minor changes in the quaternary structure (99). The unliganded structure as well as that bound with CTP is termed the T

state. ATP or CTP binding to the regulatory subunits of ATCase induce global conformational changes, hence promoting the T→R transition (100, 101).

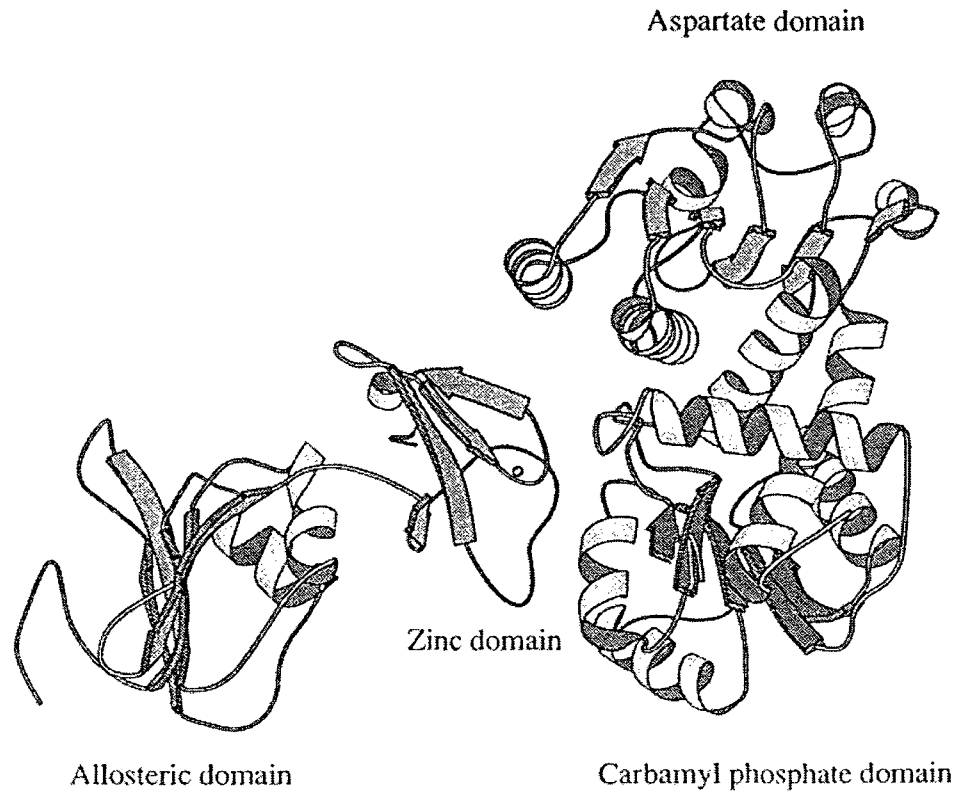


Figure 1.12: Domain structures of the catalytic and regulatory chains

The catalytic chains have two ligand-binding domains, the N-terminal carbamylphosphate domain and the C-terminal aspartate domain. The regulatory chains are also composed of two domains, namely the allosteric domain, which binds the effectors, and the zinc domain, which contains a structural zinc atom. Picture adapted from Roche, O. and Field, M.J. (102).

Key amino acid side chains are usually involved in the binding of substrates within enzyme active sites. The identity and role of these residues has been probed using x-ray crystallography for the visualization of the crystal forms of ATCase bound to either its substrates, carbamyl phosphate and/or substrate analogues. Most recently, lower resolution NMR structures have now been determined for the holoenzyme in the presence and absence of ligands (Lipscomb, W.N., unpublished). Site-directed mutagenesis and hybrid subunit exchange experiments have demonstrated that the catalytic active sites are shared at the interfaces between adjacent catalytic chains (103). Several residues have been identified as crucial for catalysis: Ser52, Thr53, Arg54, Thr55, Arg105, His134, Gln137, Arg167, Arg229, Glu231, and Ser80' and Lys84' from an adjacent catalytic chain (104) (Figure 4.5). Thus, the active site is a highly positively charged pocket. Chemical modification experiments using 5,5'-dithiobis(2-nitrobenzoate) (DTNB), a cysteine-specific chemical modifying reagent, show that Cys47, the sole cysteine residue in the catalytic polypeptide, is too far from the active site to directly interact with the substrates/PALA (105) (Figure 1.13).

Random mutagenesis experiments combined with genetic complementation were conducted by Jenness and Schachman (106). Their experiments yielded a mutant holoenzyme where Ser52 from the catalytic subunit was replaced with a phenylalanine residue (Ser52Phe). While the overall structural properties did not appear altered as a result of the substitution (extinction coefficient at 280 nm, sedimentation coefficient, electrophoretic mobilities of the chains), the variant was catalytically inactive and was unable to undergo the T→R transition upon binding of PALA (87, 107).

In order to better understand the structural importance of the substitution at position 52 in the holoenzyme, Xu and Kantrowitz constructed the Ser52Ala variant holoenzyme by site directed mutagenesis (108). The variant holoenzyme had markedly altered kinetic parameters; k_{cat} was decreased 670-fold, the K_m for aspartate and carbamyl phosphate increased 5.6-fold and 23-fold, respectively, with a loss of cooperativity in the binding of either substrate. The kinetic parameters of the isolated catalytic subunit were also affected but not to the same extent as in the holoenzyme; k_{cat} showed an 89-fold decrease, while the K_m for aspartate and carbamyl phosphate increased 6-fold and 53-fold, respectively. The K_d for carbamyl phosphate increased 75-fold and K_i for PALA increased 5.8-fold relative to the WT CSU. The conclusions drawn from these studies have shown that the Ser52 hydroxyl moiety is involved in the binding of carbamyl phosphate as well as influencing the T→R transition of the holoenzyme, possibly by stabilizing the enzyme-carbamyl phosphate complex (108).

Markby *et al.* coupled full length catalytic trimers to a 70-amino acid zinc-containing peptide originating from the RSU in order to simplify the ATCase holoenzyme model (89). This engineered holoenzyme exhibited markedly different kinetic properties compared to the WT holoenzyme, and surprisingly also corrected the catalytic differences of the Lys164Glu variant. Amino acid substitutions at position 52 were further investigated in a follow-up study by Peterson *et al.* (109). They showed by differential scanning calorimetry that the T_m of Ser52Ala CSU increased by 10.2°C relative to the WT CSU. Surprisingly, the Ser52Cys variant further increased the change in T_m to 13.3°C. The same degree of thermal stability was also observed for an engineered holoenzyme consisting of mutant CSU complexed with an isolated 70-amino

acid zinc-binding peptide originating from the RSU. Although these results were striking, Peterson's main focus was to determine the effects of the single point mutations on the thermal stabilities, notably the T_m , of the isolated single point variant CSUs compared to their respective holoenzymes, not the underlying biophysical reasons for the thermal stability.

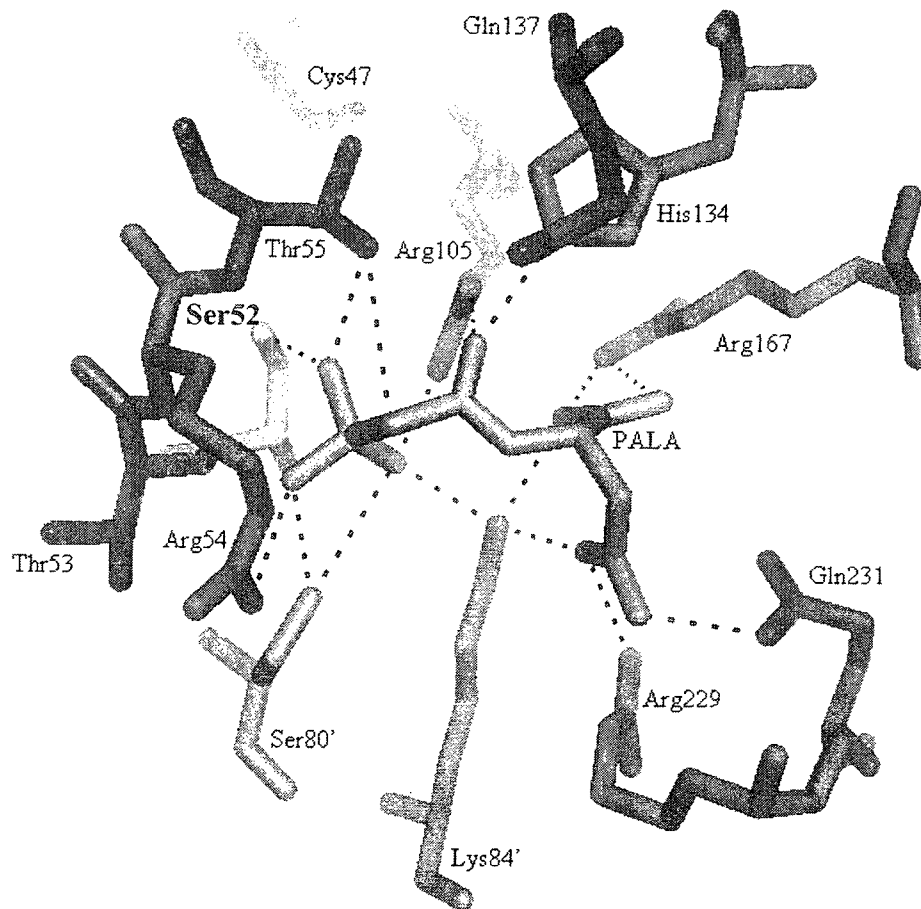


Figure 1.13: Schematic representation of WT ATCase CSU active site residues interacting with PALA

Basic amino acids are colored in red, polar uncharged residues in blue, Ser (Cys) 52 in green, Cys47 in black, residues from an adjacent monomer are in light grey and the bisubstrate analogue, PALA, in teal. The figure was generated using the PyMol software. (PDB ID: 1D09 (*110*))

1.2.1 Chemical Modification of Cysteine and Lysine Residues of Proteins

Chemical modification of proteins serves as a useful tool in biochemistry. Its applications allow for, but are not limited to, the determination of side chain reactivities, the quantitation of individual amino acids, development of cross-linking reagents, blocking reagents for peptide synthesis as well as reagents for specific cleavages of peptide bonds (*111*). Chemical modification can generate information that is complementary to that provided by site-directed mutagenesis, and has been instrumental in the identification of enzymic groups important for the biological function of enzymes and proteins (*112-115*).

Despite the informative nature of this technique, interpretation of chemical modification must be performed cautiously since several factors regulate the reactivity of amino acids. First and foremost, reactivity is highly dependent on the surface exposure of the amino acid side-chain as well as its pK_a , both of which are a function of the three-dimensional structure and the spatial arrangement of amino acids within the protein. Cysteine reactivity is also governed by the reactivity of the thiol-reactive reagent, the charge compatibility of the reagent, the environment of the cysteine, the stability of the bonds formed, and lastly, the nature of the leaving group of the sulfhydryl reagent. Hence, prominent reactivity of a given group does not automatically implicate this amino acid as being important in protein function. Loss of a given catalytic activity upon

reaction of a particular reactive amino acid may simply be due to steric hindrance caused by the chemical adduct, therefore placing its side chain in proximity of a catalytically important residue. Additional requirements for the definite assignment of importance for a specific residue include: (1) the correlation of loss of catalytic activity with the stoichiometric incorporation of a reagent into this group; (2) inhibition of inactivation in the presence of substrate or product of the reaction; (3) the observation that inhibition is invariant with the type of modifying reagent used, therefore requiring the use of a variety of reagents with different characteristics. As a consequence of the above mentioned requirements for the firm establishment of the importance of an amino acid, chemical modification should be used in combination with site-directed mutagenesis. Moreover this traditional approach of residue identification using site-specific reagents has been revitalized by recent advances in protein mass spectrometry, which allow a clearer understanding of the results of modification (116-118).

In this thesis, the role and reactivity of cysteine and lysine residues in *E. coli* CM-PD as well as cysteine residues in *E. coli* ATCase, are under investigation. Hence, the following sections provide a brief description of the chemistry of the reagents used to modify these amino acids, which is necessary for the understanding of the present work.

1.2.2 Enzyme Reaction with DTNB (Ellman's reagent)

Ellman's reagent, also known as DTNB (5,5'-dithio-bis(2-nitrobenzoic acid)), has long been used as a reagent in sulfhydryl group determination (119). It is an aromatic disulfide which specifically reacts with aliphatic thiol groups (Figure 1.14) to form a mixed disulfide of the protein with concomitant release of 2-nitro-5-thiobenzoate in 1:1 stoichiometry.

The advantage of using DTNB is the ability to monitor the reaction by UV spectrophotometry since its absorbance is negligible in the native form but intense yellow at 412 nm when it reacts with thiolate groups on proteins under mild alkaline conditions (pH 7-8) upon release of the 2-nitro-5-thiobenzoate anion (TNB²⁻) (Figure 1.14). Its disadvantages stem from the instability of the TNB adduct at both low and high pH hence eliminating its candidacy for use in mass spectrometry (120).

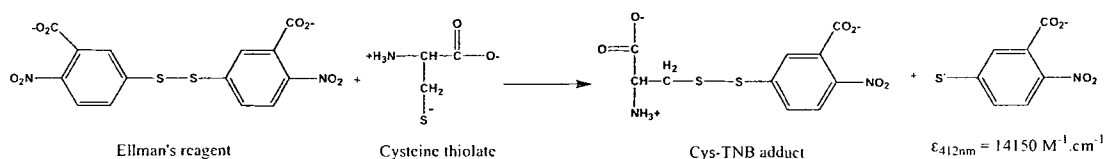


Figure 1.14: Reaction of cysteine thiol with DTNB (Ellman's reagent)

1.2.3 Enzyme Reaction with Iodoacetamide

Iodoacetamide (IAM) has long been used as a cysteine residue alkylating agent to eliminate cystine formation within proteins and hence facilitate protein digestion and analysis (121).

IAM is an alkyl thiol and is small in size relative to DTNB, which is an aromatic disulfide. Its physico-chemical properties render it less reactive than DTNB; it mainly reacts with cysteine residues but has also been reported to modify histidine and methionine residues but to a lesser extent, yielding the corresponding carboxamidomethyl derivative (77, 122). The IAM-mediated alkylation reaction involves the nucleophilic attack of the cysteine thiolate on the iodine group of the reagent, which acts as a leaving group (Figure 1.15). The alkylation of cysteine residues is irreversible and the adduct formed is stable under acidic conditions suitable for mass spectrometric analysis, exhibiting a spectral shift of +57 amu.

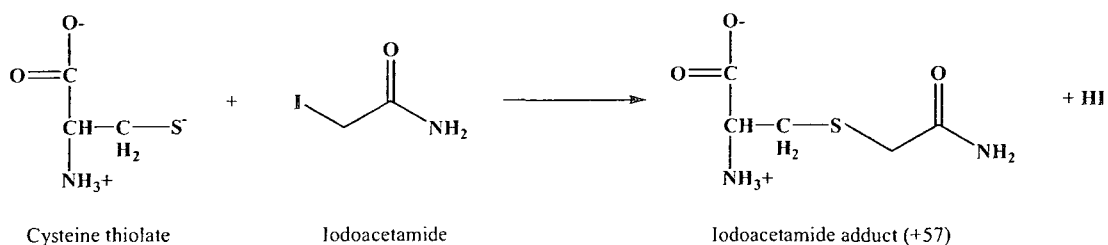


Figure 1.15: Reaction of cysteine thiol with iodoacetamide

1.2.4 Enzyme Reaction with Trinitrobenzene Sulfonic Acid (TNBS)

The reaction of 2,4,6-trinitrobenzenesulfonic acid (TNBS) with amino groups has been invaluable in studying the reactivity and function of the ϵ -amino groups of lysyl residues in proteins (123, 124). The reaction of TNBS with the primary amino groups in proteins is shown in Figure 1.16. The trinitrophenylated adduct has an extinction coefficient at 345 nm (ϵ_{345}) of $14500 \text{ M}^{-1} \text{ cm}^{-1}$ making its formation easy to monitor by UV spectrophotometry. The rate of modification is a sensitive indication of the amino group's basicity, as an amino acid must be in the deprotonated state in order to react with TNBS (77). An important reason for selecting this reagent is that the chemical modification is irreversible, allowing for the ESI-MS detection of the adduct shifted by +211 amu; the TNB-adduct may not be seen by MALDI because it absorbs strongly at the emission wavelength of the powerful laser source and is hence photodegraded (38).

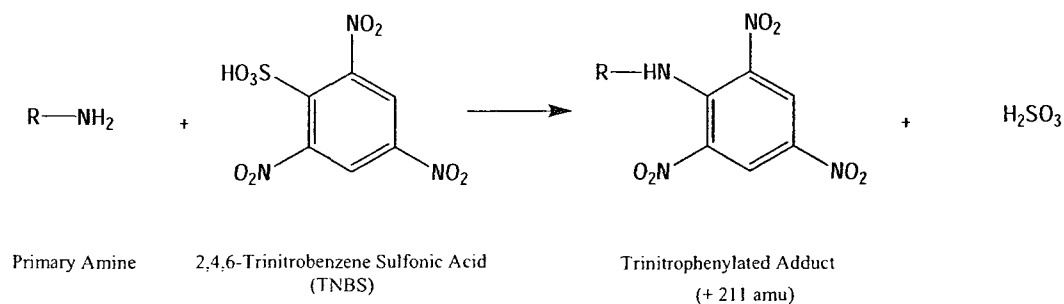


Figure 1.16: Reaction of lysine ϵ -amino with TNBS

1.3 SCOPE AND ORGANIZATION OF THIS THESIS

In chapter two, the importance of three Cys residues in the activity of CM-PD are assessed by site-directed mutagenesis and chemically modifying WT and variant forms of the enzyme. Furthermore, this chapter shows the utility of mass spectrometry in verifying the amino acid substitutions and in assessing the reactivity and accessibility of the Cys residues in the native protein.

In chapter three, we examine the reactivity and ionization state of Lys37 in WT CM-PD using TNBS for chemical modification. A Lys37Gln variant was generated by site-directed mutagenesis and was purified to homogeneity. Activity and binding studies by differential fluorescence spectroscopy using *endo*, the transition state analogue, were performed on both WT and Lys37Gln CM-PD. Ultimately, the pK_a of the Lys37 residue in WT CM-PD was determined using chemical modification by TNBS in combination with mass spectrometric peptide mapping. The biophysical reasons for the altered pK_a of Lys37 are rationalized based upon a model that was generated using the crystal structure from the *E. coli* “mini-mutase”.

In chapter 4, an improved and more efficient nickel affinity purification scheme for His-tagged ATCase holoenzyme and its separation into its constituent subunits is examined. The biophysical properties of the resulting purified CSUs were assessed using far-UV CD, fluorescence spectroscopy and mass spectrometry. The thermal stabilities of the WT and Ser52Cys CSUs were also reexamined using far-UV CD. Assessment of surface accessibility and reactivity of Cys47 in the WT CSU and both Cys47 and Cys52 in the Ser52Cys variant CSU was achieved using chemical modification by DTNB and monitored by UV spectroscopy. Ultimately, the pK_a and hence the ionization state of

Cys52 in the Ser52Cys ATCase CSU variant was examined using chemical modification by IAM and CIAM in conjunction with mass spectrometry. On the basis of the generated results and available crystal structures, we attempt to provide a rationale for the variant's altered biophysical and kinetic properties.

CHAPTER 2

Determination of the Structure/Function Relationship of Cysteine Residues in

E. coli Chorismate Mutase – Prephenate Dehydrogenase

2.1 INTRODUCTION

CM-PD of *E. coli* contains 373 amino acids, three of which are cysteine residues at positions 95, 169 and 215. Two of these cysteine residues, Cys169 and Cys215, are located in the dehydrogenase domain whereas Cys95 is found in the mutase encoding region of the enzyme. Previous chemical modification studies of CM-PD with DTNB and iodoacetamide have shown that one sulfhydryl per subunit (Cys215) was particularly reactive and the integrity of this group was essential for both enzyme activities (14, 35). In contrast, alkylation of a homologous residue in CM-PDT (Cys216) resulted in the loss of dehydratase activity with only a 5% decrease in mutase activity. More recently, site-directed mutagenesis of CM-PDT has established that substitutions at Cys216 significantly diminished prephenate binding with little or no loss of mutase activity, suggesting that this residue interacted with prephenate. Other cysteine residues have been postulated to play important roles. Cys374 was identified as a residue important in the binding of phenylalanine to the CM-PDT (80). In addition, the monofunctional CM from *Bacillus subtilis* contains an active site cysteine residue (Cys75) which has been shown by X-ray diffraction studies to interact with the ring hydroxyl group of the transition state analog (81). Moreover, it has also been postulated for CM of *E. coli* CM-PD that an active site nucleophile might assist in the rearrangement through acid/base catalysis (48).

There have been no published site-directed mutagenesis studies examining the importance of any cysteine residues in *E. coli* CM-PD. Our aims in this study were to conduct structural investigations of CM-PD, in particular to examine the reactivity of the sulfhydryl groups and to assess their importance for enzyme activity. This has been

accomplished through kinetic characterization of site-directed variants of the enzyme and by extending the chemical modification studies to those of the variant forms of the proteins performed in the presence or absence of substrates and substrate analogs. Furthermore, a 3D structural model for the PD portion of *E. coli* CM-PD has been generated using an internet based comparative modeling software package using the unpublished crystal structure of the PD portion of CM-PD from *H. influenzae*. From our studies we propose a role for Cys215 in *E. coli* CM-PD as a template.

2.2 MATERIALS AND METHODS

2.2.1 Chemicals

Chorismate was isolated from *Klebsiella pneumonia* 62-1 as described by Rieger and Turnbull (125) and prephenate was prepared as described by Dudzinski and Morrison (126). NAD⁺ (grade I) was purchased from Boehringer-Mannheim. Stock solutions of these substrates were prepared in MilliQ water or in an appropriate buffer and the pH adjusted to 7.5 prior to storage at -20°C. Their exact concentrations were determined spectrophotometrically using published extinction coefficients (127) as well as enzyme mediated end point analyses (128). *Endo-oxabicyclic diacid* (129) was a generous gift from Dr. Paul Bartlett of the University of California, Berkeley and was stored at -86°C as a 2 mM stock in distilled water. (HPP) 4-hydroxyphenylpyruvate, phenylpyruvate (PP, sodium salt) and 3-(4-Hydroxyphenyl)propionic acid (HPPionate) were obtained from Sigma-Aldrich. The keto form of HPP was prepared as described by Lindblad *et al.* (130). L-tyrosine and L-phenylalanine were purchased from ICN Biochemicals Inc. Potassium cyanide, iodoacetamide, 5,5'-dithio-*bis*-(2-nitrobenzoic acid) (DTNB or Ellman's reagent) were purchased from Sigma-Aldrich. Trypsin (modified bovine; sequencing grade) was purchased from Roche Applied Science. Dithiothreitol (DTT) was obtained from Bioshop. Methanol, chloroform, acetonitrile and trifluoroacetic acid (TFA) (HPLC grade) were purchased from Fisher. Oligonucleotides were of HPLC purity and were obtained from Integrated DNA Technologies Inc. The QuickChange XL™ site-directed mutagenesis kit was purchased from Stratagene and restriction enzymes were from MBI Fermentas. Q-Sepharose Fast Flow anion exchange resin, activated Sepharose

4B and NAP-5 pre-packed Sephadex G-25 size exclusion buffer exchange columns were purchased from Amersham Biosciences. Sepharose-AMP was synthesized in our lab; N⁶-(6-Aminohexyl)-5'-AMP was synthesized by D. Christendat as reported by Craven *et al.* (131) and was coupled to CNBr-activated Sepharose-4B as per GE Healthcare Instructions 71-7086 AE. All other chemical reagents were obtained commercially and were of the highest quality available.

2.2.2 Source of Recombinant WT and Variant CM-PD of *E. coli*

Recombinant wild-type (WT) CM-PD was expressed in *E. coli* and purified as described by Christendat (39) by subcloning *tyrA* (the gene encoding CM-PD) from plasmid pKB45 (132) into an inducible expression vector pSE380 (Novagen) to yield pVIV1 (39). Christendat and Mekhssian constructed Cys215Ala, Cys215Ser, and Cys95Ala variants as described previously by Christendat *et al.* (39) while Cys169Ala was generated with the QuikChange XL site-directed mutagenesis kit (Stratagene) following the manufacturer's instructions. The mutants were initially screened for the addition of a unique restriction site, *Sa*II. All mutations were verified by sequencing (Bio S & T, Montreal, or Centre for Structural and Functional Genomics, Concordia University). DNA was prepared for sequencing using a Promega WizardTM plasmid preparation kit.

2.2.3 Expression and Purification of WT and Variant Forms of *E. coli* CM-PD

CM-PD was purified by the method of Christendat *et al.* (39) with slight modifications. WT and variant CM-PD were expressed in *E. coli* following transformation into KB357. The resulting strain was grown at 37°C in LB medium containing 100 µg/mL ampicillin to an OD_{600nm} of 0.6 – 0.8 before overnight induction at 18°C with 0.4 mM IPTG. The cells were then harvested by centrifugation at 10000 rpm for 45 minutes at 4°C and were stored at -20°C until further use. The cell pellet was resuspended with stirring for 15 minutes on ice in buffer B (0.1 M NEM, pH 7.4, 1 mM EDTA, 1 mM DTT, 10% glycerol (v/v)). The suspension was homogenized using a Dounce homogenizer. The suspended cells were then lysed using a French pressure cell using a setting of 900 psi. The lysate was supplemented with 1 mM PMSF and was centrifuged using a Beckman centrifuge for 30 minutes at 4°C at 10000 rpm. The previously reported ammonium sulfate fractionation step was omitted. The dialyzed protein was applied to Q-Sepharose Fast Flow resin (100 mL bed volume) (2.6 x 30 cm glass column) previously conditioned with buffer B. After washing the column with 400 mL of buffer B, CM-PD was eluted with an 800 mL linear gradient of 0 – 0.4 M KCl in the same buffer. Enzymatically active fractions were pooled, dialyzed and chromatographed on Sepharose-AMP resin by the method of Turnbull *et al.* (14). The pH of the dialysate was adjusted to 6.0 using 5 M Acetic Acid (pH 4.0) and dialyzed overnight at 4°C in 4 L of buffer C (0.1 M NEM, 46 mM MES, 21 mM sodium citrate, 1 mM EDTA, 1 mM DTT, 10% glycerol (v/v) pH 6.0.). The dialyzed protein was applied to Sepharose-AMP (50 mL bed volume, 2.6 x 30 cm glass column) previously conditioned with buffer C. After washing the resin with 400 mL of buffer C, CM-PD was

eluted with an 800 mL linear gradient of 0 – 1.5 M KCl in the same buffer. Enzymatically active fractions were pooled and dialyzed overnight at 4°C in buffer D (0.1 M NEM, 21 mM sodium citrate, 1 mM EDTA, 1 mM DTT, 10% glycerol (v/v) pH 7.0). The enzyme was concentrated using Millipore 15 mL centrifugal concentrators (MWCO 30 kDa) to a concentration above 2 mg/mL in buffer D containing a final concentration of 25% glycerol and 20 mM DTT (storage buffer). Enzyme solution was stored in 100 µL flash-frozen aliquots at -86°C until ready for further use.

2.2.4 Sample Preparation of CM-PD

Frozen CM-PD protein samples were quickly thawed and then immediately placed on ice. To the samples was added DTT at a final concentration of 20 mM with subsequent incubation on ice for 30 minutes in order to reduce cysteine residues. Following DTT treatment, samples were buffer-exchanged into their intended buffer. Buffer exchange was performed using either a NAP-5 size exclusion column or a BIOMAX centrifugal concentrator (MWCO 30 kDa).

For exchange via a NAP-5 column, 10 mL of the intended buffer is used to equilibrate the column. A 500 µL aliquot of the sample is passed through the column. Once the 500 µL sample had eluted, 1 mL of buffer is applied into the column and the eluate is collected into a 1.5 mL Eppendorf tube.

For buffer exchange/concentration using a BIOMAX centrifugal concentrator, the sample is placed in the concentrator tube which had previously been conditioned with the appropriate buffer. It is then centrifuged at 12000 rpm using a benchtop centrifuge at 4°C

until the sample reaches an approximate volume of 100 μ L. Additional buffer is added to the sample up to a final volume of approximately 500 μ L. The sample is then centrifuged once again as described previously. This step is repeated two more times in order to exchange the solvent completely into the intended buffer as well as to concentrate the protein.

2.2.5 SDS—Polyacrylamide Gel Electrophoresis

Denaturing SDS-PAGE was performed using a 10% polyacrylamide gel as per the method reported by Laemmli (1970). Protein samples were diluted 1:1 (v/v) with 2 x SDS sample loading buffer (1.5 M Tris-HCl, 4% SDS, 20% glycerol, 0.002% Bromophenol blue, 200 mM DTT) and were incubated in a boiling water bath for 5 minutes in order to fully denature the protein sample. The sample was then placed on ice for 5 minutes prior to loading on the polyacrylamide gel. The gel was electrophoresed at 80 V in order for the samples to migrate through the stacking gel and the voltage was then increased to 180 V as the samples entered the resolving gel. Electrophoresis was continued until the bromophenol blue tracking dye migrated off the resolving gel. Bio-Rad broad range molecular weight protein standards were used to estimate the molecular weight of proteins in the sample. Protein was then visualized by staining the gels with Coomassie Brilliant Blue R-250. Excess dye was removed using destaining solution which consists of 10: 9: 1 methanol: distilled water: glacial acetic acid (v/v/v).

2.2.6 Protein Concentration Determination

Protein concentration was estimated using the Bio-Rad Protein Assay Kit (Bio-Rad Laboratories) with bovine serum albumin (Sigma) as a standard (134) and by recording the absorbance at 280 nm using $E^{0.1\%} = 0.818$ as reported for WT enzyme (34).

2.2.7 Determination of Enzyme Activity

Mutase and dehydrogenase activity assays were conducted at various stages of the purification procedure by adding 950 μ L CM or PD mix, respectively, to a 1 cm pathlength quartz cuvette. The assay mixtures were equilibrated for 1 minute at 30°C prior to initiation of either reaction by addition of enzyme. Assays were conducted at 30°C using a Varian Cary 50 Dual Beam Spectrophotometer equipped with a water-jacketed cell holder and thermostatted using a water circulating pump with heating/cooling capabilities. CM mix consisted of 100 mM Tris-HCl pH 7.5, 1 mM EDTA, 1 mM DTT and 500 μ M chorismate and PD mix consisted of 100 mM Tris-HCl pH 7.5, 1 mM EDTA, 1 mM DTT, 2 mM NAD^+ and 500 μ M prephenate. The conversion of chorismate to prephenate was monitored at 273 nm while the oxidative decarboxylation of prephenate in the presence of NAD^+ was followed at 340 nm as reported by Heyde and Morrison (15). Reaction rates were calculated from the linear portion of progress curves using the Cary WinUV kinetics application supplied with the spectrophotometer.

2.2.8 Kinetic Parameter Determination

Mutase and dehydrogenase kinetic parameters were determined at 30°C in 1 mL total volume, in the presence of a three-component buffer system (3CB) consisting of 0.1 M MES, 51 mM N-ethylmorpholine, 51 mM diethanolamine, 1 mM EDTA and 1 mM DTT at pH 7.2 (135). Enzyme was diluted into a three-component buffer system (buffer K) consisting of 0.1 M N-ethylmorpholine, 1 mM EDTA, 20% glycerol pH 7.5 prior to assaying. The conversion of chorismate to prephenate was monitored at 273 nm while oxidative decarboxylation of prephenate in the presence of NAD⁺ was followed at 340 nm (15). Both reactions were monitored using a Varian Cary 50 Dual Beam Spectrophotometer equipped with a water-jacketed cell holder and thermostatted using a water circulating pump with heating/cooling capabilities. Reaction rates were calculated from the linear portions of progress curves using the Cary WinUV kinetics application supplied with the spectrophotometer. Kinetic data were fitted to the Michaelis-Menten equation (equation 2.1) using GraFit v 5.0.1 from Erithacus Software in order to determine the variant kinetic parameters. Rate constants were calculated using a subunit molecular weight of 42,000. Maximum velocity (V/E_t) is expressed in units of s⁻¹ and the apparent second-order rate constant (V/KE_t) in units of M⁻¹s⁻¹. A unit of enzyme is defined as the amount of enzyme required to produce 1 μmol of product per minute at 30°C.

$$v = \frac{V_{max}[S]}{K_m + [S]} \quad (\text{Equation 2.1})$$

Residual mutase and dehydrogenase enzyme activities were determined in 3CB (pH 7.2) in reaction mixtures containing 500 μM chorismate or 500 μM prephenate and an NAD^+ concentration equivalent to 14 times the K_m for NAD^+ for the variant under investigation. DTT was omitted from the DTNB reaction mixtures to avoid reducing DTNB.

2.2.9 ESI-MS of Native and Variant CM-PD

CM-PD protein sample preparation for ESI-MS was as reported by Weinglass *et al.* (136) and was as follows: 100 μL aqueous sample (1 mg/mL) was diluted with 3 volumes of methanol with brief vortexing. To the mixture was added 1 volume of chloroform and was vortexed briefly. The sample was then precipitated with 2 volumes of MilliQ water and was vortexed briefly. The sample was then centrifuged at high speed for 2 minutes. Our protein was present as a precipitate at the interface of the two phases. Both phases were carefully removed without disturbing the precipitate. The precipitate was washed with 300 μL methanol and vortexed briefly. The sample was then centrifuged at high speed for 2 minutes in order to recover the precipitate. Methanol was removed and the pellet was allowed to air-dry at room temperature protected from light. It is noteworthy that the smallest amount of protein that was successfully precipitated was 50 μg , with a decrease in the reported volumes proportional to the decrease in the amount of protein precipitated. For ESI-MS analysis, the precipitated sample was reconstituted in 40: 60: 0.1 ACN: MilliQ water: TFA (v/v/v) to a final concentration not exceeding 5 μM monomer. The sample was applied to a Micromass Q-ToF 2 triple-quadrupole mass spectrometer by direct infusion at a flow rate of 1.0 $\mu\text{L}/\text{minute}$. Samples were analyzed in positive ion mode using Micromass MassLynx v 4.0 software. The instrument was

calibrated with [Glu]-fibrinopeptide B in the same solvent system as that used for analysis of CM-PD.

2.2.10 Chemical Modification of Native Enzymes

For DTNB experiments, 5 μM enzyme monomer was incubated with a 2-fold molar excess of DTNB with respect to the total concentration of cysteine residues, in 50 mM NEM, 50 mM MES, 1 mM EDTA, 25% glycerol (pH 7.7), at 25°C protected from light. Upon addition of DTNB, the absorbance increase at 412 nm ($\epsilon_{412} = 14150 \text{ M}^{-1} \cdot \text{cm}^{-1}$) was monitored for release of 3-carboxylate 4-nitrophenolate (137). The recorded absorbance was corrected for the contributions from buffer and DTNB. At specified time intervals after addition of DTNB, a sample aliquot was removed, diluted in buffer K without DTT and assayed for mutase and dehydrogenase activities. Control samples were incubated under the same conditions except that DTNB was omitted. For iodoacetamide, 5 μM enzyme monomer was incubated with 10 mM IAM under the same conditions as above. At specified time intervals after addition of IAM, a sample aliquot was removed, diluted into buffer K + 10 mM DTT and assayed for CM and PD activities.

NOTE: Two UV-spectrophotometers were used in order to record both the change in absorbance at 412 nm and enzyme activities.

2.2.11 Probing Cysteine Accessibility/Reactivity by Modification with IAM and CIAM Monitored by MALDI-ToF Mass Spectrometry

WT CM-PD (5 μ M monomer) was pre-treated as per section 2.2.4 and was then incubated in 50 mM NEM, 50 mM MES, 1 mM EDTA, 25% glycerol (pH 7.7) at room temperature protected from light. The modification reaction was initiated upon addition of IAM to a final concentration of 10 mM. At specified time intervals (0, 3, 10, 30 minutes and overnight). A sample aliquot was removed from the reaction in progress and immediately diluted into 10 mM ammonium bicarbonate containing 10 mM DTT. Samples were buffer exchanged into 10 mM ammonium bicarbonate using NAP-5 columns and were then lyophilized to dryness, overnight at room temperature. Lyophilized samples were then reconstituted in 50 mM ammonium bicarbonate (pH 8.0) and digested with sequencing grade trypsin (1:10 trypsin:CM-PD w/w), overnight at 37°C. Digested samples were concentrated and desalted using Millipore C4 ZipTips. Peptides were eluted using 1.5 μ L of 40: 60: 0.1 ACN: MilliQ water: TFA (v/v/v) and mixed with 1.5 μ L of 10 mg/mL α -cyano-hydroxycinnamic acid. One μ L of sample was spotted onto a MALDI plate. Samples were analyzed using Micromass M@LDI MALDI-ToF in positive ion mode using Micromass MassLynx v 4.0 software. The Mass Lynx MALDI-ToF was calibrated in positive ion mode using Bradykinin (1060.2 amu), Angiotensin (1296.5 amu), Glu-Fibrinopeptide (1570.6 amu), Renin (1759.0 amu), and ACTH (18-39 clip) (2465.7 amu) as peptide standards.

Modification by CIAM was conducted under identical conditions as those reported for modification by IAM except that only a single incubation was performed for 2 hours.

2.2.12 Ligand Protection Experiments

For all CM-PD variants, 5 μ M monomer was reacted with a 2-fold molar excess of DTNB with respect to cysteine concentration in solution, in the absence and presence of substrates. Substrates used for protection were 1 mM L-Tyr, 1 mM prephenate, 1 mM NAD⁺, 1 mM L-Tyr + 2 mM NAD⁺, and 25 μ M of mutase transition state analogue *endo*-oxabicyclic diacid (*endo*). Sixty minutes after addition of DTNB, a sample aliquot was removed, diluted into buffer K without DTT, and was assayed for mutase and dehydrogenase activities. The same experiments were performed using 10 mM iodoacetamide as the chemical modifying agent and the ligands used for protection were 1 mM L-Tyr, 1 mM L-Tyr + 2 mM NAD⁺, 1 mM HPP, 1 mM HPP + 2 mM NAD⁺. The extent of protection for both mutase and dehydrogenase activities was reported as % activity remaining with respect to unreacted enzyme.

2.2.13 DTNB Inactivation and Reactivation by Cyanolysis

For all CM-PD variants, 5 μ M monomer was reacted with DTNB in 50 mM NEM, 50 mM MES, 1 mM EDTA, 25% glycerol (pH 7.7) as previously mentioned. At specified time intervals, aliquots were removed and diluted into Buffer K (no DTT) and were immediately assayed for mutase and dehydrogenase activities. When % residual activities remained at constant levels, the CM-PD sample was buffer exchanged and concentrated into fresh buffer using Millipore Biomax centrifugal filters (MWCO 30 kDa) in order to remove any excess DTNB. Protein concentration was determined using the Biorad kit; mutase and dehydrogenase activities were reassessed in order to ensure that the buffer exchange and concentration process did not alter the DTNB-modified

sample. To this sample was added KCN to a final concentration of 10 mM. At specified time intervals, aliquots were removed and diluted into Buffer K (no DTT) and were immediately assayed for mutase and dehydrogenase activities. The percentage of mutase and dehydrogenase activities recovered was reported with respect to the control reaction without DTNB. The absorbance at 412 nm was recorded upon reaching constant % mutase and dehydrogenase activities recovered, in order to determine the concentration of TNB released by cyanolysis, which is equivalent to the concentration of modified CM-PD cysteine residues. After cyanolysis was complete, the sample was buffer exchanged and concentrated once again into fresh buffer in order to remove any excess TNB and KCN. Protein concentration was determined once again using the Biorad kit and the % mutase and dehydrogenase activities of the cyanolysis samples were assessed as previously mentioned. Controls for the experiment were assessed in the beginning of the experiment without DTNB, at the end of the experiment without DTNB as well as at the end of the experiment with 10 mM KCN in order to ensure that the KCN did not affect the enzymatic activity.

2.2.14 Determination of Cysteine pK_a Values in Native WT, Cya95Ala and Cys215Ala CM-PD Variants by ESI-MS

CM-PD variants (23 μ M monomer) (50 μ g total) were incubated in 3CB adjusted to pH values ranging from 5.77 to 9.50. The chemical modification of sulfhydryl groups was initiated upon addition of IAM, present at the same pH as the reaction mixture, to a final concentration of 500 μ M. The reaction was allowed to proceed for 30 minutes at room temperature protected from light. After 30 minutes, the reaction was quenched with

20 mM DTT and immediately precipitated and analyzed by ESI-MS as mentioned in section 2.2.8. The pK_a values were determined by plotting peak intensity ratios (adduct / (adduct + native)) vs. pH, using GraFit v 5.0.1 from Erithacus Software. Please note that the term “native” signifies non-modified enzyme.

2.2.15 Modeling of the PD Domain of *E. coli* CM-PD

Modeller 9v3 was used to model the dehydrogenase portion of the *E. coli* CM-PD monomer against the known structure of *H. influenzae* CM-PD (PDB access code 2pv7). A structure-based alignment of *E. coli* CM-PD with the *H. influenzae* protein was obtained using the FFAS03 server (<http://ffas.ljcrf.edu/ffas-cgi-cgi/ffas.pl>). The FFAS03-generated alignment was used as input for Modeller 9v3, which generated a 3 D model of the dehydrogenase portion of *E. coli* CM-PD on this input.

2.3 RESULTS

2.3.1 Purification and Determination of Kinetic Parameters of WT and Variant Forms of *E. coli* CM-PD

All the CM-PD variants expressed well and yielded active enzyme in quantities between 15 and 30 mg of CM-PD per liter of bacterial culture, comparable to those reported for WT. Purification by ion-exchange and affinity chromatography yielded homogeneous enzyme as illustrated in the SDS-PAGE analysis on Figure 2.1. The ESI-MS spectrum of WT CM-PD illustrated in Figure 2.2, exhibits 2 peaks at $[M+H^+]$ of 41913 and 42043 amu, with an m/z difference of 130 amu. The peak at $[M+H^+]$ of 42043 amu corresponds to the native full-length WT CM-PD, which is in agreement ($<0.01\%$ experimental error) with the expected molecular weight of 42042 Da for the amino acid sequence reported by Wanner *et al.* (138) for the bifunctional *E. coli* CM-PD. The peak at $[M+H^+]$ of 41913 amu corresponds to WT CM-PD where the N-terminal methionine has been post-translationally cleaved (139).

Table 2.1, summarizes the kinetic parameters for all variant CM-PDs examined in this chapter, where Cys was replaced by Ala or Ser in order to determine the effect of hydrogen bonding capabilities of the resulting side chain. This table indicates that Cys95Ala and Cys169Ala variants exhibited kinetic parameters that were comparable to those obtained for the WT enzyme, for all substrate. The k_{cat}/K_m for the mutase reaction decreased only by a factor of approximately 3. In the dehydrogenase reaction, the K_m and k_{cat} for both prephenate and NAD^+ showed less than a 2-fold difference relative to WT enzyme, with the k_{cat}/K_m remaining practically unchanged.

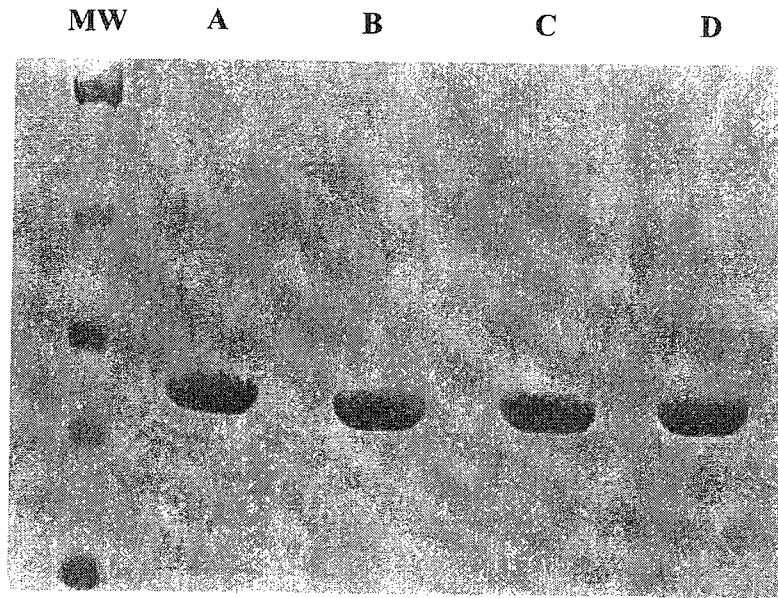


Figure 2.1: SDS-PAGE analysis of native *E. coli* CM-PD variants

Pooled protein samples after AMP-affinity chromatography from the purification of CM-PD variants as analyzed by 10% SDS-PAGE. (A) Cys95Ala, (B) Cys169Ala, (C) Cys215Ala and (D) Cys215Ser.

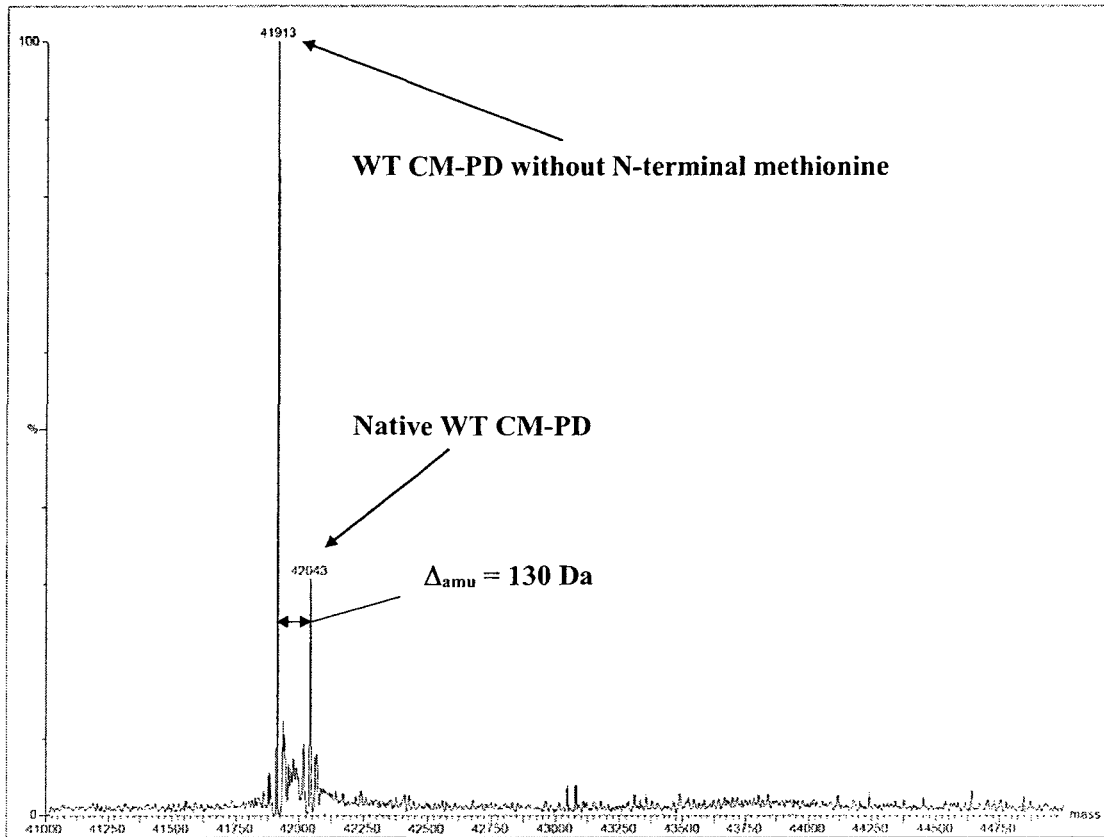


Figure 2.2: ESI-MS spectrum of native *E. coli* WT CM-PD

WT CM-PD was processed and analyzed by ESI-MS as reported in section 2.2.9. The peak at $[M+H^+]$ at 42043 amu corresponds to native full-length WT CM-PD. The peak at $[M+H^+]$ at 41913 amu corresponds to WT CM-PD with the N-terminal methionine removed.

Table 2.1: Summary of Kinetic Parameters for WT CM-PD and Variants Measured at pH 7.2 and 30°C

Protein	Mutase Activity			Dehydrogenase Activity					
	Chorismate			Prephenate			NAD ⁺		
	K _m (μM)	k _{cat} (s ⁻¹)	k _{cat} /K _m (M ⁻¹ .s ⁻¹)	K _m (μM)	k _{cat} (s ⁻¹)	k _{cat} /K _m (M ⁻¹ .s ⁻¹)	K _m (μM)	k _{cat} (s ⁻¹)	k _{cat} /K _m (M ⁻¹ .s ⁻¹)
WT	40 ± 3	54.7 ± 0.8	1.4 x 10 ⁶	35 ± 1	37.6 ± 0.3	1.1 x 10 ⁶	142 ± 13	40.7 ± 0.9	2.9 x 10 ⁵
Cys95Ala	115 ± 11	36.1 ± 1.2	3.1 x 10 ⁵	33 ± 2	31.9 ± 0.3	9.7 x 10 ⁵	172 ± 18	31.8 ± 0.7	1.8 x 10 ⁵
Cys215Ala	541 ± 42	10.2 ± 0.4	1.9 x 10 ⁴	244 ± 22	32.0 ± 0.9	1.3 x 10 ⁵	288 ± 17	27.9 ± 0.5	9.7 x 10 ⁴
Cys215Ser	727 ± 64	29.0 ± 1.1	4.0 x 10 ⁴	115 ± 10	29.2 ± 0.6	2.5 x 10 ⁵	255 ± 19	26.3 ± 0.6	1.0 x 10 ⁵
Cys169Ala	73 ± 2	25.6 ± 0.2	3.5 x 10 ⁵	29 ± 2	23.5 ± 0.3	8.1 x 10 ⁵	199 ± 6	21.4 ± 0.2	1.1 x 10 ⁵

^a Mutase and dehydrogenase kinetic parameters were determined as described in section 2.2.8. Assays were performed at 30°C in 1 mL total volume of 3CB pH 7.2.

The Cys215Ala variant, however possessed significantly altered kinetic parameters relative to the WT enzyme. Mutase activity was most affected, showing a 14-fold increase in K_m for chorismate and 5-fold decrease in k_{cat} ; the overall k_{cat}/K_m was reduced by approximately 100-fold relative to WT enzyme. PD activity was not altered to the same extent; the variant exhibited an 8-fold increase in K_m for prephenate and a 2-fold increase in K_m for NAD^+ , with only a small in dehydrogenase activity.

Cys at position 215 was also substituted for a serine yielding a side chain which is smaller and more electronegative than Cys. Unlike Cys and Ala, Ser possesses strong hydrogen-bonding capabilities. Surprisingly, the Cys215Ser substitution did not fully restore the kinetic parameters to those of the WT enzyme; the k_{cat} was reduced by only 1.6-fold (a 3-fold improvement in the k_{cat} value compared to Cys215Ala), but the K_m for chorismate was increased 18-fold, yielding a reduction in k_{cat}/K_m of 35-fold. The K_m value for prephenate was 3-fold higher for WT enzyme but a 2-fold improvement compared to the Ala variant. The K_m for NAD^+ was increased by a factor of 2. As with the Ala substitution, the Ser substitution did not markedly affect the k_{cat} of the dehydrogenase reaction.

2.3.2 Chemical Modification of Native Enzymes

CM-PD variants were subjected to chemical modification by cysteine-specific reagents in order to determine their effect on mutase and dehydrogenase activities. Figure 2.3 (panels A and B) illustrates the time-dependent chemical modification of CM-PD variants with 10 mM iodoacetamide. The results clearly indicate that all variants exhibit a loss of mutase and dehydrogenase activities with time. Inactivation by IAM of Cys215Ala and Cys215Ser resulted in a maximum loss of only 20% of both mutase and dehydrogenase activities. In contrast, reaction with the Cys95Ala variant was the most rapid where almost all of the mutase and dehydrogenase activities were lost after 60 minutes. The results for Cys169Ala are similar to those for Cys95Ala except that it retained 30% more dehydrogenase activity.

Figure 2.4 illustrates the results of chemical modification of CM-PD variants with DTNB. These results suggest that a maximum of 2 cysteine residues are accessible per WT CM-PD monomer. For the Cys95Ala and Cys215Ala/Ser variants, a single cysteine residue is being modified indicating that the cysteine residues that are titrating are Cys215 and Cys95, respectively, for each of the variants. For WT and Cys169Ala variant CM-PD, the loss of approximately 80% of both mutase and dehydrogenase activities correlates with the modification of a single cysteine residue within 10 minutes.

The protective effects of ligands on the extent of inactivation by DTNB of CM-PD activities were investigated. In the absence of substrates, WT, Cys95Ala and Cys169Ala variants show almost complete loss of both activities after 1 hour of incubation with DTNB. Furthermore, all of the ligands protected very well providing the enzymes with more than 80% residual mutase and dehydrogenase activities. Of particular

note, L-Tyr did not afford protection unless NAD^+ was present. In the absence of ligands, the Cys215Ala/Ser variants lost only 20% of activity and ligands were unable to confer any further protection from inactivation. Inactivation and protection experiments using IAM as the chemical modifying agent, yielded similar results (results not shown).

Figure 2.3: Chemical modification of WT CM-PD and variants with 10 mM IAM

CM-PD variants (5 μ M monomer) were incubated with 10 mM IAM at ambient temperature and protected from light. Experiments were performed in 50 mM NEM, 50 mM MES, 1 mM EDTA, 25% glycerol (pH 7.7). Chemical modification was initiated upon addition of IAM and enzyme was assayed for both mutase (A) and dehydrogenase (B) activities at different time points as described in section 2.2.7.

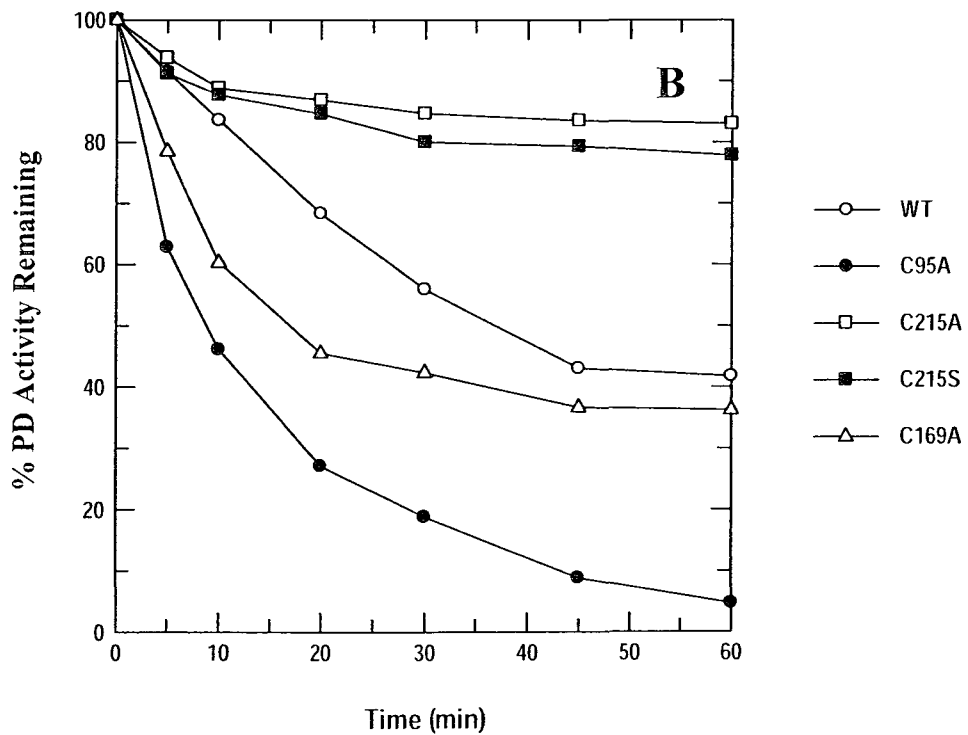
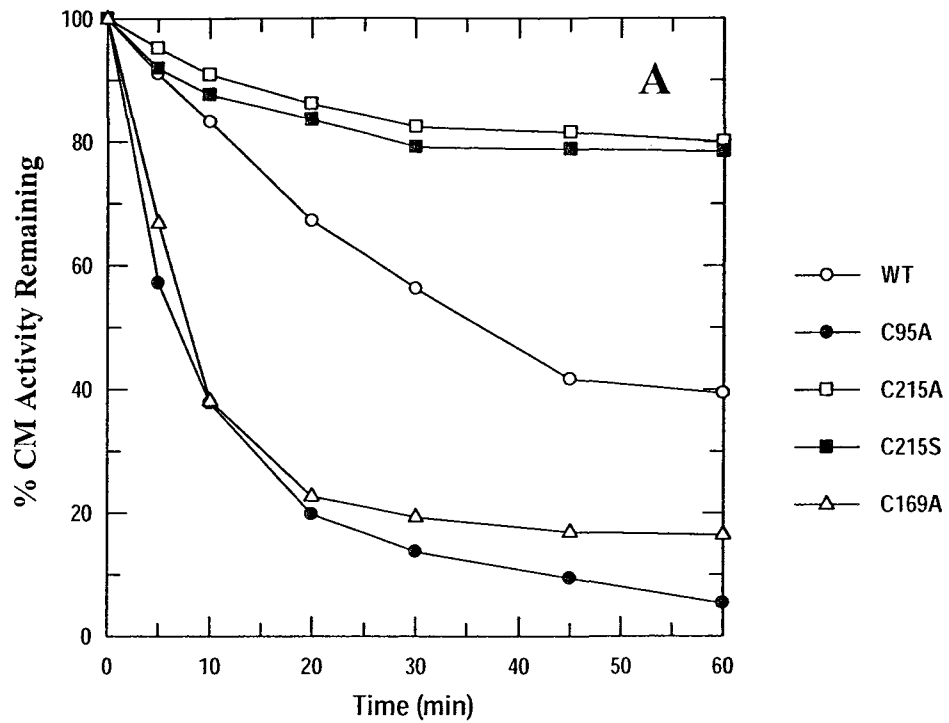
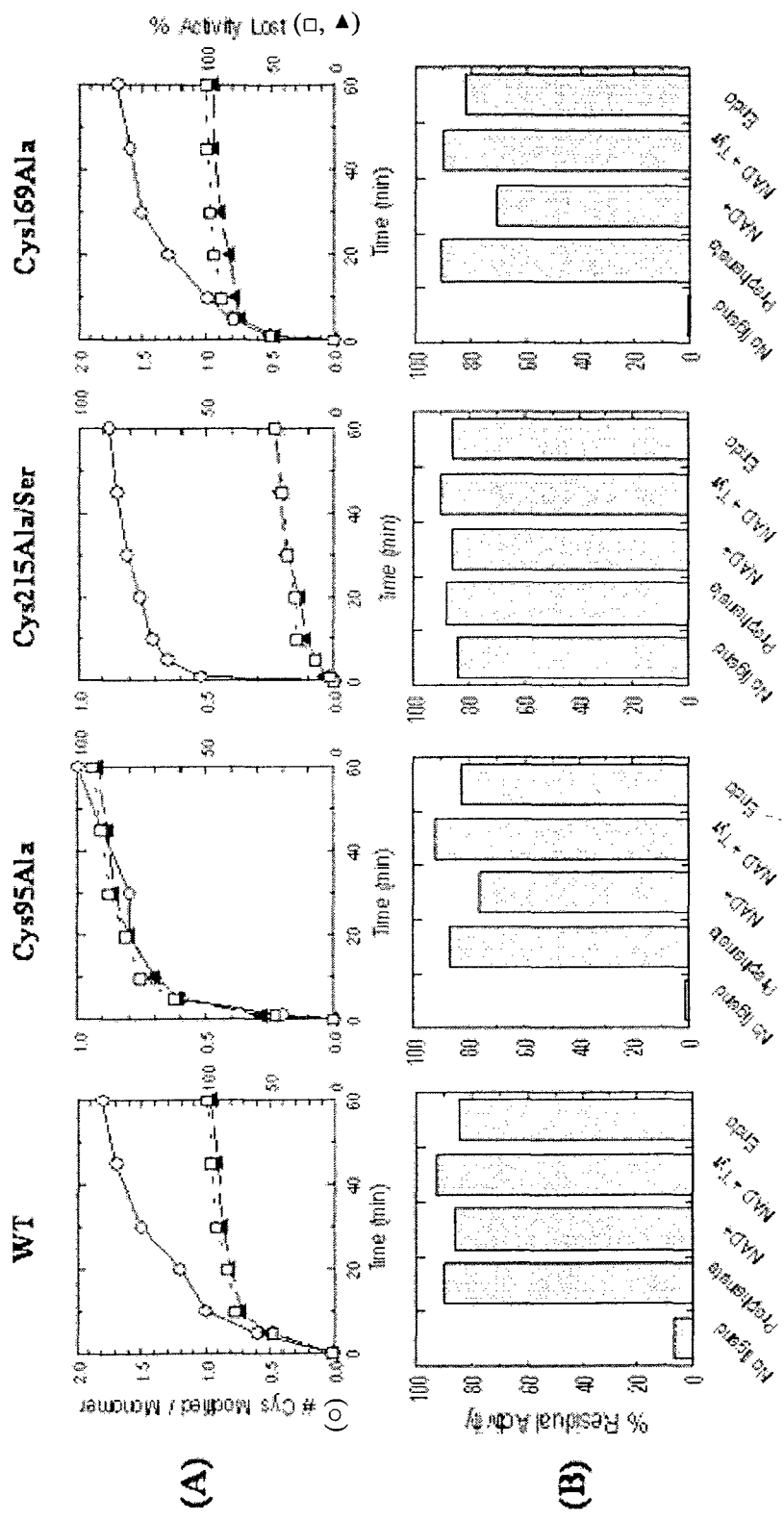


Figure 2.4: Chemical modification and ligand protection of WT CM-PD and variants using Ellman's reagent

(A) CM-PD variants (5 μ M monomer) were incubated with a 2-fold molar excess of DTNB with respect to the total concentration of cysteine residues, in 50 mM NEM, 50 mM MES, 1 mM EDTA, 25% glycerol pH 7.7, at 25°C protected from light. The chemical modification reaction was initiated upon addition of DTNB and the absorbance changes were monitored at 412 nm in order to determine the stoichiometry of modification of cysteine residues (\circ). The recorded absorbance was corrected for the contributions from buffer and DTNB. At specified time intervals after addition of DTNB, a sample aliquot was removed, diluted in buffer K without DTT and assayed for mutase (\blacktriangle) and dehydrogenase (\square) activities. Control samples were incubated under the same conditions except that DTNB was omitted.

(B) For the ligand protection experiments, the experimental conditions were identical to those reported above except substrates were added. Substrates used for protection were 1 mM L-Tyr, 1 mM prephenate, 1 mM NAD⁺, 1 mM L-Tyr + 2 mM NAD⁺, and 25 μ M *endo*-oxabicyclic diacid. Sixty minutes after initiation of the DTNB modification reaction, a sample aliquot was removed, diluted into buffer K, without DTT, and was assayed for mutase and dehydrogenase activities. The extent of protection for both mutase and dehydrogenase activities was reported in terms of % activity remaining with respect to unreacted enzyme. Results obtained for both the dehydrogenase and mutase were very similar, hence, only the effects on mutase activity are shown.



2.3.3 Inactivation of CM-PD Activities by DTNB and Reactivation by Cyanolysis

This experiment was to determine if loss of mutase and dehydrogenase activities upon chemical modification with DTNB was possibly due to steric hindrance due to the modification of the cysteine residues. Reaction of WT and Cys95Ala with DTNB resulted in complete inactivation of both mutase and dehydrogenase activities after 90 minutes; inactivation of Cys215Ala resulted in only 20% loss of both CM and PD activities. Next, the large Cys-S-TNB moiety was replaced by the smaller Cys-S-C≡N group by reaction with KCN, termed cyanolysis (140). The results of these experiments are depicted in Figure 2.5 and indicate that cyanolysis of WT lead to the partial recovery of approximately 10% of both mutase and dehydrogenase activities upon reduction of 2 cysteine residues; cyanolysis of Cys95Ala leads to the partial recovery of approximately 25% of both mutase and dehydrogenase activities upon reduction of a single cysteine residue; while cyanolysis of Cys215Ala lead to no recovery of either activity upon reduction of a single cysteine residue.

Figure 2.5: Inactivation of CM-PD variants by DTNB and Reactivation by Cyanolysis

For all CM-PD variants, 5 μ M monomer was reacted with 2-fold excess DTNB with respect to the concentration of cysteine residues, in 50 mM NEM, 50 mM MES, 1 mM EDTA, 25% glycerol pH 7.7. At specified time intervals, aliquots were removed and diluted into Buffer K (no DTT) and were immediately assayed for mutase and dehydrogenase activities. When values for percent residual activities remained at constant levels, the CM-PD sample was buffer exchanged and concentrated into fresh buffer. To this sample was added KCN to a final concentration of 10 mM. At specified time intervals, aliquots were removed and were immediately assayed for mutase and dehydrogenase activities. The percentage of mutase and dehydrogenase activities recovered was reported with respect to the control reaction without DTNB. The absorbance at 412 nm was recorded upon reaching a constant percentage of mutase and dehydrogenase activities recovered in order to determine the concentration of TNB groups released by cyanolysis. Controls for the experiment were determined at the beginning of the experiment without DTNB, at the end of the experiment without DTNB as well at the end of the experiment with 10 mM KCN present in order to ensure that KCN did not affect the enzymatic activity.

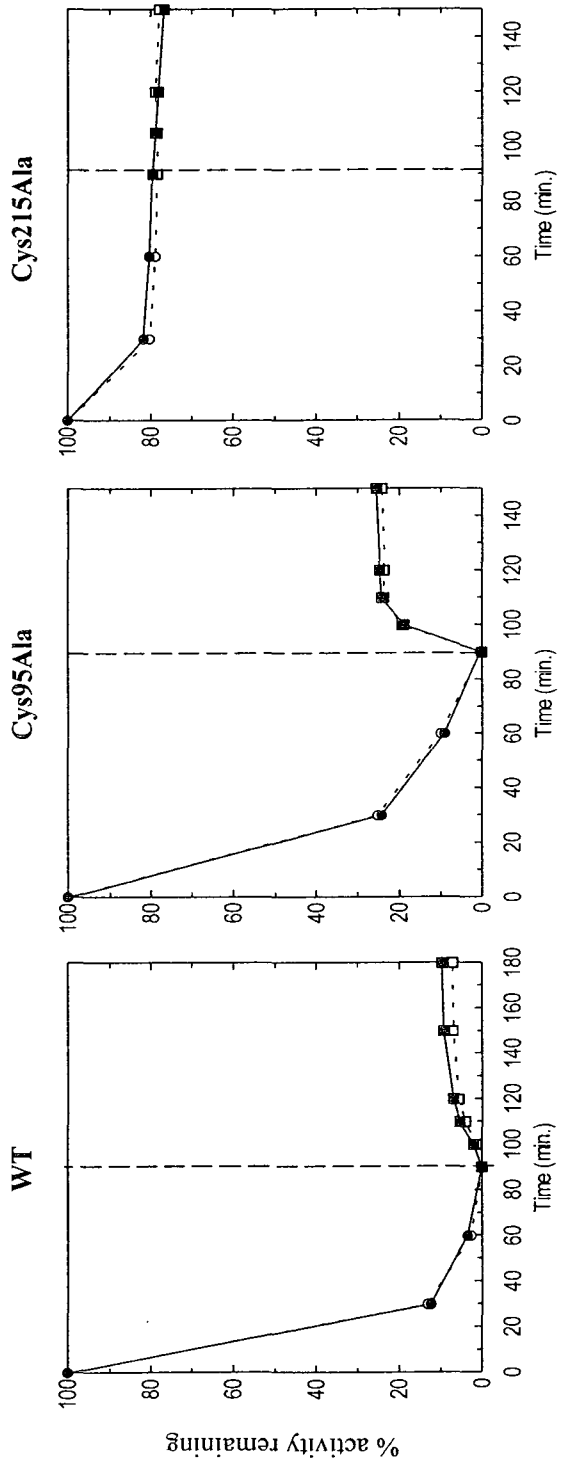


Figure 2.5: Inactivation of CM-PD variants by DTNB and Reactivation by Cyanolysis

	DTNB Inactivation		Reactivation by Cyanolysis		
	% Activity Lost		% Activity Recovered		
	PD (□)	CM (■)	PD (□)	CM (■)	# of Cyanolyzed Cys / monomer
WT	100.0	100.0	7.1	9.7	1.93
Cys215Ala	21.7	20.4	-0.5	-3.0	0.98
Cys95Ala	99.8	100.0	24.0	25.4	0.96

Table 2.2: Tabulation of results from Figure 2.5

2.3.4 Probing Cysteine Accessibility/Reactivity by Modification with IAM and Detection by MALDI

Analysis of WT CM-PD tryptic peptides by MALDI-ToF yielded coverage of more than 80% of the WT CM-PD amino acid sequence (data not shown) predicted by the web-based software PeptideMass from www.expasy.org. Although not quantitative, this method is very sensitive and generated intense and well-resolved peptide peaks for both the native peptide peaks as well as the alkylated peptides shifted by + 57 amu. The unmodified peptides containing Cys95 (T₉₃LCPSLRPVVIVGGGGQMGR₁₁₂), Cys169 (D₁₆₈CILVDLASVK₁₇₈) and Cys215 (Q₂₁₀VVWCDGR₂₁₈) were accurately detected at approximately [M+H⁺] of 1996.8, 1175.3 and 1061.3 amu, respectively, in both the control and IAM-modified samples. In the control sample (in the absence of IAM), no peaks were seen at the m/z values where alkylated peptide would be expected to appear. The results of the time-dependent modification of native WT CM-PD with 10 mM IAM at pH 7.7 indicate that the alkylated peptides containing Cys95 and Cys215 are observed by 3 minutes of the modification reaction, the earliest time point that was recorded. This is verified by the appearance of a peak at [M+H⁺] of 2053.8 amu corresponding to the IAM adduct of the peptide containing Cys95, and [M+H⁺] of 1118.30 amu for the peptide containing Cys215. This suggests that the Cys95 and Cys215 are equally accessible or reactive. The appearance of a peak at 1232.4 amu corresponding to the alkylated peptide containing Cys169 suggests that this residue is either buried within the native enzyme or is not reactive.

In order to resolve the order of alkylation of Cys95 and Cys215, we performed the alkylation reaction with CIAM instead of using IAM, we used CIAM; CIAM has been

reported to alkylate at a rate up to 300-fold slower than IAM (141). The results of this chemical modification are depicted in Figure 2.6 panels D and E, for the peptides containing Cys95 and Cys215, respectively. The results indicate in panel D that after 2 hours of reaction with CIAM, the native peptide peak containing Cys95 at $[M+H^+]$ of 1997.02 amu is essentially depleted and most of it has been modified to its alkylated form, which is the intense peak observed at $[M+H^+]$ of 2054.14 amu. In contrast, panel E suggests that after 2 hours of reaction with CIAM, the native peptide peak containing Cys215 at $[M+H^+]$ of 1061.49 amu has not been alkylated to completion, as both the native peak and the alkylated peptide peak at $[M+H^+]$ of 1118.52 amu, at equal intensity are observed. These results suggest that Cys95 reacts prior to Cys215 and may suggest that the former may possess a lower pK_a .

It is noteworthy to mention that no adducts were alkylated adducts were detected for the peptides containing Lys37 (L₂₇ELVAEVGEV**K**₃₇), His131 (I₁₂₇LEQH**D**WDR₁₃₅) and His197 (N₁₇₉GPLQAMLVAHDGPVLGLHPMFGPDSGSLAK₂₀₉), which have been reported to be essential for mutase and PD activities and may hence be ruled out as the cause for loss of mutase and dehydrogenase activities upon chemical modification by IAM and CIAM..

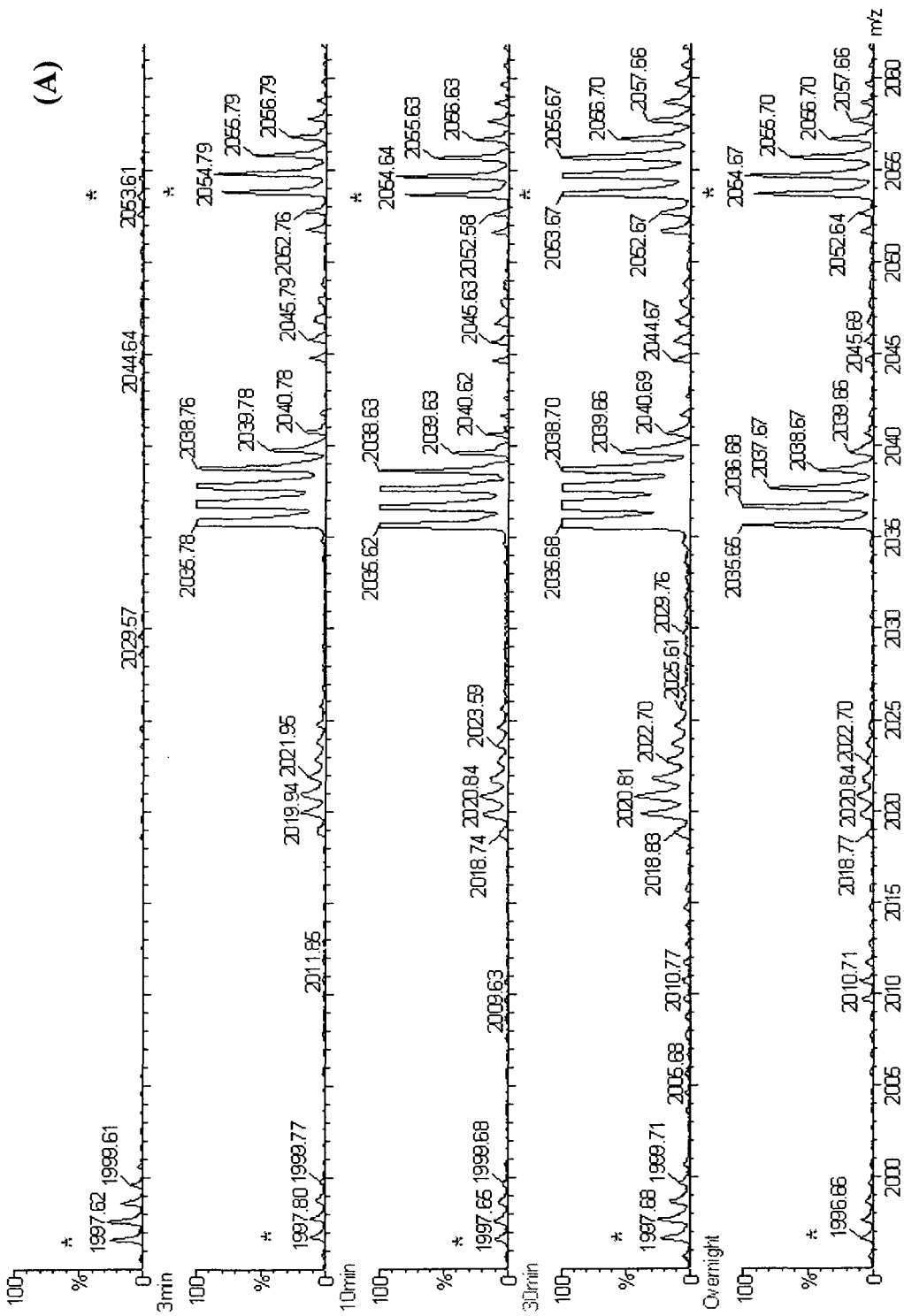
Figure 2.6: Time dependent chemical modification of WT CM-PD with 10 mM IAM and 10 mM CIAM

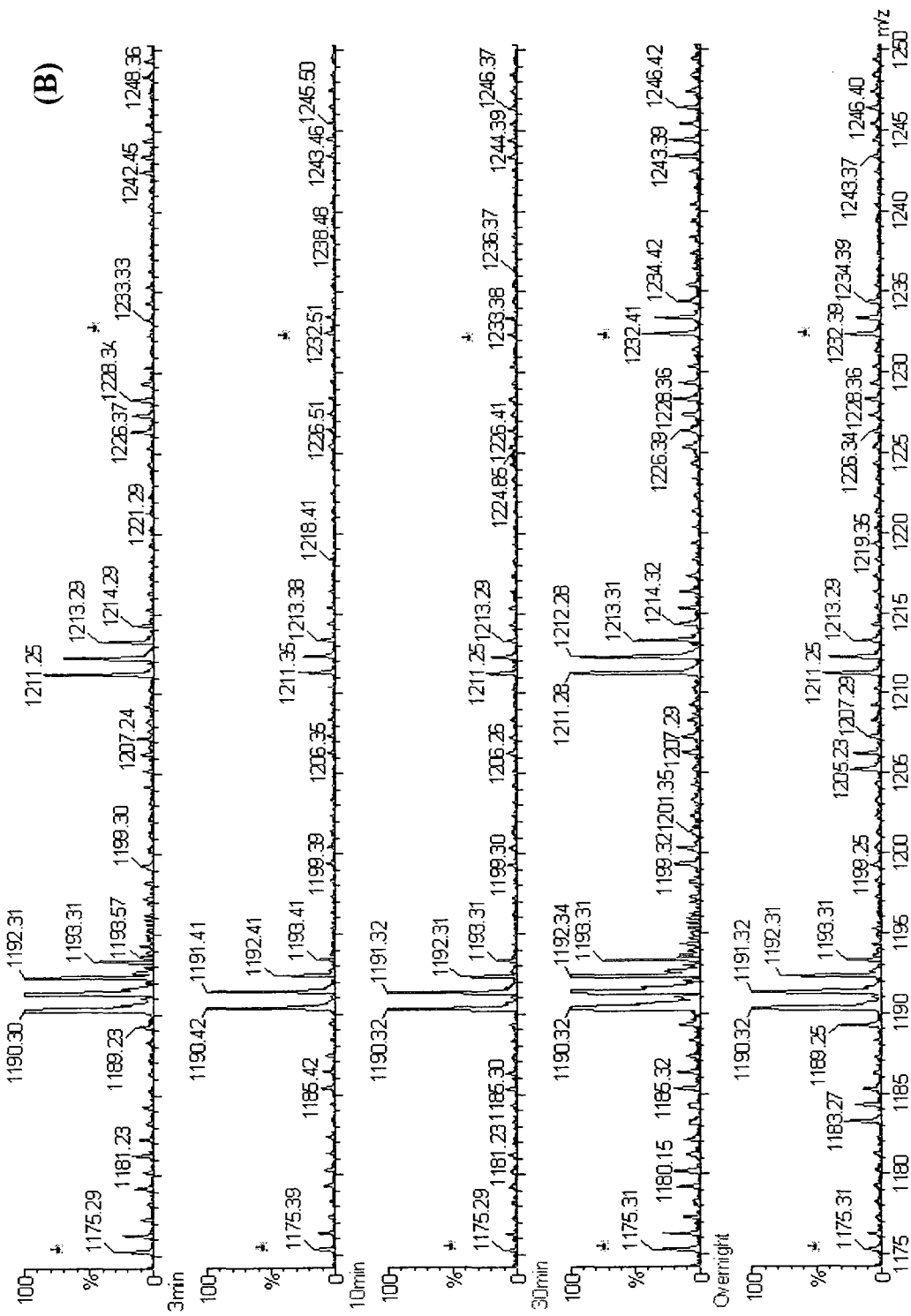
WT CM-PD (5 μ M monomer) was incubated in 50 mM NEM, 50 mM MES, 1 mM EDTA, 25% glycerol (pH 7.7) at room temperature protected from light. The modification reaction was initiated upon addition of IAM to a final concentration of 10 mM. At specified time intervals, a sample aliquot was removed and immediately diluted into 10 mM ammonium bicarbonate containing 10 mM DTT. Samples were buffer exchanged into 10 mM ammonium bicarbonate and were then lyophilized to dryness. Samples were reconstituted in 50 mM ammonium bicarbonate (pH 8.0) and digested with sequencing grade trypsin. Digested samples were desalted using C4 ZipTips. Peptides were mixed using α -cyano-hydroxycinnamic acid as the matrix. 1 μ L of sample was spotted onto a MALDI plate. Samples were analyzed using Micromass M@LDI MALDI-ToF in positive ion mode using Micromass MassLynx v 4.0 software.

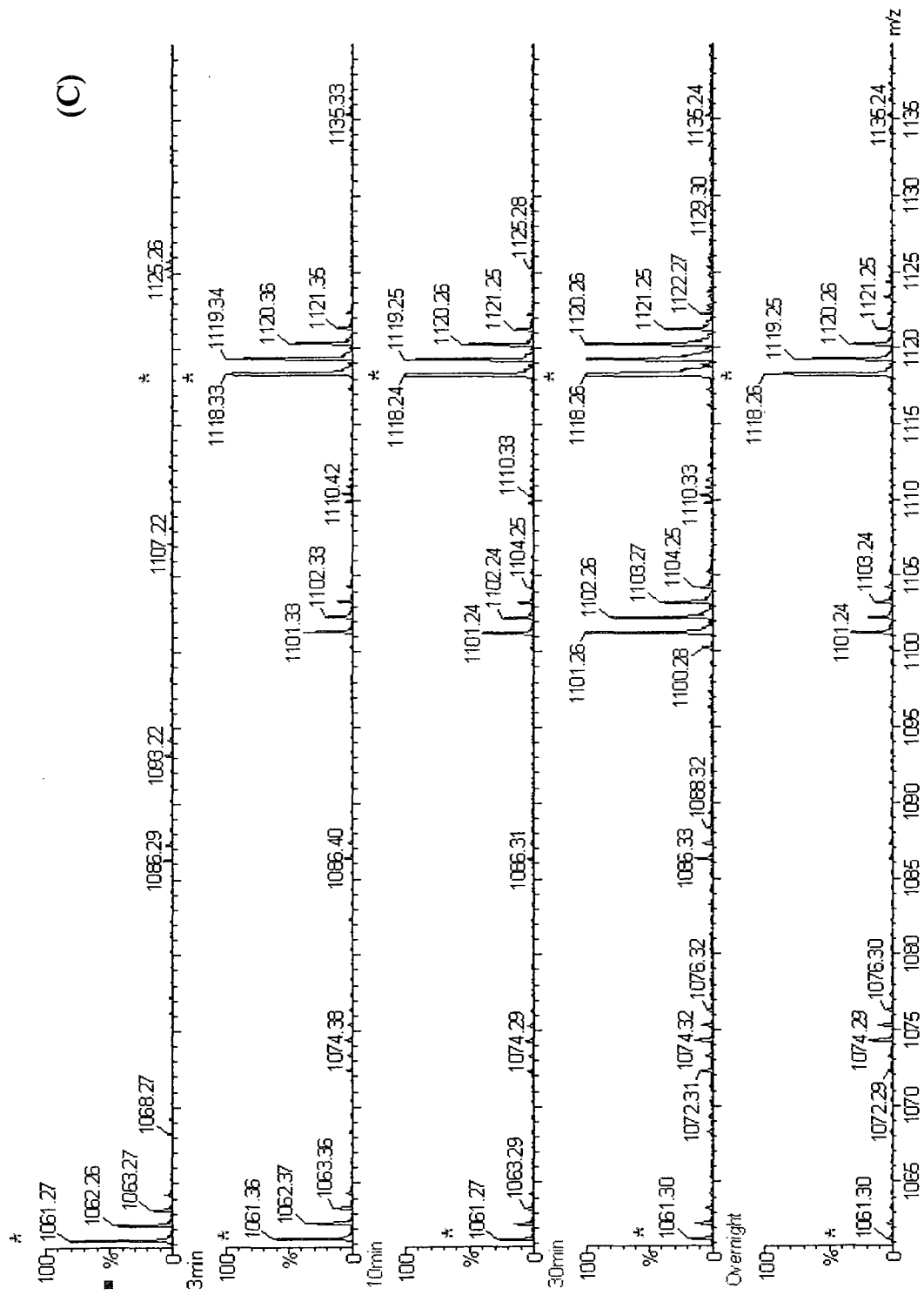
Peptide alkylated by IAM containing **(A)** Cys95, **(B)** Cys169 and **(C)** Cys215, respectively, were resolved by MALDI ToF. Time-points include 0, 3, 10, 30 minutes and overnight from top to bottom. Asterisks (*) indicate peaks of interest. IAM adducts correspond to a shift of native peptide peaks by +57 amu.

Peptide alkylated by CIAM containing **(D)** Cys95 and **(E)** Cys215, respectively, were resolved by MALDI ToF. The chemical modification was performed exactly as described for IAM, except that a single incubation for 2 hours was performed.

Asterisks (*) indicate peaks of interest. IAM and CIAM adducts correspond to a shift of native peptide peaks by +57 amu.







2.3.5 Determination of Cysteine pK_a Values in Native WT, Cys95Ala and Cys215Ala CM-PD Variants by ESI-MS

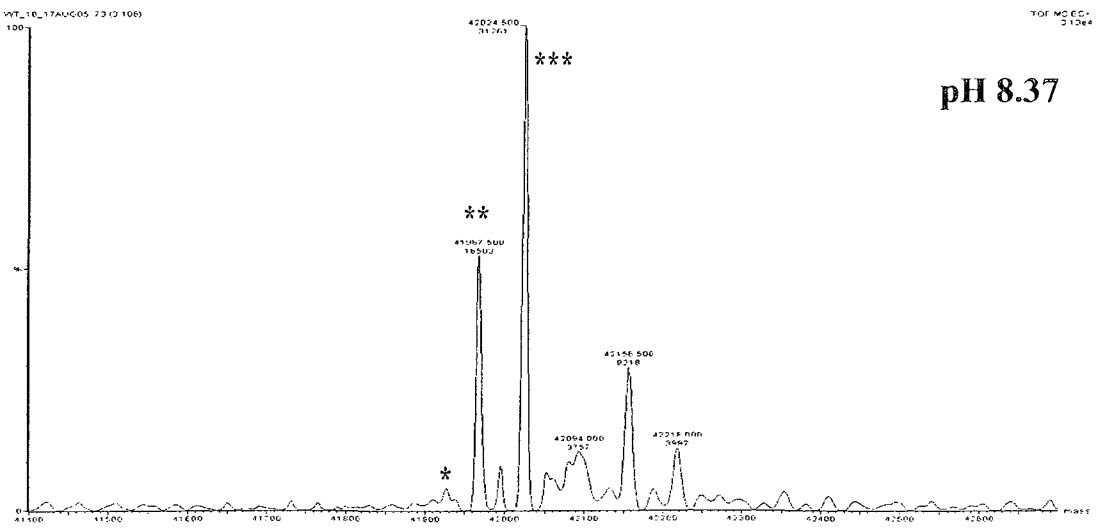
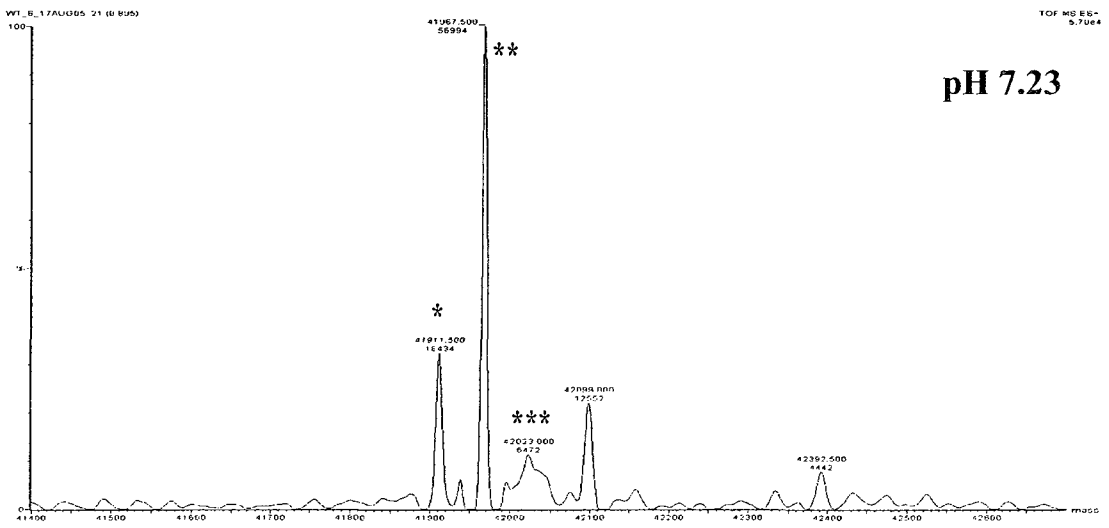
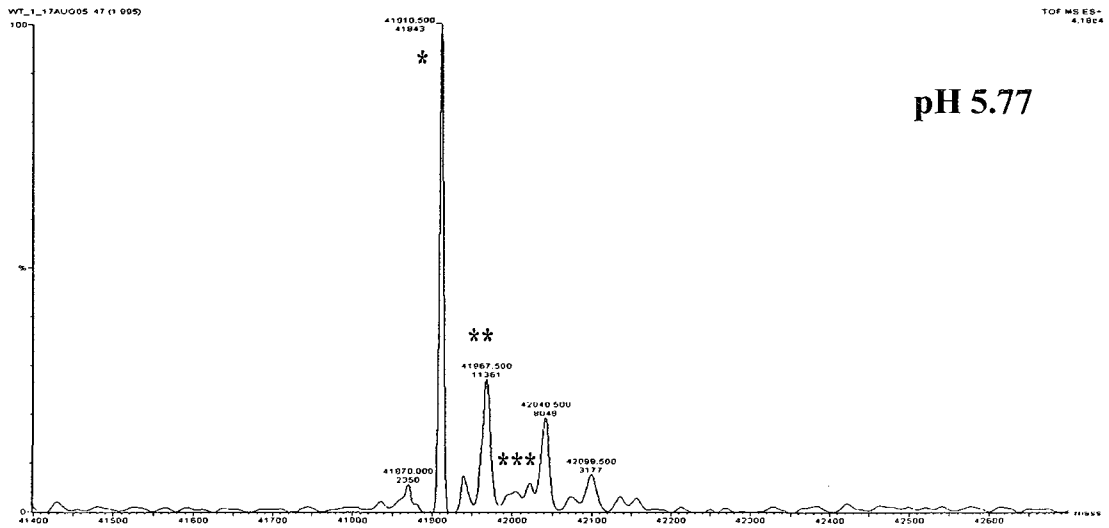
CM-PD proteins were reacted with 0.5 mM IAM at various pH values ranging from 5.77 to 9.50 in order to determine the pH-dependent reactivity of the cysteine residues. ESI-MS analysis of unmodified CM-PD variants yielded well-resolved peaks corresponding to the full-length CM-PD as well as full-length enzyme with single and multiple IAM adducts (+ (n x 57 amu)) (representative data for WT enzyme are shown in Figure 2.7). For both Cys95Ala and Cys215Ala (data not shown), a peak at $[M+H^+]$ of 41880 amu was observed corresponding to the unmodified enzyme; upon modification with IAM, a single peak at $[M+H^+]$ of 41937 amu appeared corresponding to the alkylated enzyme with a single IAM adduct, with a concomitant decrease in the intensity of the unmodified enzyme. For Cys95Ala, the alkylated enzyme exhibits a peak at $[M+H^+]$ of 41937 amu, which appears at higher pH values, whereas it appears at lower pH values for the Cys215Ala variant, suggesting that the pK_a for Cys215 is higher than that of Cys95.

The ESI-MS data taken together with the results from MALDI-ToF indicate the reactivity of the different cysteine groups, as shown in Figure 2.7. The appearance of a single peak at lower pH values was observed, corresponding to the modification of Cys95. A second adduct also appeared with increasing pH, corresponding to the modification of Cys215.

**Figure 2.7: Representative ESI-MS spectra of the pH-dependent alkylation of WT
CM-PD with IAM**

CM-PD variants of 23 μM monomer (50 μg total) were incubated in 3CB buffer adjusted to pH values ranging from 5.77 to 9.50. The chemical modification of sulfhydryl moieties was initiated upon addition of IAM, present at the same pH as the reaction mixture, to a final concentration of 500 μM . The reaction was allowed to proceed for 30 minutes at room temperature protected from light. After 30 minutes, the reaction was quenched with 20 mM DTT and immediately precipitated and analyzed by ESI-MS as described previously. The $\text{p}K_a$ values were determined by plotting the ratios of peak intensity (adduct / (adduct + native)) vs. pH, using GraFit v 5.0.1.

- * denotes unmodified WT CM-PD
- ** denotes WT CM-PD with a single IAM adduct
- *** denotes WT CM-PD with two IAM adducts



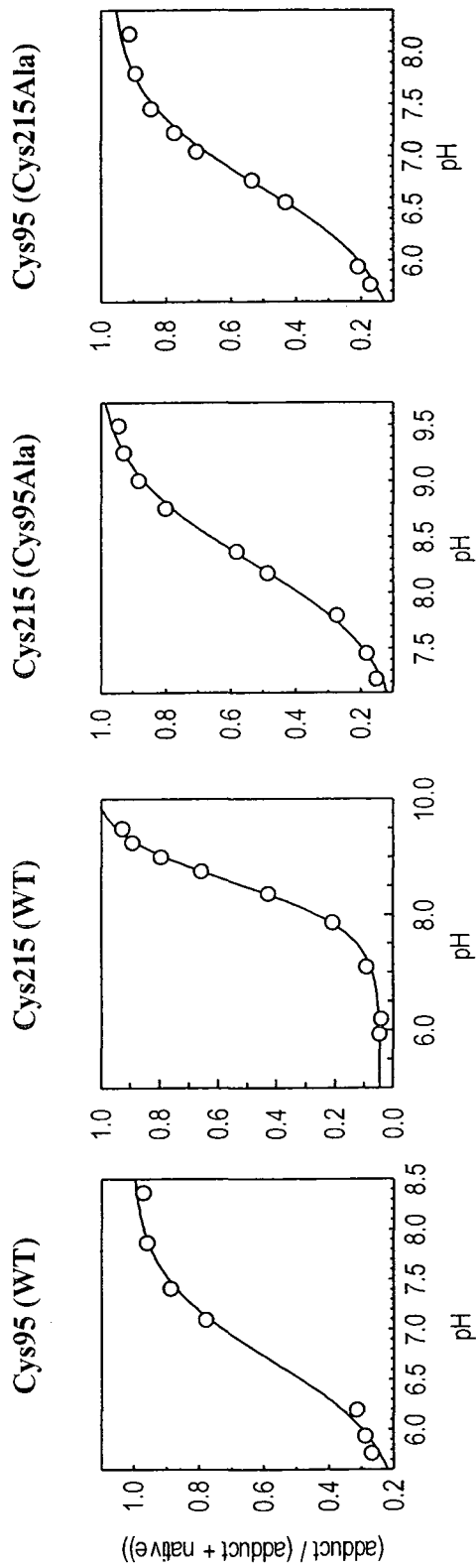


Figure 2.8: Plot of peak intensity ratios of (adduct / (adduct + native)) for WT, Cys95Ala and Cys215Ala CM-PD

Enzyme	pKa Values	
	Cys95	Cys215
WT	6.70 ± 0.10	8.57 ± 0.03
Cys215Ala	6.73 ± 0.07	N/AP
Cys95Ala	N/AP	8.28 ± 0.04

Table 2.3: Tabulation of pKa values of Cys95 and Cys215 in CM-PD variants

2.4 DISCUSSION

In the present investigation, we have studied the role of the cysteine residues in the function and structure of the *E. coli* bifunctional CM-PD. Toward this goal, site-directed mutants were characterized to more precisely define the role of the three cysteine residues (Cys95, Cys169 and Cys215) in substrate binding and catalysis. Cys to Ala substitutions were introduced at all three positions in order to eliminate H-bonding capabilities at that position. In addition, a Cys215 to Ser change was made. Although Cys and Ser are relatively isosteric, the polar hydroxyl group of Ser is capable of forming stronger H-bonds compared to the sulfhydryl group of Cys.

The kinetic parameters obtained for the mutase and dehydrogenase reactions catalyzed by Cys95Ala and Cys169Ala variant proteins were similar to those obtained for WT enzyme. Hence, it appears that Cys95 in the mutase portion of CM-PD does not contribute to the binding energy of the diaxial form of chorismate and of the transition state of the mutase reaction as proposed for Cys75 in the monofunctional CM from *B. subtilis* (142). Kinetic analysis of the Cys75Ala variant of the monofunctional CM from *B. subtilis* has shown that the binding of both chorismate and the mutase TS analog are reduced by over 10-fold.

Replacing the sulfhydryl group of Cys215 with a methyl (Cys215Ala) resulted in a significant decrease in the efficiency constant for the mutase reaction of k_{cat}/K_m of $1.9 \times 10^4 \text{ M}^{-1} \cdot \text{s}^{-1}$ and only a moderate decrease for the dehydrogenase reaction of k_{cat}/K_m of $1.3 \times 10^5 \text{ M}^{-1} \cdot \text{s}^{-1}$ compared to the WT k_{cat}/K_m of $1.4 \times 10^6 \text{ M}^{-1} \cdot \text{s}^{-1}$ for CM activity and $1.1 \times 10^6 \text{ M}^{-1} \cdot \text{s}^{-1}$ for PD activity. Moreover, replacing Ala with Ser restored, only partially, the enzyme's affinity for prephenate to values comparable to the WT protein.

Taken together, the data suggest that the Cys215 thiol moiety plays only a modest role in the proper binding of prephenate. These results partially support the findings of Zhang *et al.* (79) who showed that the Cys216Ala variant in the related bifunctional enzyme CM-PDT possessed a 10-fold higher K_m for prephenate, which was restored with the Ser substitution.

In contrast to the dehydrogenase reaction, replacing Ala with Ser further reduced the binding of chorismate at the mutase site suggesting that the presence of a smaller, more polar group than cysteine perturbed the proper binding of chorismate. In contrast, Zhang *et al.* (79) reported that the mutase activity and the K_m for chorismate were not altered by the Cys216 to Ala substitution, supporting the idea that the reactions catalyzed by CM and PDT occur at distinct non-interacting sites. In summary, our observations suggest that Cys215 is the only cysteine residue whose substitution affects both the mutase and dehydrogenase activities of CM-PD and hence highlight the interdependence of the sites at which the two reactions occur.

The pH dependence of the kinetic parameters V and $(V/K)_{\text{prephenate}}$ for the WT dehydrogenase reaction as performed by Mekhssian (143) and others (36) indicated that a protonated group with a pK_a value of about 8.4 was essential for the binding of prephenate to the enzyme-NAD⁺ complex. This value is close to that expected for a free cysteine residue at neutral pH (2). However this titrating residue was not Cys215 as the $(V/K)_{\text{prephenate}}$ pH profiles for Cys215Ser and WT enzyme were essentially identical. Hence, the residue titrating with a pK_a of ~ 8.4 is still present when this cysteine is missing (143), suggesting that the ionization state of Cys215 was not essential for substrate binding.

Reaction of CM-PD variants with the cysteine modifying reagents DTNB and iodoacetamide support the conclusion drawn from site-directed mutagenesis that Cys at position 215 may be important for both mutase and dehydrogenase activity. Modification of WT CM-PD with these reagents resulted in the time-dependent loss of both mutase and dehydrogenase activities (Figures 2.3 and 2.4). This agreed with previous reports by Hudson *et al.* (16) using the aforementioned reagents and by Turnbull *et al.* (14) who monitored alkylation by the active site directed reagent, iodoacetic acid. However, this was in contrast to the results obtained by Zhang *et al.* (79) and Gething *et al.* (78) in which modification of CM-PDT with DTNB and N-ethylmaleimide (NEM) resulted in the inactivation of only the dehydratase.

Extending these studies to the inactivation of variant forms of CM-PD by DTNB and iodoacetamide (Figures 2.3 and 2.4), showed conclusively that it was Cys215, presumably at or near the active site(s), which upon chemical modification rendered the enzyme inactive. The fact that Cys215Ala/Ser proteins retained approximately 80% residual mutase and dehydrogenase activities upon modification with cysteine specific reagents support the idea that the loss of both activities in the WT enzyme was due to the chemical modification of the same group (Cys215). In the case of modification by DTNB, steric effects associated with the formation of the bulky Cys-TNB moiety is, in part responsible for the inactivation of the enzyme as cyanolysis of the adduct results in the smaller C≡N moiety, allowing for up to 25% recovery of both of the enzyme's activities.

In order to determine the reactivity/accessibility of the 3 cysteine residues in WT CM-PD, a time-dependent chemical modification was conducted at pH 7.7, using the

cysteine-specific reagent iodoacetamide. The results of this modification in tandem with peptide mapping using MALDI-ToF mass spectrometry first confirmed that Cys169 is not readily accessible and/or relatively reactive to iodoacetamide under the experimental condition that were used since an adduct of the peptide containing this residue only appeared after 30 minutes into the reaction (Figure 2.6 panel B). Unfortunately, under these experimental conditions, both Cys95 and Cys215 reacted to appreciable degrees within 3 minutes (Figure 2.6, panels A and C, respectively). Only with the use of CIAM, which reacts by the same mechanism as IAM but 300 times slower (141), could it be shown that Cys95 is slightly more sensitive to alkylation than to Cys215. Figure 2.9, illustrates a space filling model of *E. coli* CM-PD.

The chemical modification experiments in tandem with mass spectrometry were extended to determine of the ionization state of the cysteine residues in the WT and Cys95Ala and Cys215Ala variant CM-PDs. Iodoacetamide, which reacts with a thiolate, forms a stable adduct that is readily detectable by ESI-MS as a shift of +57 amu. Thus, performing the alkylation reaction at various experimental pHs will result in the sulfhydryl alkylation, that is dependent on the pK_a of the cysteine residue under investigation. The ESI-MS spectra of the WT CM-PD (Figure 2.7) clearly show an increase in the amount of alkylated enzyme relative to the unmodified enzyme, with increasing pH. Since we know the order of modification to be Cys95>Cys215, we were able to determine that, in WT CM-PD, the pK_a of Cys95 is 6.70 ± 0.10 and that of Cys215 is 8.15 ± 0.03 . Experiments conducted on the variant CM-PDs, verified our assignments for the WT CM-PD; in the Cys215Ala enzyme, the pK_a of Cys95 was

determined to be 6.73 ± 0.07 while in the Cys95Ala variant, the pK_a of Cys215 was calculated to be 8.28 ± 0.04 (Table 2.3).

Further complementary chemical modification studies consisted of chemically modifying WT, Cys95Ala and Cys215Ala CM-PD variants with DTNB, which leads to the formation of the bulky Cys-S-TNB moiety, whose steric properties may be the cause of the loss of both mutase and dehydrogenase activities. In order to assess the contribution to steric hindrance of the TNB moiety with inactivation, the DTNB-modified enzyme was treated with KCN, which results in the cleavage of Cys-S-TNB and leads to the formation of Cys-S-C \equiv N, which is much smaller; recovery of activity upon cyanolysis would be an indication that loss of activity is due to steric hindrance of the TNB adduct. Figure 2.5 and Table 2.2 illustrate the results of the cyanolysis experiments and indicate that upon modification of a single residue in the Cys215Ala variant (Cys95), 20% of mutase and dehydrogenase activities are lost, which are not recoverable upon cyanolysis of Cys95-TNB. In contrast, when Cys215 is chemically modified by DTNB in the Cys95Ala variant, both activities are completely lost, highlighting the importance of this residue. Upon cyanolysis, approximately 25% of both activities are recovered in this variant. In keeping with the results of the modification of the individual cysteine residues in the CM-PD variants, WT CM-PD recovered approximately 7-10% of both activities, which is consistent with the recovery of 25% of both activities upon cyanolysis of Cys215-TNB excluding the 20% of both activities that is not recoverable upon cyanolysis of Cys95-TNB in the Cys215Ala variant CM-PD. These results suggest that inactivation of both activities in CM-PD must be due to a conformational change in the enzyme upon chemical modification for Cys95. On the other hand, the cyanolysis results for the

Cys215-TNB in the Cys95Ala variant indicate that loss of both activities is due to steric hindrance of the adduct, which may interfere with a residue that is important for activity or important for the orientation of an important residue within the active site. These results are in keeping with the inactivation studies by chemical modification with iodoacetamide, which forms a larger adduct than the Cys-S-C≡N, hence leading to mutase and dehydrogenase inactivation.

Although the Ala substitution at positions 95 and 169 did not affect the kinetic parameters of the enzyme catalyzed reaction, they did appear to affect their reactivity with the cysteine modifying reagents. Inactivation of Cys169Ala dehydrogenase activity by DTNB was faster and more complete compared to WT enzyme. Clearly the Cys to Ala substitution resulted in changes that rendered the reactive group(s) more prone to modification by the different reagents. This result clearly demonstrates the necessity of combining site-directed mutagenesis with protein modification to better understand the function of the different residues under investigation.

In agreement with studies by Hudson *et al.* (35), incubation of WT CM-PD with DTNB resulted in the modification of 2 cysteine residues per monomer (Figure 2.4), indicating that one cysteine was inaccessible or not reactive to DTNB. In the present study, identical studies with the cysteine variants identified this sulfhydryl group as Cys169. Furthermore, alkylation of the enzyme with iodoacetamide followed by peptide mapping using mass spectrometry clearly identified Cys95 and Cys215 as more reactive and surface accessible than Cys169. These findings are in agreement with peptide mapping experiments of Hudson *et al.* using radiolabelled iodoacetamide (35).

Comparison of the chemical modification of WT and variant forms of CM-PD in the absence and presence of substrates and substrate analogs have affirmed that only Cys215 is at or near the active site(s) of CM-PD. Incubation of the enzyme with prephenate, NAD^+ + tyrosine and mutase TS analog prior to inactivation with DTNB or iodoacetamide, led to the protection of both mutase and dehydrogenase activities. This was expected as prephenate is a product inhibitor of the mutase reaction as well as a substrate in the dehydrogenase reaction. NAD^+ plus L-Tyr also afforded protection. NAD^+ structurally affects the CM domain as its presence activates mutase activity. As expected the protective effect of NAD^+ was enhanced in the presence of tyrosine presumably by increasing the enzyme's affinity for this cofactor (15, 35). Cys169Ala and Cys95Ala variant proteins, which possess a cysteine residue at position 215, could be protected against inactivation by these ligands whereas Cys215Ala and Cys215Ser were not.

Similarly, preincubation of the enzyme with prephenate, NAD^+ plus L-Tyr, and mutase TS analog, prevented one cysteine residue from being modified by DTNB. These results clearly indicated the presence of a reactive thiol group near or at the binding site of these ligands. Similar studies with the Cys variants clearly identified this reactive sulfhydryl as Cys215. However, from the conclusion that Cys169 was buried and that Cys215 could be protected against alkylation by any one of the ligands, modification of Cys95Ala in the presence of ligands did not result in an absence of cysteine modification as predicted (143). This might arise if the substitution at position 95, caused a conformational change in the structure of this variant. In summary, these results suggest that the substrates may interact with or be in the same vicinity with the Cys215 residue in

the active site, since its presence seems to both allow inactivation of mutase and dehydrogenase activities in the absence of substrates as well as protection from inactivation in the presence of substrates.

Surprisingly, the mutase transition state analogue protected PD from inactivation by the cysteine specific reagents. Moreover our kinetic studies indicated that this protection was afforded through binding to the mutase site and not the dehydrogenase site. In support of this idea was the finding that the dehydrogenase activity of Lys37Gln (a CM-PD variant unable to bind the mutase TS analog; discussed in Chapter 3) was inactivated by iodoacetamide in the presence of the analog (143).

The present study reports the first reproducible ESI-MS analysis of intact *E. coli* CM-PD. The difficulty in analyzing CM-PD by ESI mass spectrometry is presumably due to the protein's surface hydrophobicity. Marked hydrophobicity can reduce the ability of a protein's residues to ionize, a feature which is essential for ESI-MS. Sixty percent of the CM-PD's 373 amino acid residues are large (L, I, V, M, F, Y, W) and small (A, G) non-polar groups; L, I, V alone constitute 26% of the total residues. Recent results from ANS coupled fluorescence experiments (69) and the observation that CM-PD binds very tightly to phenyl sepharose and to C₁₈ reverse phase columns highlight the fact that the protein's surface is highly hydrophobic.

Mass spectrometry has yielded an accurate determination of the molecular weight of the CM-PD subunit (42042 Da). Furthermore, mass spectrometric analysis of native and tryptic digests of the protein has been used in this study to verify the presence and identity of the site-directed variants (143).

Mass spectrometric analysis of CM-PD has also identified a post-translational modification common to many proteins. Deconvolution of the mass spectra of WT and variant enzyme yielded two peaks with a difference in mass of 130 amu. These two peaks corresponded to the enzyme with or without the N-terminal methionine. More than 60% of all proteins lose their N-terminal methionine (144), a feature, which governs, in part, the half-life of proteins (145). The extent of N-terminal methionine excision from *E. coli* proteins is inversely proportional to the side-chain length of the penultimate amino acid (144). In *E. coli* CM-PD, the amino acid at position 2 is a valine. Studies by Meinnel *et al.* (146) have shown that when valine is the amino acid at position 2 in a series of different proteins, the extent of methionine cleavage was around 80%. This ratio was not observed in our studies, where the two peaks in the deconvoluted spectra of WT and Cys variants were of unequal intensity, with the non-cleaved enzyme intensity predominated. This could be explained if the over expression of CM-PD in *E. coli* cells, leads to a high ratio of the bifunctional enzyme versus the enzyme responsible of cleaving the N-terminal residue, thus decreasing the extent of methionine cleavage.

In the absence of a crystal structure for the bifunctional *E. coli* CM-PD, we resorted to comparative modeling of the dehydrogenase using the PD domain of the bifunctional CM-PD from *H. influenzae* as a template, which possesses 57.6% sequence identity. Based on all the results obtained in the studies by site-directed mutagenesis, comparative modeling and chemical modification, we propose a model where Cys215 is at the interface of both active sites. This would be consistent with the decrease in the enzyme's affinity for both chorismate and prephenate as observed by site-directed

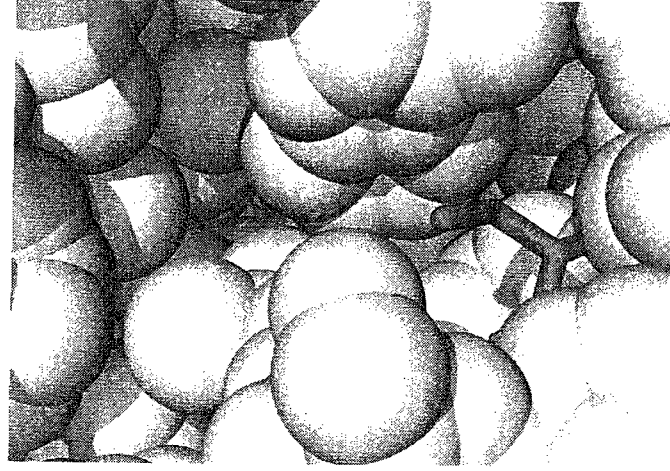
mutagenesis. The inactivation of both activities by alkylation with cysteine specific reagents, notably iodoacetamide that is smaller than DTNB, also supports our hypothesis.

The fact that both K_m of prephenate and the turnover number are affected by the Cys215Ala mutation suggests that Cys215 may play an indirect role in correctly orienting the catalytic residue, His197. Interestingly, in our PD model, Cys215 is located near residues, which have been determined in the Turnbull lab to play a key role in catalysis (His197) and tyrosine binding (His245) (Figure 2.10) (39, 68) T. Lee, unpublished). Figure 2.10 illustrates a close-up of the dehydrogenase active site bound with L-tyrosine. It is clear that Cys215 is very near His245, approximately 4.77 Å away, which seems to coordinate the catalytic base His197. Substitution of His245 with a glutamine in our lab, lead to insoluble protein suggesting that it may have an important role in PD activity (T. Lee, unpublished). The proximity of Cys215 to His245 explains the loss of dehydrogenase activity upon chemical modification since adduct formation at position 215, whether small like $-C\equiv N$ or big as $-TNB$, must perturb His245 out of position, which in turn cannot effectively coordinate His197 to its intended position for dehydrogenase activity.

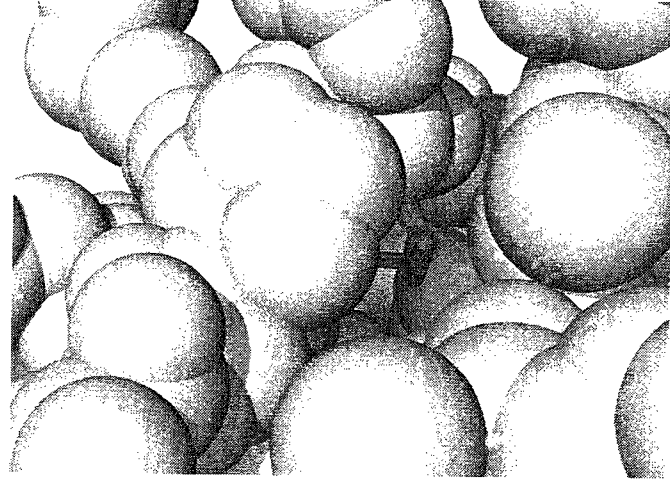
Moreover, Figure 2.10 illustrates a complex network of hydrogen bonding in helix 240-269, in which His245 is suitably positioned for the proper coordination of His197; Cys215 can be seen interacting with the backbone carbonyl group of Ile240. Substitution of Cys215 for an alanine residue, which has no hydrogen bonding capabilities, seems to be sufficient to destabilize the position of the helix and hence His245, leading to inactivation of PD.

In addition, the model is in keeping with the protective effect of *endo*-oxabicyclic diacid against inactivation of PD, assuming that the binding of the mutase TS analog to the CM site blocks the interaction of the modifying reagents with Cys215. Alternatively, the interaction of the *endo*-oxabicyclic diacid at the mutase site could promote a conformational change in the enzyme propagated to the dehydrogenase site.

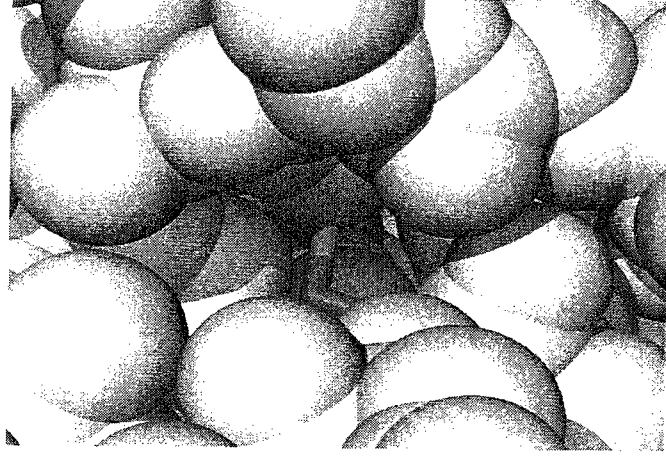
Unfortunately, the mutase domain could not be modeled together with PD since there is no crystal structure of the bifunctional enzyme. This capability would have helped us pinpoint the location of both active sites relative to each other and understand the role of Cys215 in the mutase reaction.



Cys95



Cys169



Cys215

Figure 2.9: Spacefill representation of the modeled *E. coli* CM-PD PD domain illustrating the accessibility of the cysteine residues

The PD domain of *E. coli* CM-PD was modeled using the crystal structure of the PD domain of *H. influenzae* (PDB ID: 2PV7). The image was created using PyMol software (DeLano, W.L., The PyMOL Molecular Graphics System (2002) Delano Scientific, San Carlos, CA, USA. <http://www.pymol.org>).

Figure 2.10: Modeled PD active site of *E. coli* CM-PD

The PD domain of *E. coli* CM-PD was modeled using the crystal structure of the PD domain of *H. influenzae* (PDB ID: 2PV7) as described in section 2.2.15. The multitude of hydrogen-bonding interactions between the residues (colored by element: yellow = carbon, blue = nitrogen, red = oxygen, green = sulfur) at the N-terminus of helix 240-261 can be seen. The sulfhydryl moiety of Cys215 can be seen hydrogen-bonding with residues at the N-terminus of helix 240-261 effectively orienting the helix in the correct position in order for His245 to coordinate the catalytic base, His197. This image was created using PyMol software.

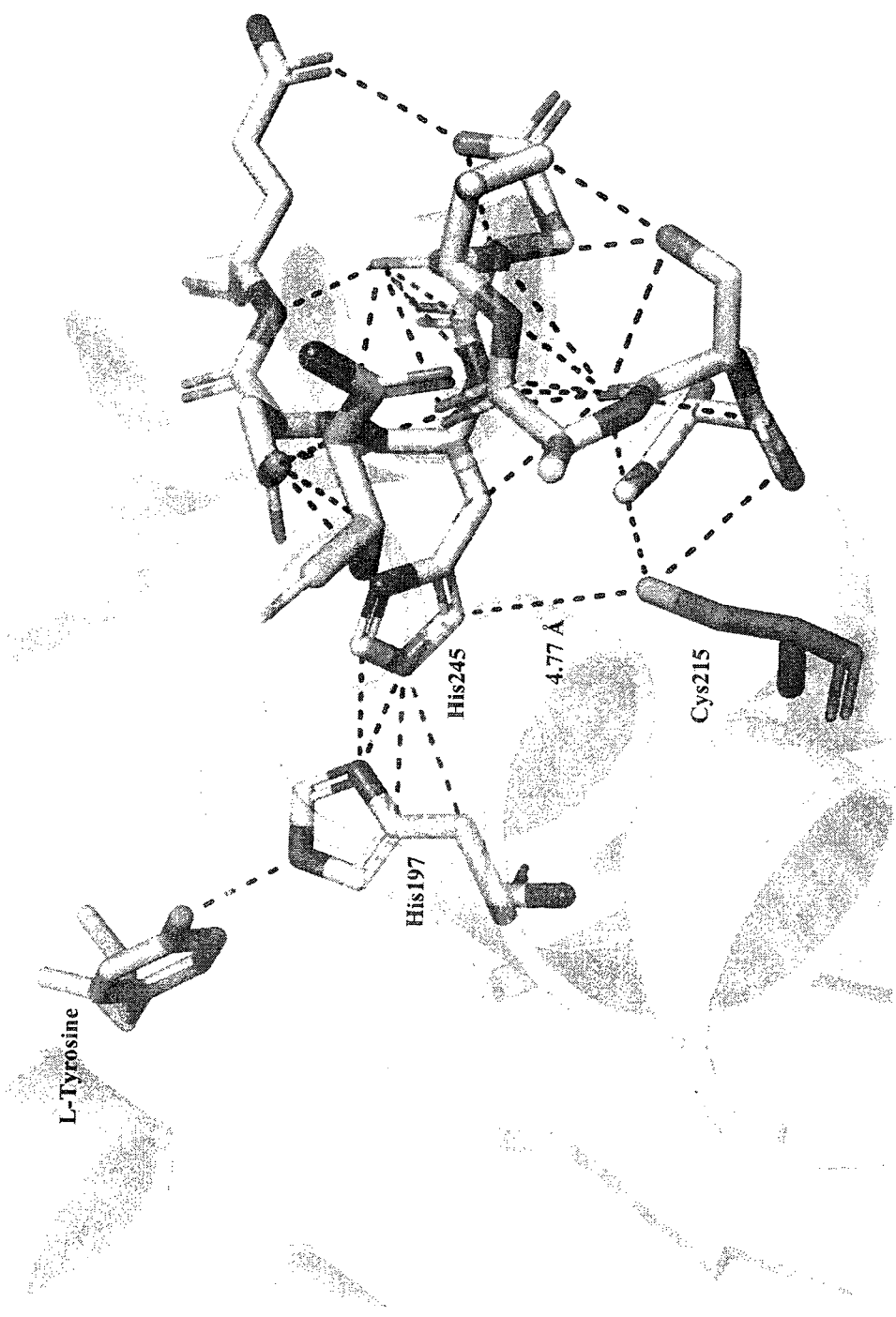


Figure 2.10: Modeled PD domain of *E. coli* WT CM-PD and key amino acids

CHAPTER 3

Determination of the pK_a of Lys37 in

E. coli Chorismate Mutase – Prephenate Dehydrogenase

3.1 INTRODUCTION

Lys37 possesses a pivotal role in the mutase domain of the bifunctional *E. coli* chorismate mutase – prephenate dehydrogenase. Sequence alignments with the mutase portions of *E. coli* CM-PD and CM-PDT reveal a conserved lysine residue at positions 37 and 39, respectively (16, 35). Despite the low sequence identity that is exhibited between chorismate mutases from different organisms, the overall electrostatic environment of the mutase active site is conserved (59, 147). Careful investigation of the crystal structures of the mini-mutase, which is the engineered monofunctional mutase from CM-PDT, as well as native monofunctional mutases from *B. subtilis* and *S. cerevisiae* have identified a cationic residue homologous to Lys37, whose presence is essential for the stabilization of the transition state of the mutase reaction. Furthermore, the substitution of Lys37 in the bifunctional *E. coli* CM-PD with glutamine results in a complete loss of mutase activity (39). Similarly, site-directed mutagenesis of homologous residues of mutases in other organisms result in variants with low or no activity.

Earlier studies performed by Turnbull *et al.* (36) and more recently by K. Bull (unpublished), which examined the pH dependence of $V/K_{\text{chorismate}}$ in the mutase reaction of the bifunctional *E. coli* CM-PD, established that an unidentified group with a pK_a of approximately 7.5 had to be protonated in order to assist in the binding of chorismate and the transition state analog to the mutase active site. Furthermore, chemical modification experiments by Christendat and Turnbull determined that Lys37 was particularly reactive with the histidine-specific reagent diethylpyrocarbonate, implying that the pK_a of this residue is depressed.

The purpose of this chapter is to establish the pK_a of Lys37 in the bifunctional *E. coli* CM-PD as a goal towards identifying the catalytically important group whose ionization is observed in the $V/K_{\text{chorismate}}$ pH rate profile. This is achieved by monitoring the pH-dependence of the reactivity and inactivation by the lysine-specific chemical modifying reagent TNBS.

3.2 EXPERIMENTAL PROCEDURES

3.2.1 Materials

Chorismate, prephenate and NAD⁺ (grade I) were prepared as described in section 2.2.1. *Endo*-oxabicyclic diacid (*endo*) (129) was a generous gift from Dr. Paul Bartlett of the University of California, Berkeley and was stored at -86°C as a stock of 2 mM in distilled water. 2,4,6-trinitrobenzenesulfonic acid (TNBS) and BSA were purchased from Sigma-Aldrich. GluC endopeptidase from *Staphylococcus aureus* strain V8 was purchased from Roche Applied Science. All other chemical reagents and resins were obtained as described in section 2.2.1.

3.2.2 Source of Recombinant WT and Variant CM-PD of *E. coli*

Recombinant WT CM-PD and Lys37Gln were constructed in *E. coli* by Christendat *et al.* (39).

3.2.3 Expression and Purification of WT and Variant Forms of *E. coli* CM-PD

CM-PD was expressed as described in section 2.2.3. It should be noted however that ammonium sulfate precipitation was included in the procedure here as described in the method of Christendat *et al.* (39) but was later omitted.

3.2.4 Sample Preparation of CM-PD

Frozen CM-PD protein samples were quickly thawed and then immediately placed on ice. To the samples was added DTT at a final concentration of 20 mM with subsequent incubation on ice for 30 minutes in order to reduce cysteine residues. Following DTT treatment, samples were buffer-exchanged into their intended buffer. Buffer exchange was performed using either a NAP-5 size exclusion column or a BIOMAX centrifugal concentrator (MWCO 30 kDa).

For exchange via a NAP-5 column, 10 mL of the intended buffer is used to equilibrate the column. A 500 μ L aliquot of the sample is passed through the column. Once the 500 μ L sample had eluted, 1 mL of buffer is applied into the column and the eluate is collected into a 1.5 mL Eppendorf tube.

For buffer exchange/concentration using a BIOMAX centrifugal concentrator, the sample is placed in the concentrator tube which had previously been conditioned with the appropriate buffer. It is then centrifuged at 12000 rpm using a benchtop centrifuge at 4°C until the sample reaches an approximate volume of 100 μ L. Additional buffer is added to the sample up to a final volume of approximately 500 μ L. The sample is then centrifuged once again as described previously. This step is repeated two more times in order to exchange the solvent completely into the intended buffer as well as to concentrate the protein.

3.2.5 SDS—Polyacrylamide Gel Electrophoresis

Denaturing SDS-PAGE was performed as described in section 2.2.5.

3.2.6 Protein Concentration Determination

Protein concentrations were estimated as described in section 2.2.6.

3.2.7 Determination of Enzyme Activity

Mutase and dehydrogenase activities were determined as described in section 2.2.7.

3.2.8 Determination of Kinetic Parameters

Mutase and dehydrogenase kinetic parameters were determined as described in section 2.2.8.

3.2.9 ESI-MS of Native WT and Variant CM-PD

CM-PD protein samples for ESI-MS were prepared using the protocol described in section 2.2.9.

3.2.10 Time-Dependent Chemical modification of WT CM-PD with TNBS at Neutral pH

3.2.10.1 Inactivation of Mutase by TNBS

WT CM-PD (5 μ M monomer) was incubated with a 3-fold molar excess of TNBS with respect to the total concentration of monomer, at ambient temperature and protected from light. Experiments were performed in 50 mM N-ethylmorpholine, 50 mM 2-morpholinoethanesulfonic acid, 1 mM EDTA, 25% glycerol at neutral pH. Mutase activity of the unmodified WT CM-PD (t_0) was assessed at pH 7.2 as outlined in section 3.2.8 using 500 μ M chorismate. Chemical modification was initiated upon addition of TNBS and mutase activity was assayed at different time points as described above. Changes in mutase activity were reported as percent mutase activity remaining relative to activity at t_0 .

The Lys37Gln variant was chemically modified with TNBS under the experimental conditions described above for WT CM-PD. Dehydrogenase activity was monitored as described in section 3.2.8, using 500 μ M prephenate and 1.6 mM NAD^+ . The data were collected using a Varian Cary 50 Dual Beam Spectrophotometer and the absorbances were corrected for the contributions from buffer and TNBS.

3.2.10.2 Quantitation of Stoichiometry of Trinitrophenylation

WT CM-PD (5 μ M monomer) was incubated with TNBS under identical conditions as in the previous section. Upon addition of TNBS, the absorbance increase at

345 nm ($\epsilon_{345\text{nm}} = 1.45 \times 10^4 \text{ M}^{-1}\cdot\text{cm}^{-1}$) was monitored for the formation of the trinitrophenylated adduct (148). The data were collected using a Varian Cary 50 Dual Beam Spectrophotometer and the absorbances were corrected for the contributions from buffer and TNBS.

3.2.11 pH-Dependent Inactivation of WT CM-PD by Chemical modification Using TNBS

WT CM-PD (5 μM monomer) was incubated with a 3-fold molar excess of TNBS with respect to the total concentration of monomer, at ambient temperature and protected from light. Experiments were performed in 3-component buffer denoted 3CB (0.05M 2-morpholinoethanesulfonic acid (MES), 0.05M N-ethylmorpholine, 0.1M diethanolamine) at various pH values ranging from 6.0 to 8.7. Mutase activity of the unmodified WT CM-PD, denoted as the t_0 time point, was assessed at pH 7.2 in 3CB using 500 μM chorismate. Chemical modification was initiated upon addition of TNBS and mutase activity was assayed at different time points as described above. Changes in mutase activity were reported as percent mutase activity remaining relative to the mutase activity at t_0 .

3.2.12 pH-Dependency of WT CM-PD Mutase Activity

The pH dependency of the mutase reaction was determined in a 3-component buffer (0.05 M 2-morpholinoethanesulfonic acid (MES), 0.05M N-ethylmorpholine, 0.1M diethanolamine) at 30°C from pH 5.23 to 8.33. The values of V and $(V/K)_{\text{chorismate}}$

were determined by performing activity assays, where the initial velocities were measured, while varying the concentration of chorismate, as outlined in section 3.2.8. In these assays, the ionic strength of this reaction buffer remains essentially constant (135). The final pH was determined on assay mixtures pooled after the reaction and equilibrated at 30°C in a water bath.

The variation of the values for V/K as a function of pH was fitted to the log form of Equation 3.1 (below) using Erithacus Software GraFit 5.0:

$$y = ((\text{Limit} * 10^{\text{pH} - \text{pKa1}}) / (10^{(2 * \text{pH} - \text{pKa1} - \text{pKa2})} + (10^{\text{pH} - \text{pKa1}} + 1))) \quad (\text{Equation 3.1})$$

where y represents the value of V/K at a particular pH value, *Limit* represents the pH-independent value of the parameters, K_1 and K_2 are dissociation constants for ionizable groups on the enzyme and/or substrate.

3.2.13 *In-silico* Digestion of WT CM-PD with Endopeptidase GluC

In-silico digestion was performed on the amino acid sequence of WT CM-PD (Table 3.3) using the PeptideCutter software (149) at www.expasy.org. Endopeptidase GluC from *Staphylococcus aureus* V8 was used for the *in-silico* digestion.

3.2.14 *In-vitro* Digestion of WT CM-PD with Endopeptidase GluC

Both native and trinitrophenylated samples of WT CM-PD (from section 3.2.10) were buffer exchanged into MilliQ water using NAP-5 size exclusion columns. The samples were lyophilized overnight at room temperature using a Speedvac and were then dissolved in 30 μ L of 50 mM ammonium bicarbonate (pH 7.8). The samples were then digested using endopeptidase GluC at a ratio of 20:1 CM-PD:GluC (w/w) overnight at room temperature protected from light. The GluC-digested CM-PD samples were analyzed by LC-MS using a 45 minute linear acetonitrile gradient from 5 – 95 % containing 0.1% TFA. Peptide peaks were detected in positive mode from 200 – 3000 amu using the same instrument and parameters as described in section 3.2.9.

3.2.15 Peptide Sequencing by ESI-MS/MS

A sample of GluC-digested WT CM-PD peptides was subjected to LC-MS analysis as per section 3.2.14. The peptide at $[M+H^{2+}]$ of 858.4 amu corresponding to the trinitrophenylated P(36-48) was selected at the first quadrupole, fragmented at the second quadrupole, and the resulting amino acid peaks were detected from 100 – 1400 amu in positive mode at the third quadrupole. Parameters used were: Cone voltage: 35 V, Collision Cell voltage: 35 V, Argon gas used for fragmentation and the resolution was approximately 0.5 Da.

3.2.16 Determination of Dissociation Constants for the Transition State Analogue by Fluorescence Emission

Values for the dissociation constant of *endo* from the complex with WT CM-PD or Lys37Gln variant were determined at 25°C by monitoring the changes in protein intrinsic fluorescence using a Shimadzu fluorimeter. The excitation wavelength was set at 280 nm and emission was monitored from 300 – 400 nm. Instrument parameters were set at 845 V for the lamp voltage, 2 nm/minute for the scan speed and 4 nm for the bandwidth; the fluorescence emission of each sample was recorded twice. Protein samples (0.24 μ M CM-PD monomer) were prepared in a 1-cm quartz cuvette (total volume 3 mL) in 50 mM N-ethylmorpholine, 50 mM 2-morpholinoethanesulfonic acid, 1 mM EDTA and 25% glycerol pH 7.7. *Endo* oxabicyclic diacid was available as a 2 mM stock in water and subsequent dilutions were prepared in the same buffer as for the

enzymes. Titrations were performed by the progressive addition of *endo* to a final concentration of 7 μM for WT and 10 μM for Lys37Gln CM-PD but not exceeding 3% of the total sample volume. Samples were mixed by gentle pipetting and binding was allowed to proceed for 2 minutes prior to recording measurements. The areas under the fluorescence signal from 325 – 360 nm were determined using the software that was included with the spectrophotometer. The fluorescence data were corrected for dilution and background fluorescence; no inner filter effect was observed.

A dissociation constant was determined by fitting the data to the Michaelis-Menten equation or the quadratic equation (150) (Equation 3.2) using Erithacus Software Grafit 5.0:

$$\Delta F = \Delta F_m \left(\frac{([L_t] + [E_t] + K_d) - \left(([L_t] + [E_t] + K_d)^2 - 4[L_t][E_t] \right)^{0.5}}{2[E_t]} \right) \quad (\text{Equation 3.2})$$

ΔF is the difference in fluorescence intensities in the presence and absence of the titrant, ΔF_m is the maximum change in fluorescence intensity, $[L_t]$ is the total concentration of titrant, $[E_t]$ is the total enzyme concentration and K_d is the dissociation constant.

3.2.17 Substrate Protection from Chemical Modification

In order to determine whether the mutase transition state analogue afforded protection from chemical modification of the cysteine residues in CM-PD by iodoacetamide, WT and Lys37Gln variants (5 μM monomer) were incubated for 5 minutes with *endo* at concentrations of 20 and 200 μM in 3CB at pH 7.2. After 5 minutes, IAM was added to the each enzyme sample to a final concentration of 10 mM and was allowed to react for 60 minutes. Upon completion of the reaction, samples were

immediately quenched with DTT at a final concentration of 20 mM and were kept on ice. Samples were then processed for ESI-MS analysis as described in section 3.2.9. A negative control was prepared for each sample, where neither IAM nor *endo* was added to the enzyme sample. A positive control was prepared by adding enzyme and IAM to a final concentration of 10 mM and was allowed to react for 60 minutes under identical conditions as reported above and then quenched with DTT. Controls were prepared for ESI-MS analysis as reported in section 3.2.17.

3.2.18 Determination of Lys37 pK_a by Titration With TNBS

The ionization state and surface accessibility of Lys37 in WT CM-PD was determined by reaction with TNBS for 10 minutes at several pH values, ranging from 5.94 to 9.26. WT CM-PD was treated as reported in section 3.2.4 prior to chemical modification. The sample was then buffer exchanged using a BIOMAX centrifugation filter (MWCO 30 kDa) into 1 x 3-component buffer (pH 7.0). WT CM-PD (5 μ M monomer) prepared above, was incubated for 10 minutes at ambient temperature in 2 x 3-component buffer at each pH value. A 178 μ M substock of TNBS was prepared in MilliQ water by performing a 1/1000 dilution of the stock TNBS solution (0.18 M). The trinitrophenylation reaction was initiated upon addition of 8.4 μ L of 178 μ M TNBS; the mixture was gently vortexed for 5 seconds and the reaction was then allowed to proceed for 10 minutes. The reaction was then quenched with the addition of 2 M ammonium bicarbonate, to a final reaction mixture volume of 500 μ L and the samples were kept on ice. Samples were buffer-exchanged into MilliQ water using individual NAP-5 size exclusion columns in order to avoid cross-contamination, and were then lyophilized

overnight using a SpeedVac at room temperature and protected from light. Samples were then dissolved in 30 μ L of 50 mM ammonium bicarbonate (pH 7.8) and were digested using endopeptidase GluC at a ratio of 20:1 CM-PD:GluC (w/w) overnight at room temperature protected from light. The GluC-digested WT CM-PD samples were analyzed by LC-MS using a 45 minute linear acetonitrile gradient from 5 – 95 % containing 0.1% TFA. Peptide peaks were detected in positive mode from 200 – 3000 amu using the same instrument and parameters as described in section 3.2.9.

For the analysis of the ESI-MS data, the ratio of peak intensity of trinitrophenylated P(36-48) / (peak intensity of native P(36-48) + peak intensity of trinitrophenylated P(36-48)) was calculated in order to determine the ratio of trinitrophenylated P(36-48) at different pHs relative to native P(36-48). The pK_a of the trinitrophenylated lysine residue was determined using Erithacus Software Grafit 5.0 software by plotting the above mentioned ratios versus pH values and using the equation for a single pK_a which is included in the software:

$$y = \frac{Limit_1 + Limit_2 \cdot 10^{(pH - pK_a)}}{10^{(pH - pK_a)} + 1} \quad (\text{Equation 3.3})$$

3.2.18 Modeling of CM Domain of *E. coli* CM-PD

Modeller 9v3 was used to model the mutase portion of the *E. coli* CM-PD monomer against the known structure of *E. coli* CM-PDT (PDB access code 1ecm). A structure-based alignment of *E. coli* CM-PD with the *E. coli* CM-PDT protein was obtained using the FFAS03 server (<http://ffas.ljcrf.edu/ffas-cgi-cgi/ffas.pl>). The FFAS03-generated alignment was used as input for Modeller 9v3, which generated a 3 D model of the mutase portion of *E. coli* CM-PD on this input.

3.3 RESULTS

3.3.1 Purification and Purity Assessment of WT and Lys37Gln Variant CM-PD

Both WT and Lys37Gln CM-PD were purified using a combination of ion-exchange and sepharose-AMP affinity chromatography as previously reported (39). As noted in Table 3.1, the purification of the variant led to a recovery of 9.3% or 82 mg of the proteins present in the cell-free extract. We were unable to calculate a purification factor for Lys37Gln since it did not possess any detectable mutase activity and fractions prior to Q-Sepharose were contaminated with other enzymes, which are NAD^+ -dependent. Figure 3.1 shows the SDS-PAGE analysis of purified *E. coli* Lys37Gln CM-PD indicating the purity of CM-PD after purification by AMP-affinity chromatography, suggesting that there is a homogeneous preparation of CM-PD.

ESI-MS was used in order to confirm the exact molecular weight of the purified CM-PD proteins. The deconvoluted mass spectrum of native WT CM-PD (Figure 3.3 panel A) clearly shows two major peaks at $[\text{M}+\text{H}^+]$ of 41913 and 42043 amu. The protein peaks display a difference of 130 amu. The peak at $[\text{M}+\text{H}^+]$ of 42043 amu corresponds to the full-length WT CM-PD and is exactly as expected from the literature molecular weight. Similar results were seen for the Lys37Gln variant CM-PD, since the substitution of lysine for glutamine does not yield a significant change in the molecular weight relative to the WT.

Table 3.2 shows a summary of the kinetic parameters that were determined for both the WT and Lys37Gln CM-PDs. The data clearly indicate that mutase activity is

abolished, while the kinetic parameters for the dehydrogenase reaction remain essentially identical to those of WT CM-PD. These results confirm the importance of Lys37 in the mutase activity of CM-PD. It is worth noting that the k_{cat} values of the purified enzymes in this report are approximately 20% higher than those previously reported by Christendat *et al.* (39).

Table 3.1: Purification table for WT (A) and Lys37Gln (B) CM-PD

(A)

Purification Step	Volume (mL)	Total Protein (mg)	Chorismate Mutase Activity		Prephenate Dehydrogenase Activity		Recovery (%)	Purification Factor	CM:PD ratio
			Units	Units / mg	Units	Units / mg			
Cell-free extract	112	1397	9918	7.1	Nd ¹	Nd ¹	100.0	1.00	nd
1 st Ammonium Sulfate Supernatant	118	950	9500	10.0	Nd ¹	Nd ¹	73.2	1.41	nd
2 nd Ammonium Sulfate Supernatant	122	540	3510	4.6	Nd ¹	Nd ¹	N/AP	N/AP	N/AP
2 nd Ammonium Sulfate Pellet	79	396	6574	16.6	Nd ¹	Nd ¹	28.3	2.34	nd
Q-Sepharose Purification	104	179	3866	21.6	8595	32.2	12.8	3.04	0.67
Sepharose-AMP Purification	211	69	4644	67.3	5996	86.9	5.0	9.48	0.77

(B)

Purification Step	Volume (mL)	Total Protein (mg)	Chorismate Mutase Activity		Prephenate Dehydrogenase Activity		Recovery (%)	Purification Factor	CM:PD ratio
			Units	Units / mg	Units	Units / mg			
Cell-free extract	78	886	ND*	ND*	Nd ¹	Nd ¹	100.0	1.00	Nd
1 st Ammonium Sulfate Supernatant	81	886	ND*	ND*	Nd ¹	Nd ¹	100.0	1.00	Nd
2 nd Ammonium Sulfate Supernatant	84	212	ND*	ND*	Nd ¹	Nd ¹	N/AP	N/AP	N/AP
2 nd Ammonium Sulfate Pellet	42	744	ND*	ND*	Nd ¹	Nd ¹	84.0	Nd	Nd
Q-Sepharose Purification	125	225	ND*	ND*	8595	38.2	25.4	Nd	Nd
Sepharose-AMP Purification	152	82	ND**	ND**	5486	66.9	9.3	Nd	Nd

Nd: activity not determined ND: no activity detected N/AP: not applicable

¹ PD activity cannot be readily determined because of the presence of other NADH-oxidizing enzymes

* No CM activity detected (50 µg CM-PD used for assay)

** No CM activity detected (300 µg CM-PD used for assay)

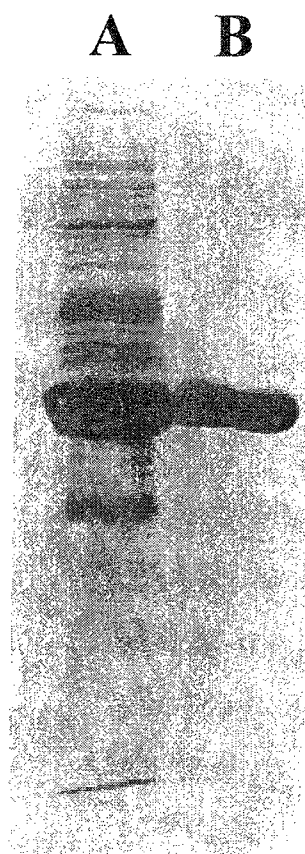


Figure 3.1: SDS-PAGE Analysis of ion-exchange and AMP-affinity purification of Lys37Gln CM-PD

Selected samples from the purification steps of variant CM-PD as analyzed by 10% SDS-PAGE. (A) Pooled protein after ion-exchange chromatography and (B) pooled protein after AMP-affinity chromatography.

Table 3.2: Kinetic Data for WT and Lys37Gln CM-PD Measured at pH 7.2 and 30°C

Protein	Mutase Activity			Dehydrogenase Activity					
	Chorismate			Prephenate			NAD ⁺		
	K_m (μM)	k_{cat} (s^{-1})	k_{cat} / K_m ($\text{M}^{-1}\cdot\text{s}^{-1}$)	K_m (μM)	k_{cat} (s^{-1})	k_{cat} / K_m ($\text{M}^{-1}\cdot\text{s}^{-1}$)	K_m (μM)	k_{cat} (s^{-1})	k_{cat} / K_m ($\text{M}^{-1}\cdot\text{s}^{-1}$)
WT	40 ± 3	54.7 ± 0.8	1.4 × 10 ⁶	35 ± 1	37.6 ± 0.3	1.1 × 10 ⁶	142 ± 13	40.7 ± 0.9	2.9 × 10 ⁵
K37Q	ND	ND	N/A	42 ± 4	39.2 ± 0.1	9.3 × 10 ⁵	112 ± 7	31.7 ± 0.4	2.8 × 10 ⁵

Kinetic parameters for the mutase and dehydrogenase reactions were determined at 30°C and pH 7.2 as reported in section

3.2.8.

3.3.2 *In-silico* Digestion of WT CM-PD With Endopeptidase GluC

In-silico digestion was performed on the amino acid sequence of WT CM-PD (Table 3.3) with GluC using PeptideCutter, an internet-based prediction software (<http://ca.expasy.org/tools/peptidecutter/>). WT CM-PD possesses fifteen lysine residues, five in the mutase domain and ten in the dehydrogenase domain. *In-silico* digestion of this protein with GluC yields 21 peptides of widely varying sizes from 572.2198 to 6850.6434 Da. Interestingly, Lys37 is associated with a single peptide free from other lysine groups. P(36-48) consists of residues 36 – 48 (VKSRFGLPIYVPE) with a mass of 1504.8522 Da.

Peptide Mass (Da)	Position	Peptide Sequence
448.535	1 - 4	MVAE
1173.288	5 - 14	LTALRDQIDE
1595.946	15 - 28	VDKALLNLLAKRLE
430.502	29 - 32	LVAE
303.315	33 - 35	VGE
1504.792	36 - 48	VKSRFGLPIYVPE
303.318	49 - 50	RE
1091.251	51 - 60	ASMLASRAE
218.21	61 - 62	AE
1023.194	63 - 72	ALGVPPDLIE
1173.399	73 - 81	DVLRVMRE
571.541	82 - 86	SYSSE
3076.625	87 - 115	NDKGFKTLCPSLRPVVIVGGGGQMGRLE
1650.997	116 - 129	KMLTLSGYQVRILE
2945.3	130 - 156	QHDWDRAADIVADAGMVIVSVPIHVTE
6854.123	157 - 221	QVIGKLPPLPKDCILVDLASVKNGPLQAMLVAHDGPVLGLHPMFGPDSGLAKQVVVWCDGRKPE
956.065	222 - 228	AYQWFLE
1863.153	229 - 244	QIQVWGARLHRISAVE
2902.282	245 - 269	HDQNMAFIQALRHFATFAYGLHLAE
147.131	270	E
601.657	271 - 275	NVQLE
1502.774	276 - 288	QLLALSSPIYRLE
2568.986	289 - 311	LAMVGRLEAQPQLYADIIMSSE
1927.283	312 - 326	RNLALIKRYKRFGE
331.369	327 - 329	AIE
373.450	330 - 332	LLE
1767.959	333 - 347	QGDKQAFIDFRKVE
1670.761	348 - 360	HWFGDYAQRQSE
1569.744	361 - 373	SRVLLRQANDNRQ

Table 3.3: *In-silico* digest of WT CM-PD with endopeptidase GluC in bicarbonate buffer

3.3.3 Time-Dependent Chemical modification of WT CM-PD with TNBS at Neutral pH

In order to determine the reactivity and surface accessibility of the lysine residues in WT CM-PD, a time-dependent modification of the enzyme was performed at neutral pH with an equimolar concentration of TNBS relative to CM-PD monomer. Figure 3.2 illustrates that there is a time-dependent loss of mutase activity, which reaches 80% of activity lost within 45 minutes of chemical modification. The formation of trinitrophenylated-adduct was monitored by UV spectrophotometry at 345 nm. Figure 3.2 clearly indicates that under the experimental conditions that were used, 0.8 lysine residues are modified within 45 minutes. More importantly, time-dependent modification directly coincides with the loss of mutase activity. Chemical modification was performed for Lys37Gln under identical experimental conditions as for the WT enzyme. Figure 3.2 clearly indicates that there is no loss in dehydrogenase activity upon the incubation of the variant enzyme with TNBS.

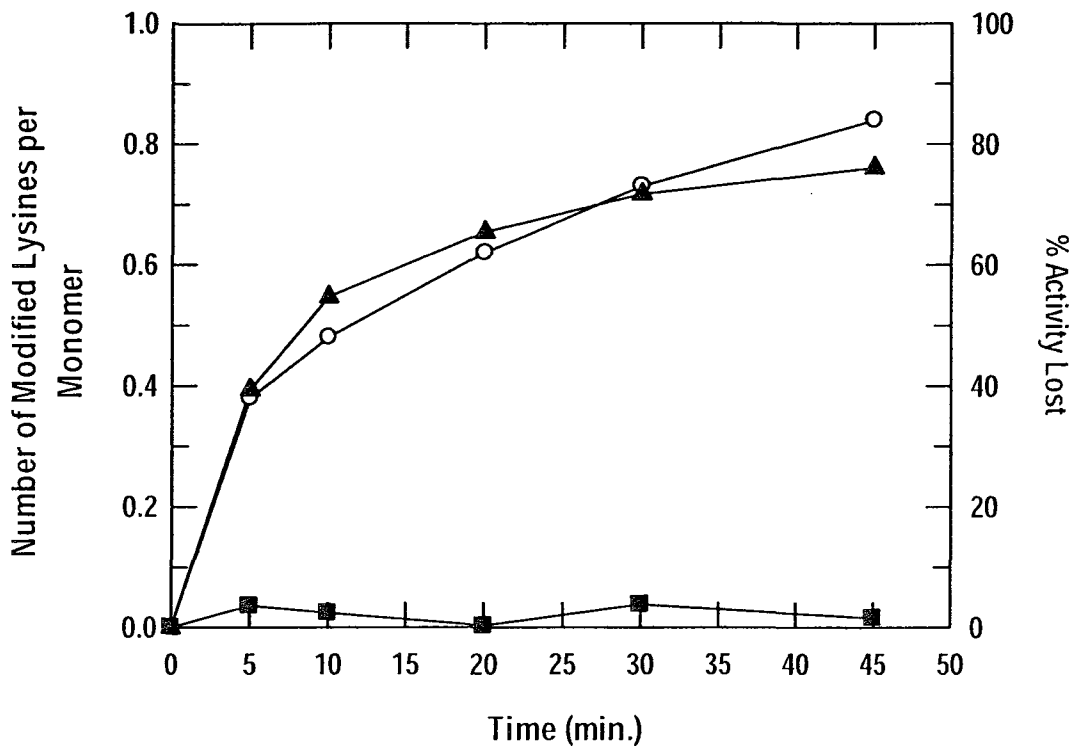
These samples were also subjected to mass spectrometric analysis in order to confirm the results. Figure 3.3 illustrates the ESI-MS spectra of native and trinitrophenylated WT CM-PD from section 3.2.10. In Panel A, the deconvoluted spectrum of native WT CM-PD shows two major peaks with a difference of 130 amu; at $[M+H^+]$ of 41913 amu is the WT CM-PD with its N-terminal methionine removed and at $[M+H^+]$ of 42043 amu is the full-length WT CM-PD. Panel B illustrates the ESI-MS spectrum of trinitrophenylated WT CM-PD. In this spectrum, we see 4 major peaks; two of these are the same as those mentioned for native WT CM-PD and the other two are

shifted by +211 amu relative to the native protein, at $[M+H]^+$ of 42123 and 42254 amu.

These correspond to the singly trinitrophenylated WT CM-PD polypeptide peaks.

Figure 3.2: Correlation of TNBS adduct formation with mutase inactivation at neutral pH

WT CM-PD (5 μM monomer) was incubated with a 3-fold molar excess of TNBS with respect to the total concentration of monomer at pH 7.0, at ambient temperature and protected from light. Chemical modification was initiated upon addition of TNBS and mutase activity was assayed at different time points as described in section 3.2.10. Changes in mutase activity were reported as percent activity remaining relative to activity at t_0 . TNBS adduct formation was monitored at 345 nm and calculated using $\epsilon_{345\text{nm}} = 1.45 \times 10^4 \text{ M}^{-1}\cdot\text{cm}^{-1}$. Identical experimental conditions were used for trinitrophenylation of the Lys37Gln variant. Changes in dehydrogenase activity were monitored as mentioned in section 3.2.7, using 500 μM prephenate and 1.6 mM NAD^+ . The absorbances were corrected for the contributions from buffer, enzyme and TNBS.



○ Number of Modified Lysines per Monomer
 ▲ % CM Activity Lost
 ■ % PD Activity Lost

Figure 3.3: Deconvoluted ESI-MS spectra following the time-dependent modification of WT CM-PD with TNBS

WT CM-PD (5 μ M monomer) was reacted with 15 μ M TNBS for 15 minutes at pH 7.0 in 2 x 3-component buffer at room temperature and protected from light. After 15 minutes, the modification reaction was quenched using 2 M ammonium bicarbonate and the samples were kept on ice. Protein samples (2-5 μ M monomer) were prepared as described in section 3.2.9 immediately prior to direct injection. (A) WT CM-PD; unmodified polypeptide peaks observed at $[M+H^+]$ of 41913 and 42043 amu. (B) Trinitrophenylated WT CM-PD unmodified polypeptide peaks observed at $[M+H^+]$ of 41912 and 42043 amu; modified polypeptide peaks observed at $[M+H^+]$ of 42123 and 42254 amu.

A

WT CM-PD w/o N-Terminal Met

Δ amu = 130

Native WT CM-PD

B

WT CM-PD w/o N-Terminal Met

+211 amu

WT CM-PD w/o N-Terminal Met
+ 1 TNB Adduct

Native WT CM-PD

Native WT CM-PD + 1 TNB Adduct

3.3.4 *In-vitro* Digestion of WT CM-PD With Endopeptidase GluC

In-vitro digestion was performed on native WT CM-PD using endopeptidase GluC, in order to determine the extent of detection of the expected peptides generated by the *in-silico* digestion show in Table 3.3. The data in Table 3.4 was generated from Figure 3.4 and indicates that for WT CM-PD, 251 of 373 amino acids were accounted for, yielding a sequence coverage of 67.3%. The peptides were detected as singly and doubly charged peaks. The peptide of interest containing Lys37, denoted P(36-48), was detected as a doubly charged peak at $[M+2H^+]$ of 752.90 amu (Figure 3.5).

In order to confirm that trinitrophenylation occurred on Lys37 of P(36-48), the trinitrophenylated form of WT CM-PD, generated as described in section 3.2.10, was also digested with GluC and analyzed as for the unmodified form of the enzyme. Since P(36-48) was identified as a doubly charged peak $[M+2H^+]$ at 752.90 amu, the trinitrophenylated form of P(36-48) would be expected at $[M+2H^+]$ of 858.37 amu. Figure 3.5 (Panel A) corresponding to unmodified WT CM-PD polypeptide, clearly show that there is no interfering peak at 858.37 amu. Panel B corresponding to the variant polypeptide, clearly illustrates the appearance of a intense doubly charged peptide peak at $[M+2H^+]$ of 858.37 amu as well as a concomitant decrease in the intensity of the unmodified P(36-48) peptide peak at 752.90 amu. The results of these digestions confirm that trinitrophenylation of Lys37 occurs on P(36-48). ESI-MS/MS peptide sequencing performed as described in section 3.2.15 identified the amino acid sequence of P(36-48) as **VK(TNB)SRFGLPLYVPE** but most importantly confirmed that the site of trinitrophenylation was on the lysine at position 37 (Figure 3.6).

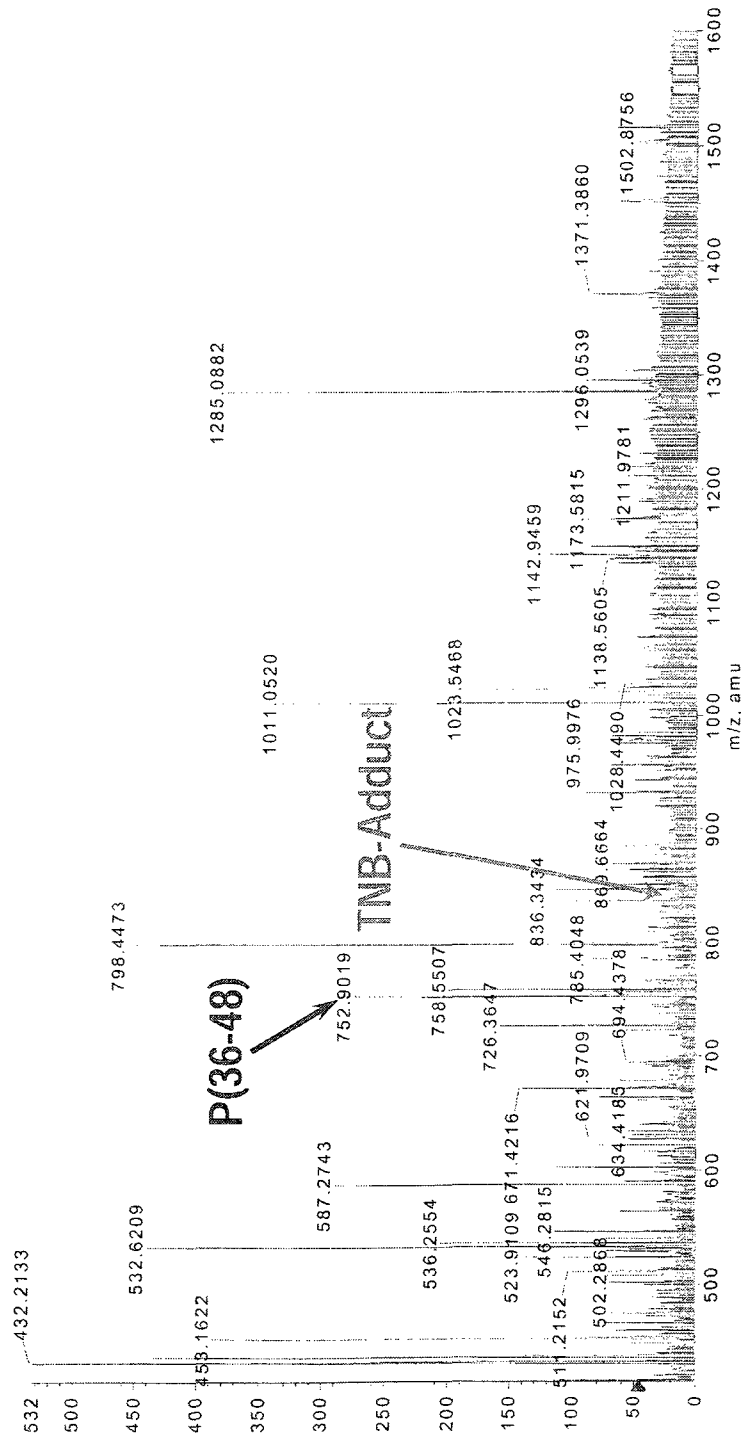


Figure 3.4: ESI-MS spectrum of the WT CM-PD digestion profile with endopeptidase GluC in bicarbonate buffer

WT CM-PD was digested using endopeptidase GluC in 30 μ L of 50 mM ammonium bicarbonate (pH 7.8), at a ratio of 20:1 CM-PD:GluC (w/w), overnight at room temperature protected from light. The GluC-digested CM-PD samples was analyzed by LC-MS, using a linear 45 minute acetonitrile gradient form 5 – 95 % containing 0.1% TFA. Peptides were detected in positive mode from 400 – 3000 amu using the same instrument and parameters as described in section 3.2.9.

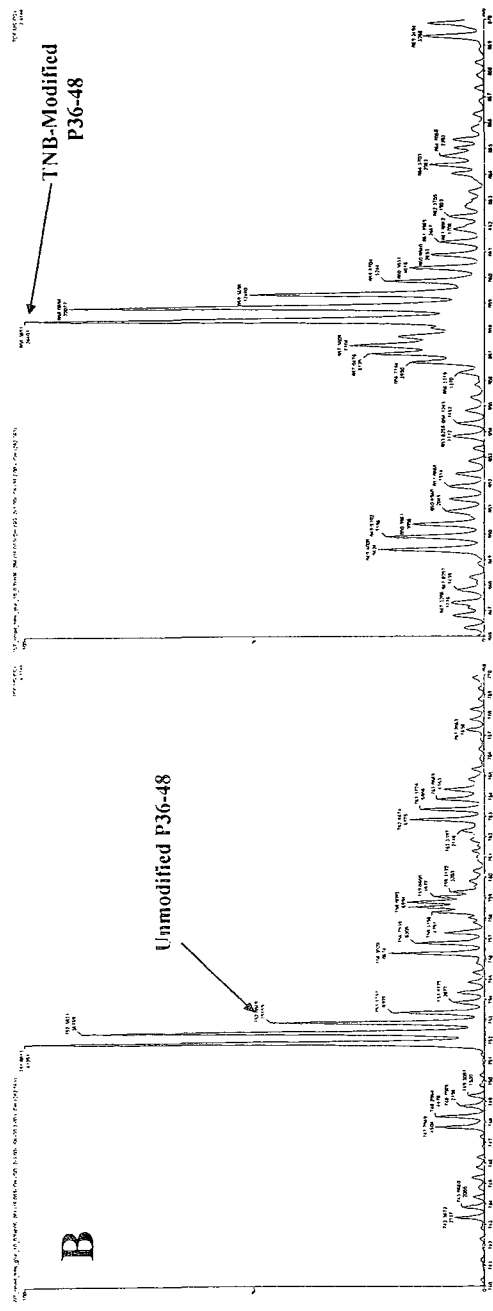
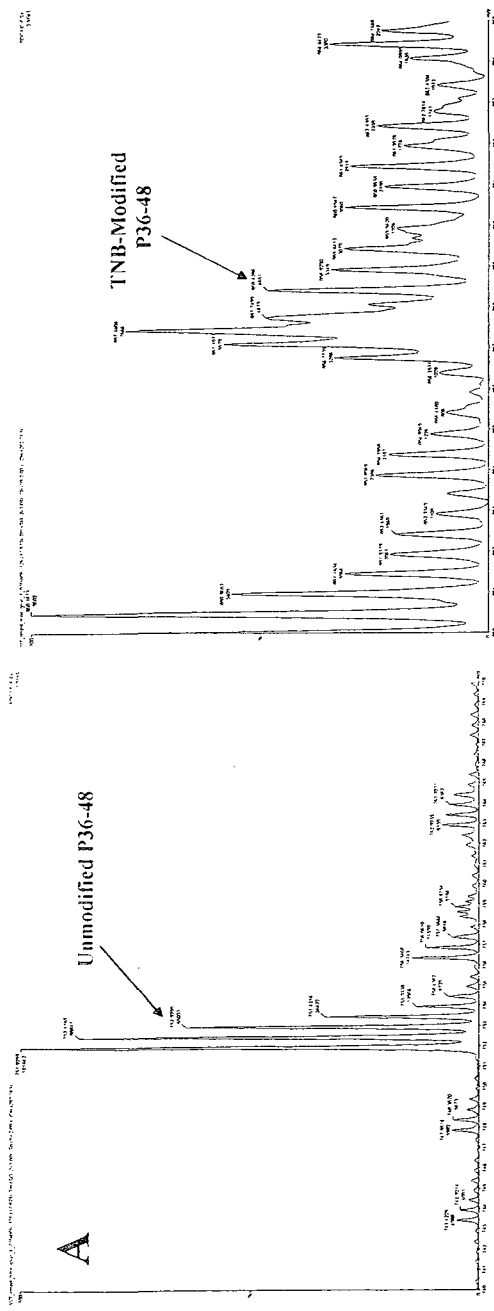
Peptide Mass (Da)	Charge	Position	Peptide Sequence
448.5350	+1	1-4	MVAE
587.3261	+2	5-14	LTALRDQIDE
1173.6110	+1	5-14	LTALRDQIDE
798.4921	+2	15-28	VDKALLNLLAKRLE
1004.6082	+2	15-32	VDKALLNLLAKRLELVAE
716.3825	+1	29-35	LVAEVGE
1101.6084	+2	29-48	LVAEVGEVKSFRGLPIYVPE
752.9261	+2	36-48	VKSFRGLPIYVPE
1376.7063	+1	49-60	REASMLASRAE
1091.5626	+1	51-60	ASMLASRAE
788.8930	+2	49-62	REASMLASRAEAE
1148.5983	+2	51-72	ASMLASRAEAEALGVPPDL IE
612.3259	+2	61-72	AEALGVPPDLIE
1023.5720	+1	63-72	ALGVPPDLIE
1089.6032	+2	63-81	ALGVPPDLIEDVLRVMRE
587.3055	+2	73-81	DVLRVMRE
1173.6521	+1	73-81	DVLRVMRE
572.2198	+1	82-86	SYSSE
825.9624	+2	116-129	KMLTSLSGYQVRILE
956.4512	+1	222-228	AYQWFLE
478.7256	+2	222-228	AYQWFLE
932.0174	+2	229-244	QIQVWGARLHRISAVE
1515.7340	+2	245-270	HDQNMAFIQALRHFATFAYGLHLAEE
1043.5771	+2	271-288	NVQLEQLLALSSPIYRLE
602.3144	+1	271-275	NVQLE
751.9289	+2	276-288	QLLALSSPIYRLE
1284.2836	+2	289-311	LAMVGRFLFAQDPQLYADIIM SSE
1120.6331	+2	312-329	RNLALIKRYKRFGEAIE
835.8673	+2	348-360	HWFGDYAQRQSE
785.4284	+2	361-373	SRVLLRQANDNRQ

Table 3.4: *In-vitro* digest of WT CM-PD with endopeptidase GluC in bicarbonate buffer

The table indicates the peptides that were detected upon GluC digestion of WT CM-PD shown in Figure 3.4. The ionization state of the peaks that were detected by LC-MS is indicated in the Charge column.

Figure 3.5: *In-vitro* digest of WT CM-PD with endopeptidase GluC in bicarbonate buffer

Unmodified and trinitrophenylated WT CM-PD from section 3.2.10 were digested using endopeptidase GluC in 30 μ L of 50 mM ammonium bicarbonate (pH 7.8), at a ratio of 20:1 CM-PD:GluC (w/w), overnight at room temperature protected from light. The GluC-digested samples were analyzed by LC-MS, using a linear 40 minute acetonitrile gradient from 5 – 95 % containing 0.1% TFA. Peptides were detected in positive mode from 200 – 3000 amu using the same instrument and parameters as described in section 3.2.9. Panel A illustrates the GluC digest spectrum of unmodified WT CM-PD: in the left pane, the unmodified P(36-48) peptide is observed as a doubly charged peak at $[M+2H^+]$ of 752.9 amu; in the right pane, no interfering peak is seen at 858.4 amu, where the trinitrophenylated form of P(36-48) is expected (spectrum enlarged to baseline). Panel B illustrates the GluC digest spectrum of trinitrophenylated WT CM-PD: in the left pane, the unmodified P(36-48) peptide is observed as a doubly charged peak at $[M+2H^+]$ of 752.9 amu; in the right pane, the trinitrophenylated appears as an intense doubly charged peak at $[M+2H^+]$ of 858.4 amu.



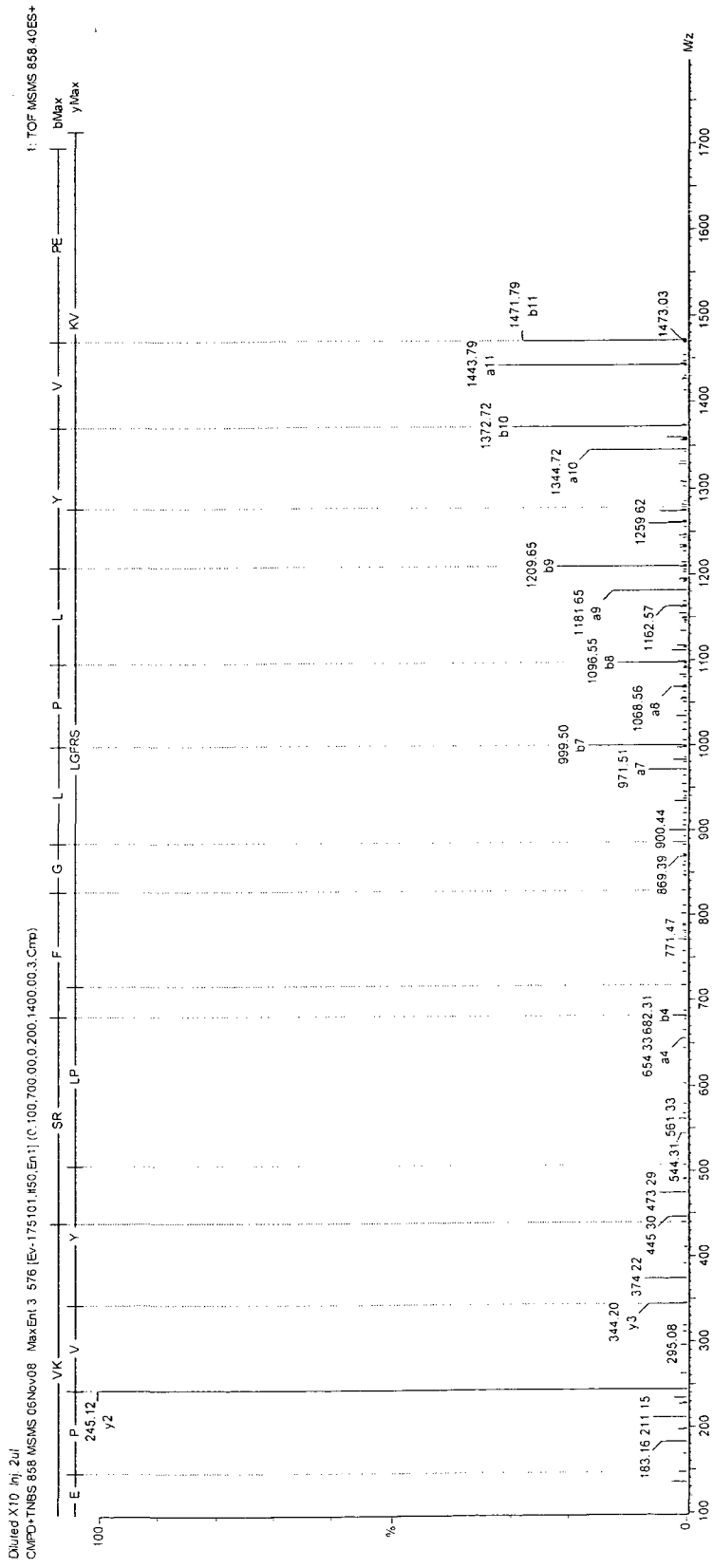


Figure 3.6: ESI-MS/MS spectrum of peptide sequencing data for alkylated P(36-48)

Trinitrophenylated peptide P(36-48) was subjected to ESI-MS/MS analysis as described in section 3.2.15 in order to determine the amino acid sequence of the peptide. Analysis of the sequence data revealed the sequence of trinitrophenylated P(36-48) to be **VK(TNB)SRFGLPL YVPE**, which confirms the identity of the peptide and the site of alkylation on residue Lys37.

3.3.5 pH-Dependent Inactivation of WT CM-PD by Chemical Modification Using TNBS

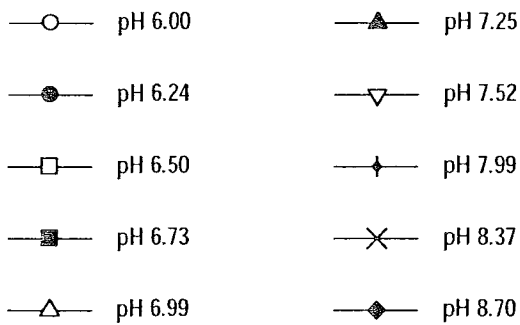
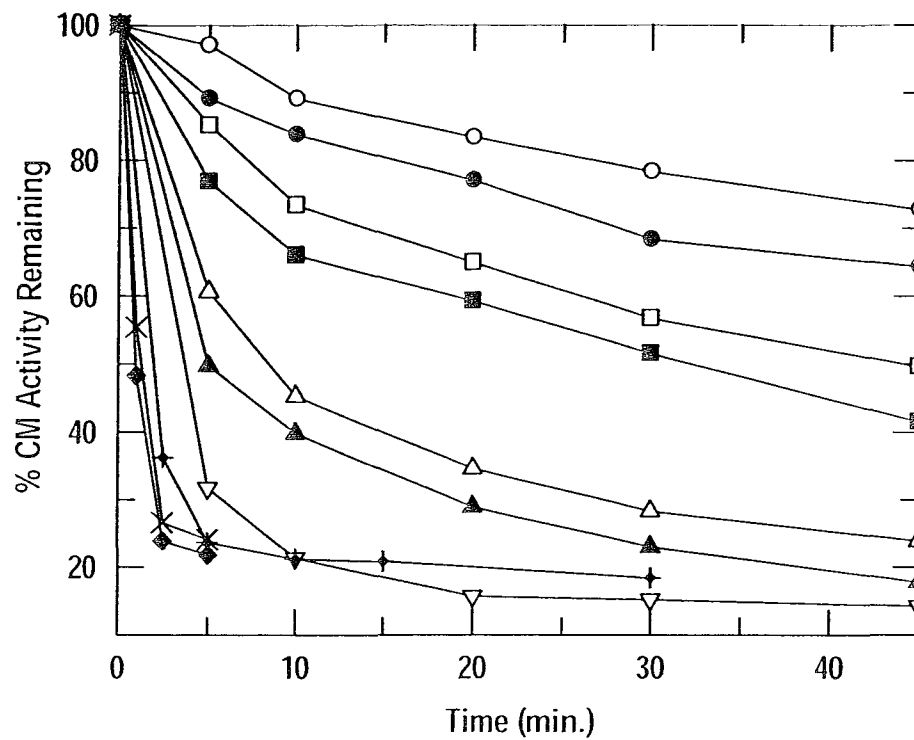
Inactivation of mutase activity by TNBS was monitored as a function of pH in order to determine the pK_a of the ionizable residue being chemically modified. Loss of mutase activity due to trinitrophenylation was time-dependent and pH-dependent over the experimental pH range of 6.00 to 8.70 (Figure 3.7). When reaction rates were plotted as a function of time, apparent second-order rate constants could be calculated at each pH value by fitting the data to Equation 3.4 (151) (data not shown). The rates of inactivation were slow at lower pH values (pH 6.00 – 6.73) but increased rapidly at higher pH values from 6.99 to 8.70. The apparent pK_a of the reacting group was estimated by following the pH dependence of the rate constants for TNBS inactivation of the mutase. Over the pH range of 6.00 - 8.70, the ionization of a single group was observed (Figure 3.8) with a pK_a value of 7.69 ± 0.08 .

$$k_{app} = \frac{C_{CM-PDTNB}}{t \cdot C_{CM-PD0} (C_{CM-PD0} - C_{CM-PDTNB})} \quad (\text{Equation 3.4})$$

,where the concentrations of trinitrophenylated CM-PD ($C_{CM-PDTNB}$) were derived from CM activity at time zero (C_{CM-PD0}) and the activity at a given time point.

Figure 3.7: Stoichiometric chemical modification of WT CM-PD with TNBS at various pH values

WT CM-PD (5 μ M monomer) was incubated with a 3-fold molar excess of TNBS with respect to the total concentration of monomer, at ambient temperature and protected from light. Experiments were performed in 3-component buffer at various pH values. Chemical modification was initiated upon addition of TNBS and mutase activity was assayed at different time points as noted in section 3.2.7. Changes in mutase activity were reported as percent activity remaining relative to activity at t_0 for each pH value.



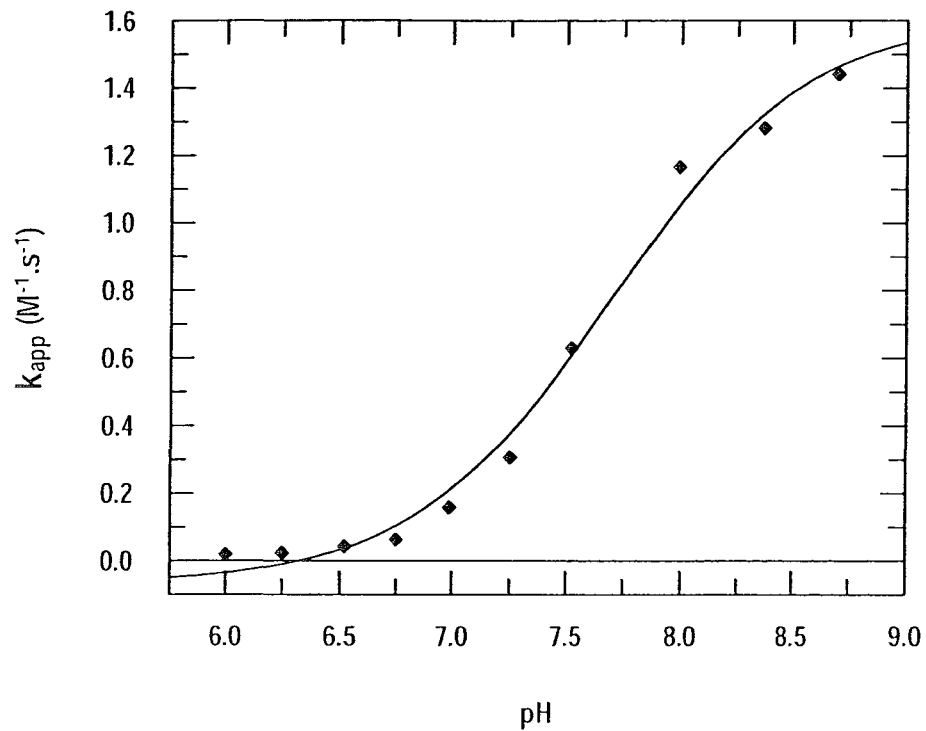


Figure 3.8: Titration of trinitrophenylated residue by reaction of WT CM-PD with TNBS for 40 minutes at different pH values

Graph illustrating the second-order rate constants, k_{app} , plotted versus the different experimental pH values into the Erithacus Grafit 5.0 software by using the equation for a single pK_a (Equation 3.3).

3.3.6 pH-Dependence of the Mutase Reaction

In order to assess the pH dependence of the mutase reaction, a pH rate profile was constructed for WT CM-PD from pH 5.23 to 8.33, by varying the concentration of chorismate. The $V/K_{\text{chorismate}}$ profile for WT CM-PD is bell-shaped with slopes of +1 and -1 and illustrates the decrease in the rate of reaction of chorismate at both high and low pH values (Figure 3.9). The variation of $\log V$ with pH indicates that there are no ionizable residues that participate in catalysis and/or product release, that titrate within our experimental range. Fit of the data to the Equation 3.1 indicate in the $V/K_{\text{chorismate}}$ profile, that a residue with a pK_a of about 6.3 must be deprotonated and another with a pK_a of about 7.5 must be protonated for maximal activity. The $\log V$ and $V/K_{\text{chorismate}}$ imply that these 2 residues associated with the free enzyme and/or free substrate are involved in chorismate binding and/or catalysis.

Unfortunately, since the Lys37Gln CM-PD variant lacks mutase activity, construction of a pH rate profile for the mutase reaction was not possible.

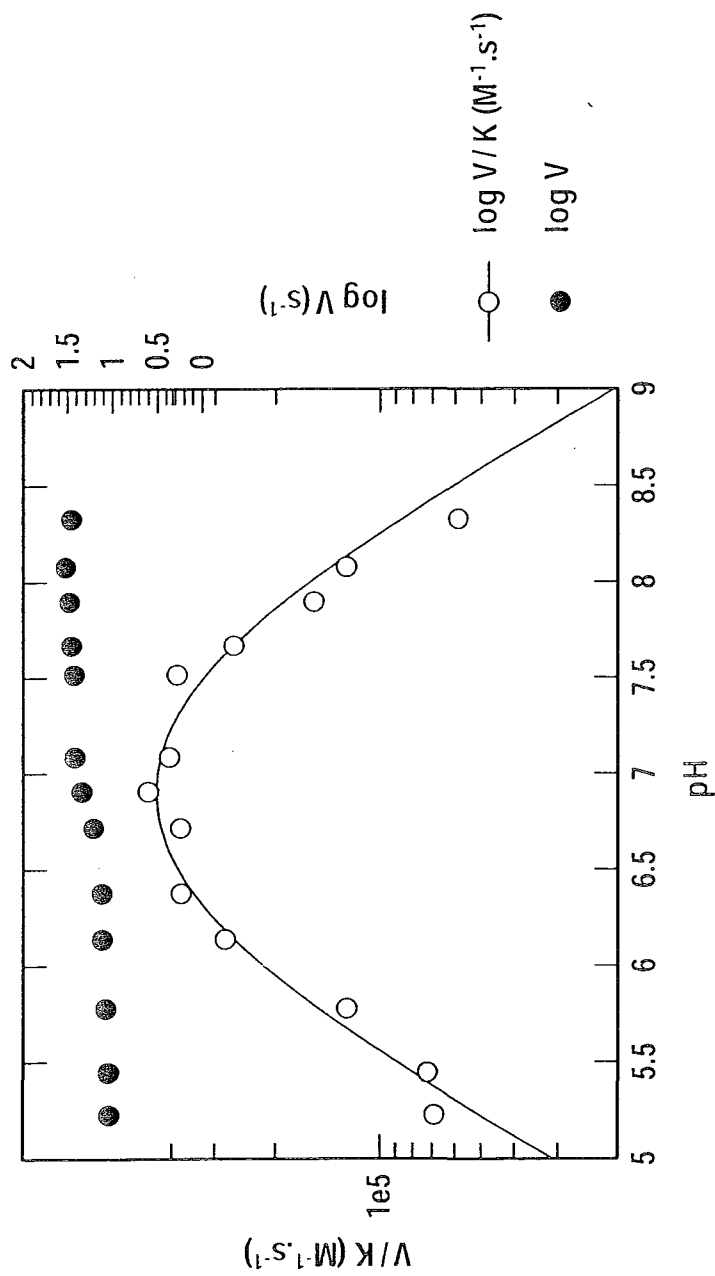


Figure 3.9: Variation of $\log V$ and $\log V/K$ with pH for the chorismate mutase reaction catalyzed by WT CM-PD. Mutase activity was recorded at 30°C from pH 5.23 to 8.33 in a three-component buffer consisting of 0.1 M MES, 51 mM N-ethylmorpholine, 51 mM diethanolamine, 1 mM EDTA and 1 mM DTT at pH 7.2. The curve for $V/K_{\text{chorismate}}$ represents the best fit of the data to Equation 3.1 using GraFit 5.0, yielding pK_a values of 6.32 ± 0.12 and 7.50 ± 0.11 .

3.3.7 Determination of Dissociation Constant of Mutase Transition State Analogue WT and Lys37Gln CM-PD by Fluorescence Spectroscopy

Fluorescence spectroscopy was used in order to determine the binding affinity of the mutase transition state analogue *endo* for both WT CM-PD and Lys37Gln. This experiment should address the question if the variant is inactive because it cannot bring about the conversion of substrate to product or because it cannot bind chorismate. Figure 3.10 displays the overlays of the fluorescence emission spectra following excitation at 280 nm, in the absence and in the presence of increasing concentrations of *endo*, for WT and Lys37Gln CM-PD. For both enzymes, the fluorescence signal decreases with increasing concentrations of *endo*. WT CM-PD exhibits a slight shift in λ_{max} of emission, at higher *endo* concentrations, from 333 to approximately 336 nm; no such shift is observed for the variant, which may be an indication of its change in affinity of binding for the transition state analogue.

The area under the fluorescence emission band was determined from 325 – 360 nm at increasing concentrations of *endo*. The differences in the areas relative to that of the enzyme in the absence of *endo* were plotted as a function of inhibitor concentration, and values for K_d were determined using Equation 3.2 (Figure 3.11). The data indicates that WT CM-PD binds the transition state analogue 10-fold more tightly than does Lys37Gln (compare K_d value of $0.05 \pm 0.01 \mu\text{M}$ and $0.51 \pm 0.04 \mu\text{M}$, respectively).

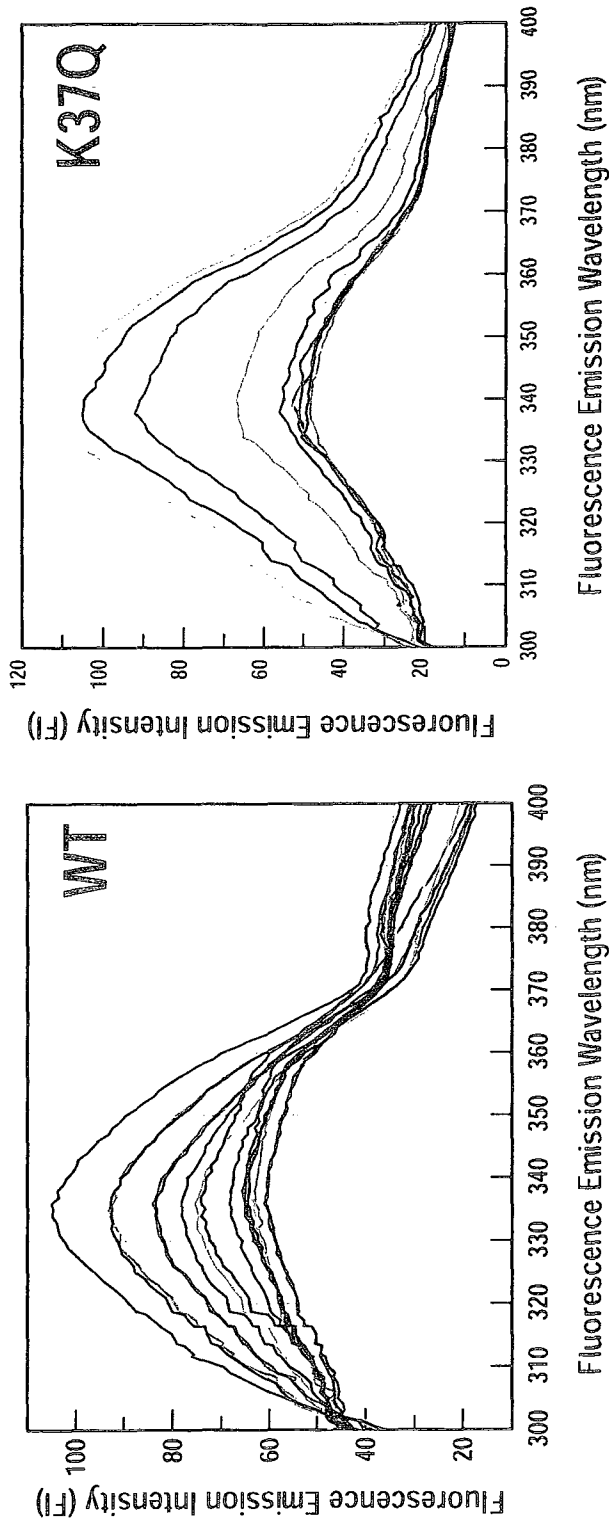
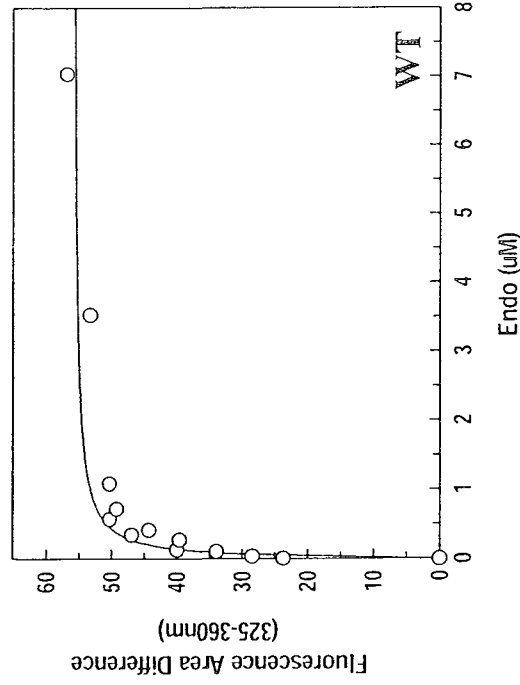


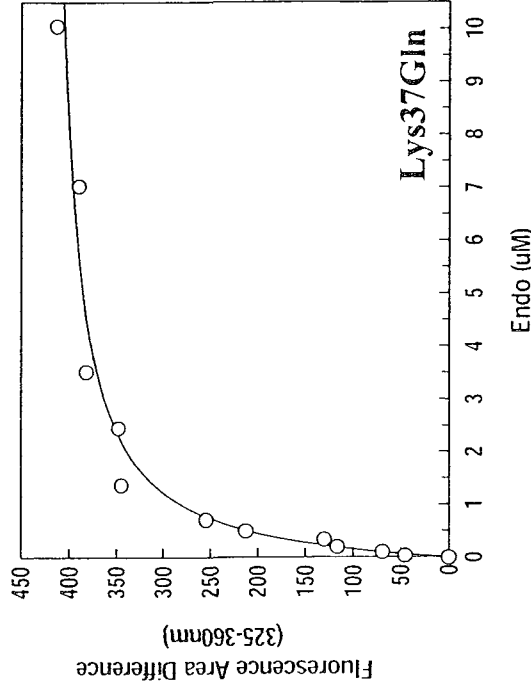
Figure 3.10: Fluorescence emission spectra of WT and Lys37Gln CM-PD in the presence of increasing amounts of

endo

Fluorescence emission spectra recorded for WT and Lys37Gln variant CM-PD (0.24 μ M monomer) recorded in 50 mM N-ethylmorpholine, 50 mM 2-morpholinoethanesulfonic acid, 1 mM EDTA and 25% glycerol pH 7.7 in the presence of increasing amounts of *endo* (from 0 - 7 μ M for WT and 0 - 10 μ M for Lys37Gln) from using an excitation wavelength of 280 nm. All spectra were corrected for contribution from buffer.



Parameter	Value	Std. Error
Dissociation Constant	0.05	0.01



Parameter	Value	Std. Error
Dissociation Constant	0.51	0.04

Figure 3.11: Changes in fluorescence intensity of WT and Lys37Gln variant CM-PD upon binding of *endo*

The intrinsic Tyr fluorescence of WT and Lys37Gln CM-PD (0.24 µM monomer) was observed by excitation at 280 nm and measuring the emission from 300 to 400 nm. Changes in the area under the fluorescence signal from 325 – 360 nm were plotted versus *endo* concentration from 0 – 7 µM for WT and 0 -10 µM for Lys37Gln. The dissociation constants (K_d) for *endo* were determined by fitting the data to Equation 3.2.

3.3.8 Substrate Protection from Chemical Modification

The cysteine residues of WT and Lys37Gln CM-PD variants were chemically modified with 10 mM IAM for 60 minutes at pH 7.2 in the absence and presence of both 20 and 200 μM *endo*, respectively.

Figure 3.12 panel (A1), show the negative control for WT CM-PD, where no IAM and no *endo* has been added. This spectrum illustrates the 2 peaks expected for WT CM-PD, notably at $[\text{M}+\text{H}^+]$ of 41911 and 42042 amu. For simplicity, we will be observing modifications noted on the peak at $[\text{M}+\text{H}^+]$ of 41911 amu. Panel (A2) represents the spectrum of the positive alkylation control, where IAM is added and the reaction allowed to proceed for 60 minutes. The major peak at $[\text{M}+\text{H}^+]$ of 42025 amu represents WT CM-PD without the N-terminal methionine that has been alkylated at 2 sites, notably $[\text{M}+\text{H}^+]$ of 41911 amu + (2 x 57 amu). Panels (A3) and (A4) represent the spectra of the alkylation experiment in the presence of 20 and 200 μM *endo*, respectively. In the presence of 20 μM *endo*, the spectrum is essentially identical to that of panel (A2), where the major peak at $[\text{M}+\text{H}^+]$ of 42025 amu is that of a doubly-alkylated WT CM-PD. In Panel (A4) however, two major peaks are observed at $[\text{M}+\text{H}^+]$ of 41968 and 42025 amu. The latter peak corresponds once again to the doubly-alkylated WT CM-PD, whereas the presence of 200 μM *endo* seems to have protected against the partial modification of a single cysteine residue, which is suggested by the appearance of a novel peak at $[\text{M}+\text{H}^+]$ of 41968 amu corresponding to native WT CM-PD with a single alkylation site, shifted by -57 amu.

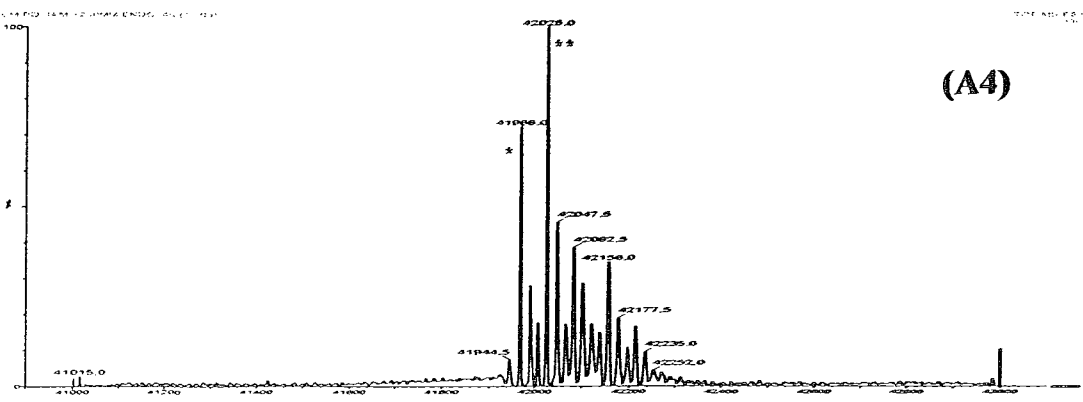
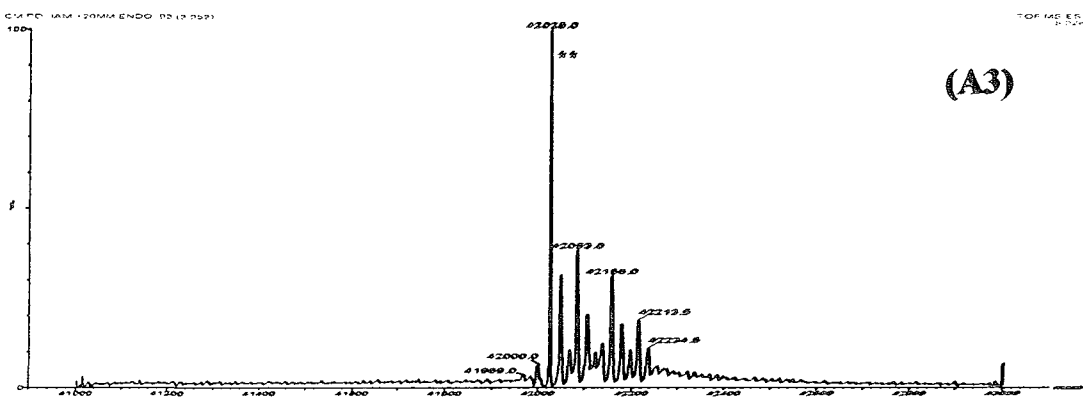
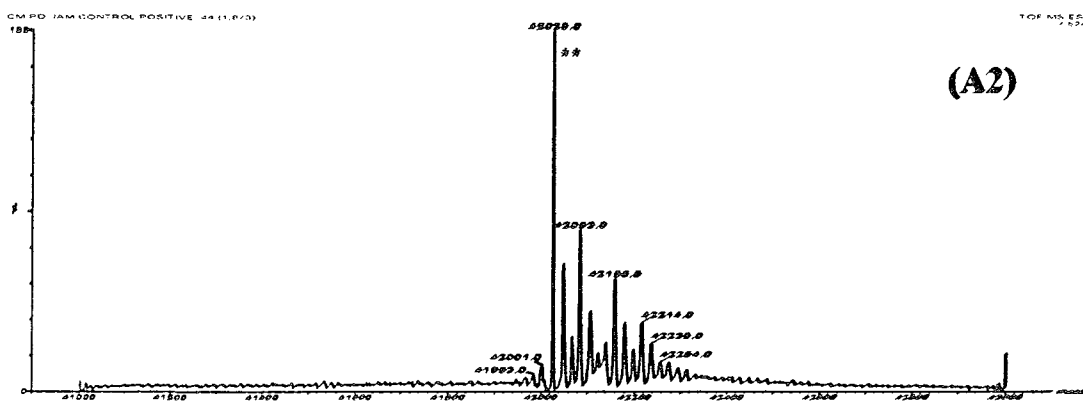
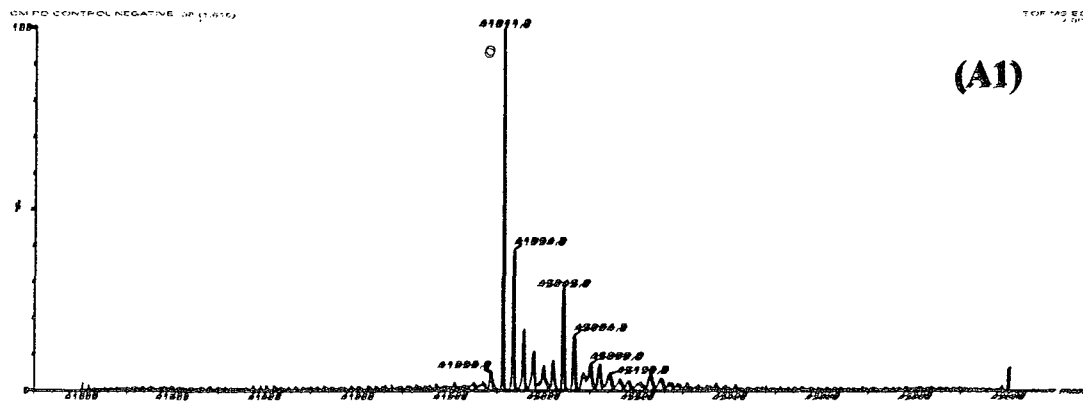
Panel (B1) illustrates the negative control for the Lys37Gln variant CM-PD, where incubations are performed in the absence of IAM and *endo*. This spectrum

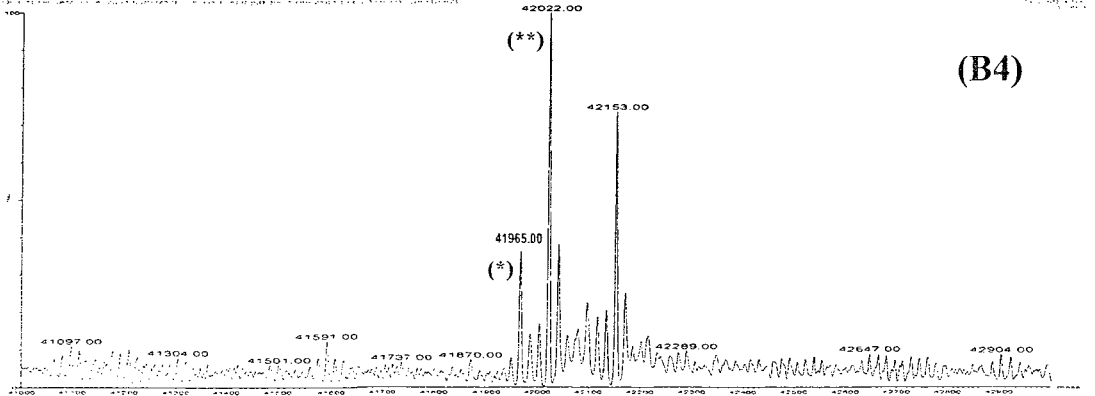
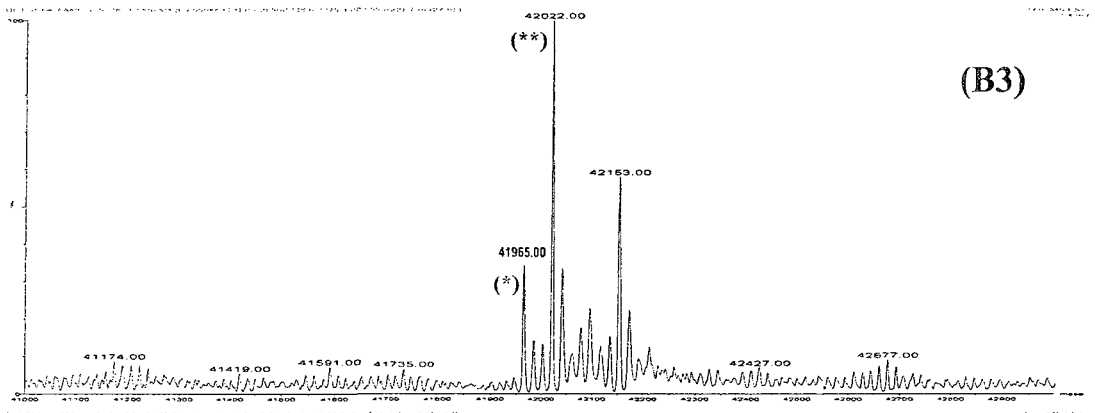
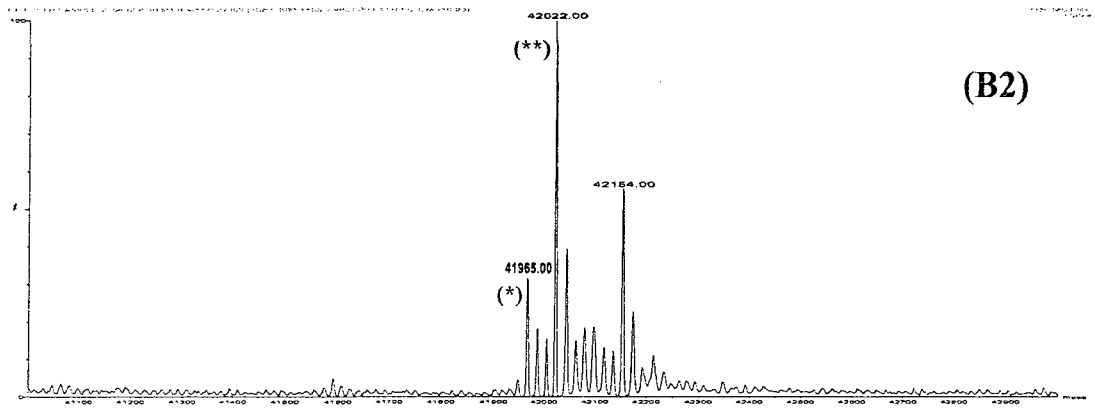
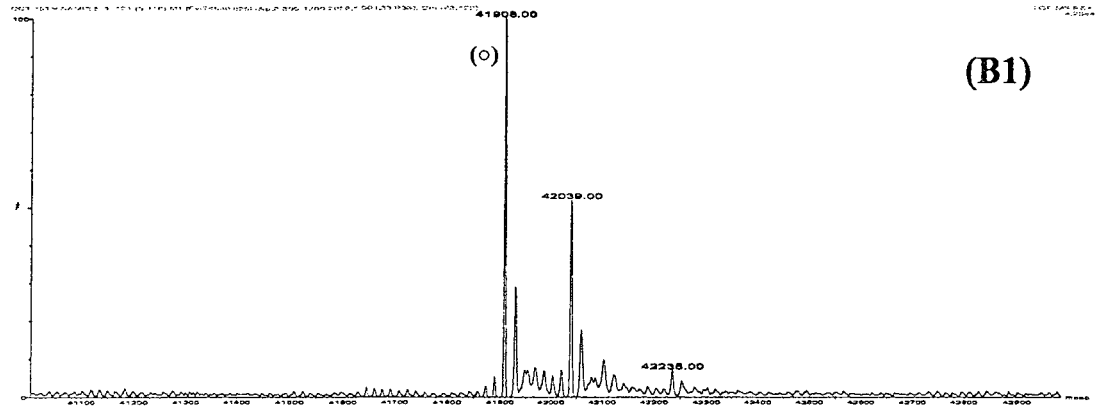
illustrates the 2 peaks expected for the variant, notably at $[M+H^+]$ of 41908 and 42039 amu. Panel (B2) represents the spectrum of the positive alkylation control, where IAM is added and the reaction allowed to proceed for 60 minutes. The peaks of interest at $[M+H^+]$ of 41965 and 42022 amu represent the native variant CM-PD without the N-terminal methionine that has been partially alkylated at 1 site and fully alkylated at 2 sites, respectively, at a peak height ratio of approximately 1.65: 5 (1 site: 2 site alkylation). Panels (B3) and (B4) represent the spectra of the alkylation experiment in the presence of 20 and 200 μM *endo*, respectively. For both 20 and 200 μM *endo*, the spectra are essentially identical to that of panel (B2), where the peak height ratio of the singly alkylated polypeptide at $[M+H^+]$ of 41965 amu is still 1.65: 5 with respect to the doubly charged polypeptide peak at $[M+H^+]$ of 42022 amu.

Figure 3.12: Mass spectrometric analysis of ligand protection experiments for WT and Lys37Gln CM-PD

WT and Lys37Gln variant CM-PD were reacted with 10 mM IAM for 60 minutes at pH 7.2 in order to determine whether the mutase transition state analogue afforded protection from chemical modification by IAM, WT and Lys37Gln variant CM-PD (5 μ M monomer) were incubated for 5 minutes with *endo* at concentrations of 20 and 200 μ M in 3CB at pH 7.2 at room temperature. After 5 minutes, IAM was added to the each enzyme sample to a final concentration of 10 mM and was allowed to react for 60 minutes. Upon completion of the reaction, samples were immediately quenched with DTT at a final concentration of 20 mM. Samples were then processed for ESI-MS analysis as described in section 3.2.9. A negative control was prepared for each sample, where neither IAM nor *endo* was added to the enzyme sample. A positive control was prepared by adding enzyme and IAM to a final concentration of 10 mM and was allowed to react for 60 minutes under identical conditions as reported above and the reaction was quenched with 20 mM DTT. Controls were prepared for ESI-MS analysis as reported in section 3.2.9.

The panel annotations in this figure correspond to (A) WT, (B) Lys37Gln, (1) positive control, (2) negative control, (3) alkylation in the presence of 20 μ M *endo* and (4) alkylation in the presence of 200 μ M *endo*. Peaks of interest are marked as: (°) for native enzyme, (*) for singly alkylated enzyme and (**) for doubly alkylated enzyme.





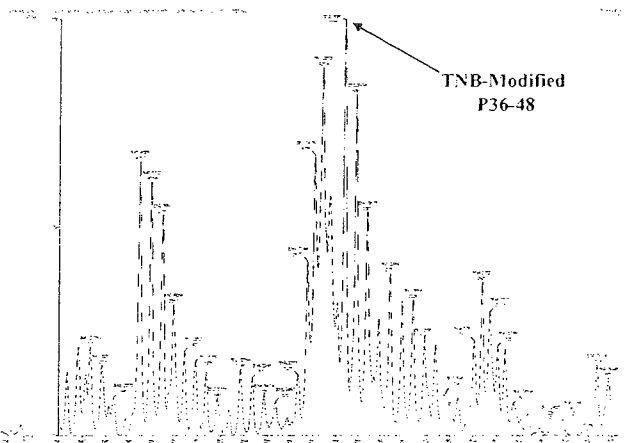
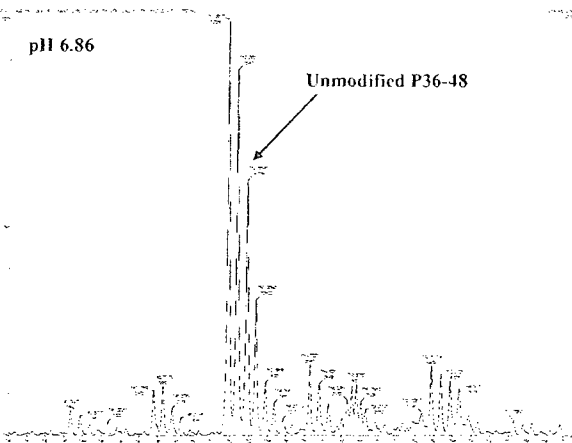
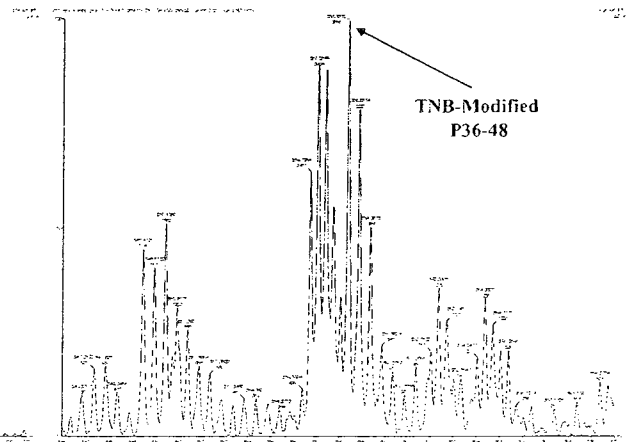
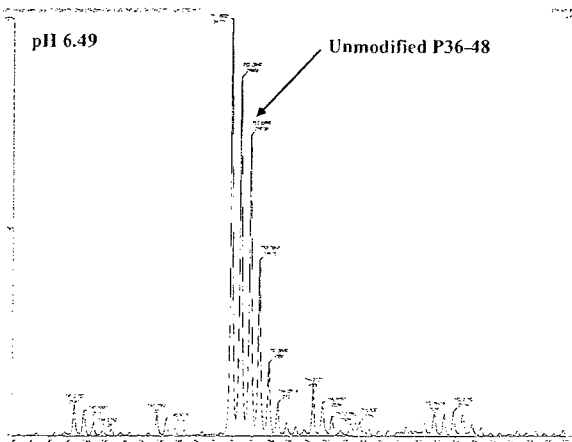
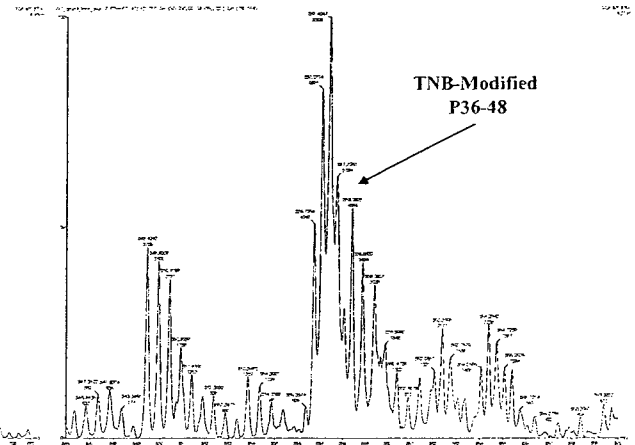
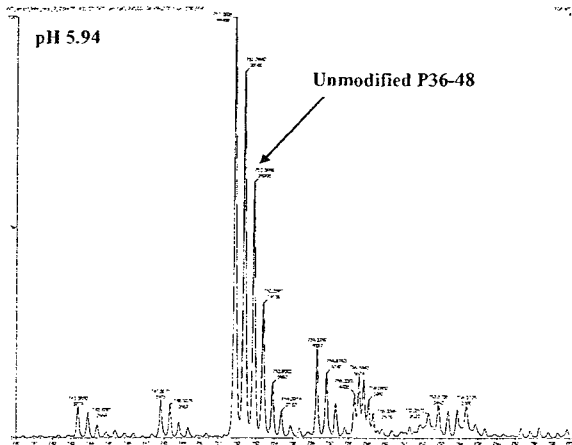
3.3.9 Determination of Lys37 pK_a by Titration with TNBS

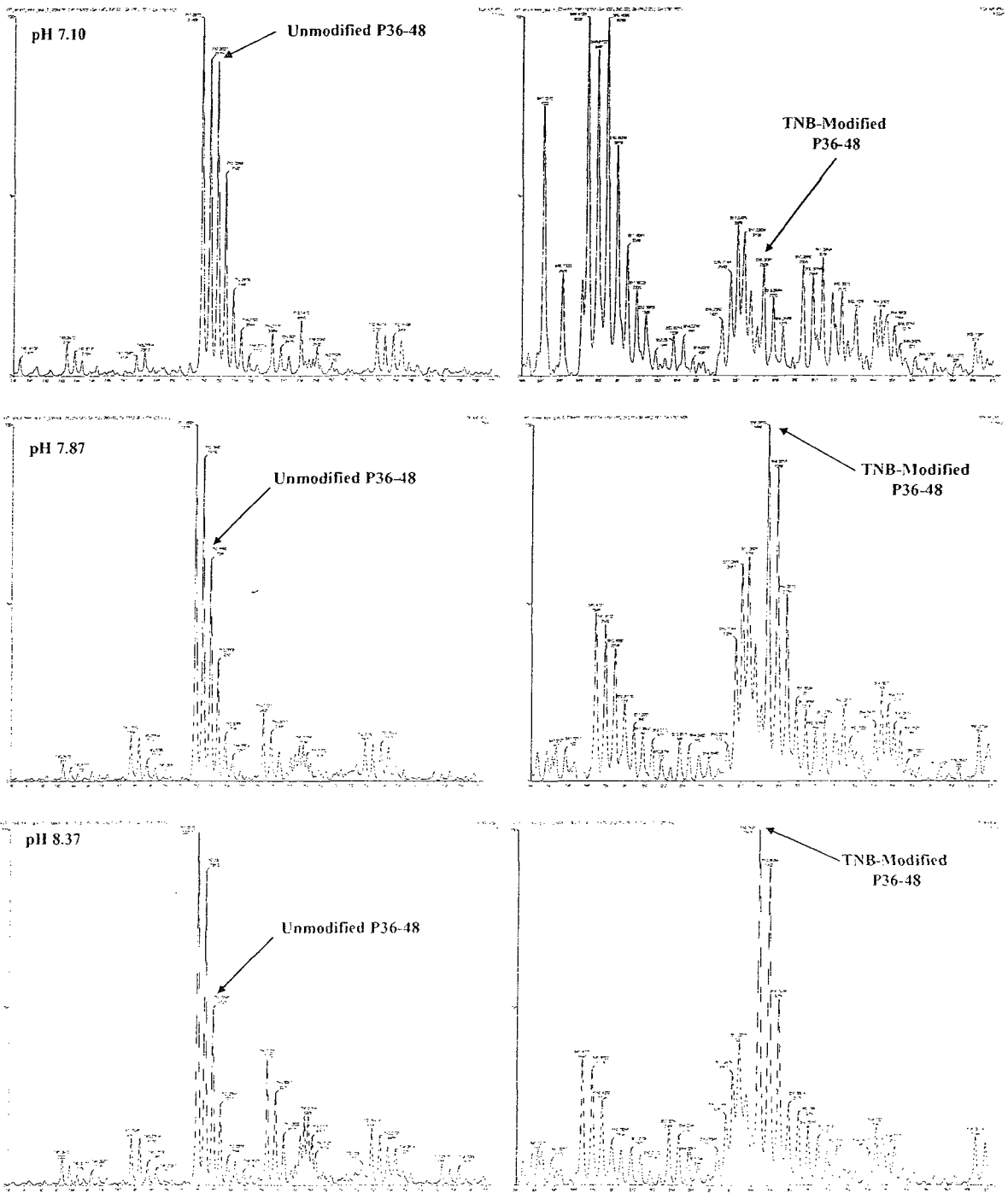
ESI-MS was used to monitor the trinitrophenylation of Lys37 in WT CM-PD (5 μ M monomer) by reaction with 15 μ M TNBS for 10 minutes at various pH values, ranging from 5.94 to 9.26. The parameters of the chemical modification in this experiment allowed us to probe the ionization state and surface accessibility of Lys37 in WT CM-PD. The pH-dependent trinitrophenylation reaction was carried out in a 2 x 3-component buffer (0.1 M 2-morpholinoethanesulfonic acid (MES), 0.1 M N-ethylmorpholine, 0.2 M diethanolamine) at room temperature.

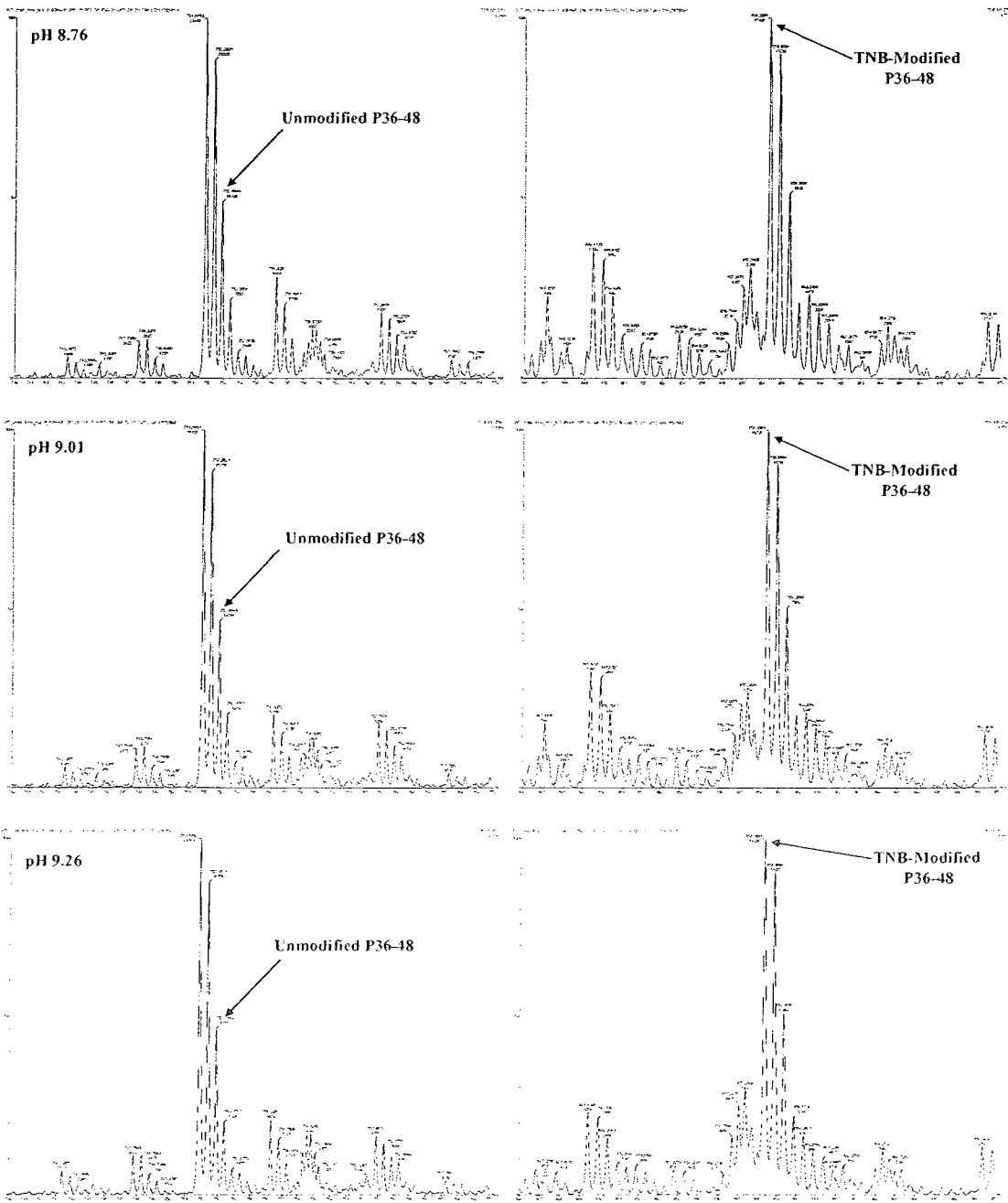
Panels A – H of Figure 3.13 represent the ESI-MS spectra of the GluC-digested WT CM-PD polypeptide after the 10 minute reaction with 15 μ M TNBS at pH values of 5.94, 6.86, 7.10, 7.87, 8.37, 8.76, 9.01 and 9.26, respectively. For all samples, the left panel examines the unmodified P(36-48) peptide, which is observed as a doubly charged peak at $[M+2H^+]$ of 752.9 amu; the right panel examines the trinitrophenylated peptide, which appears as an intense doubly charged peak at $[M+2H^+]$ of 858.4 amu. The intensity of the unmodified P(36-48) decreases and the intensity of trinitrophenylated P(36-48) increases with increasing pH, respectively.

Figure 3.13: ESI-MS Spectra of the GluC-digested WT CM-PD after pH-dependent modification with TNBS

WT CM-PD (5 μ M monomer) was reacted with 15 μ M TNBS for 10 minutes in 2 x 3-component buffer at several pH values ranging from 5.94 to 9.26 at room temperature and protected from light. After 10 minutes, the modification reaction was quenched using 2 M ammonium bicarbonate and samples were then buffer-exchanged into MilliQ water and lyophilized overnight at room temperature. Samples were reconstituted into 30 μ L of 50 mM ammonium bicarbonate (pH 7.8) and were digested using endopeptidase GluC at a ratio of 20:1 WT CM-PD:GluC w/w, overnight at room temperature protected from light. The GluC-digested samples were analyzed by LC-MS, using a linear 40 minute acetonitrile gradient from 5 – 95 % containing 0.1% TFA. Peptides were detected in positive mode from 200 – 3000 amu using the same instrument and parameters as described in section 3.2.9. Figure 3.13 illustrates the ESI-MS spectra of the GluC-digested WT CM-PD, which was trinitrophenylated at pH values of 5.94, 6.86, 7.10, 7.87, 8.37, 8.76, 9.01 and 9.26, respectively. In the left panels, the unmodified P(36-48) peptide is observed as a doubly charged peak at $[M+2H^+]$ of 752.9 amu; in the right panels, the trinitrophenylated peptide appears as an intense doubly charged peak at $[M+2H^+]$ of 858.4 amu.







3.3.10 Determination of Lys37 pK_a in WT CM-PD by Titration with TNBS

The results depicted in the spectra of Figure 3.13 clearly indicate that the extent of trinitrophenylation of Lys37 is pH-dependent. As pH is increased, the ratio of trinitrophenylated to unmodified P(36-48) increases proportionately to pH. The extent of trinitrophenylation was quantified by using the relationship:

$$\frac{\text{Intensity of trinitrophenylated P(36-48)}}{\text{Intensity (native + trinitrophenylated) P(36-48)}}$$

When plotted as a function of the experimental pH values, the data fit well to a single titrating group with a pK_a of 7.68 ± 0.13 (Equation 3.3).

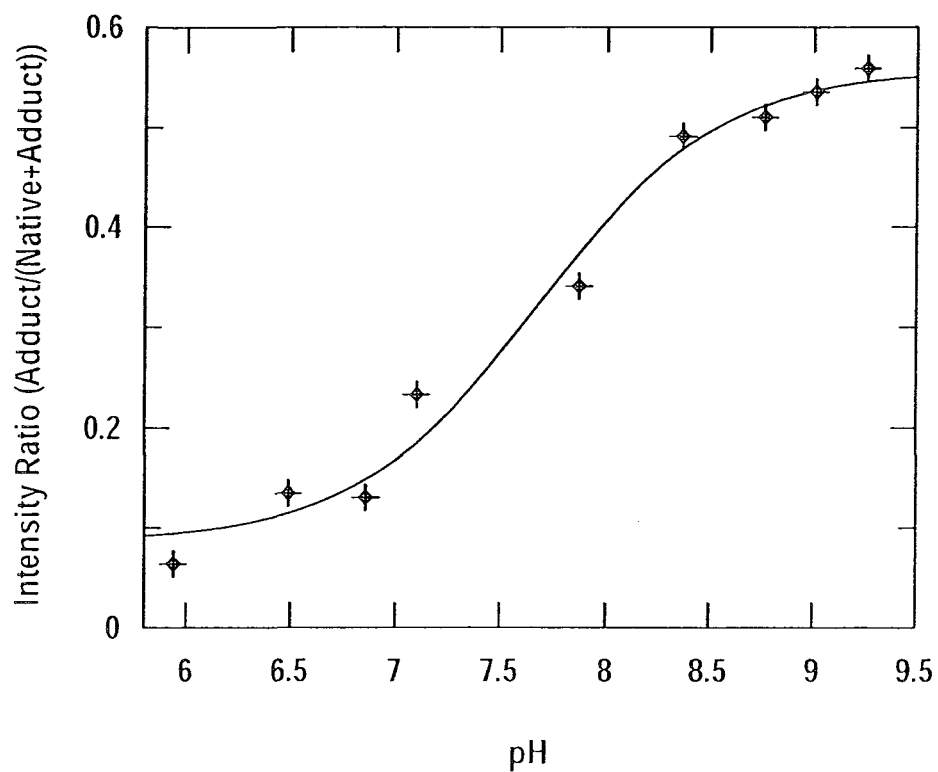


Figure 3.14: Titration of Lys37 in P(36-48) of WT CM-PD by reaction with TNBS for 10 minutes at different pH values

The ratios of (trinitrophenylated P(36-48) / (unmodified P(36-48) + trinitrophenylated P(36-48))) were plotted as a function of experimental pH values. The curve represents the fit of the data to Equation 3.3 using Erithacus Grafit 5.0 software.

3.4 DISCUSSION

The focus of this chapter was to determine the pK_a of a catalytically important residue, Lys37, in the mutase reaction of *E. coli* CM-PD and to further probe the role that it plays in the Claisen rearrangement of chorismate to prephenate. Our goal was accomplished by a combination of chemical modification using the lysine-specific reagent TNBS in tandem with mass spectrometry, kinetic and binding studies on both the WT enzyme and Lys37Gln CM-PD. The work presented in this chapter provides one of the few detailed examples reporting the titration of active site residues using chemical modification in conjunction with peptide mass mapping, and hence outlines the utility of this approach. Krekel *et al.* (151) demonstrated by MS analysis that Cys115 of *Enterobacter cloacae* MurA was only alkylated by IAM at pHs > 7. Measurement of the enzymatic inhibition by IAM as a function of pH revealed a $pK_a \sim 8.3$.

Christendat and Turnbull (38) previously reported that Lys37 in WT CM-PD is very reactive based on the results of chemical modification experiments with diethylpyrocarbonate (DEPC); DEPC is a histidine-specific modifier and does not usually react with lysine residues unless they are partially or fully deprotonated.

In agreement with the histidine results of Christendat *et al.* (39), we show that the Lys37Gln mutation abolishes mutase activity while not affecting dehydrogenase activity (Table 3.2) and hence is in accord with the crystal structure of the homologous “mini-mutase” from CM-PDTase, which clearly shows that this lysine residue can stabilize the ether oxygen in the transition state of the reaction (Figure 1.6).

Similarly, site-directed mutagenesis of homologous residues of CM in other organisms results in enzymes that are inactive or show low activity. These results confirm the importance of Lys37 in the mutase activity of CM-PD (39). The possibility arises that a substitution of Lys37 (or an analogous residue) affects binding of chorismate, or catalysis, or both.

Since Lys37Gln possesses no mutase activity kinetic studies cannot be used to establish its role. Binding studies were performed by fluorescence spectroscopy in order to determine the dissociation constants (K_d) of the transition state analogue for both the WT and Lys37Gln variants. CM-PD possesses 5 tryptophan and 10 tyrosine residues per monomer; only 2 tyrosine residues are located in the mutase domain at positions 45 and 83 and they are within 4.5 Å of the binding site of the transition state analogue as deduced by a model of the mutase domain from CM-PD generated using the structure of the “mini-mutase” as the template. Decreases in fluorescence intensity of emission (λ_{ex} 280 nm) in the presence of increasing concentrations of *endo* were observed for both WT and Lys37Gln CM-PD from which the dissociation constants for the interaction of the enzyme with *endo* could be calculated. WT CM-PD binds the transition state very tightly with a dissociation constant of $0.05 \pm 0.01 \mu\text{M}$, whereas the *endo* K_d for the Lys37Gln variant is $0.51 \pm 0.04 \mu\text{M}$. Our experimentally determined dissociation constant for *endo* for the WT CM-PD is similar to the K_i of $0.062 \mu\text{M}$ reported in Chapter 2 and in the same range with the K_i of $0.11 \mu\text{M}$ previously reported by Turnbull *et al.* (14). These results indicate that although the variant is devoid of all mutase activity, it surprisingly appears to be able to bind the transition state analogue, albeit 10-fold less tightly than the WT.

The ability of the Lys37Gln variant to bind *endo* was further tested by examining the ability of the transition state analogue to protect against the alkylation of cysteine residues. Mekhssian (143) had previously shown that incubation of the Lys37Gln variant with 25 and 200 μM *endo* did not prevent the loss of dehydrogenase activity from alkylation with IAM (presumably because the mutant could not bind *endo*), whereas both concentrations of *endo* afforded full protection of the mutase activity in WT enzyme. Furthermore, we demonstrated in Chapter 2 that loss of activity was due to the chemical modification of Cys215, which might place the cysteine near the mutase active site where the transition state analogue binds. The results of mass spectrometric ligand protection studies (Figure 3.12) revealed that 200 μM *endo* partially protected a single cysteine residue in WT CM-PD from alkylation (likely Cys215) judging by the appearance of a singly alkylated polypeptide peak at $[M+H^+]$ of 41968 amu in addition to the doubly alkylated polypeptide at $[M+H^+]$ of 42025 amu. In contrast, in absence of ligand, the Lys37Gln variant was alkylated at two sites (Cys95 and Cys215) and the addition of 200 μM *endo* did not prevent alkylation. Taken all together, the results of ligand protection experiments by kinetic and mass spectrometric studies, in parallel with the dissociation constants for *endo* determined by fluorescence spectroscopy, confirm that binding of *endo* to Lys37Gln is decreased/abolished relative to WT CM-PD. However, the 10-fold decrease in the K_d of *endo* binding in the Lys37Gln variant may simply be the result of binding at a site other than the mutase active site or perhaps binding to an alternative conformation of the enzyme under these experimental conditions.

The pH dependence of the $V/K_{\text{chorismate}}$ for the mutase reaction is bell-shaped and reveals that a group with a $\text{p}K_a \sim 7.5$ must be protonated for binding of chorismate to the

free enzyme. This agrees with the studies of Turnbull (72) who showed that a group with a $pK_a \sim 7.5$ must be protonated to assist in the binding of chorismate or the transition state analogue. Furthermore, it is possible that the group is also important for catalysis but does not titrate in the V profile if only the protonated form of the residue can bind the substrate. If this residue is Lys37, then it has a markedly depressed pK_a and would be very reactive at neutral pH.

Previous studies performed by Mekhssian (143) on the modification of CM-PD by the lysine-specific reagent TNBS showed that under pseudo-first order conditions of reagent to enzyme (30-75 fold excess reagent to enzyme monomer concentration), complete inactivation of mutase activity was too rapid to be monitored accurately. In addition, the biphasic time-dependent mutase inactivation profile suggested that more than one reactive group was being trinitrophenylated. Lower concentrations of TNBS were thus used for all studies involving mutase inactivation (3-fold excess of reagent to monomer). Similarly, 25% glycerol was used to increase the reaction solution density and hence slow down the rate of inactivation of the enzyme.

Hence, in the present study, the reactivity of Lys37 was investigated with TNBS under near-stoichiometric conditions at neutral pH (section 3.2.10) and in the presence of 25% glycerol. Since the pK_a of lysine in solution is above 10 and trinitrophenylation occurs on deprotonated ϵ -amino groups, only very reactive lysine residues should react at this pH. Figure 3.7 illustrates the results of this chemical modification and indicates that there is a time-dependent loss of 80% of mutase activity after 45 minutes. Further investigation revealed that under identical conditions, a single lysine residue out of 15 total lysine residues per monomer is trinitrophenylated in the time frame of the

experiment. These results imply that loss of mutase activity correlates with the trinitrophenylation of a single lysine residue. This suggests that this lysine residue is either critical in the mutase reaction or may be spatially near to a residue that is critical. Additional protection experiments reported previously by Mekhssian (143) indicated that incubation of WT CM-PD with stoichiometric amounts of *endo*-oxabicyclic diacid inhibited the time-dependent inactivation by TNBS and hence prevented the trinitrophenylation of a residue that is important for the catalytic mechanism of the mutase reaction. This result is not surprising since *endo* mimics the proposed transition state for the chorismate mutase reaction (59) and binds tightly with a K_i of 0.062 μM . Similarly, preincubation of the enzyme with the product of the mutase rearrangement (prephenate) protected from inactivation of mutase activity.

A similar chemical modification experiment performed with the Lys37Gln variant enzyme did not exhibit any loss in dehydrogenase activity, suggesting that no lysine residues are involved in the dehydrogenase reaction or none were reactive/accessible under our experimental conditions (Figure 3.2). In contrast, Turnbull *et al.* noted a loss of dehydrogenase activity of approximately 40% for the WT CM-PD. However, this may be a consequence of the longer exposure to 20-fold molar excess of reagent to monomer CM-PD that was used compared to 45 min incubation with 3-fold excess used in the present study. It is worth noting that TNBS can react slowly with cysteine residues (148, 151), although this seems unlikely in the present studies since modification of cysteine

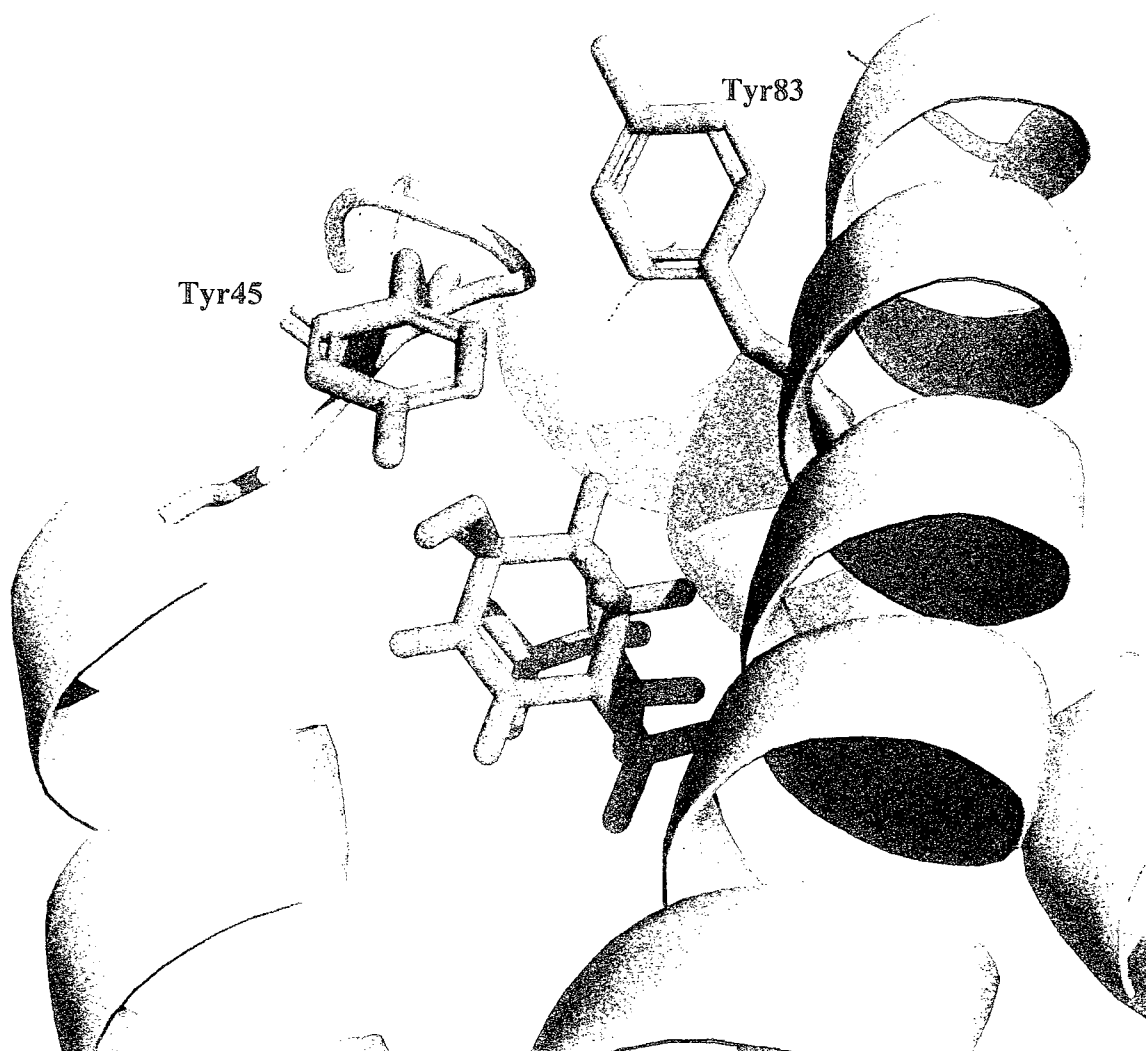


Figure 3.15: Schematic representation of the mutase active site in the *E. coli* CM-PD model

Close-up of the *E. coli* model CM active site. Tyrosine residues are in orange and the transition state analogue (*endo*) is in blue. The model of the mutase portion of *E. coli* CM-PD was generated as described in section 3.2.18; the image was created using the PyMol software.

residues by sulfhydryl-specific reagents is expected to inactivate both mutase and dehydrogenase activities.

ESI-MS was used to verify the stoichiometry of trinitrophenylation. Figure 3.3 illustrates the deconvoluted mass spectra of the trinitrophenylated sample after 15 minutes and exhibits two sets of peaks; the first set corresponding to the 2 forms of the native enzyme at $[M+H^+]$ of 41913 and 42043 amu and the second set, shifted by +211 amu, at $[M+H^+]$ of 42123 and 42254 amu, corresponding to the native enzyme with a single TNBS adduct, hence confirming the results reported above.

Digestion was performed on the trinitrophenylated enzyme using endopeptidase GluC, in order to pinpoint the site of trinitrophenylation upon chemical modification. The peptide containing Lys37, P(36-48), was identified as a doubly charged peak $[M+2H^+]$ at 752.90 amu and the trinitrophenylated form of P(36-48), which was expected at $[M+2H^+]$ of 858.37 amu was only detected for the chemically modified enzyme. Further ESI-MS/MS peptide sequencing of this peptide P(36-48) confirmed the expected amino acid sequence as being **VK(TNB)SRFGLPLYVPE**, with the trinitrophenylation occurring on the Lys37 residue (Figure 3.6). It is worthy mentioning that in the sequence determined by MS/MS, the residue reported at position 44 is a leucine, whereas the known amino acid at that position from the amino acid sequence of CM-PD is an isoleucine. This is due to the fact that there is no change in molecular weight for the respective residues and should have no impact on the identification of the peptide and site of trinitrophenylation.

The above-mentioned data allowed for the identification of a single lysine residue whose trinitrophenylation abolishes mutase activity at neutral pH. The reactivity and hence the changes in the rate of inactivation with pH would shed light on the ionization

state and hence allow for the determination of the pK_a of Lys37. Figure 3.7 illustrates the pH-dependent inactivation of mutase activity upon chemical modification by TNBS, which has been reported to be stable under alkaline conditions (123). These results clearly indicate that the rate of inactivation increases with increasing pH and thus correlates with the deprotonation of the ϵ -amino group of Lys37. By fitting the experimentally determined apparent rates of inactivation (k_{app}) with pH, to Equation 3.3 for a single titrating residue, we were able to determine that the pK_a of Lys37 is 7.69 ± 0.08 . This result suggests within reasonable error, that Lys37 is the residue identified in the mutase pH-rate profile that must be protonated for mutase activity (Figure 3.9).

ESI-MS was used to monitor the trinitrophenylation of Lys37 in WT CM-PD (5 μ M monomer) by reaction with 15 μ M TNBS for 10 minutes at various pH values, ranging from 5.94 to 9.26. Figure 3.13 represents the ESI-MS spectra of the GluC-digested WT CM-PD polypeptide after the 10 minute reaction with 15 μ M TNBS at pHs 5.94, 6.86, 7.10, 7.87, 8.37, 8.76, 9.01 and 9.26, respectively. A trend is clearly visible in the spectra, wherein the intensity of the unmodified P(36-48) at $[M+2H^+]$ of 752.90 amu decreases and the intensity of trinitrophenylated P(36-48) at 858.37 amu increases with increasing pH. The results depicted in Figure 3.13 clearly indicate that the extent of trinitrophenylation of Lys37 is pH-dependent; as pH is increased, the ratio of trinitrophenylated to unmodified P(36-48) increases proportionately to pH. The pH-dependent trinitrophenylation was quantified using Equation 3.3 for the titration of a single residue which yielded a pK_a for Lys37 in the WT CM-PD of 7.68 ± 0.13 .

The results of the studies reported in this chapter have provided evidence that Lys37 is likely the residue that titrates at pH 7.5 in the $V/K_{chorismate}$ profile. At

physiological pH, this residue is protonated but readily capable of donating a proton. The biophysical reasons for the major shift of the pK_a of Lys37 to 7.5 from 10 in solution are unclear and must hence be inspected. Careful examination of a model of the mutase domain of the bifunctional CM-PD of *E. coli* complexed with *endo*, using the CM domain of *E. coli* CM-PDT as a structure template reveals several charged amino acid residues in proximity to Lys37, which may affect its ionization state. As shown in Figure 3.17, the net negatively charged residue Glu50 is at 7.65 Å. Interestingly, the side chain of Glu86 (4.76 Å) has been proposed to be protonated in order to interact with the ether oxygen of the transition state analogue. The positively charged residues in the vicinity of Lys37 are Arg26 (10.69 Å), Arg49 (7.24 Å), Arg57 (15.97 Å) and Lys89 (8.20 Å). Arg11', which has also been implicated in the binding of the carboxylate moiety of *endo* at C₁₁, originates for the second monomer of the mutase dimer in *E. coli* CM-PDT and is 4.48 Å from the ϵ -amino group of Lys37. Honig and Nicholls (152) have reported that electrostatic interactions operate over long ranges; they suggest that a single charged amino acid 10 – 20 Å away can have a net effect on the pK_a of a titratable group. Hence, the combined effect of multiple charged residues could conceivably induce a much larger perturbation in pK_a . It is noteworthy to mention that Lys37 is present near the C-terminus of a long helix (4 – 40) and a protonated form may stabilize the δ^- charge at that site.

A possible role for Lys37 in the mechanism of the mutase reaction is shown in Figure 3.16. In this mechanism, groups involved in binding may also participate in catalysis. The ϵ -amino group of Lys37 may form a hydrogen bond with the ether oxygen of *endo*; the participation of Lys37 in catalysis would involve the protonation of the ether oxygen, which would facilitate the cleavage of the C₅-O bond and subsequently, the

nucleophilic attack on C₁ by the electron pair of the endolpyruvyl side chain of chorismate (36). Thus, a reduced p*K*_a would facilitate Lys37's function as a hydrogen bond donor.

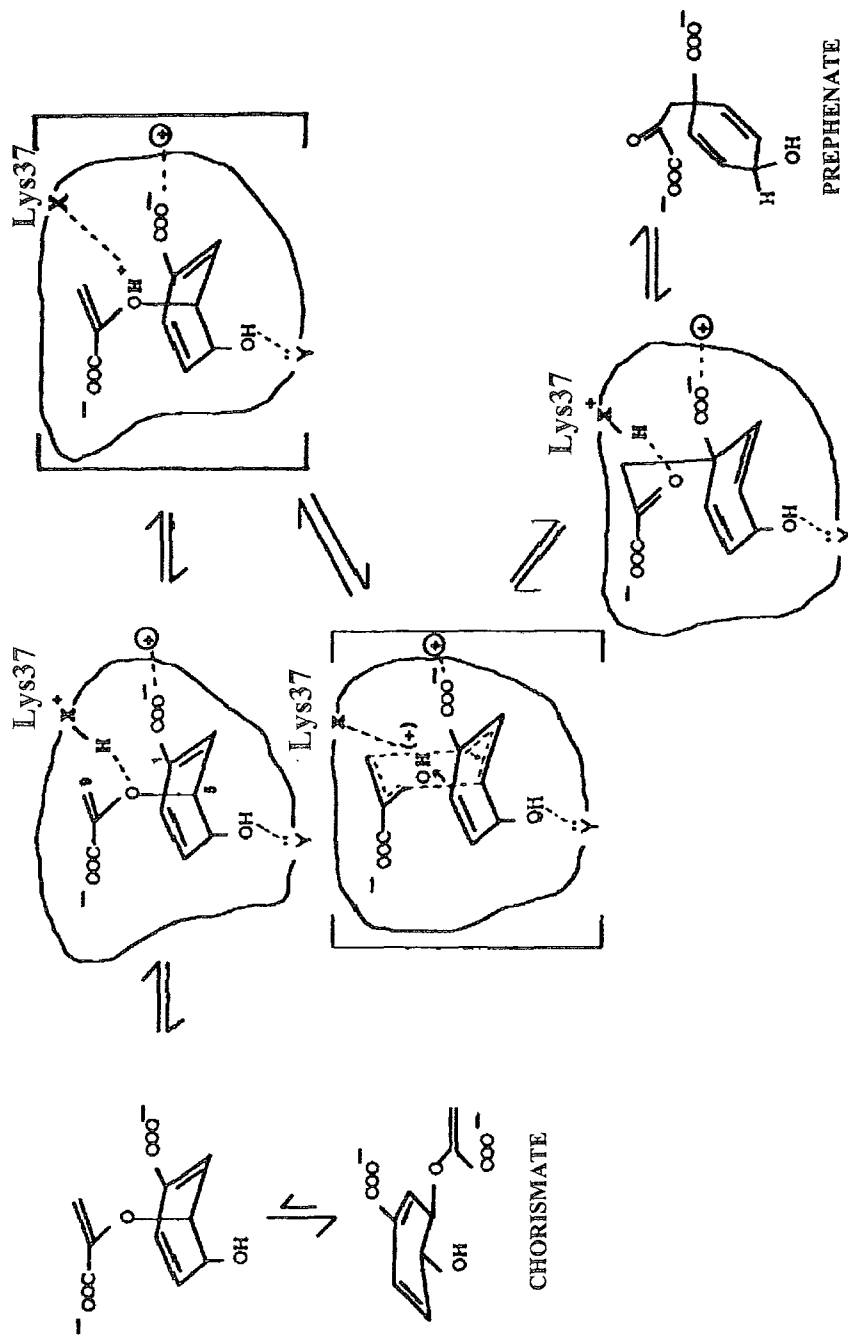


Figure 3.16: Possible mechanism for the chorismate mutase mechanism

Lys37 binds the diaxial form of chorismate and protonates the ether oxygen. This subsequently causes the cleavage of the C₅-O bond and allows for the formation of the C₉-C₁ bond through the transition state complex (36).

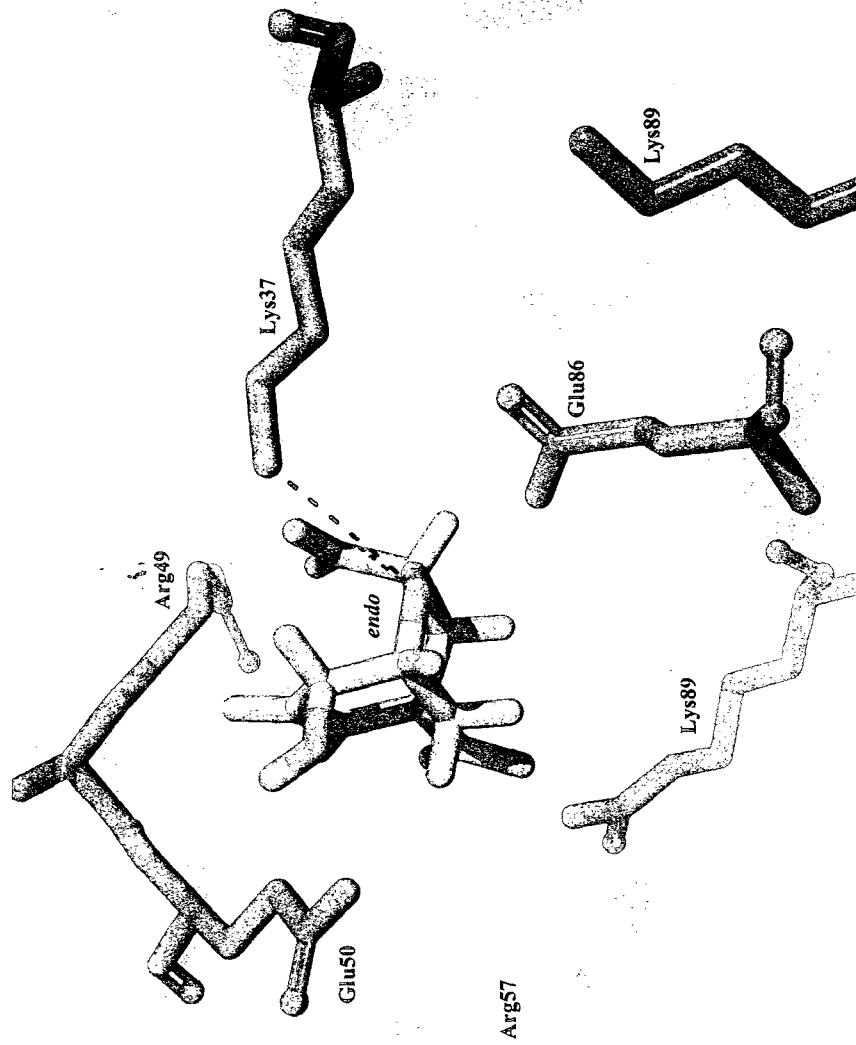


Figure 3.17: Illustration of mutase active site in the monomer model of *E. coli* CM-PD

The CM domain of *E. coli* CM-PD was modeled using the crystal structure of the CM domain of *E. coli* (PDB ID: 1ecm) as described in section 3.2.18. This image was created using PyMol software.

Chapter 4

Investigating the Ionization State of Active Site Cysteine Residues
in the Catalytic Trimer of *E. coli* Aspartate Transcarbamylase

4.1 INTRODUCTION

The catalytic subunit of aspartate transcarbamylase in *E. coli* is composed of three identical polypeptide chains, each possessing a single cysteine residue at position 47. Sequence alignments reported in this chapter indicate that this residue is not conserved, since it is frequently replaced by methionine as well as other non-polar amino acids.

Earlier studies on the WT CSU performed by Vanaman and Stark (105) indicated that Cys47 is not reactive towards small, cysteine-specific alkylating agents, but was somewhat reactive toward the bulkier reagents DTNB and p-hydroxymercuribenzoate. Chemical modification of the WT CSU by DTNB resulted in a time-dependent loss of activity. Moreover, inorganic phosphate and succinate, competitive inhibitors of the ATCase reaction, afforded protection against inactivation by chemical modification, exhibiting K_i values of 1.5 and 37 mM, respectively, which were in agreement with previously reported results (153, 154). Derivatization of the DTNB-modified CSU using nucleophiles, restored activity for the most part, suggesting that the Cys47 residue is in or very near the active site. Subsequent experiments which followed the pH-dependence of DTNB modification determined the apparent pK_a of Cys47 to be ~ 7.9 . This depressed pK_a led to the hypothesis that the Cys47 thiol group must be near a cluster of cations.

Previous studies have indicated that Ser52 is critical for binding of carbamyl phosphate, in agreement with the crystal structure of the enzyme bound with PALA (Figure 1.13) As expected, an Ala substitution at position 52 caused a decrease in activity, decrease in ability to bind PALA and carbamyl phosphate, but also, surprisingly, an increase in thermal stability (108, 109). Interestingly, the decrease in catalytic and

binding efficiency as well as increase in thermal stability were further magnified with the substitution with a cysteine at position 52 (109, Turnbull unpublished). These results allowed for speculation that this group is present in the active site and that the unusual properties caused by the Ser to Cys substitution are a consequence of a negative charge on the Cys52 sulfhydryl group.

The aforementioned results lay the groundwork for the present chapter. Here, we describe an improved method for the isolation of CSU from His-tagged ATCase holoenzyme, consisting of a one step Nickel affinity chromatography in conjunction with the treatment of column-bound holoenzyme with the mercurial reagent neohydrin. The purified CSU was assayed for residual mercury by mass spectrometry. We also determined the ionization state of Cys52, since the presence of the thiolate anion at position 52 may be the underlying cause of the observed kinetic and biophysical characteristics of the variant CSU. Chemical modification and mass spectrometric studies were performed on WT and Cys52 CSUs to determine the reactivity of both cysteine residues and to determine the pK_a of Cys52's sulfhydryl group. Using the structural information available for the catalytic trimer of ATCase, we propose why the pK_a of Cys52 is unusually low.

4.2 EXPERIMENTAL PROCEDURES

4.2.1 Materials

Both WT and Ser52Cys ATCase holoenzymes were expressed as recombinant proteins with an engineered hexa-histidine tag on the N-terminus of their respective regulatory chains. His-tagged WT ATCase holoenzyme, a gift from Dr. H.K. Schachman, was obtained from *E. coli* HS1061 containing plasmid pax4 which encompasses the *pyrB* and *pyrI* genes, and which encode the c and r chains of ATCase, respectively. His-tagged Ser52Cys ATCase holoenzyme was obtained from HS533 *E. coli* strain HS533, which was constructed by Dr. J. Turnbull while on sabbatical in the lab of Dr. H.K. Schachman at the University of California, Berkeley. In this latter strain, endogenous ATCase and ornithine transcarbamylase have been inactivated. DTNB (5,5'-dithiobis(2-nitrobenzoate)), iodoacetamide (IAM), chloroacetamide (CIAM) and imidazole were purchased from Sigma. Dialysis membranes (10 kDa MWCO) were purchased from Fisher Scientific. Biomax centrifugal concentrators (10 kDa MWCO) were purchased from Millipore, while size-exclusion NAP-5 columns were purchased from Amersham Pharmacia Biotech. Ni-NTA Superflow resin was purchased from Qiagen. Bradford dye reagent was purchased from Biorad. Protein molecular ladder used for SDS-PAGE was obtained from Fermentas Life Sciences. Neohydrin was synthesized as reported by Rowland *et al.*(155) and was stored in 50 mg aliquots until use. All other chemicals were purchased at the highest quality commercially available.

4.2.2 Expression and Purification of WT ATCase CSU

An agar stab of the permanent bacterial stock of the recombinant strain HS1061 of *E. coli* was inoculated into 50 mL LB medium supplemented with 100 µg/mL ampicillin in a rotating incubator shaker (225 rpm) at 37°C for 12 – 16 hours. The inoculated HS1061 culture was then streaked onto an LB/agar plate supplemented with 100 µg/mL ampicillin. The streaked plate was incubated overnight at 37°C. A single colony was then selected and inoculated overnight in 50 mL LB medium supplemented with 100 µg/mL ampicillin in a rotating incubator shaker (225 rpm) at 37°C. Ten mL of this culture were then inoculated overnight into each of two Fernbach flasks each containing 1.5 L of LB medium supplemented with 100 µg/mL ampicillin and the cultures were additionally incubated with shaking (225 rpm) at 37°C. Cells were then harvested by centrifugation at 10000 rpm for 30 minutes at 4°C. The bacterial pellet was kept at -20°C until ready for further processing. The cells were later resuspended in about 90-100 mL of sterile and chilled phosphate buffer (50 mM NaH₂PO₄, 0.3 M NaCl, 20 mM imidazole pH 8.0). The cells were lysed by sonication using a Branson/VWR sonicator on setting 3. Samples were subjected to six bursts of 15 seconds each with one minute on ice between bursts. The lysate was subsequently clarified by centrifugation at 90 000g for at least 30 minutes at 4°C using a Beckman ultracentrifuge.

The purification of CSU was performed as described by Yang *et al.* (156) with specific modifications, which included the elimination of an ion-exchange chromatography step and the inclusion of neohydrin treatment Nickel affinity resin-bound holoenzyme. Briefly, the cleared lysate was applied to a glass column containing 25 mL of Qiagen Ni-NTA Superflow resin previously washed and equilibrated with the

phosphate buffer mentioned above in order to bind the His-tagged holoenzyme. Protein was allowed to bind to the affinity resin by recirculating the supernatant through the column using a peristaltic pump for 1.5 hours at 4°C. The resin was then washed with about 150 mL of phosphate buffer and the flow-through was collected in 10 ml aliquots. The presence of protein was verified by monitoring the increase in absorbance at 280 nm and the protein was quantified by the Bradford assay. The amount of His-tagged holoenzyme bound to the resin was then determined by subtracting the amount of protein in the wash from the total protein initially found in the supernatant. In order to separate the holoenzyme subunits, neohydrin dissolved in phosphate buffer mentioned above, was added to the column dropwise with gentle swirling; 30 mg neohydrin was used for each 100 mg of holoenzyme (double the amount suggested by Yang *et al.* (156)). Neohydrin was allowed to react for 45-60 minutes while slowly rotating the column at 4°C. After the reaction, the resin was allowed to settle by gravity and 4 mL aliquots of eluate were collected. DTT was added to each aliquot to a final concentration of 10 mM. The resin was then washed with 60 mL of 10 mM Tris, 0.1 M KCl buffer (pH 8.7) and subsequent 4 mL fractions were collected. These fractions were examined for the presence of CSU by monitoring the absorbance at 280 nm. The samples containing CSU were pooled and dialyzed overnight at 4°C in 2 L 10 mM Tris (pH 8.7) with 1 mM DTT, in order to remove imidazole. The dialyzed sample was dialyzed once again overnight in 4 L of 3.6 M ammonium sulphate (pH 7.0) with 10 mM β -mercaptoethanol at 4°C. The protein was stored as an ammonium sulphate precipitate at 4°C until further.

Elution of the bound RSU and remaining holoenzyme was performed using imidazole at a concentration of 250 mM. Imidazole was subsequently dialyzed away in

4 L of 10 mM Tris (pH 8.7) with 1 mM DTT. Subsequently, 5 mM zinc acetate was added in order to refold RSU to its native conformation and avoid precipitation. The dialyzed sample was dialyzed once again overnight in 4 L of 3.6 M ammonium sulphate (pH 7.0) with 10 mM β -mercaptoethanol at 4°C. The protein was stored as an ammonium sulphate precipitate at 4°C until ready for use.

4.2.3 Expression and Purification of Ser52Cys ATCase CSU

Expression and purification of Ser52Cys ATCase holoenzyme was performed using the recombinant strain HS533 of *E. coli*. The procedures for expression and purification were exactly as those reported for WT ATCase holoenzyme in section 4.2.2.

4.2.4 Determination of Protein Concentration

Protein concentrations were estimated using the Bio-Rad Protein Assay Kit (Bio-Rad Laboratories) (134) and bovine serum albumin (BSA) (Sigma) as the standard protein. BSA was dissolved in 10 mM Tris-HCl (pH 7.4), filtered using a 0.2 μ m syringe-driven filter to remove any particulates and its concentration was determined spectrophotometrically at 280 nm using $\epsilon_{280\text{nm}}$ 0.667 mg/mL (157).

4.2.5 Polyacrylamide Gel Electrophoresis of Proteins

Denaturing SDS-PAGE was performed using 10% polyacrylamide gels as described in section 2.2.4 for CM-PD.

4.2.6 Electrospray Ionization Mass Spectrometry (ESI-MS)

Both WT and Ser52Cys CSU protein samples were prepared for ESI-MS analysis by adapting the procedure reported by Weinglass *et al.* (136) and as reported for CM-PD in section 2.2.8. The sample was applied to a Micromass Q-ToF 2 triple-quadrupole mass spectrometer by direct infusion at a flow rate of 1.0 $\mu\text{L}/\text{min}$. Samples were analyzed in positive ion mode scanning over a m/z range of 500 - 2500. A spray voltage of 3.5 kV and a cone voltage of 35 V were used. No auxiliary gas was used. The data were generated and analyzed using Micromass MassLynx v 4.0 software. The instrument was calibrated with [Glu]-fibrinopeptide B in the same solvent system as that used for analysis of ATCase CSU. In all mass spectra, the x-axis represents mass (amu) and the y-axis % relative intensity to most intense peak in spectrum.

4.2.7 ICP-MS for Detection of Mercury in CSU Sample

All materials used for the handling and preparation of ICP-MS samples were made of polypropylene; these materials were soaked overnight in trace metal free 7% HNO_3 , rinsed with MilliQ water and dried in an incubator at 37°C before use. Metal-free 100 mM Tris buffer (pH 8.7) was prepared by chelation of metal ions using Chelex®100 resin. CSU was diluted into 100 mM Tris buffer (pH 8.7) and was then buffer exchanged using a NAP-5 size exclusion column to a final concentration of about 1 mg/ml. A 500 μL aliquot of the sample was mixed with 143.7 μL of 10% HNO_3 and 356.3 μL of MilliQ water and the sample was then allowed to digest overnight at 60°C. The sample was then diluted 10-fold in MilliQ water to a final volume of 3.5 mL for sample reading. The bound metals were evaluated using the helium mode reaction cell (in order to decrease

non-specific signal by decomposing molecules into its basic elements). External calibration was used in a range of 1 ppb to 1 ppm with the 202 amu mercury isotope in metal-free 1% HNO₃. The amount of mercury bound to the enzyme was back-calculated from the linear regression generated from the standard solution calibration curve. Sampling rate was 300 µL/minute using a peristaltic pump.

4.2.8 Sample Preparation of Ammonium Sulfate Precipitated ATCase CSUs

An aliquot of ammonium sulfate precipitated ATCase CSU from section 4.2.2 was placed in a 1.5 mL Eppendorf tube. The precipitate was centrifuged at 14000 rpm at 4°C for 5 minutes. The supernatant was removed and 400 µL of appropriate buffer was added. The precipitated sample was dissolved in the buffer by repeated gentle aspiration and release using a micropipettor. The sample was then centrifuged at 14000 rpm at 4°C for 5 minutes in order to clarify the solution from particulate matter. In order to remove any traces of mercury potentially bound to the catalytic chains, samples were treated with 10 mM EDTA and 20 mM DTT for 30 minutes on ice prior to buffer exchange or concentration.

Buffer exchange was performed using either a NAP-5 size exclusion column or a BIOMAX centrifugal concentrator (10 kDa MWCO).

For exchange via a NAP-5 column, 10 mL of the intended buffer is used to equilibrate the column. A 500 µL aliquot of the sample is passed through the column. Once the 500 µL sample had eluted, 1 mL of buffer is applied into the column and the eluate is collected into a 1.5 mL Eppendorf tube.

For buffer exchange/concentration using a BIOMAX centrifugal concentrator, the dissolved sample is placed in the concentrator tube which had previously been conditioned with the appropriate buffer. It is then centrifuged at 12000 rpm using a benchtop centrifuge at 4°C until the sample reached an approximate volume of 100 µL. Additional buffer is added to the sample up to a final volume of approximately 500 µL. The sample is then centrifuged once again as mentioned earlier. This step is repeated two more times in order to exchange the solvent completely into the intended buffer as well as to concentrate the protein.

4.2.9 WT ATCase CSU Multiple Sequence Alignments

Multiple sequence alignments were performed on the amino acid sequence of the WT ATCase CSU from *E. coli* using the web-based software ClustalW (www.ebi.ac.uk/clustalw/) (158, 159). The amino acid sequences of 13 diverse species were used for these alignments and consisted of the sequences of *Escherichia coli*, *Campylobacter jejuni* RM1221, *Photobacterium profundum* SS9, *Yersinia pestis* CO92, *Methanocaldococcus jannaschii*, *Bacillus subtilis*, *Pyrococcus abyssi*, *Arabidopsis thaliana*, *Saccharomyces cerevisiae*, *Candida albicans* SC5314, *Homo sapiens*, *Mus musculus* (house mouse) and *Danio rerio* (zebrafish).

4.2.10 Far-UV Circular Dichroism Spectroscopy for Assessment of Secondary Structure

Far-UV circular dichroism (far-UV CD) studies were performed to assess global secondary structure using a JASCO J-815 Spectropolarimeter which was connected to a Pelletier heating/cooling system. WT and Ser52Cys ATCase CSU samples were prepared in 100 mM Tris-HCl (pH 7.0) at a concentration of 0.20 mg/mL (5 μ M monomer) and scans were performed from 200 – 260 nm at 25°C in a 2 mm pathlength quartz cuvette. The resulting spectra were obtained by averaging 5 scans. at a bandwidth of 1 nm, a wavelength scanning rate of 50 nm/minute and 0.25 second response. The data were corrected for the contribution of the solvent and cuvette system using software included in the Jasco J-815 spectropolarimeter.

4.2.11 Fluorescence Spectroscopy for Assessment of Tertiary Structure

The tertiary structures of WT and Ser52Cys CSU were probed by monitoring fluorescence emission using Shimadzu fluorimeter. WT and Ser52Cys ATCase CSU were prepared at approximately 0.06 mg/mL (1.5 μ M monomer) in 10 mM HEPES (pH 7.5) with 1 mM DTT. The samples were placed in a 3-mL quartz fluorescence cuvette. The fluorescence spectra were recorded at excitation wavelengths of 280 and 295 nm, while emission was recorded from 300-400 nm. Buffer signal was subtracted from fluorescence scans. The settings used were slow scan speed, 4 nm bandwidth and the instrument was set on high sensitivity.

4.2.12 Thermal Denaturation of WT and Ser52Cys CSU Secondary Structure Monitored by Circular Dichroism

In order to determine the thermal stability of the secondary structure of both WT and Ser52Cys ATCase CSUs, the enzymes were subjected to thermal denaturation from 30 to 95°C at a rate of 30°C/hour. Identical experimental conditions were used as in section 4.2.10 except that samples were prepared in 10 mM HEPES (pH 7.5). Loss of α -helical structure was monitored at 222 nm. The first order derivative of the change in CD signal with temperature was determined using analysis software included in the Jasco J-815 spectropolarimeter in order to determine the actual melting temperatures of the CSUs.

4.2.13 Chemical Modification of WT and Ser52Cys CSU by Cysteine-Specific Modifying Reagents

4.2.13.1 Sample Preparation Prior to Chemical Modification

A final protocol developed for all subsequent analyses of the CSU is described below. An aliquot of either WT or Ser52Cys ammonium sulfate precipitated ATCase CSU was centrifuged for 5 minutes at 14000 rpm using a benchtop microcentrifuge at 4°C. The supernatant was removed using a micropipettor and the pellet was resuspended in 0.5 mL of the appropriate buffer containing 10 mM EDTA and 20 mM DTT. The sample was then allowed to incubate for 30 minutes on ice to ensure the reduction of the cysteine residues as well for the chelation of any mercury that might be present from the purification process. EDTA and DTT were then removed by buffer exchange into the

intended buffer without EDTA and DTT, using NAP-5 columns. Protein concentration was then determined using the BioRad assay kit.

4.2.13.2 Chemical Modification Using Ellman's reagent (DTNB)

The concentration/accessibility of the CSU cysteine residues was determined for both the WT and Ser52Cys CSUs by assaying with DTNB. The assays were performed under both native and denaturing conditions. Native conditions were maintained by using a buffer of 200 mM Tris-HCl, 20 mM EDTA (pH 8.5) buffer while denaturing conditions using the same buffer but with 6 M GuHCl present. CSU monomer (40 μ M for WT/ 20 μ M for Ser52Cys) was incubated with a 2-fold molar excess of DTNB with respect to the total concentration of cysteines at 30°C protected from light. Upon addition of DTNB, an absorbance increase was monitored for release of 3-carboxylate 4-nitrophenolate at 412 nm for both the native and denaturing conditions but using slightly different extinction coefficients for the calculation of the cysteine residue concentrations, notably $\epsilon_{412} = 14150 \text{ M}^{-1} \cdot \text{cm}^{-1}$ for native conditions and $\epsilon_{412} = 13700 \text{ M}^{-1} \cdot \text{cm}^{-1}$ for denaturing conditions (137). The recorded absorbance was corrected for the contributions from buffer and DTNB.

Briefly, for performing the DTNB assay under native conditions, the CSU was incubated in buffer in a 1.0 mL cuvette for 10 minutes at 30°C in the spectrophotometer interfaced to a circulating thermostatted water bath. Under denaturing conditions, the CSU was incubated for 60 minutes at room temperature in 6 M GuHCl prior to assaying in order to ensure complete protein denaturation. The absorbance of the enzyme solution

at 412 nm was zeroed and the reaction was initiated with the addition of DTNB; measurements were recorded at 0, 1, 2, 3, 4, 5, 10, 15, 20, 30, 40, 50 and 60 minutes, with gentle mixing using a pipette prior to every reading. A DTNB control was prepared as for the above samples (but without protein) and its absorbance at 412 nm was monitored at the same time points. The absorbance values for the DTNB control were subtracted from the sample absorbances in order to correct for auto-hydrolysis as well as baseline drift.

4.2.13.3 Time-Dependent Chemical Modification Using Iodoacetamide (IAM) and Chloroacetamide (CIAM)

ESI-MS was used to monitor the alkylation of cysteine residues in WT and Ser52Cys ATCase CSU by reaction with either IAM or CIAM. Alkylation involved reaction of 10 μ M CSU monomer with 10 mM IAM in a total volume of 50 μ L of 100 mM Tris-HCl (pH 7.0) at room temperature and protected from light. Time-dependent modification using either IAM or CIAM was followed at $t = 0, 5, 10, 20, 30$ minutes. Samples were allowed to equilibrate at room temperature for 10 minutes prior to initiation of the alkylation reaction. The modification reaction was initiated upon addition of either IAM or CIAM. At the end of each time point, the modification reaction was stopped using DTT at a final concentration of 20 mM. Samples were kept on ice and were then processed and analyzed by ESI-MS as reported in section 4.2.6.

4.2.14 *In-silico* Digestion of WT and Ser52Cys ATCase CSU With Endopeptidase

GluC

In-silico digestions were performed on the amino acid sequences of both WT and Ser52Cys CSUs (Tables 4.1 and 4.2) using the PeptideCutter software (149) found at www.expasy.org. Endopeptidase GluC from *Staphylococcus aureus* V8 was used for the *in-silico* digestion.

4.2.15 Digestion of WT and Ser52Cys ATCase CSU With Endopeptidase GluC

Both native and alkylated WT and Ser52Cys CSU samples (from section 4.2.13.3) were lyophilized overnight at room temperature using a Speedvac and then dissolved in 30 μ L of 50 mM ammonium bicarbonate (pH 7.8). Next, the samples were digested using endopeptidase GluC at a ratio of 100:1 CSU:GluC (w/w) overnight at room temperature protected from light.

The GluC-digested CSU samples were analyzed by LC-MS using a 45 minute linear acetonitrile gradient from 5 – 95 % containing 0.1% TFA. Peptide peaks were detected in positive mode from 200 – 3000 amu using the same instrument and parameters as described in section 4.2.6.

4.2.16 Peptide Sequencing by ESI-MS/MS

A sample of GluC-digested Ser52Cys ATCase CSU peptides was subjected to LC-MS analysis as per section 4.2.17. The peptide at $[M+H^{2+}]$ of 620.787 amu corresponding to the alkylated P(51-60) was selected at the first quadrupole, fragmented at the second quadrupole, and the resulting amino acid peaks were detected from 100 – 1400 amu in positive mode at the third quadrupole. Parameters used were as follows: Cone voltage: 35 V; Collision Cell voltage: 35 V; Argon gas used for fragmentation and the resolution was approximately 0.5 Da.

4.2.17 Determination of Cys52 pK_a by Titration With Chloroacetamide

The ionization state and surface accessibility of Cys52 of the variant CSU was determined by reaction with CIAM for 40 minutes at several pH values, ranging from 3.93 to 9.01. The pH-dependent alkylation reaction was carried out in a 2 x 3-component buffer (0.1 M 2-morpholinoethanesulfonic acid (MES), 0.1 M N-ethylmorpholine, 0.2 M diethanolamine). Ser52Cys CSU was prepared as reported in section 4.2.8 prior to chemical modification with CIAM. The protein was then buffer exchanged by NAP-5 into 3-component buffer (pH 7.01). CSU monomer (10 μ M), was incubated for 10 minutes at ambient temperature in 2 x 3 component buffer at several pH values ranging from 3.93 to 9.01. The alkylation reaction was initiated upon addition of 0.5 μ L of a stock solution of 1 M CIAM in MilliQ water to a final reaction volume of 50 μ L. The reaction mixture was gently vortexed for 5 seconds and the reaction was then allowed to

proceed for 40 minutes as described in section 4.2.13.3. Samples were then prepared for ESI-MS analysis as reported in section 4.2.6.

For the analysis of the ESI-MS data, the ratio of peak intensity of adduct / (peak intensity of native CSU + peak intensity of adduct) was calculated in order to determine the ratio of alkylated CSU at different pHs relative to unmodified CSU. The pK_a of the alkylated cysteine residue was determined by plotting peak intensity ratios versus pH values and fitting the data to the equation for a single pK_a using Erithacus Software Grafit 5.0 software:

$$y = \frac{Limit_1 + Limit_2 \cdot 10^{(pH - pK_a)}}{10^{(pH - pK_a)} + 1} \quad (\text{Equation 4.1})$$

4.3 RESULTS

4.3.1 Purification and Purity Assessment of WT and Ser52Cys CSU

Both WT and Ser52Cys ATCase holoenzymes were engineered with a hexahistidine tag at the N-terminus of the RSU to facilitate purification of the holoenzyme by Ni-NTA affinity chromatography. The location of this tag did not interfere with the non-covalent association of the catalytic chain with the regulatory chain in the holoenzyme. In order to minimize non-specific binding of proteins lacking a His-tag, the resin was washed with a phosphate buffer containing a low concentration of imidazole (20 mM) after applying the cell-free extract to the column. The results in Figure 4.1 (lanes B-E) indicate that a significant amount of unbound protein as well as a small amount of holoenzyme eluted upon washing with this low imidazole-containing wash buffer. Holoenzyme may have eluted at 20 mM imidazole if the binding capacity of the Ni-NTA resin was exceeded.

In order to separate the catalytic subunit from the regulatory subunit, holoenzyme was reacted with neohydrin as reported in section 4.2.2. The bound His-tagged holoenzyme was treated with neohydrin while still bound to the nickel resin, using a ratio of neohydrin:holoenzyme 3:10 (w/w), which is approximately 3-fold higher than previously reported by Yang *et al.* (156). SDS-PAGE analysis shown in Figure 4.1 (lanes F and G) indicates that the reaction of the holoenzyme with neohydrin yields a protein resolved as a single band which migrated with an approximate molecular weight of 35 kDa suggesting that the preparation of CSU was homogeneous.

In order to elute the bound RSUs and any intact holoenzyme, the resin was subsequently washed with a Tris buffer containing 250 mM imidazole. Denaturing PAGE analysis of fractions 4 and 7 (Figure 4.1 (lanes I-J)) of the wash performed at a high imidazole concentration yielded a protein which migrated at an approximate molecular weight of 18 kDa, corresponding to the molecular weight of RSU. Also resolved were a few faint bands corresponding to possible unidentified proteins. No bands corresponding to the CSU were seen in lanes I and J which indicates that neohydrin-mediated reaction of the holoenzyme likely lead, to the complete dissociation of the holoenzyme into its subunits. Identical results were obtained during the purification of WT ATCase CSU (results not shown). Hence, purification of His-tagged ATCase holoenzyme by Ni-NTA affinity chromatography followed by subsequent treatment with neohydrin leads to a yield of approximately 35 mg of CSU and 50 mg RSU per liter of culture, although the CSU is homogeneous.

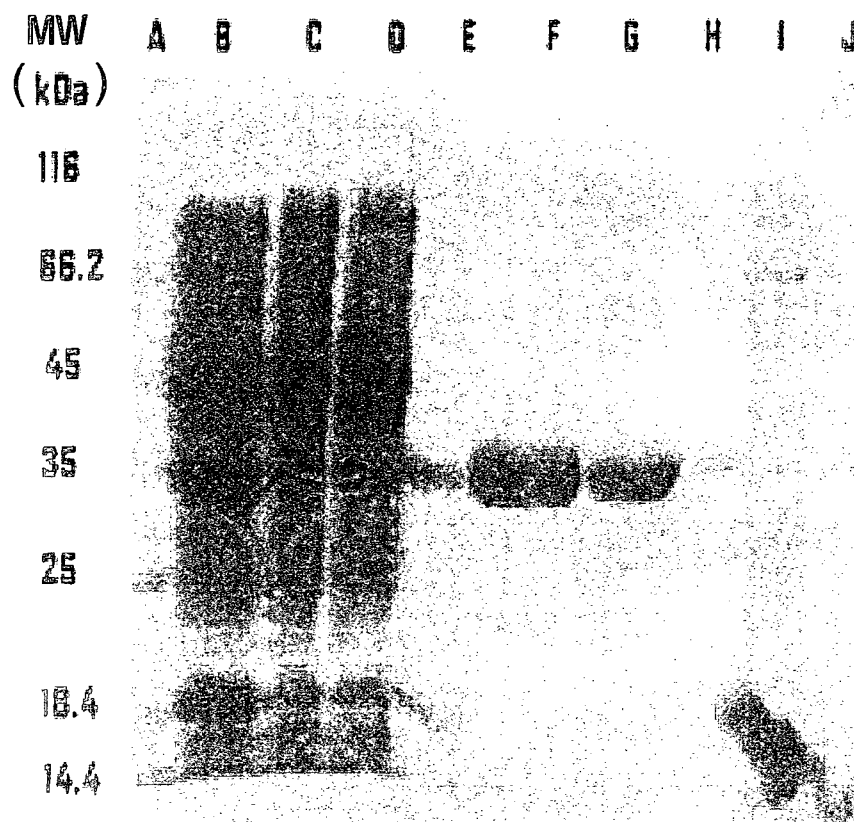


Figure 4.1: SDS-PAGE analysis of the nickel affinity purification of Ser52Cys CSU. Selected samples from the purification scheme as analyzed by 10% SDS-PAGE. They include: (A) broad range molecular weight ladder, (B) crude extract, (C) flow-through from nickel column; (D-E) wash fractions 1 and 12 collected prior to treatment with neohydrin, (F-H) fractions 2, 9, and 12 in the wash after treatment of holoenzyme with neohydrin, (I-J) fractions 4 and 7 from the 250 mM imidazole wash.

ESI-MS was used to confirm the exact molecular weight of the proteins that had been purified by Ni-NTA affinity chromatography. The literature molecular weight value from the updated amino acid sequence of pyrB from *E. coli* K12 (accession number: P0A786) is 34427 Da. The mass spectrum of native WT CSU (Figure 4.2, panel A) clearly shows a single peak at $[M+H^+]$ of 34294 amu. The value obtained by mass spectrometry has a discrepancy of -130 amu with the literature value. This discrepancy corresponds to the removal of the N-terminal methionine in the catalytically active polypeptide (139). The results indicate that the WT CSU indeed undergoes post-translational modification and also confirms that the molecular weight of the purified fully folded WT ATCase CSU is in excellent agreement with the expected value reported in the literature with an experimental error less than $\pm 0.01\%$.

The mass spectrum of Ser52Cys CSU clearly indicates the presence of two major peaks at $[M+H^+]$ of 34312 amu and 34511 amu (Figure 4.2 panel B). The peak identified at $[M+H^+]$ of 34312 amu once again illustrates a discrepancy of -131 amu with respect to the molecular weight of the full length polypeptide (34443 Da). The Ser52Cys CSU variant also undergoes cleavage of the N-terminal methionine as reported for the WT CSU. The second peak identified at 34511 amu (an adduct of +199 amu) corresponds to a bound Hg^{+2} originating from the neohydrin treatment for the dissociation of the holoenzyme into its constituent subunits. It is not uncommon to detect mercury adducts by ESI-MS on polypeptides containing cysteine residues (160).

The ESI-MS spectrum (Figure 4.2, panel B) shows only the formation of a single +199 amu adduct, suggesting that not more than one Hg^{+2} binds per catalytic chain. Hence, conditions must be determined to ensure that the metal is removed before any

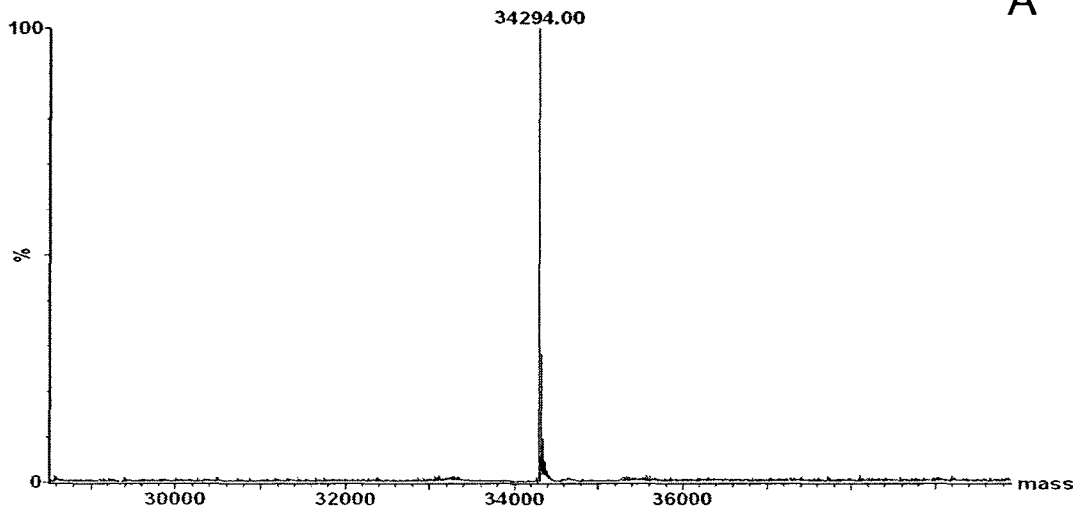
further experiments may be conducted. It is also noteworthy that the +199 amu adduct was not seen for the WT CSU.

ICP-MS was used in order to determine the presence or absence of metal, and to determine the nature of the metal. The results of Ser52Cys CSU analysis by ICP-MS indicate that the metal bound was mercury and that there were 1.7 mercury bound per variant CSU trimer.

Figure 4.2: Deconvoluted electrospray ionization mass spectra of untreated CSU

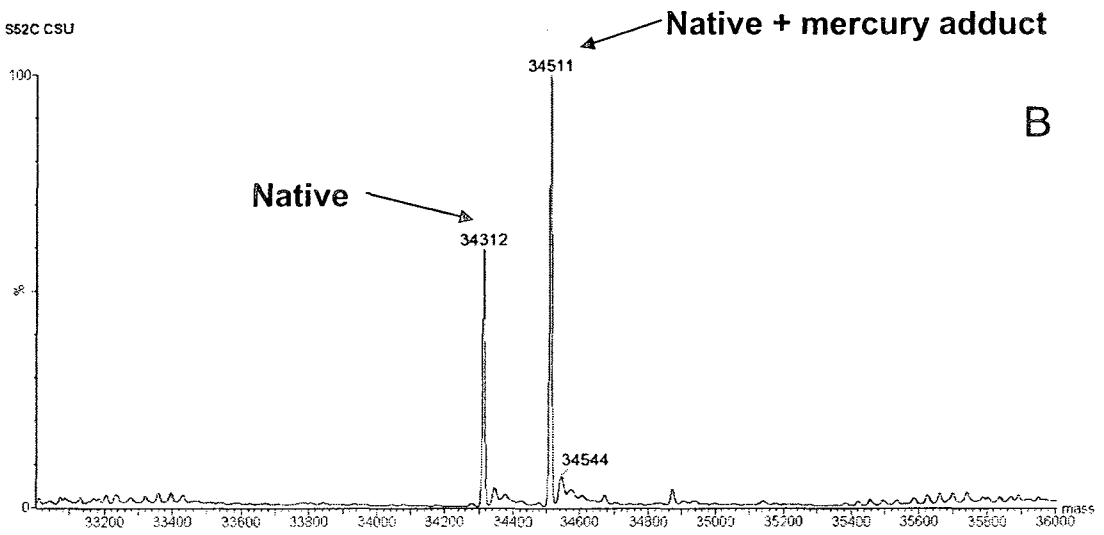
(A) Untreated WT CSU, observed $[M+H^+]$ of 34294 amu. **(B)** Untreated Ser52Cys CSU; minor species corresponding to Ser52Cys CSU observed at $[M+H^+]$ 34312 amu and major species corresponding to Ser52Cys CSU bound with a mercury adduct at $[M+H^+]$ of 34511 amu. The enzymes (2-5 μ M monomer) were prepared as described in section 4.2.8 immediately prior to direct injection.

WT ATCase CSU



A

S52C CSU



B

4.3.2 Sample Preparation of Ammonium Sulfate Precipitated ATCase CSUs

Ammonium sulfate precipitated samples of Ser52Cys CSU were subjected to various treatments in order to determine experimental conditions under which a metal-free polypeptide may be obtained for use in further experiments. In the untreated sample (Figure 4.3, panel A), two major species are observed: the unmodified variant polypeptide at $[M+H^+]$ of 34312 amu and the protein with the mercury adduct at $[M+H^+]$ of 34511 amu. From their relative intensities, a ratio of native protein: mercury-adduct of 4:7 was determined.

EDTA, a divalent metal chelator, was not present during the Ni-NTA purification step (given that it will bind the resin-bound nickel and prevent binding of the hexahistidine tag). Hence, an initial treatment was performed by incubating the variant CSU with 10 mM EDTA on ice for 30 minutes in an attempt to bind the contaminating mercury. The ESI-MS spectrum of the sample treated with 10 mM EDTA (Figure 4.3, panel B), indicates that two major species are still present: the variant protein peak observed at $[M+H^+]$ of 34311 amu, and the protein bound with mercury at $[M+H^+]$ of 34510 amu. Their relative peak intensities do however, indicate a slight improvement of the ratios of uncomplexed mercury-adduct protein from 4:7 to 4.5:6, thus suggesting that increasing the concentration of EDTA may aid in the chelation of mercury from the variant protein.

Surprisingly, further treatment with a higher EDTA concentration of 100 mM indicates no noticeable improvement in mercury chelation as suggested by the two major species seen in (Figure 4.3, panel C). In contrast, the data indicate a decrease in the ratio of uncomplexed:mercury-adduct protein to its original untreated value of 4:7. Hence,

increasing the concentration of EDTA appeared to confer an undesirable effect on the removal of mercury from the metal-bound polypeptide.

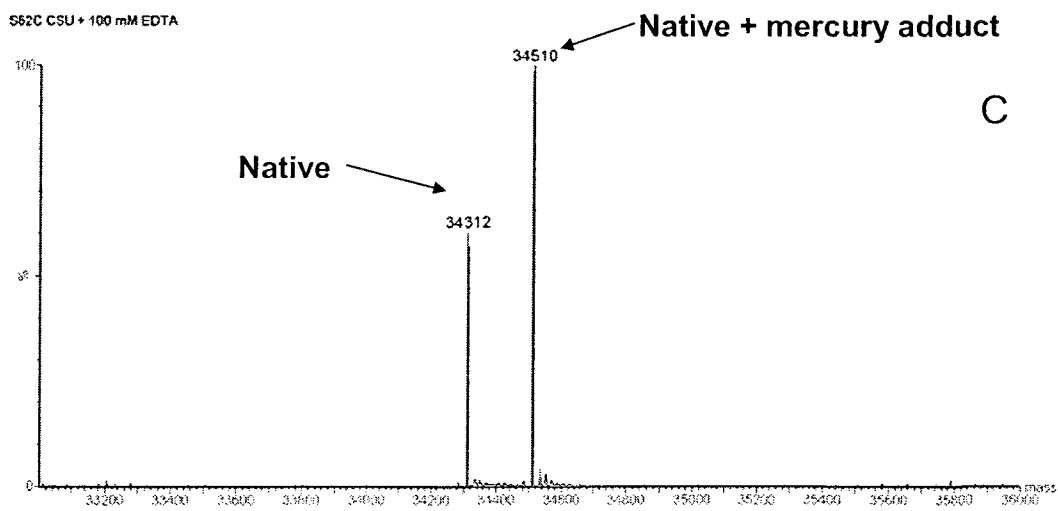
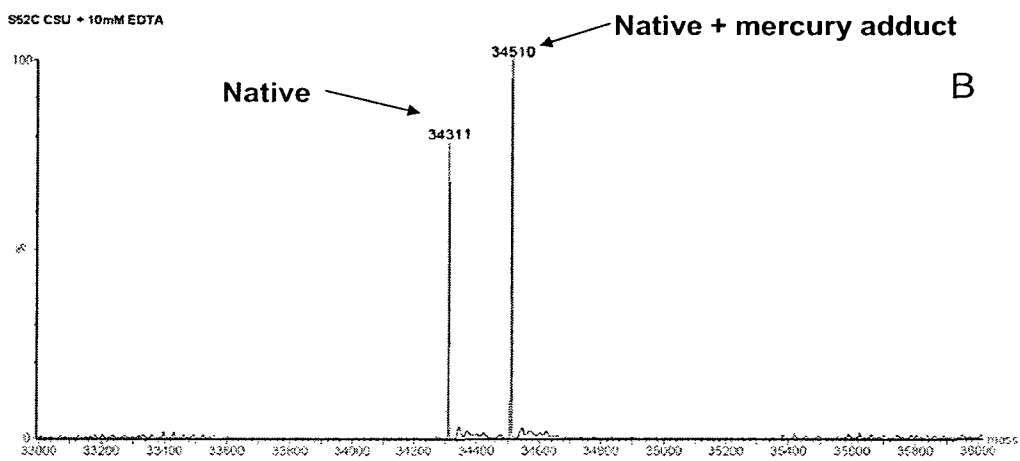
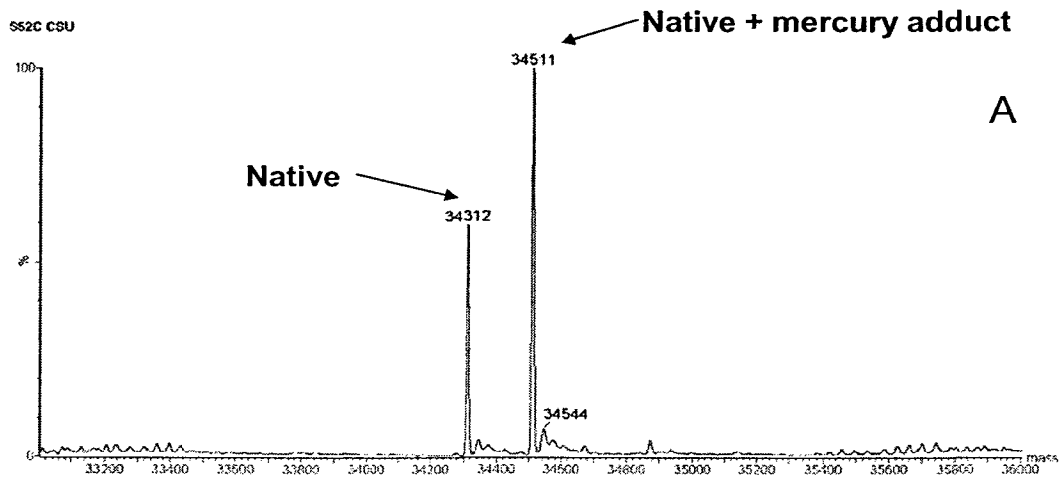
The use of thiol-reducing agent DTT as a chelator of heavy metals for toxicological studies has frequently been reported (161). Thus, DTT was utilized at a concentration of 20 mM in conjunction with 10 mM EDTA in order to remove the contaminating mercury from the neohydrin-treated variant polypeptide. Incubations conditions with DTT and EDTA were identical to those reported for EDTA alone. As predicted from the literature, the ESI-MS results of this treatment (depicted in Figure 4.3, panel D), reveals that the only species is observed at $[M+H^+]$ of 34312 amu corresponding to the unmodified variant polypeptide; the peak corresponding to the protein complexed with mercury has disappeared, as indicated by the arrow. Several sample preparations with 10 mM EDTA and 20 mM DTT confirm that this protocol is effective at removing the mercury bound to the Ser52Cys CSU.

WT CSU was subjected to the same protocol in order to ensure that treatment with 10 mM EDTA and 20 mM DTT did not result in any protein modification. The ESI-MS spectrum of treated WT CSU seen in Figure 4.3, panel E indicates that a single major peak is observed at $[M+H^+]$ of 34374 amu corresponding to the unmodified WT CSU. The ESI-MS spectra of several subsequently treated WT CSU samples confirmed that no adverse effects are caused during this sample treatment (data not shown).

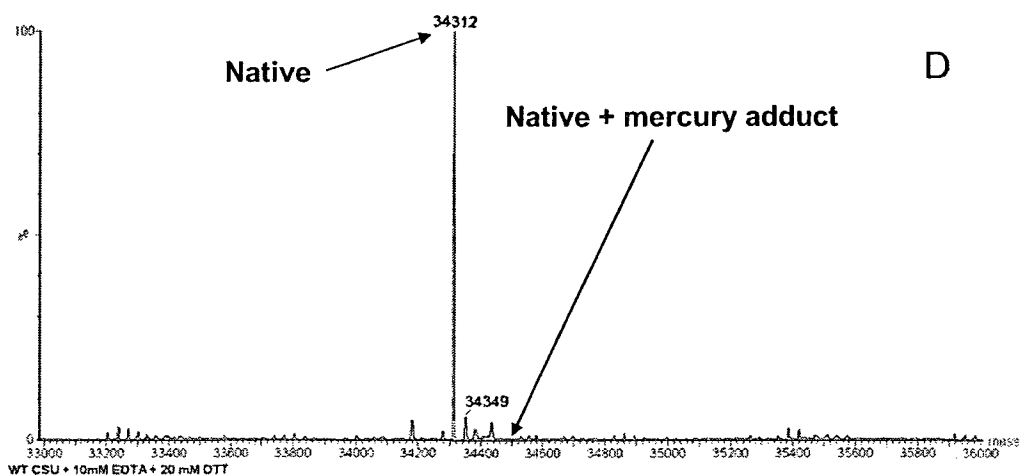
In light of the previous results, all subsequent sample preparations for WT and variant proteins, included 10 mM EDTA and 20 mM DTT, in order to minimize variations between protein sample preparations.

Figure 4.3: Deconvoluted electrospray ionization mass spectra of treated CSU

(A) Untreated Ser52Cys CSU; unmodified polypeptide peak observed at $[M+H^+]$ of 34312 amu and protein with a mercury adduct observed at $[M+H^+]$ of 34511 amu. (B) Unmodified Ser52Cys CSU treated with 10 mM EDTA; native polypeptide peak observed at $[M+H^+]$ of 34311 amu and protein with a mercury adduct observed at $[M+H^+]$ of 34510 amu. (C) Unmodified Ser52Cys CSU treated with 100 mM EDTA; unmodified polypeptide peak observed at $[M+H^+]$ of 34312 amu and protein with a mercury adduct observed at $[M+H^+]$ of 34510 amu. (D) Unmodified Ser52Cys CSU treated with 10 mM EDTA and 20 mM DTT; single major peak observed at $[M+H^+]$ of 34312 amu corresponding to variant polypeptide without mercury bound. The enzymes were treated with EDTA and DTT as mentioned in section 4.2.8 for 30 minutes on ice. Protein samples (2-5 μ M monomer) were prepared as described in section 4.2.6 immediately prior to direct injection. The term “native” denotes the protein that is unmodified and not complexed with mercury.

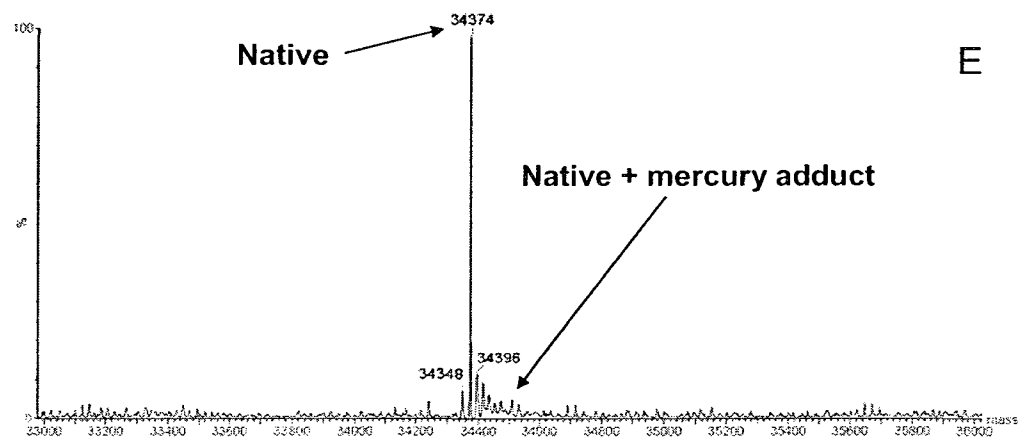


SS2C CSU + 10mM EDTA + 20mM DTT



D

WT CSU + 10mM EDTA + 20 mM DTT



E

4.3.3 WT CSU Multiple Sequence Alignments

In order to determine the importance of the Ser52 residue which is substituted for a cysteine residue in the Ser52Cys CSU variant protein, the amino acid sequence of WT CSU was aligned with those of 12 diverse species from different kingdoms using the internet-based software ClustalW (www.ebi.ac.uk/clustalw/). The results of the sequence alignments seen in Figure 4.4 are striking; Ser52 in WT CSU from *E. coli* is conserved in all species surveyed despite the difference in the organization of ATCase within multifunctional proteins as well as in the length of ATCase's primary sequence. By contrast, the cysteine at position 47 is not conserved; it is frequently replaced by methionine or non-polar amino acids. It is of interest to note that in the bacteria represented in the sequence alignments, ATCase is present as a monofunctional enzyme, as opposed to the eukaryotic organisms, where it is a component within a multifunctional enzyme, notably, Carbamyl-phosphate synthetase 2, aspartate transcarbamylase and dihydroorotase.

```

Escherichia P-----E L L K H K V I A S C F F E A S T R T R L S F E T S M H R L G A S V V G F S D S A N T S L G K K G E T I A D T 92
Yersinia P-----E L L K H K V I A S C F F E A S T R T R L S F E T S I H R L G A S V V G F S D S S N T S L G K K G E T I A D T 92
Photobacterium P-----E L L K N V V A S C F F E F S T R T R L S F E T A V Q R L G G T V I G F D N G C N T S L A K K G E T I A D S 92
Methanocaldococcus T K R P L K L L E G K I L A T V F Y E F S T R T R L S F E T A M K R L G G E V I T M D L K S S S V A K - G E S L I D T 89
Pyrococcus E K Q L E Y A K G K I L A T L F F E F S T R T R L S F E S A M H R L G G A V I G F A E A S T S S V K K - G E S I R D T 93
Arabidopsis S S S Q S E I L K G Y L M A T L F Y E F S T R T R L S F E S A M K R L G G E V L T T E N A R E F S S A A K G E T L E D T 173
Saccharomyces R E G V L D L M K G H V I T T I F F E F S T R T C S S F I A A M E R L G G R I V N V N P L - V S S V K K G E T L Q D T 1997
Candida R Q G V L D L L Q G R V L A T M F Y E F S T R T S T S F D A A M Q R L G G R V V A V D H G - - S S S V K K G E T L Q D T 1999
Homo K E R S L D I L K G K V M A S M F Y E V S T R T S S S F A A A M A R L G G A V L S F S E A - - T S S V Q K G E S L A D S 2010
Mus K E R S L D I L K G K V M A S M F Y E V S T R T S S S F A A A M A R L G G A V L S F S E A - - T S S V Q K G E S L A D S 2010
Danio K E R P L D I L K G K V M A S M F Y E V S T R T S S S F A A A M H R L G G S V V H F C E S - - T S S T Q K G E S I V D S 1956
Campylobacter R-----T F L E C K S I T T I F F E N S T R T L S S F E S A A R R L G A R V L R L D V S - - R S S S S K G E T I Y D T 84
Bacillus D-----N Q L T G K F A A N L F F E F S T R T R F S F E V A E K K L G M V L N L D G T - - S T S V Q K G E T I Y D T 84
: . * : * * * * * : : * * * : : * * * * * :

```

Figure 4.4: Multiple sequence alignments for *E. coli* WT CSU

The amino acid sequences of WT CSU from *Escherichia coli*, *Campylobacter jejuni* RM1221, *Photobacterium profundum* SS9, *Yersinia pestis* CO92, *Methanocaldococcus jannaschii*, *Bacillus subtilis*, *Pyrococcus abyssi*, *Arabidopsis thaliana*, *Saccharomyces cerevisiae*, *Candida albicans* SC5314, *Homo sapiens*, *Mus musculus* (house mouse) and *Danio rerio* (zebrafish) were subjected to multiple sequence alignments using the internet-based software ClustalW (www.ebi.ac.uk/clustalw/).

4.3.4 Secondary and Tertiary Structure Assessment of WT and Ser52Cys CSU

Circular dichroism (CD) spectroscopy is an important and sensitive biochemical tool for the characterization of proteins. In the far UV, CD is invaluable as a solution technique for the determination of protein secondary structures such as α -helices and β -sheets. Depending on the type of secondary structure, protein peptide bonds exhibit differential absorbance of right versus left-circularly polarized light (162).

CD spectra for WT and Ser52Cys ATCase CSU were recorded in the far UV (200 – 260 nm). Figure 4.5 clearly illustrates that both spectra are dominated by a double minimum at 207 and 222 nm, which is characteristic of predominantly α -helical proteins. Moreover, the CD signals of both enzymes almost completely overlap, suggesting that their global secondary structures remain essentially unchanged despite the substitution of Ser52 for a cysteine residue. These results are in agreement with crystal structures of the isolated CSU, which illustrate ~ 52% helical content (163, 164).

The tertiary structures of both WT and Ser52Cys CSU were probed using fluorescence spectroscopy. This technique consists of exciting the enzyme's fluorophores (2 Trp and & Tyr/monomer) and measuring the emission intensity from 300 – 400 nm. Excitations at 280 nm preferentially targets Trp and Tyr residues, while excitation at 295 nm targets Trp preferentially. An overlay of the spectra of both proteins at each respective excitation wavelength indicates that the Ser to Cys substitution at position 52 does not cause any significant changes in the environment surrounding Trp and Tyr residues within the variant CSU. The λ_{max} of emission for both proteins is at 335 nm regardless of λ_{ex} and with comparable intensities (Figure 4.6).

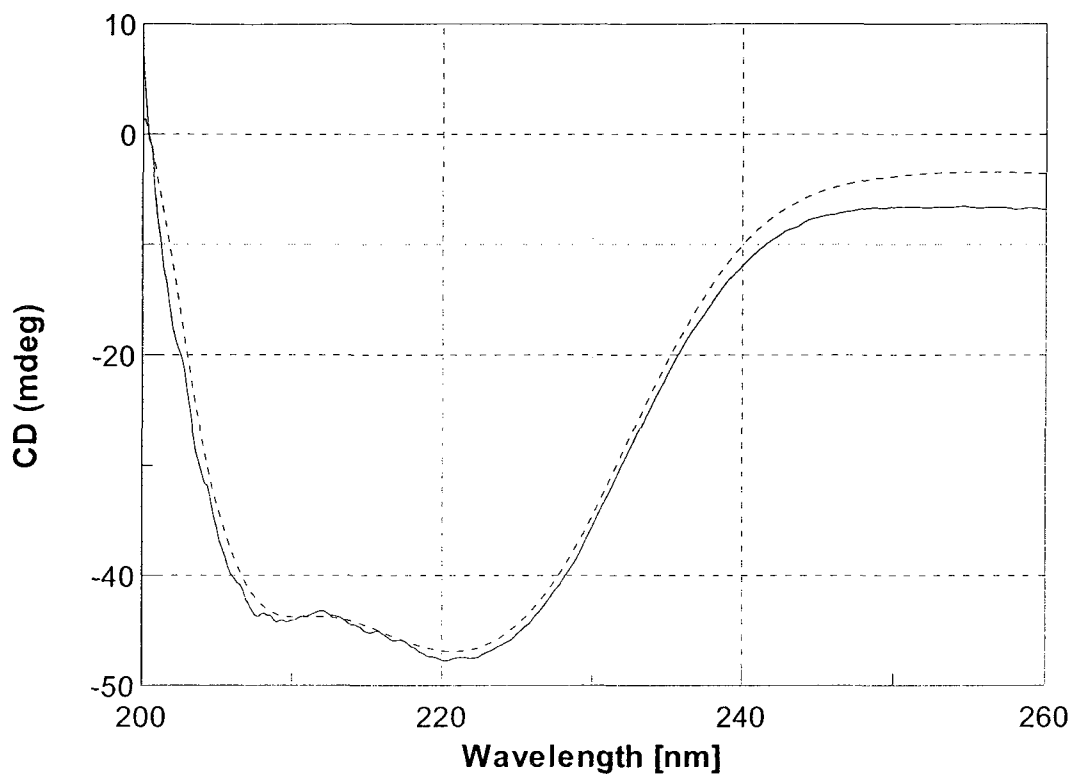


Figure 4.5: Far-UV CD spectra analysis of WT and Ser52Cys CSU

Protein samples of WT CSU (—) and Ser52Cys CSU (----) were prepared at a concentration of 0.2 mg/mL in 100 mM Tris-HCl (pH 7.0). Spectra were recorded at 25°C using a Jasco J-815 spectropolarimeter interfaced with a Pelletier temperature controller unit. Measurements were performed in a 2 mm pathlength quartz cuvette, averaging 5 wavelength scans from 260 to 200 nm (1 nm bandwidth) in 0.2 nm steps at a rate of 50 nm/minute, and 0.25 second response. Data were corrected for the signal contribution of the buffer and cuvette using software supplied by Jasco.

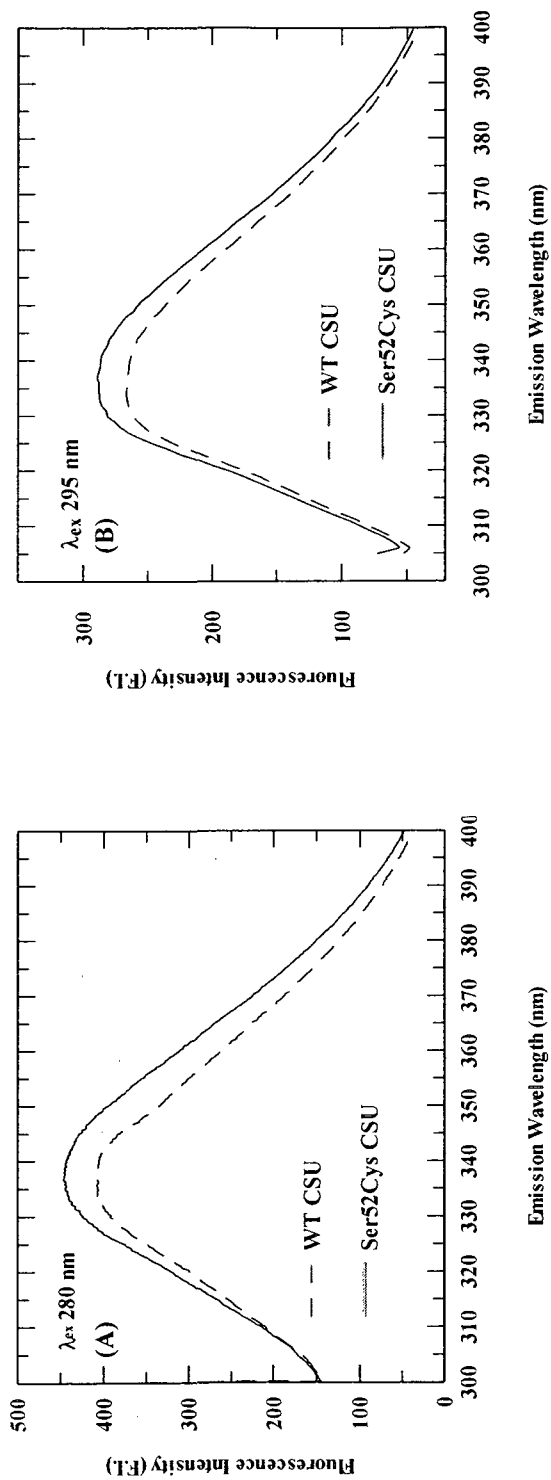


Figure 4.6: Fluorescence spectroscopy of WT and Ser52Cys ATCase CSU

WT and Ser52Cys CSU (0.06 mg/mL) were prepared in 10 mM HEPES (pH 7.5) with 1 mM DTT and placed in a 3 mL (1cm) quartz fluorescence cuvette. The fluorescence spectra were recorded using a Shimadzu fluorimeter at excitation wavelengths of 280 (A) and 295 nm (B), while emission was recorded from 300-400 nm. Contributions from buffer were subtracted from fluorescence scans. The differences in intensity between WT and variant are due to small variations in protein concentrations.

4.3.5 Thermal Stability of WT and Ser52Cys CSU Secondary Structure Monitored by Circular Dichroism

In order to determine the thermal stability of the secondary structures of both WT and Ser52Cys CSUs, both enzymes were subjected to thermal denaturation from 30 to 95°C at a rate of 30°C/hour. Loss of α -helical structure was monitored at 222 nm. Identical experimental conditions were used as in section 4.2.10. The data (Figure 4.7) show sigmoidal shaped curves indicating a highly-cooperative two-state unfolding process for the variant protein and possibly an intermediate species in the less cooperative unfolding of WT CSU. The results yield melting temperatures of 62.4°C for WT and 73.9°C for Ser52Cys CSU, indicating that the variant CSU is 11.5°C thermally more stable than the WT CSU .

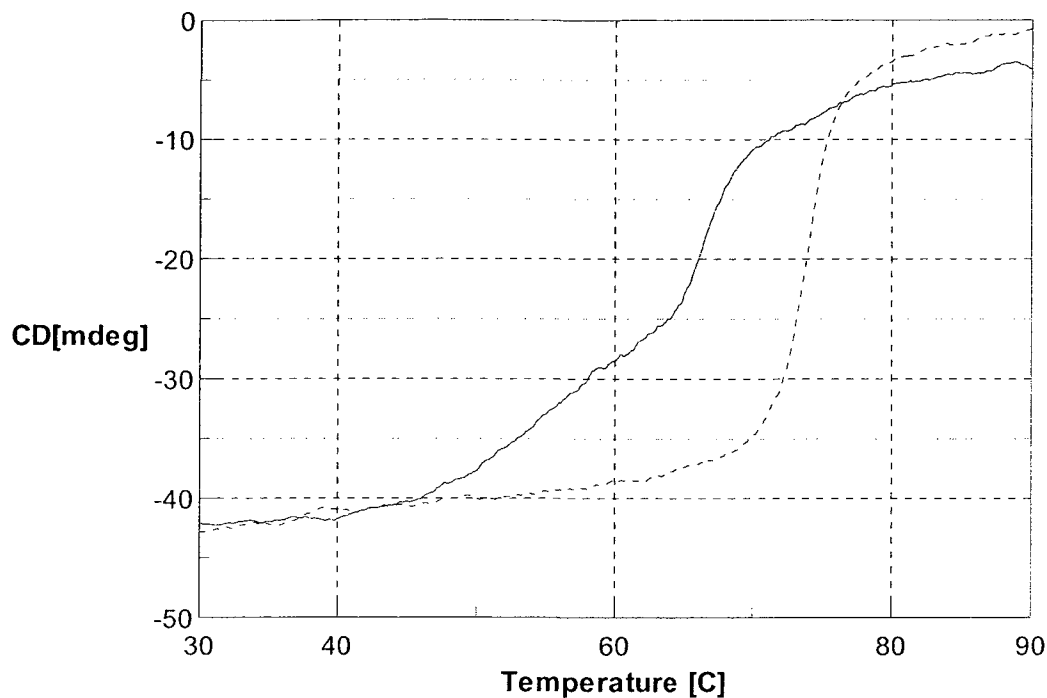


Figure 4.7: Thermal denaturation curves for WT and Ser52Cys CSUs monitored by circular dichroism

Thermal denaturation of WT (—) and Ser52Cys (---) CSU were monitored by circular dichroism at a wavelength of 222 nm. Samples were prepared at a concentration of about 0.2 mg/mL in 10 mM HEPES (pH 7.5). Denaturation was performed from 30° to 95°C, at a ramp speed of 30°C/hour, 1 nm bandwidth and a 0.25 second response. T_m values were determined as described in section 4.2.12.

4.3.6 Chemical Modification of WT and Ser52Cys CSU by Cysteine-Specific Modifying Reagents

4.3.6.1 Chemical Modification Using Ellman's Reagent (DTNB)

The concentration/accessibility of the CSU cysteine residues was determined spectrophotometrically for both the WT and Ser52Cys CSUs by assaying with DTNB. The assays were performed under both native and denaturing conditions. The rate of this reaction is dependent on the pH of the solution, the pK_a of the target cysteine residue and the residue's surface accessibility.

The results of the chemical modification for the WT CSU in the presence of 6M GuHCl, illustrate in Figure 4.8, that the equivalent of a single cysteine residue per catalytic chain has reacted within a minute and no additional adducts are formed even by 60 minutes. This result is not surprising since only a single cysteine residue, Cys47, is present in the amino acid sequence of the WT CSU.

The results of the chemical modification under non-denaturing conditions exhibit that the reaction follows second order kinetics with a second order rate constant of $1.9 \text{ M}^{-1} \cdot \text{s}^{-1}$ for the rapid phase between 0 and 5 minutes, and $0.13 \text{ M}^{-1} \cdot \text{s}^{-1}$ for the slower phase between 5 and 60 minutes. The formation of trinitrophenylated is slow and steadily increases over 60 minutes to yield approximately 0.55 cysteine residues per monomer. This result contrasts that reported by Vanaman and Stark (105), where Cys47 reacted at a slower rate but to the same extent as those we are reporting. This may be due to the fact that the two experiments were conducted under different experimental conditions; experiments conducted by Stark were under conditions where pseudo first-order kinetics are taking place.

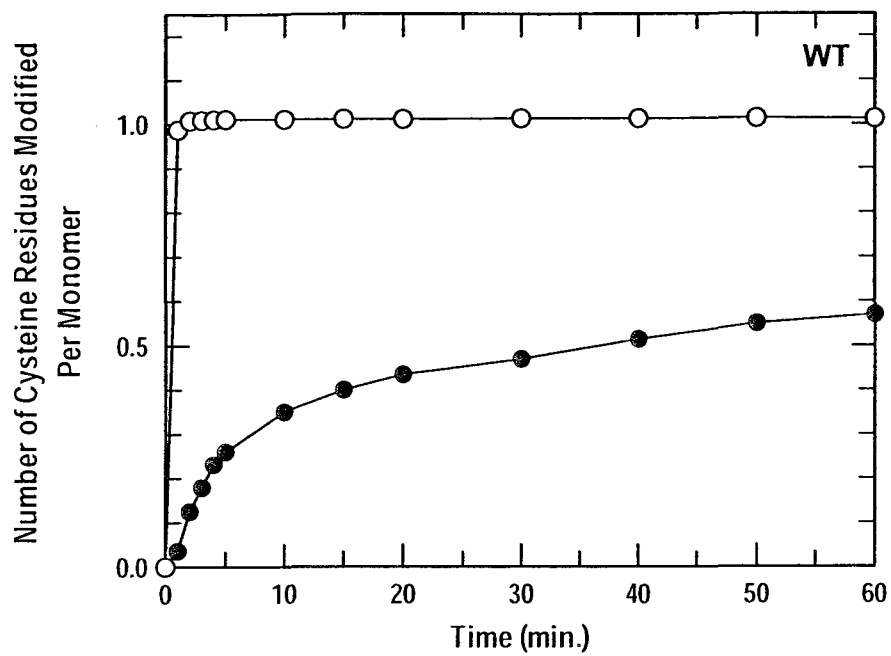
Results for the DTNB reaction with Ser52Cys CSU revealed that under denaturing conditions, the equivalent of a two cysteine residues have reacted within a minute and once again, the signal remains at a plateau until the end of the experiment at 60 minutes. This result confirms that only two cysteine residues are present in the amino acid sequence of the Ser52Cys CSU, notably Cys47 and Cys52.

Under non-denaturing conditions, Figure 4.8, panel B illustrates that a single cysteine residue reacts rapidly within 1 minute, and a second cysteine residue appears to react slowly until a further 0.25 more cysteine residues per monomer have been modified by 60 minutes.

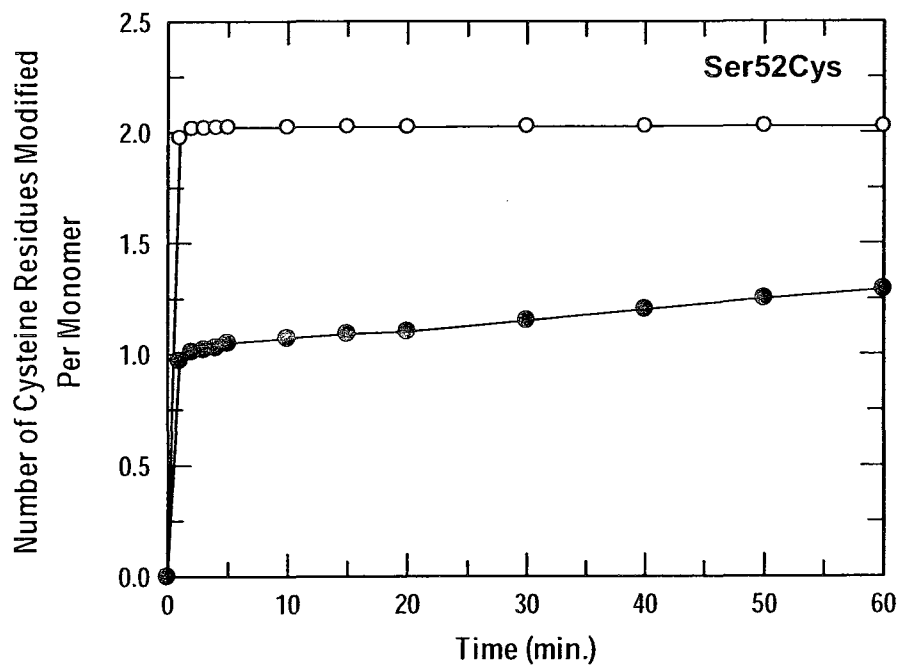
Figure 4.8: Chemical Modification of WT (A) and Ser52Cys (B) CSU With Ellman's Reagent

CSU (40 μM monomer for WT and 20 μM monomer for Ser52Cys) was incubated with a 2-fold molar excess of DTNB with respect to the total concentration of cysteines at 30°C, protected from light. Experiments under native conditions, denoted by (•), were performed in 200 mM Tris-HCl, 20 mM EDTA (pH 8.2), while those under denaturing conditions, denoted by (○) were performed in 6M GuHCl in the same buffer. Upon the addition of DTNB, absorbance increases were monitored at 412 nm for the release of 3-carboxylate-4-nitrophenolate. Extinction coefficients used were $\epsilon_{412} = 14150 \text{ M}^{-1} \cdot \text{cm}^{-1}$ and $\epsilon_{412} = 13700 \text{ M}^{-1} \cdot \text{cm}^{-1}$ for reactions conducted under native and denaturing conditions, respectively. The data were recorded on a Varian Cary 50 Dual Beam Spectrophotometer and the absorbances were corrected for the contributions from buffer and DTNB.

(A)



(B)



4.3.6.2 Time-Dependent Chemical Modification Using Iodoacetamide (IAM) and Chloroacetamide (CIAM)

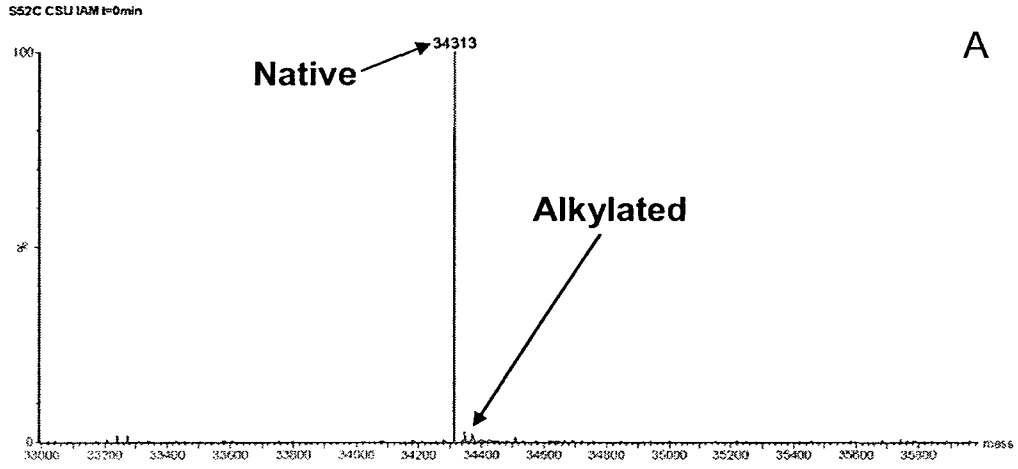
DTNB is very unstable under acidic conditions thus eliminating its use in mass spectrometry. In contrast, the small cysteine-specific alkylating agents IAM and CIAM, which form stable adducts over a large pH range are ideally suited for applications in mass spectrometry. Thus, ESI-MS was used to monitor the alkylation of cysteine residues by reaction with either IAM or CIAM. Since Cys47 in the WT CSU has been reported by Vanaman and Stark to be unreactive with IAM (105), we followed the IAM-mediated alkylation reaction using the Ser52Cys CSU instead. The reaction was followed at neutral pH since the variant was very reactive with DTNB at pH ~8 (section 4.2.13).

Figure 4.9, panels A-E show the time course of the reaction of Ser52Cys CSU with 10 mM IAM at pH 7.0. Panel A represents the reaction at $t = 0$ minutes, where the enzyme is incubated in the absence of IAM, while panels B-E represent the incubations of the enzyme with 10 mM IAM at 5, 10, 20 and 30 minutes, respectively. Panel A shows a single peak at $[M+H^+]$ of 34313 amu, which corresponds to the unmodified enzyme. Panels B-E clearly exhibit a single peak at $[M+H^+]$ of 34370 amu, corresponding to the alkylated enzyme, which is shifted by +57 amu upon reaction with IAM. These findings suggest that the alkylation reaction is extremely rapid since the results of the modification after 5 minutes or 30 minutes are identical. Additionally, the results also indicate that the reactivity of the variant CSU with IAM is limited to a single cysteine residue, presumably Cys52, since there are no other observable peaks other than that at $[M+H^+]$ of 34370 amu. This reaction of enzyme with IAM is too rapid even at neutral pH and is not

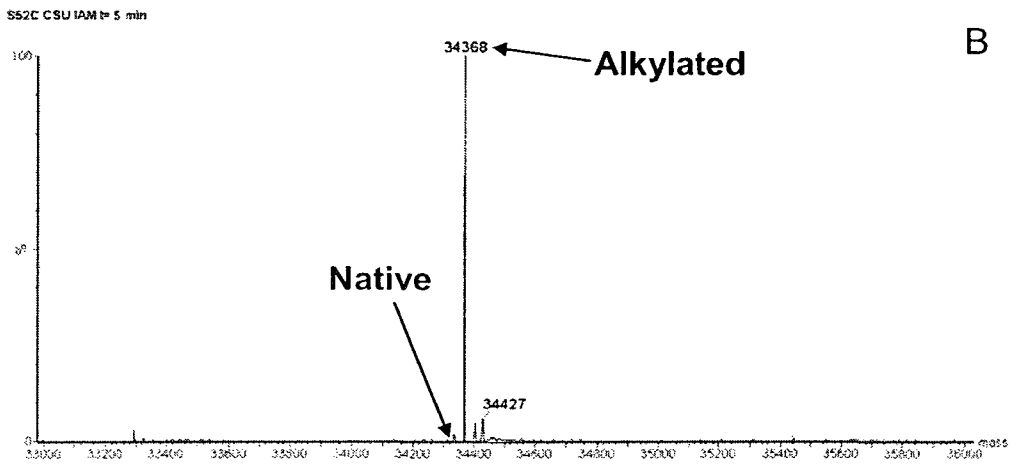
convenient for the determination of the extent of alkylation of the Cys52 in the Ser52Cys
CSU.

Figure 4.9: Deconvoluted electrospray ionization mass spectra displaying time-course modification of Ser52Cys CSU with 10 mM IAM

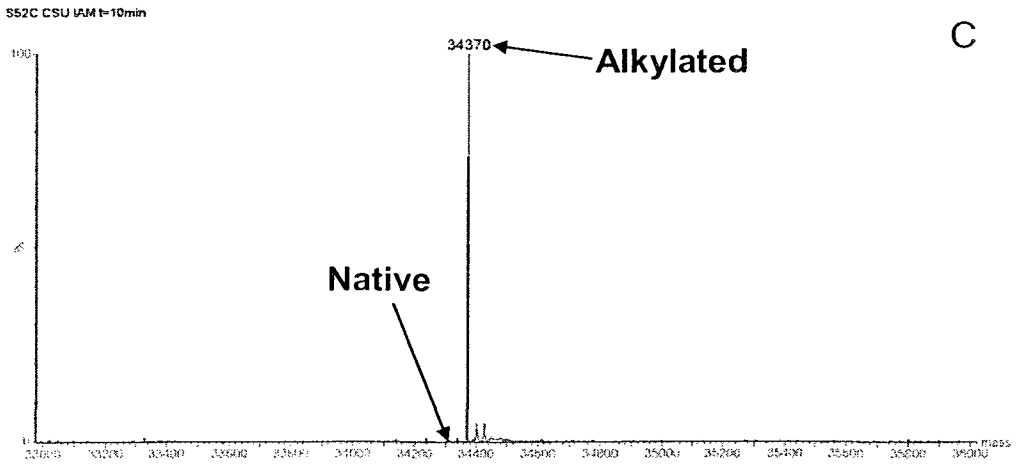
CSU (10 μ M monomer) was reacted with 10 mM IAM in 100 mM Tris-HCl (pH 7.0) at room temperature and protected from light. The alkylation reaction, initiated upon addition of IAM, was monitored for 5, 10, 20 and 30 minutes. At the end of each time point, the modification reaction was quenched using DTT at a final concentration of 20 mM and samples were kept on ice. Protein samples (2-5 μ M monomer) were prepared as described in section 4.2.6 immediately prior to direct injection. (A) Ser52Cys CSU's unmodified (native) polypeptide is observed at $[M+H^+]$ of 34313 amu ($t = 0$ minutes). Ser52Cys CSU after incubation with 10 mM IAM for 5 minutes (B), 10 minutes (C), 20 minutes (D) and 30 minutes (E). The alkylated polypeptide was observed at $[M+H^+]$ of 34368 amu, 34370 amu, 34370 amu and 34369 amu, respectively, for each of the time points.



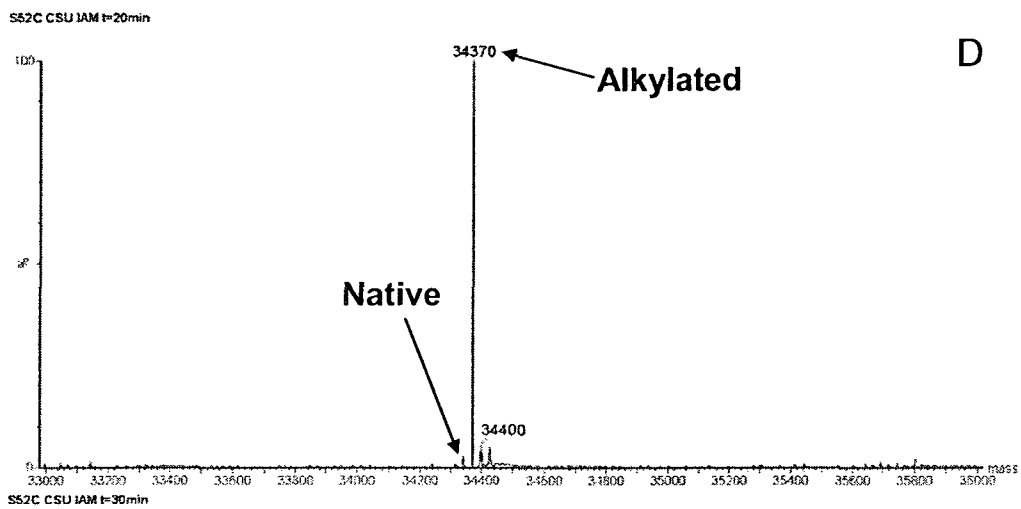
A



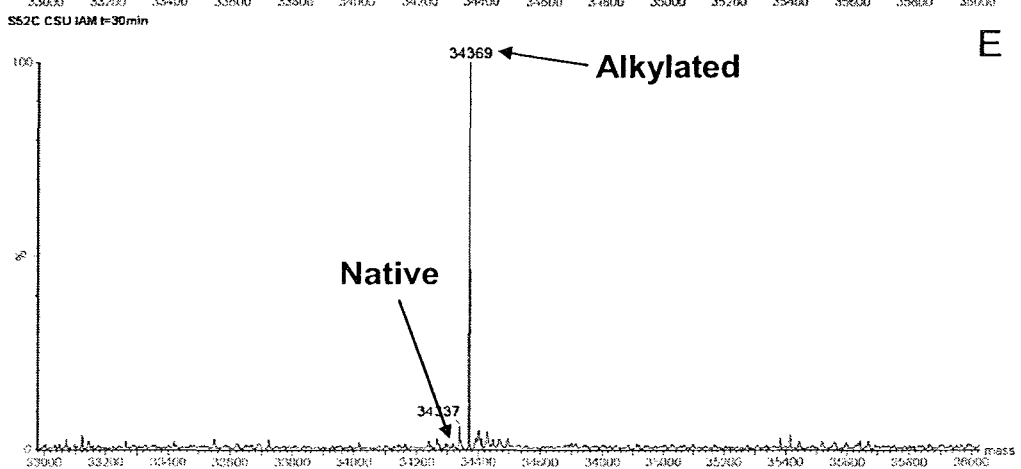
B



C



D



E

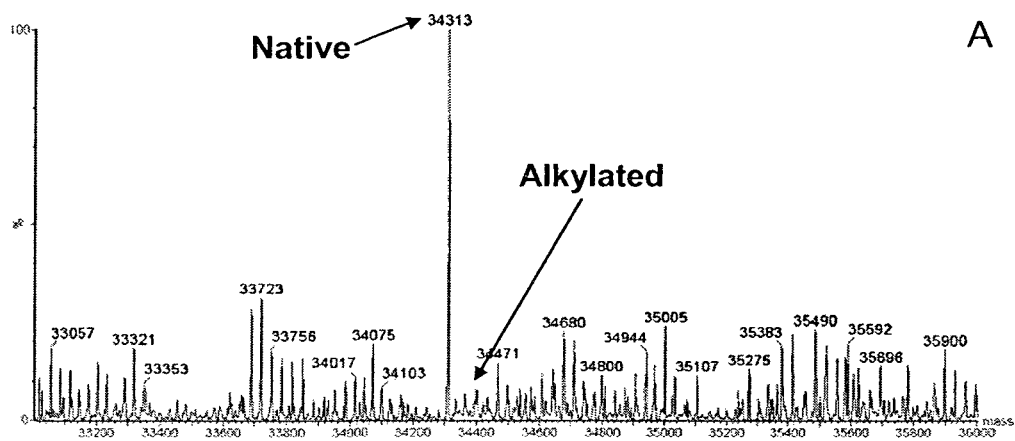
Since the alkylation reactions were too rapid when performed using IAM, the former reagent was replaced with CIAM, which is known to alkylate by the same mechanism but which proceeds at a much slower rate, and hence is more convenient for the purpose of this study (141).

Figure 4.10 shows the ESI-MS spectra produced by reaction of Ser52Cys CSU with CIAM for 0, 10, 20, 30 and 40 minutes, respectively. At $t=0$ minutes, Panel A exhibits a single peak at $[M+H^+]$ of 34313 amu, corresponding to the unmodified Ser52Cys CSU. In panel B, two peaks are present at $[M+H^+]$ of 34312 and 34372 amu. The spectrum shows the presence of unmodified variant at $[M+H^+]$ of 34312 amu and the appearance of a peak at $[M+H^+]$ of 34372 amu, shifted by +60 amu, which corresponds to the alkylated form of the Ser52Cys CSU. By increasing the incubation time with CIAM to 20, 30 and 40 minutes, panels C, D and E, respectively, we observe a time-dependent decrease in the proportion of unmodified variant polypeptide at $[M+H^+]$ of 34312 amu, 34312 amu and 34311 amu, respectively, concomitant with an increase in the alkylated variant polypeptide at $[M+H^+]$ of 34370 amu, 34370 amu, and 34368 amu, respectively. These results show that the reaction of Ser52Cys CSU with CIAM occurs over a much more reasonable time-frame, which will allow for a more accurate assessment of the pH-dependent alkylation of the Cys52 residue, the ultimate goal of our study.

Figure 4.10: Deconvoluted electrospray ionization mass spectra following the time-dependent modification of Ser52Cys CSU with CIAM

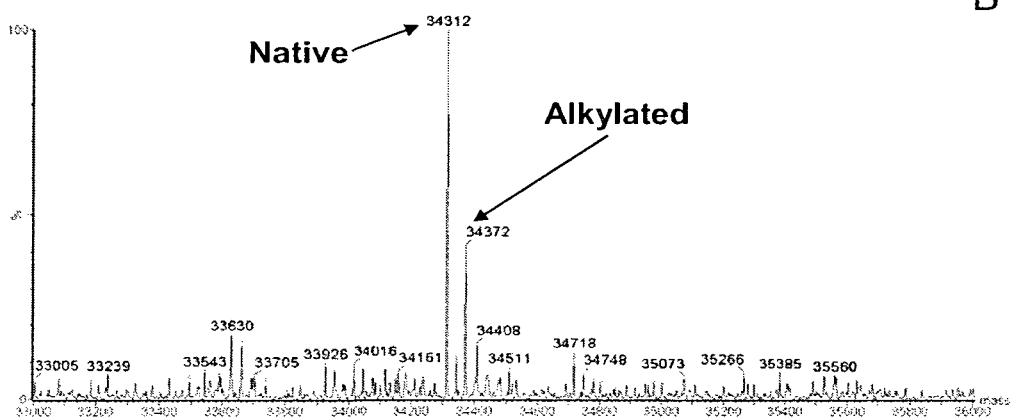
CSU (10 μM monomer) was reacted with 10 mM CIAM in 100 mM Tris-HCl (pH 7.0) at room temperature and protected from light. The alkylation reaction was initiated upon addition of CIAM was monitored for 0, 10, 20, 30 and 40 minutes. At the end of each time point, the modification reaction was quenched using DTT at a final concentration of 20 mM and samples were kept on ice. Protein samples (2-5 μM monomer) were prepared as described in section 4.2.6 immediately prior to direct injection. (A) Ser52Cys CSU's unmodified polypeptide peak observed at $[\text{M}+\text{H}^+]$ of 34313 amu. Ser52Cys CSU after incubation with 10 mM CIAM for 10 minutes (B), 20 minutes (C), 30 minutes (D) and 40 minutes (E). Unmodified polypeptide was observed at $[\text{M}+\text{H}^+]$ of 34312 amu, 34312 amu, 34312 amu and 34311 amu, respectively, while alkylated polypeptide was observed at $[\text{M}+\text{H}^+]$ of 34372 amu, 34370 amu, 34370 amu and 34368 amu, respectively, for each of the time points.

S52C CSU CIAM t=0



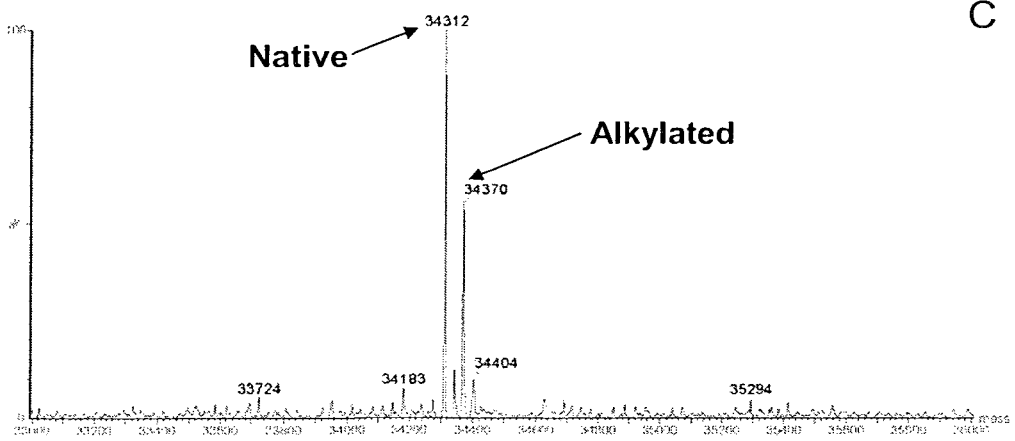
A

S52C CSU CIAM t=10min

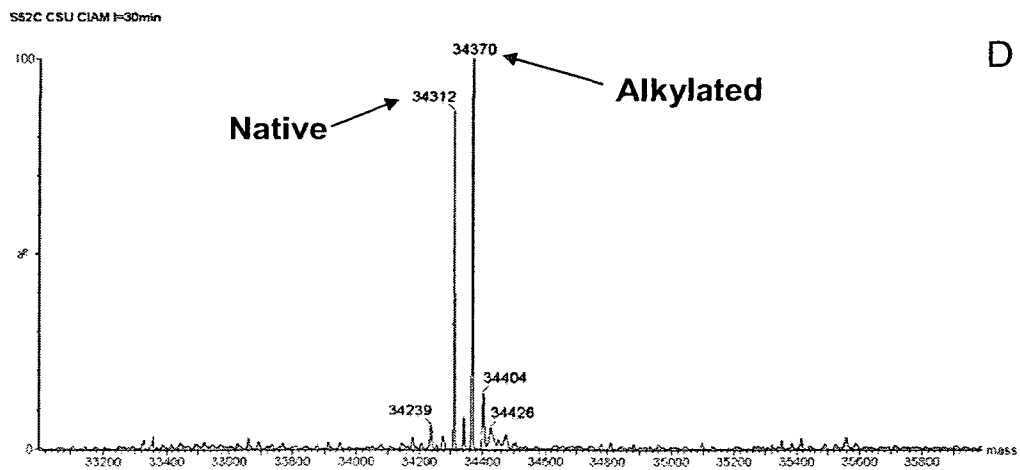


B

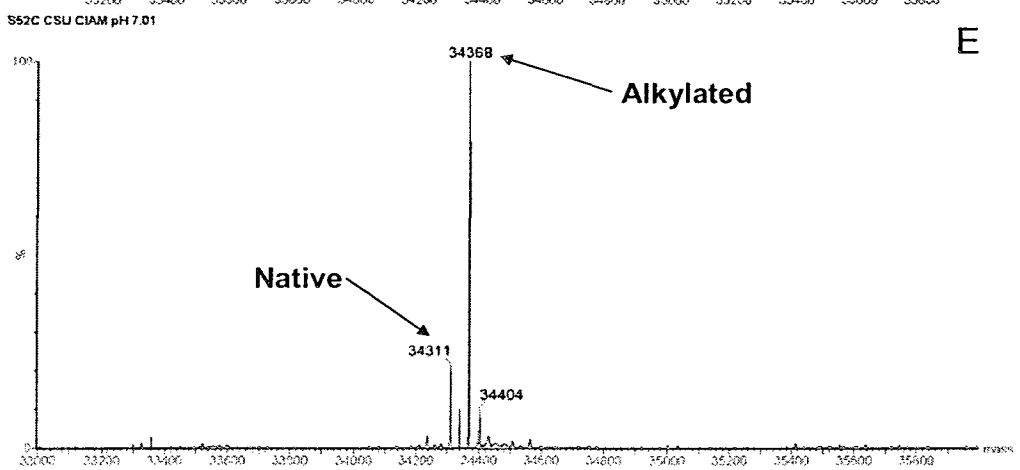
S52C CSU CIAM t=20min



C



D

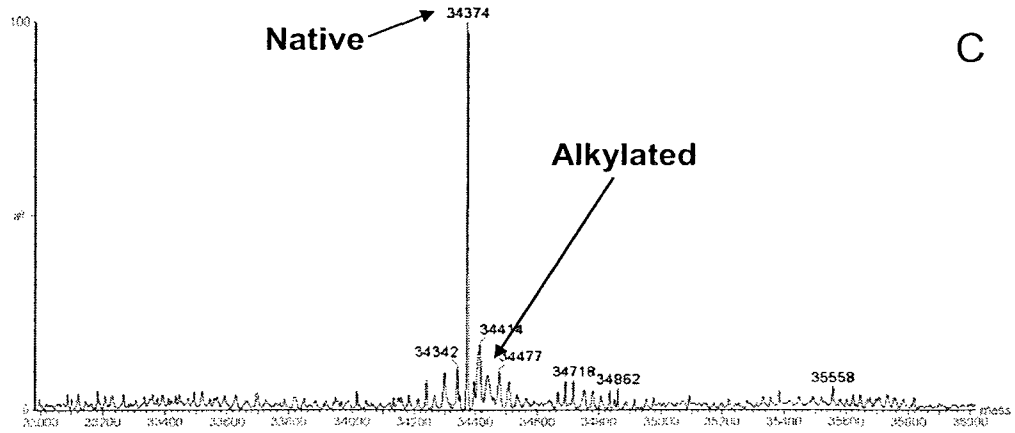
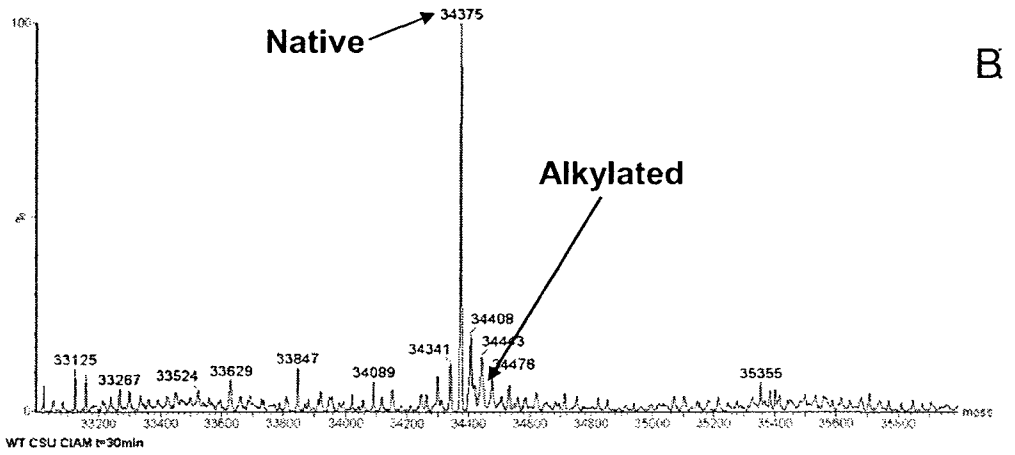
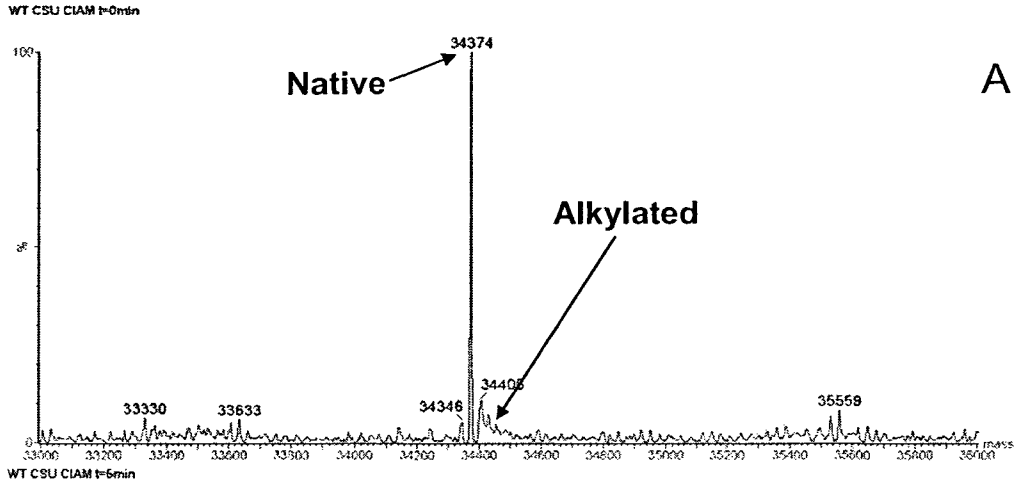


E

The same experiment was performed using the WT CSU in order to determine the reactivity of Cys47 with CIAM. These results are depicted in Figure 4.11 Panel A illustrates a single peak at $[M+H^+]$ of 34374 amu corresponding to the unmodified WT polypeptide. Further reaction of the WT CSU with CIAM for 5 and 30 minutes (panels B and C, respectively) continued to show only a single peak at $[M+H^+]$ of 34375 and 34374 amu, respectively. The results indicated that over the time course of this study, Cys47 was not alkylated and suggested that this residue was either inaccessible or unreactive to CIAM.

Figure 4.11: Deconvoluted electrospray ionization mass spectra displaying time-course modification of WT CSU with 10 mM CIAM

CSU (10 μ M monomer) was reacted with 10 mM CIAM in 100 mM Tris-HCl (pH 7.0) at room temperature and protected from light. The alkylation reaction was initiated upon addition of CIAM was monitored for 0, 5, and 30 minutes. At the end of each time point, the modification reaction was quenched using DTT at a final concentration of 20 mM and samples were kept on ice. Protein samples (2-5 μ M monomer) were prepared as described in section 4.2.6 immediately prior to direct injection. **(A)** WT CSU's unmodified polypeptide. WT CSU after incubation with 10 mM CIAM for 5 minutes **(B)** and 30 minutes **(C)**. Unmodified polypeptide was observed at $[M+H^+]$ of 34374 amu and 34375 amu, respectively, while alkylated polypeptide was not observed.



4.3.7 *In-silico* Digestion of WT and Ser52Cys CSU With Endopeptidase GluC

In-silico digestion consists of a software-based prediction of the digestion profile of a known polypeptide amino acid sequence based on the known properties of the endopeptidase selected. *In-silico* digestion was performed on the amino acid sequences of WT and Ser52Cys CSUs of ATCase (Table 4.1) with GluC using PeptideCutter (<http://ca.expasy.org/tools/peptidecutter/>). GluC from *Staphylococcus aureus* V8 is a serine protease which cleaves peptide bonds at the C-terminus of glutamic acid; it also cleaves at aspartic acid residues but with a 3000-fold lower efficiency (165). Moreover, the specificity for glutamate is higher relative to aspartate when the protein is digested in ammonium bicarbonate (pH 7.8) and ammonium acetate (pH 4.0) (166, 167).

In-silico digestion of the WT CSU with endopeptidase GluC yields 15 peptides ranging from 147.13 to 6442.39 Da. As shown in Table 4.1, Cys47, common to WT and variant, is present on a peptide consisting of residues 38 – 50 (LLKHKVIASCFFE) with a mass of 1534.88 Da (denoted P38-50).

Ser52Cys CSU possesses an additional Cys group, Cys52. Interestingly, upon *in-silico* digestion, the two cysteine residues, although in close proximity in the primary sequence, are segregated into two different peptides: P(38-50) housing Cys47 is mentioned above, whereas Cys52, is associated with residues 51 – 60 (ACTRTRLSFE) with a mass of 1183.35 amu, denoted P(51-60). The amino acid composition of P(38-50) and P(51-60) suggest that these peptides should be easily protonated for ESI-MS analysis. Thus, the *in-silico* results show that GluC digestion of CSU could be used to unambiguously identify the adducts on each of the cysteine residues by chemical modification studies and ESI-MS analysis.

Mass (Da)	Position	Peptide Sequence
4085.67	1 - 37	ANPLYQKHIISINDLSRDDLNLVLATAAKLKANPQPE
1534.88	38 - 50	LLKHKVIASCFFE
1167.29	51 - 60	ASTRIRLSFE
2636.92	61 - 86	TSMHRLGASVVGFSANTS LGKKGE
2559.92	87 - 109	TLADTISVISTYVDAIVMRHPQE
787.87	110 - 117	GAARLATE
3213.51	118 - 147	FSGNVPVLNAGDGSNQHTQTLDDLFTIQE
6442.39	148 - 204	TQGRDLNLHVAMVGDLYGRTVHSLTQALAKFDGNRFYFIAPDALAMPQYILDMLDE
1327.50	205 - 216	KGIAWSLHSSIE
147.13	217	E
448.54	218 - 221	VMAE
1494.77	222 - 233	VDILYMTRVQKE
715.76	234 - 239	RLDPSE
3746.35	240 - 272	YANVKAQFVLRASDLHNAKANMKVLHPLPRVDE
4239.89	273 - 310	IATDVDKTPHAWYFQQAGNGIFARQALLALVLRDLVL

Table 4.1: *In-silico* digest of WT CSU with endopeptidase GluC in bicarbonate buffer

Mass (amu)	Position	Peptide Sequence
4085.67	1 - 37	ANPLYQKHIISINDLSRDDLNLVLATAAKLKANPQPE
1534.88	38 - 50	LLKHKVIASCFE
1183.35	51 - 60	AC ⁺ TRIRLSFE
2636.92	61 - 86	TSMHRLGASVVGFSANTSLSGKKGE
2559.92	87 - 109	TLADTISVISTYVDAIVMRHPQE
787.87	110 - 117	GAARLATE
3213.51	118 - 147	FSGNVPVLNAGDGSNQHPTQTLLDLFTIQE
6442.39	148 - 204	TQGRLDNLHVAMVGDLYGRTVHSLTQALAKFDGNRFYFIAPDALAMPQYILDMLDE
1327.50	205 - 216	KGIAWSLHSSIE
147.13	217	E
448.54	218 - 221	VMAE
1494.77	222 - 233	VDILYMTRVQKE
715.76	234 - 239	RLDPSE
3746.35	240 - 272	YANVKAQFVLRASDLHNAKANMKVLHPLPRVDE
4239.89	273 - 310	IATDVKTPHAWYFQQAGNGIFARQALLALVLNRDLVL

Table 4.2: *In-silico* digest of Ser52Cys CSU with endopeptidase GluC in bicarbonate buffer

4.3.8 *In-vitro* Digestion of WT and Ser52Cys CSU With Endopeptidase GluC

In-vitro digestion was performed on native WT and variant CSU using endopeptidase GluC, in order to determine the extent of detection of the expected peptides generated by the *in-silico* digestion. The data depicted in Figures 4.12, 4.13 and 4.14 as well as Table 4.3, indicate that for both the WT and variant CSU, 11 of the 15 peptides were detected, yielding 65.3% sequence coverage. The peptides for both forms of the enzyme were detected in different ionization states ranging from $[M+H^+]$ to $[M+3H^+]$. The peptide of interest containing Cys52, henceforth denoted P(51-60), was detected as a doubly charged peak at $[M+2H^+]$ of 592.281 amu (Figure 4.14, Panel A). The peptide containing Cys47 was not detected under the same conditions.

In order to confirm that alkylation was performed on P(51-60) containing Cys52, the alkylated form of Ser52Cys CSU, was also digested with GluC and analyzed as for the unmodified forms of the CSU. Since P(51-60) was identified as a doubly charged peak $[M+2H^+]$ at 592.281 amu, the alkylated form of P(51-60) would be expected at $[M+2H^+]$ of 620.781 amu. Panel A, corresponding to the unmodified variant polypeptide, clearly shows that there is no interfering peak at 620.781 amu. Panel B corresponding to the alkylated variant polypeptide, clearly illustrates the appearance of a intense doubly charged peptide peak at $[M+2H^+]$ of 620.781 amu as well as a concomitant decrease in the intensity of the unmodified P(51-60) peptide peak at 592.281 amu. The results of these digestions confirm that alkylation of Ser52Cys CSU occurs on P(51-60).

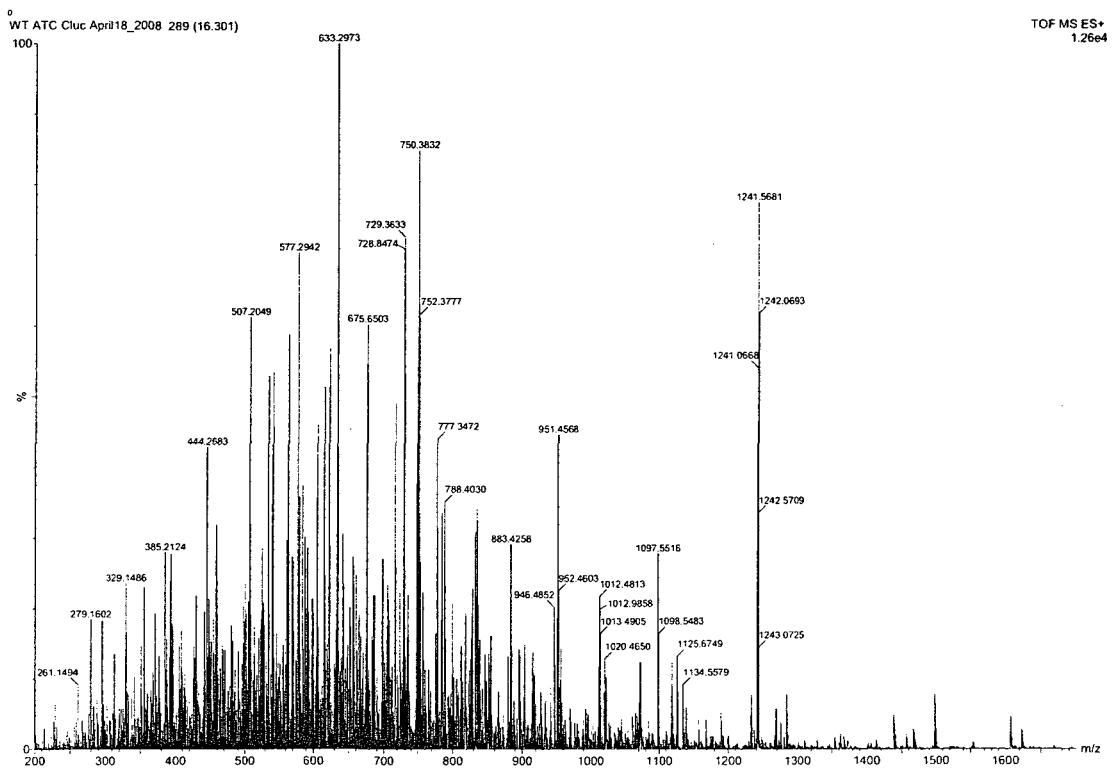


Figure 4.12: ESI-MS spectrum of WT CSU digestion profile with endopeptidase GluC in bicarbonate buffer

WT CSU was digested using endopeptidase GluC in 30 μ L of 50 mM ammonium bicarbonate (pH 7.8), at a ratio of 100:1 CSU:GluC (w/w), overnight at room temperature protected from light. The GluC-digested CSU samples were analyzed by LC-MS, using a linear 45 minute acetonitrile gradient from 5 – 95 % containing 0.1% TFA. Peptides were detected in positive mode from 200 – 3000 amu using the same instrument and parameters as described in section 4.2.6.

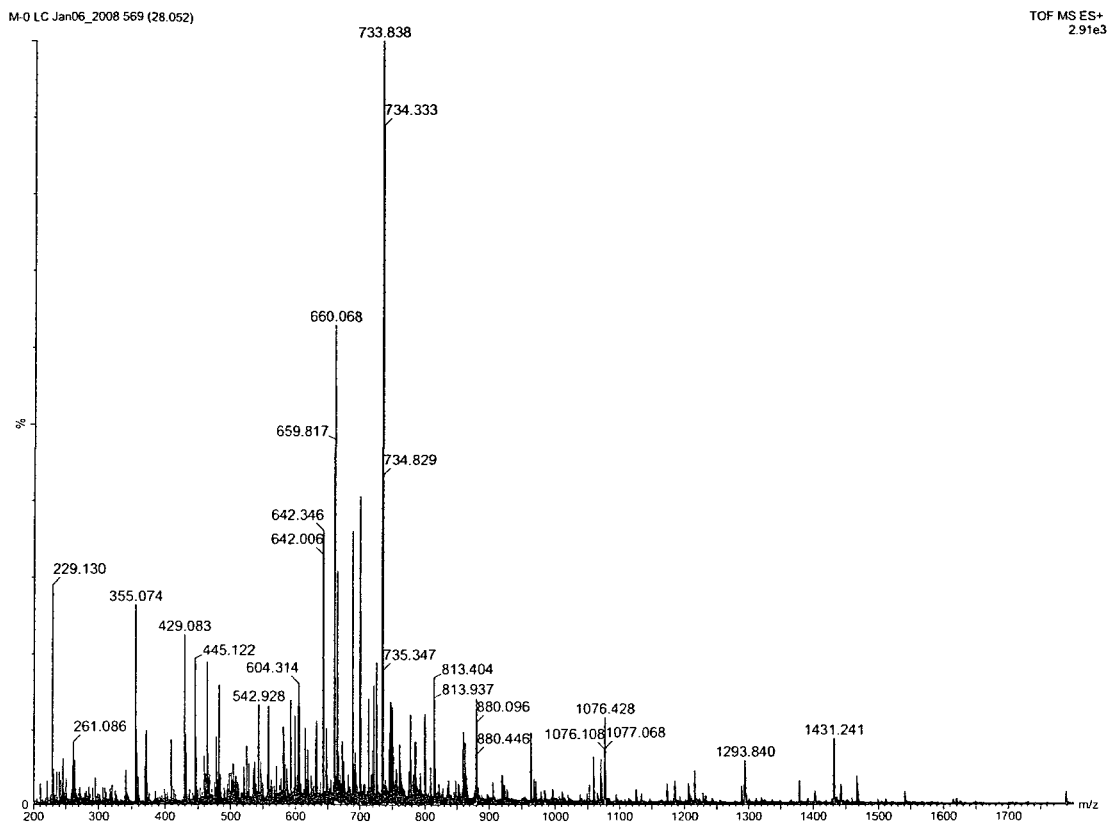


Figure 4.13: ESI-MS spectrum of Ser52Cys CSU digestion profile with endopeptidase GluC in bicarbonate buffer

Ser52Cys CSU was digested using endopeptidase GluC in 30 μ L of 50 mM ammonium bicarbonate (pH 7.8), at a ratio of 100:1 CSU:GluC (w/w), overnight at room temperature protected from light. The GluC-digested CSU samples were analyzed by LC-MS, using a linear 45 minute acetonitrile gradient from 5 – 95 % containing 0.1% TFA. Peptides were detected in positive mode from 200 – 3000 amu using the same instrument and parameters as described in section 4.2.6.

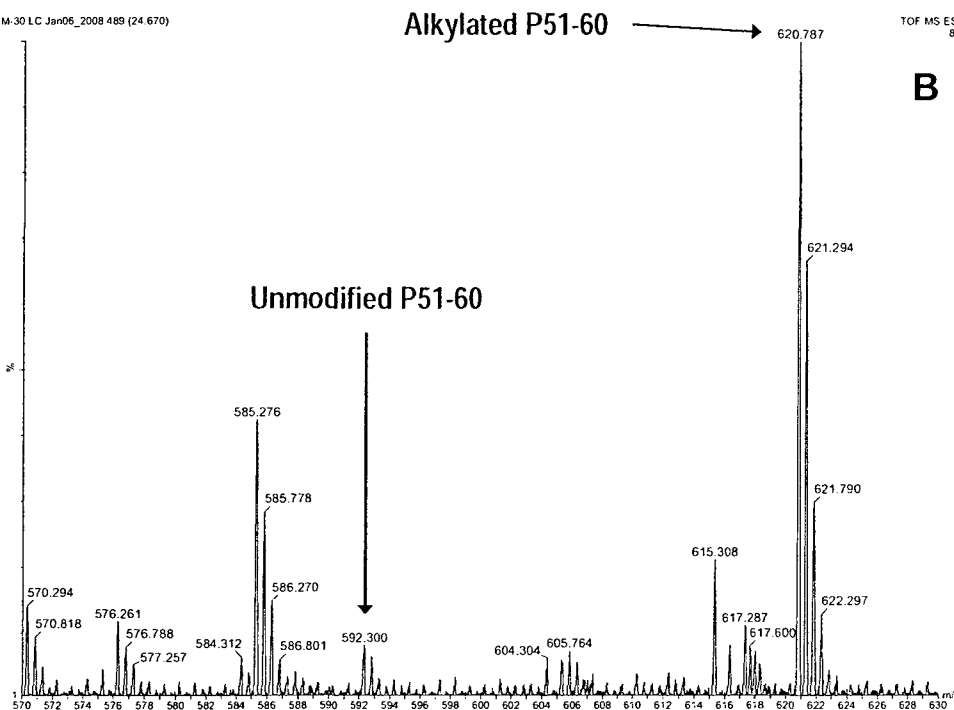
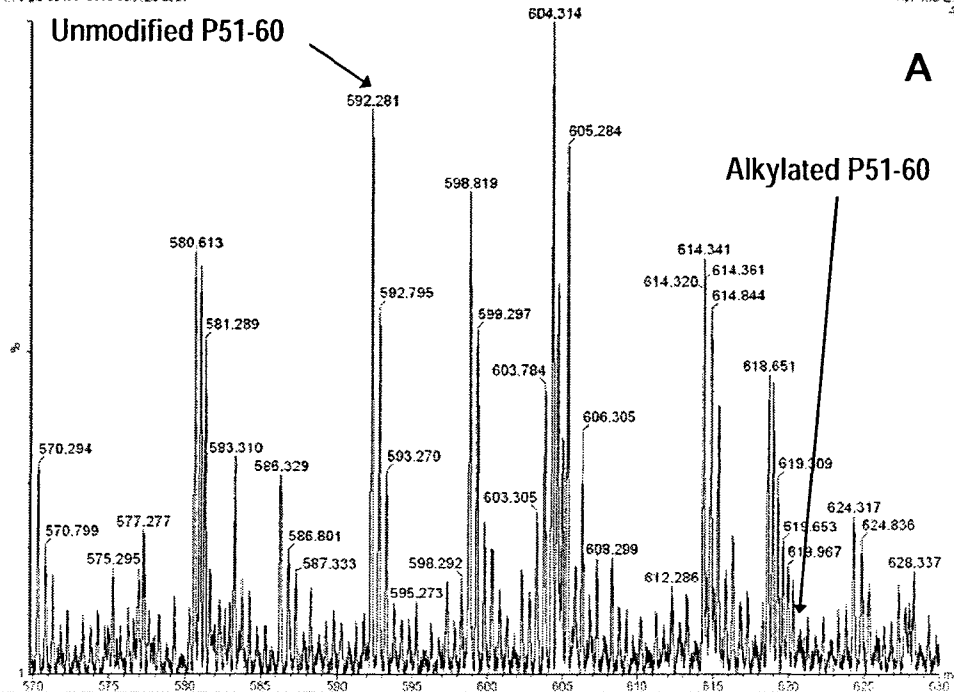
Mass (amu)	Position	Peptide Sequence	Ionization State
4085.67	1 - 37	ANPLYQKHHSINDLSRDDLNLVLATAAKLKANPQPE	+3
1534.88	38 - 50	LLKHKVIASCFFE	ND
1167.29	51 - 60	ASTRTRLSFE	+1
1183.35	51 - 60	AC ⁺ TRTRLSFE	+2
2636.92	61 - 86	TSMHRLGASVVGFSANTSLSGKKGE	+3
2559.92	87 - 109	TLADTISVISTYVDAIVMRHPQE	+3
787.87	110 - 117	GAARLATE	+1
3213.51	118 - 147	FSGNVPVLNAGDGSNQHTQTLLDLFTIQE	+2
6442.39	148 - 204	TQGRDLNLHVAMVGDLYGRTVHSLTQALAKFDGNRFYFIAPDALAMPQYILDMLDE	ND
1327.50	205 - 216	KGIAWSLHSSIE	+2
147.13	217	E	ND
448.54	218 - 221	VMAE	ND
1494.77	222 - 233	VDILYMTRVQKE	+2
715.76	234 - 239	RLDPSE	+1
3746.35	240 - 272	YANVKAQFVLRASDLHNAKANMKVLIHPLPRVDE	ND
4239.89	273 - 310	IATDVDKTPHAWYFQQAGNGIFARQALLALVLRDLVL	+3

Table 4.3: *In-vitro* digest of WT and Ser52Cys CSU with endopeptidase GluC in bicarbonate buffer

Table indicating the expected peptides for both WT and Ser52Cys CSU. Two P(51-60) peptides are indicated; the shaded line corresponds to Ser52Cys CSU and the other to WT CSU. The ionization state of the peaks that were detected by LC-MS is indicated in the Ionization State column. Peptides that were not detected are marked as ND (not detected).

Figure 4.14: *In-vitro* digest of WT and Ser52Cys CSU with endopeptidase GluC in bicarbonate buffer

Unmodified and alkylated Ser52Cys CSU were digested using endopeptidase GluC in 30 μ L of 50 mM ammonium bicarbonate (pH 7.8), at a ratio of 100:1 CSU:GluC (w/w), overnight at room temperature protected from light. The GluC-digested CSU samples were analyzed by LC-MS, using a linear 45 minute acetonitrile gradient from 5 – 95 % containing 0.1% TFA. Peptides were detected in positive mode from 200 – 3000 amu using the same instrument and parameters as described in section 4.2.6. Panel A corresponds to the unmodified GluC digest of the variant CSU; the unmodified P(51-60) peptide is observed as an intense peak at $[M+2H^+]$ of 592.281 amu. No interfering peak is seen at 620.781 amu, where the alkylated form of P(51-60) is expected. Panel B corresponds to the alkylated GluC digest of the variant CSU; unmodified P(51-60) peptide is seen as a small peak at $[M+2H^+]$ of 592.281 amu and the alkylated P(51-60) peptide is seen as an intense peak at $[M+2H^+]$ of 620.787 amu.



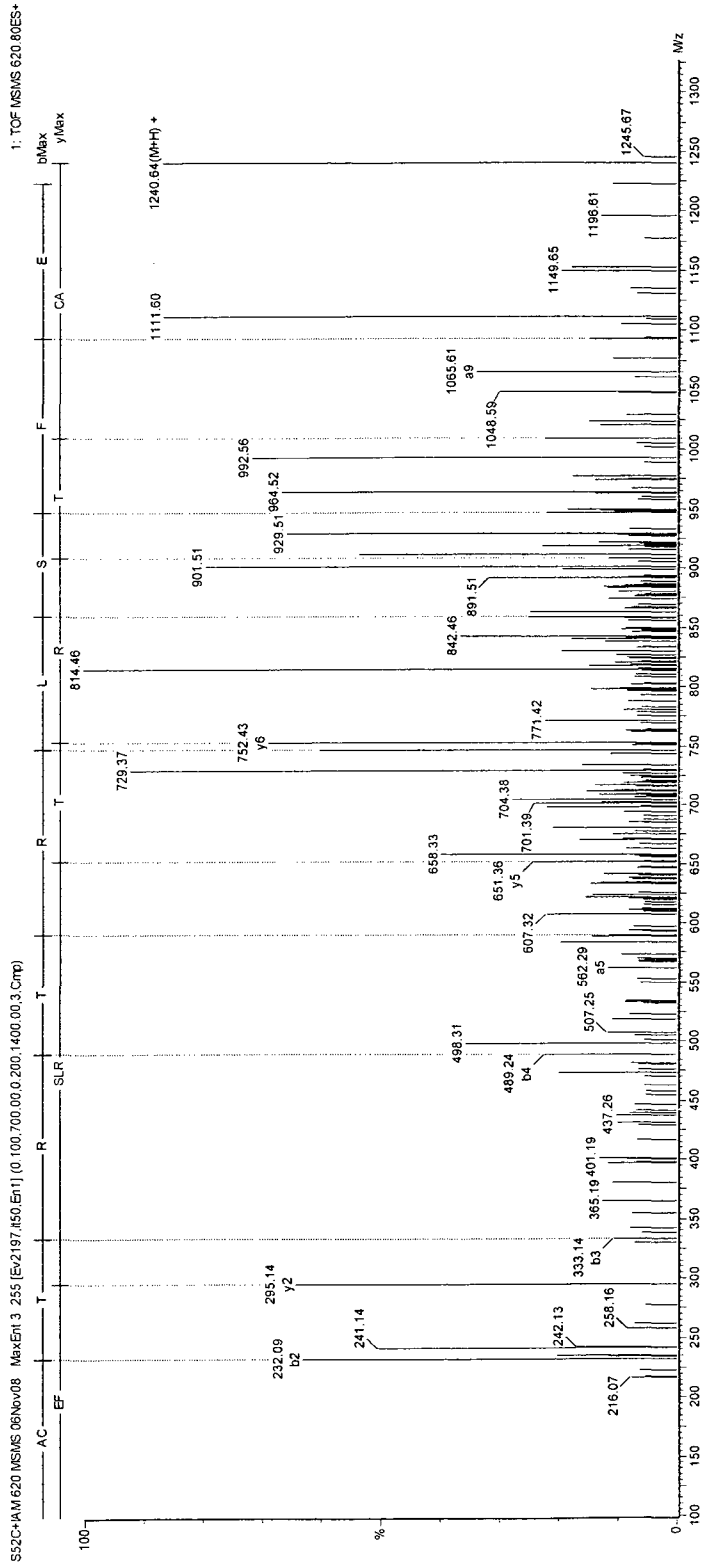


Figure 4.15: ESI-MS/MS spectrum of peptide sequencing data for alkylated P(51-60)

Alkylated peptide P(51-60) was subjected to ESI-MS/MS analysis described in section 4.2.6 in order to determine the amino acid sequence of the peptide. Sequencing data revealed the sequence of alkylated P(51-60) to be AC(IAM)TRTRLSFE, which confirms the identity of the peptide and the residue alkylated (Cys52).

4.3.9 Determination of Cys52 pK_a by Titration with Chloroacetamide

ESI-MS was used to monitor the alkylation of Cys52 in Ser52Cys CSU by reaction with 10 mM CIAM for 40 minutes at various pH values, ranging from 3.93 to 9.01. The parameters of the chemical modification in this experiment allowed us to probe the ionization state and surface accessibility of Cys52 in the variant CSU.

The pH-dependent alkylation reaction was carried out in a 2 x 3-component buffer (0.1 M 2-morpholinoethanesulfonic acid (MES), 0.1 M N-ethylmorpholine, 0.2 M diethanolamine), which ensured an appropriate buffering capacity within the experimental pH range being studied.

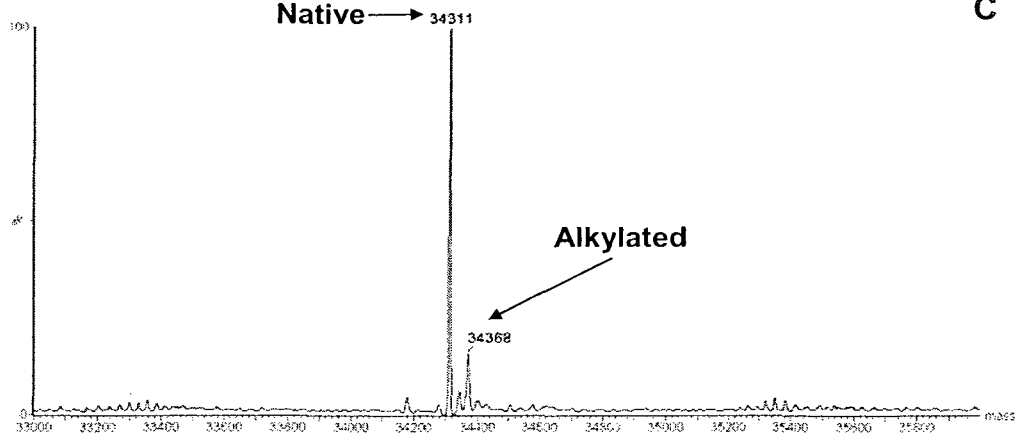
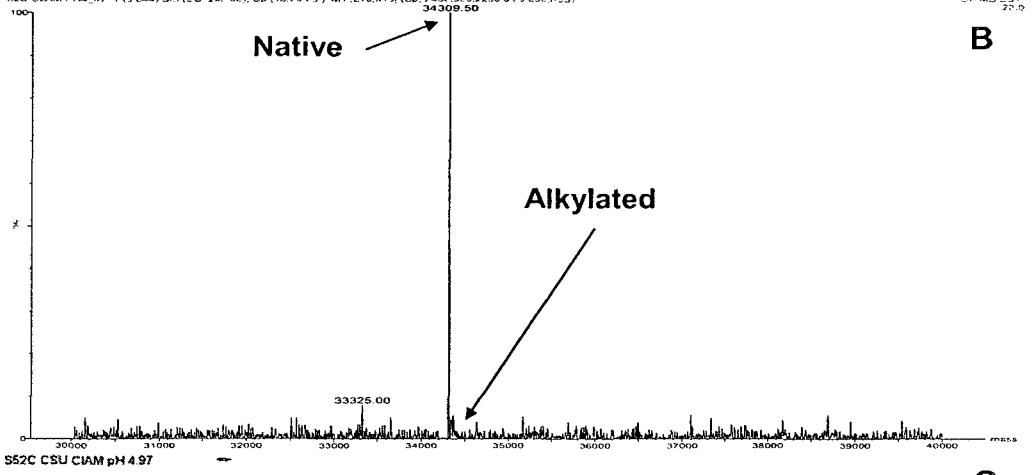
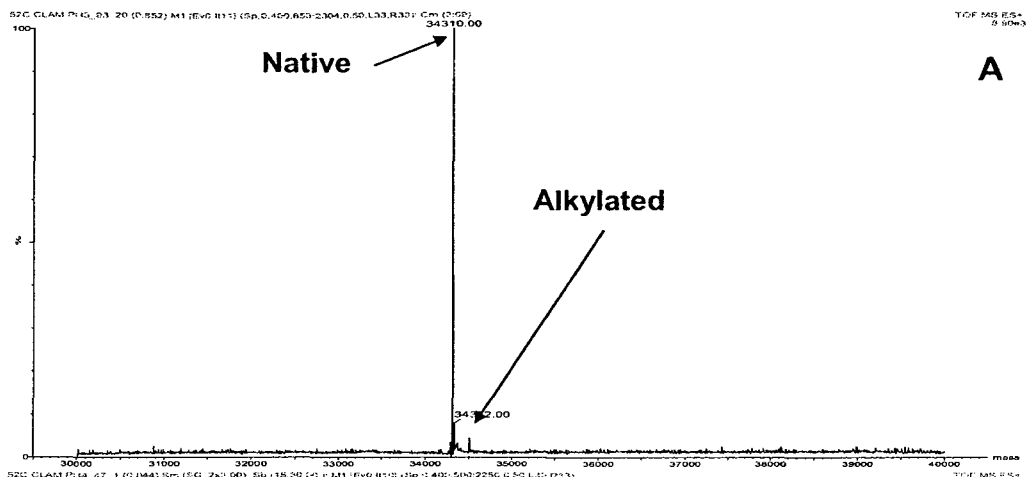
Figure 4.16, panels A and B represent the deconvoluted ESI-MS spectra of the Ser52Cys CSU polypeptide after the 40 minute reaction with 10 mM CIAM at pHs 3.93 and 4.47, respectively. The spectra both exhibit a single major peak at $[M+H^+]$ of 34310 amu corresponding to the unmodified Ser52Cys CSU; a second minor peak can be seen at $[M+H^+]$ of 34367 amu when zoomed to baseline, corresponding to the alkylated Ser52Cys CSU.

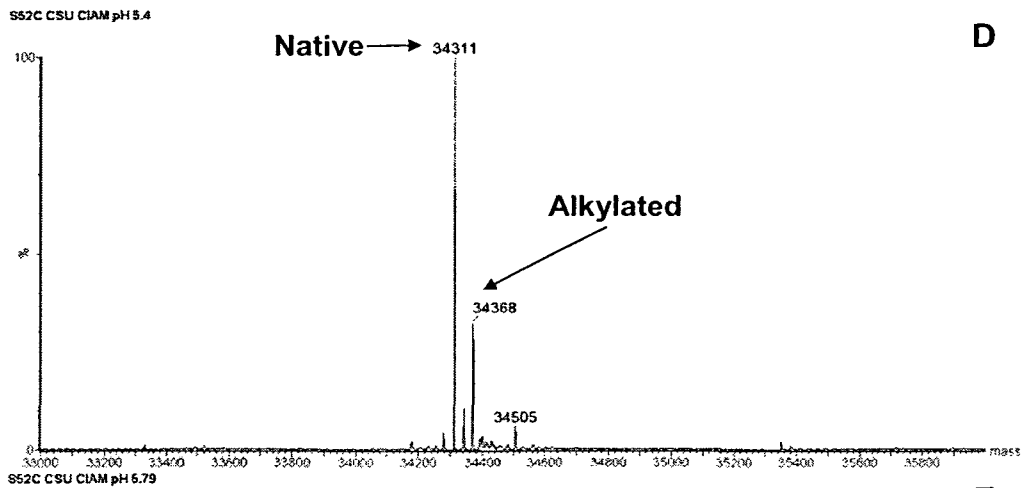
Panel C represents the deconvoluted ESI-MS spectrum of the Ser52Cys CSU polypeptide after the 40 minute reaction with 10 mM CIAM at pH 4.97. The spectrum exhibits two major peaks; the first at $[M+H^+]$ of 34311 amu corresponding to the unmodified Ser52Cys CSU and the second at $[M+H^+]$ of 34368 amu corresponding to the alkylated Ser52Cys CSU. Panels D-N illustrate the deconvoluted ESI-MS spectra of the Ser52Cys CSU polypeptide after the 40 minute reaction with 10 mM CIAM at increasing pH values. All spectra display two major peaks at $[M+H^+]$ of 34311 amu and $[M+H^+]$ of 34368 amu, corresponding to the unmodified Ser52Cys CSU and the alkylated Ser52Cys

CSU, respectively. A trend is clearly visible in the spectra, wherein the ratio of alkylated CSU: unmodified CSU increases with increasing pH. However, the above mentioned ratios seem to reach a plateau at pH values higher than 7.01. This observation suggests that the pK_a of Cys52 is less than 7.01 and beyond that pH; the ionization state of the thiol of Cys52 is completely in its anionic form and is fully deprotonated.

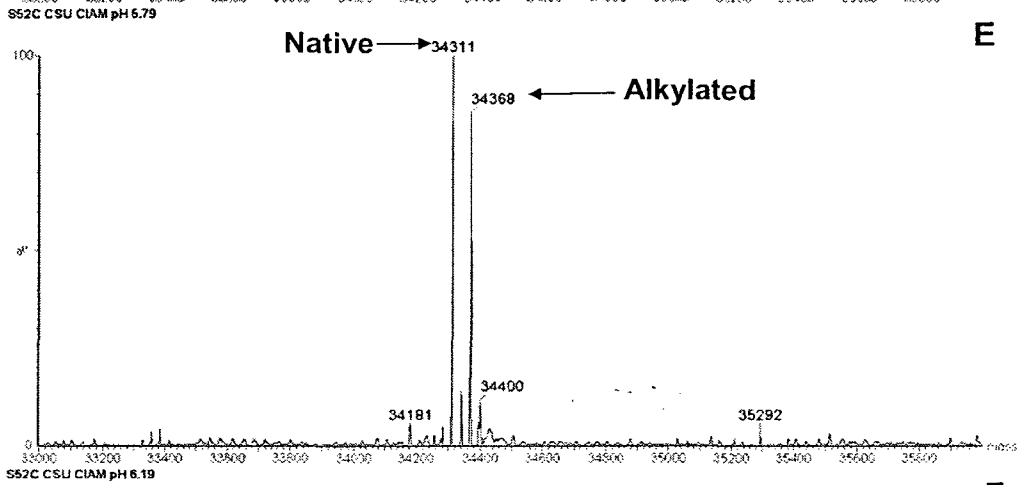
Figure 4.16: Deconvoluted electrospray ionization mass spectra of the pH-dependent modification of Ser52Cys CSU with 10 mM CIAM

Variant CSU (10 μ M monomer) was reacted with 10 mM CIAM for 40 minutes in 2 x 3-component buffer (0.1 M 2-morpholinoethanesulfonic acid (MES), 0.1 M N-ethylmorpholine, 0.2 M diethanolamine) at room temperature and protected from light at several pH values ranging from 3.93 to 9.01. After 40 minutes, the modification reaction was quenched using DTT at a final concentration of 20 mM and the samples were kept on ice. Protein samples (2-5 μ M monomer) were prepared as described in section 4.2.6 immediately prior to direct injection. Panels A-N illustrate the results of the alkylation reaction of Ser52Cys CSU with CIAM at pH values of 3.93 (A), 4.47 (B), 4.97 (C), 5.40 (D), 5.79 (E), 6.19 (F), 6.60 (G), 7.01 (H), 7.41 (I), 7.80 (J), 7.99 (K), 8.19 (L), 8.53 (M), 9.01 (N), respectively. Native Ser52Cys CSU polypeptide is observed at $[M+H^+]$ of 34311 amu and alkylated Ser52Cys CSU polypeptide is observed at $[M+H^+]$ of 34368 amu.

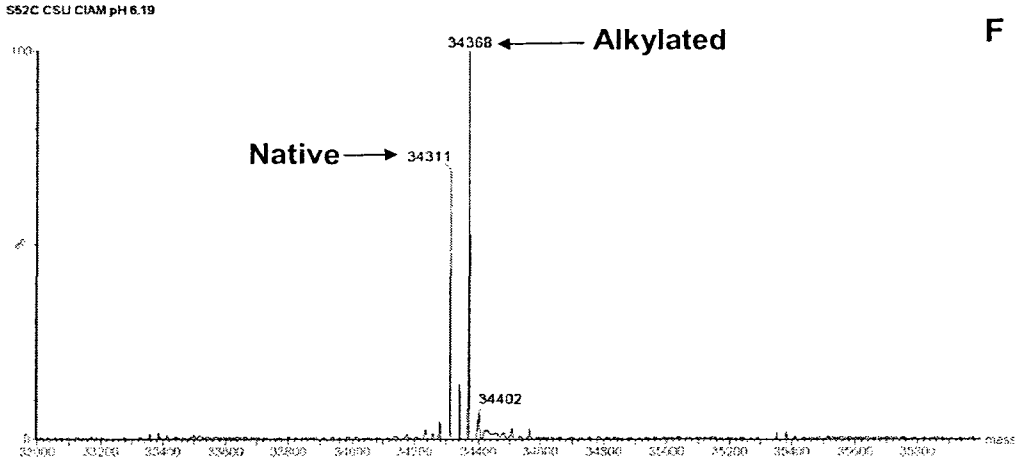




D

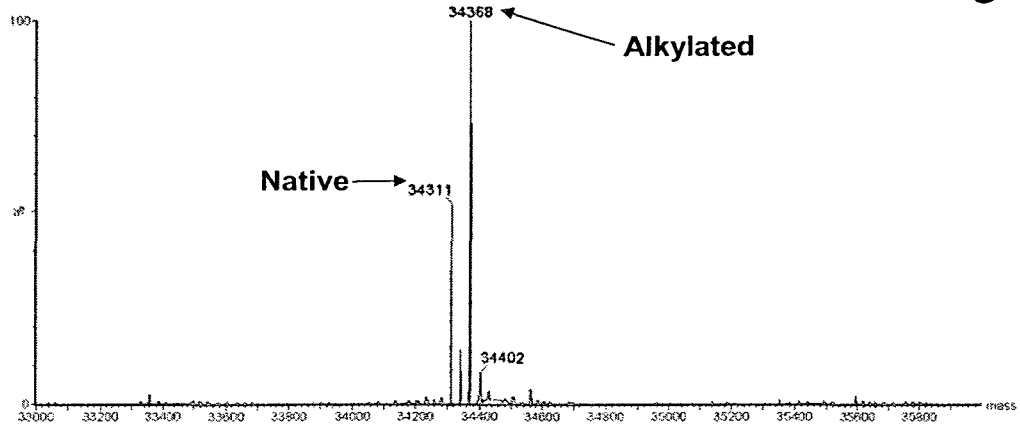


E



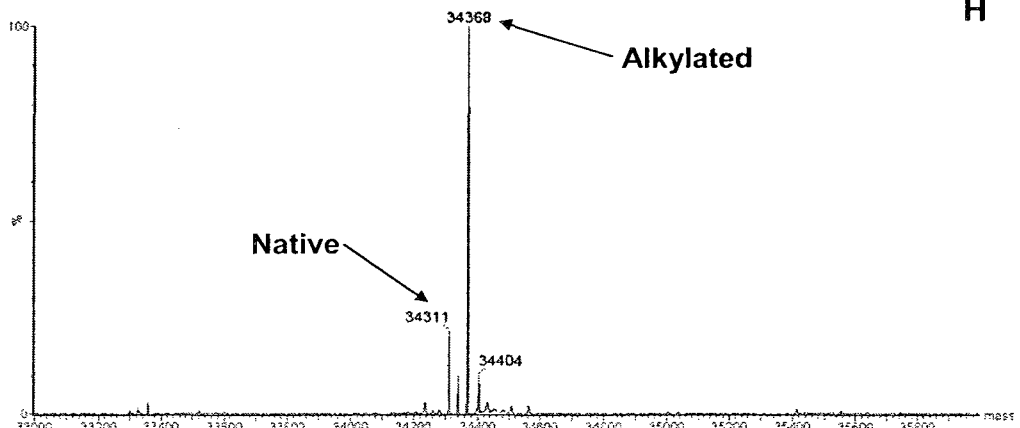
F

S52C CSU CIAM pH 6.60



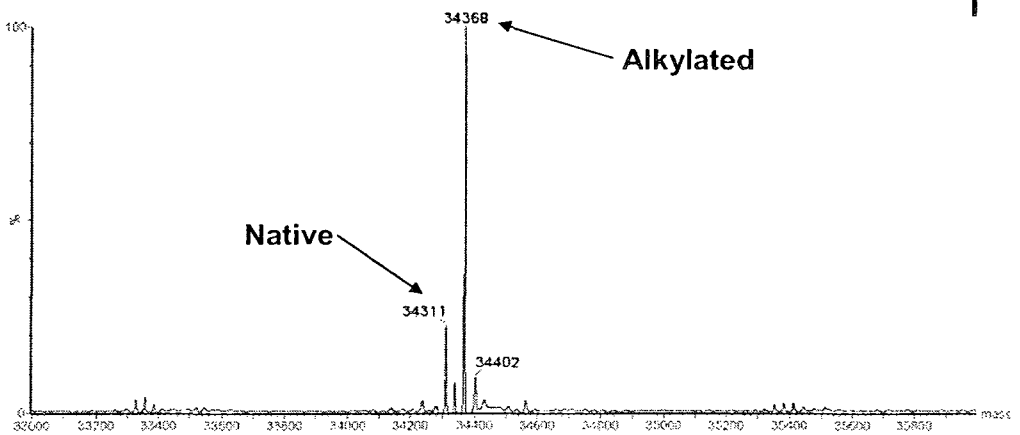
G

S52C CSU CIAM pH 7.01



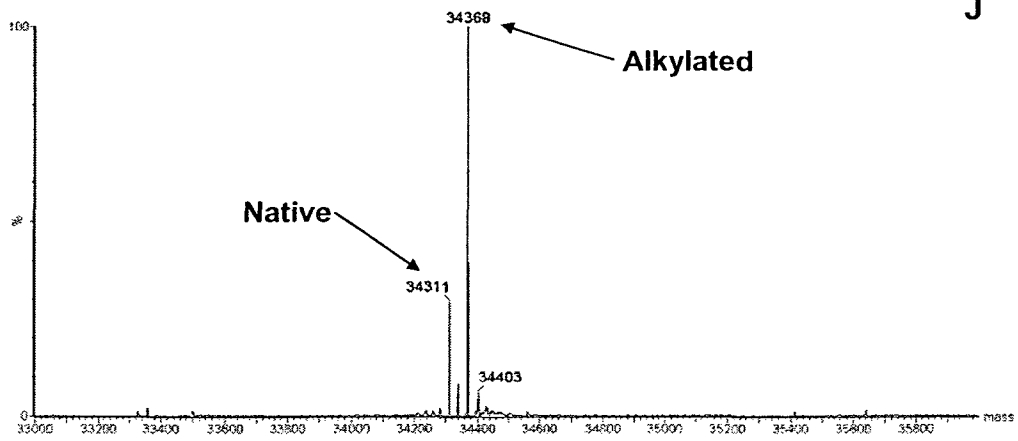
H

S52C CSU CIAM pH 7.41



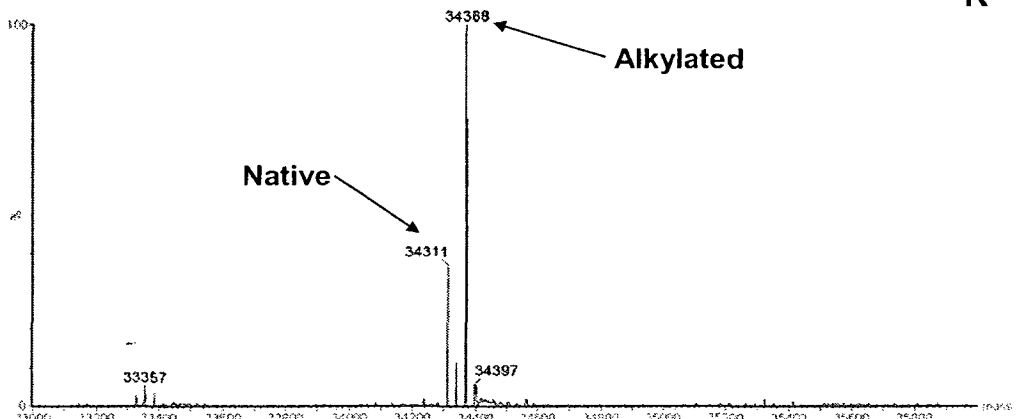
I

S52C CSU CIAM pH 7.80



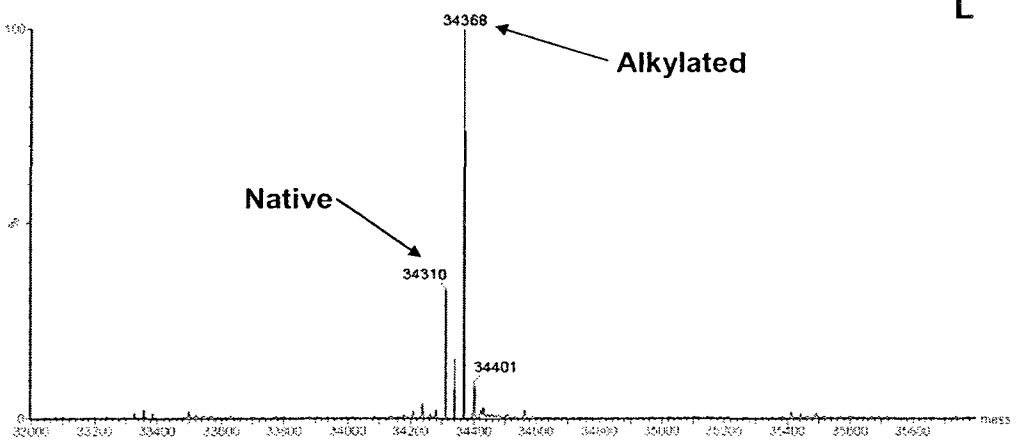
J

S52C CSU CIAM pH 7.99



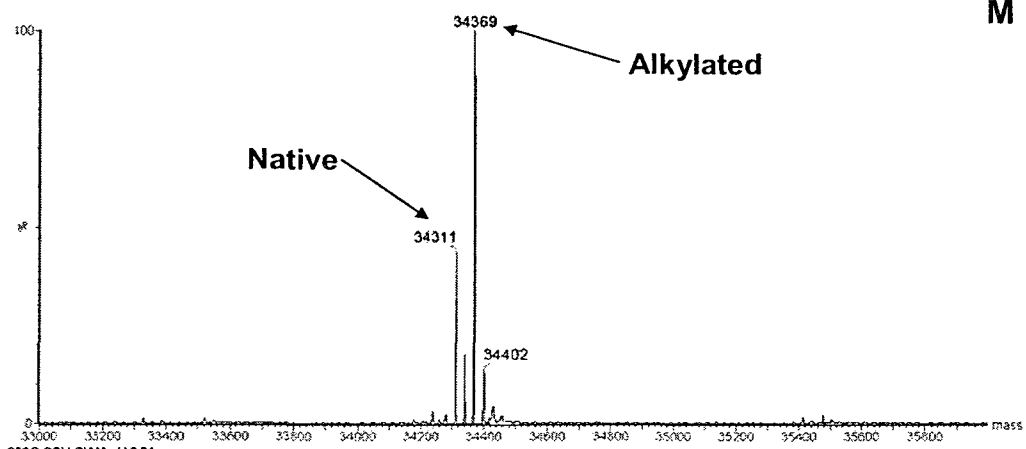
K

S52C CSU CIAM pH 8.19



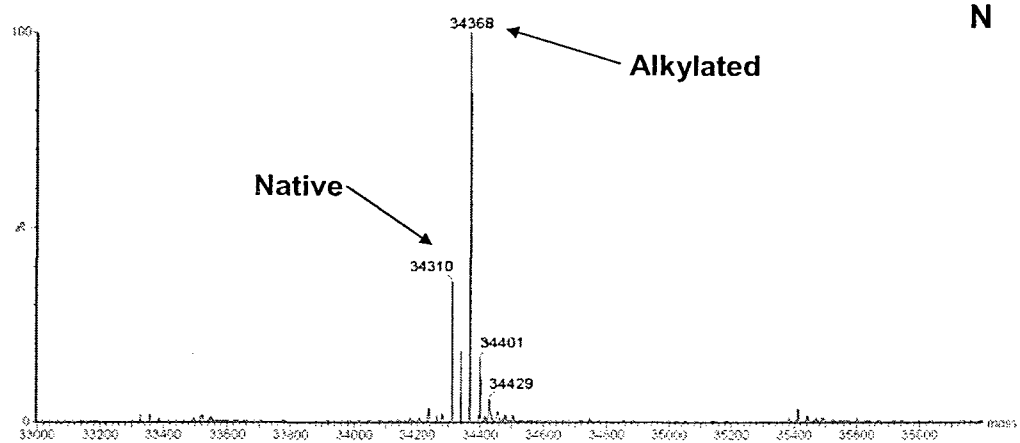
L

S52C CSU CIAM pH 8.53



M

S52C CSU CIAM pH 9.01



N

4.3.10 Determination of Cys52 pK_a in Ser52Cys CSU by Titration With CIAM

The results depicted in Figure 4.16 clearly indicate that the extent of alkylation of Ser52Cys, and hence that of Cys52, is pH-dependent. As pH is increased, the ratio of alkylated to unmodified CSU increases proportionately to pH; the extent of modification then remains constant from pH 7.01 to 9.01. The extent of alkylation was quantified by using the relationship:

$$\frac{\text{Intensity of alkylated Ser52Cys CSU}}{\text{Intensity of (unmodified + alkylated) Ser52Cys CSU}}$$

When plotted as a function of the experimental pH values, the data fit well to the Equation 4.1 describing the ionization of a single residue (Figure 4.17). A pK_a of 5.63 ± 0.05 was determined for Cys52.

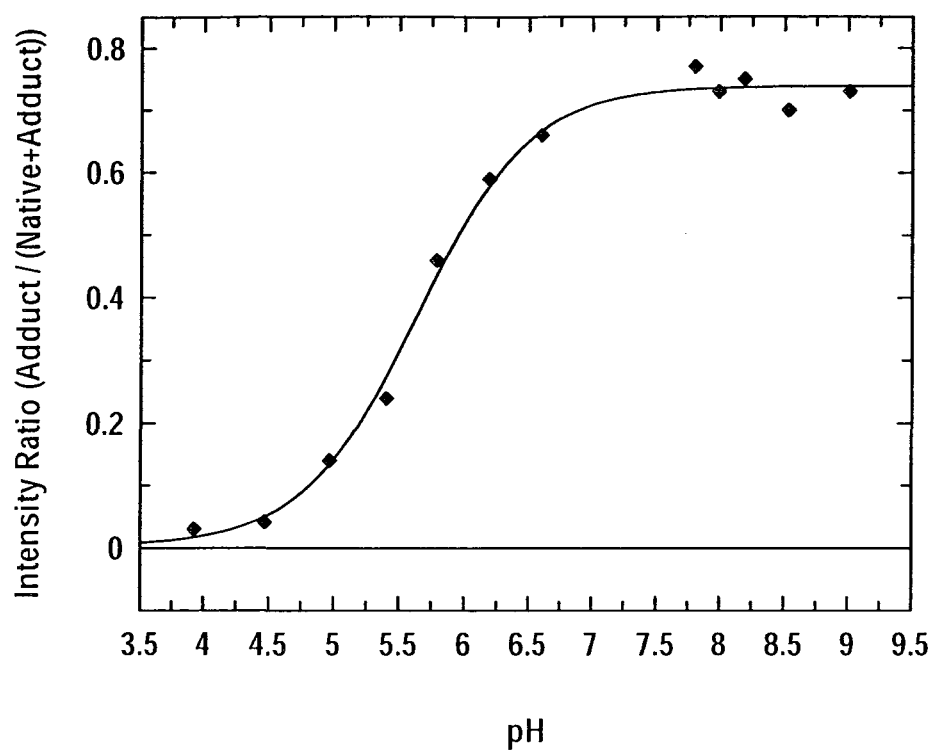


Figure 4.17: Titration of Cys52 residue by reaction of Ser52Cys catalytic trimer with CIAM for 40 minutes at different pH values

Graph illustrating the ratios of (alkylated Ser52Cys CSU / (unmodified Ser52Cys CSU + alkylated Ser52Cys CSU)) plotted versus the different experimental pH values into the Erithacus Grafit 5.0 software by using the equation for a single pK_a .

4.4 DISCUSSION

The focus of this chapter was to develop a simple purification scheme for His-tagged holoenzyme, to separate CSU from His-tagged RSU, to determine the biophysical characteristics of WT and Ser52Cys CSU, and to determine the reactivity, accessibility and stoichiometry of the cysteine residues in both variants, as well as to determine the pK_a of the Cys52 residue in Ser52Cys CSU.

An initial protocol for the purification of CSU of ATCase involved purification of the holoenzyme first with ion-exchange followed by size exclusion chromatography (168). CSU and RSU were then dissociated by treatment of the purified holoenzyme with neohydrin, followed by separation of the CSUs by ion exchange chromatography (156). Hence, upon separation of the CSUs from the RSUs, the additional purification step using ion-exchange chromatography renders the procedure time-consuming. In this report, we have further simplified the purification strategy by performing the on-column reaction of neohydrin with the holoenzyme and also eliminated the need of subsequent ion-exchange purification for the isolation of the CSU from the RSU.

The results from SDS-PAGE and ESI-MS analyses clearly indicate that the CSU, which eluted from the Ni-NTA affinity resin upon reaction with neohydrin, was homogeneous and devoid of any protein impurities. It is noteworthy that upon elution of CSU, the His-tagged RSU was still bound to the nickel resin and was successfully eluted with buffer containing 250 mM imidazole, as per the Qiagen Handbook. The initial RSU fractions were, however, contaminated with protein which may very well include unreacted holoenzyme. These results suggest that a second round of neohydrin reaction

may be necessary to ensure that no unreacted holoenzyme remains bound to the resin. The results of this quick purification scheme highlight the efficiency of this procedure yielding high amounts of pure CSU and RSU, notably 35 mg CSU and 50 mg RSU per liter of culture, which is approximately double the amount previously reported by Graf and Schachman (169).

ESI-MS analysis of both WT and variant CSUs showed a discrepancy of approximately -130 amu, relative to the molecular weight calculated from their respective amino acid sequences. The molecular weights obtained by ESI-MS (Figure 4.2 panels A and B) do however agree with reports by Hoover *et al.* (139) that the CSU undergoes post-translational modification, notably cleavage of the N-terminal methionine in the catalytically active polypeptide. Cleavage of N-terminal methionine residues has been reported for many enzymes, including CM-PD in *E. coli*, discussed in Chapter 2 of this thesis. N-terminal methionine cleavage is dictated mainly by the nature of the second amino acid and is catalyzed by methionyl-aminopeptidase (170).

The mercury-containing reagent, neohydrin, is essential for the isolation of the CSU from the holoenzyme by chelating the 4 cysteine residues in the RSU within the zinc binding domain (Figure 1.12). WT and Ser52Cys CSUs possess a cysteine residue at position 47 and the latter, a second engineered cysteine residue at position 52. Cysteine is known to bind mercury with reported K_d values ranging from 0.17 – 3.70 μM (171, 172). Hence, it was important to ensure that no mercury remained bound to the CSUs prior to experimental use. Both the WT and variant CSU were subjected to mass spectrometric analysis, in order to assess the presence or absence of mercury, which is possible by ESI-MS as reported by Cohen *et al.* (160). The ESI-MS spectrum of WT CSU (Figure 4.2,

panel A) illustrates a single peak at $[M+H^+]$ of 34294 amu, which is in excellent agreement with the expected value discussed previously. The ESI-MS spectrum of Ser52Cys CSU exhibits two peaks at $[M+H^+]$ of 34312 amu and 34511 amu, the former being in excellent agreement with the expected molecular weight of Ser52Cys CSU and the latter peak corresponding to the variant CSU with a single mercury adduct, exhibiting a shift of +199 amu. The intensity ratio of mercury-adduct: native Ser52Cys polypeptide in Figure 4.2 panel B was determined to be 5:3, suggesting that approximately 60% of each monomer is bound with a mercury ion. Furthermore, ICP-MS confirmed the nature of the metal ion bound as mercury, and also confirmed the stoichiometry determined by ESI-MS; 1.7 μM of mercury is bound per μM of CSU, which corresponds to 0.57 mercury ions for each monomer of the CSU. Assuming that the WT and variant CSU were purified under identical conditions, the absence of mercury in the WT CSU suggests that in contrast to the engineered cysteine at position 52, Cys47 was either inaccessible or unreactive toward mercury. In any event, our studies suggest that treatment of the CSU with 10 mM EDTA and 20 mM DTT for 30 minutes on ice prior to experimental use is an effective method to remove and residual mercury which may be bound to the CSU (Figure 4.3).

The reactivity of cysteine residues toward cysteine-specific reagents is dependent on several factors. These factors include solvent accessibility, pK_a , reactivity of the reagent, compatibility of the reagent with the cysteine environment, the stability of the bonds formed between cysteine and the reagent, and finally, the nature of the leaving group of the sulfhydryl reagent (141). As expected, titration with DTNB of both denatured WT and variant CSU indicated that a single cysteine residue (Cys47) was

modified in the WT enzyme and two cysteines (Cys47 and Cys52) were modified in the variant. For the variant under non-denaturing conditions, a single cysteine residue reacted within 1 minute, and a second cysteine residue appears to react slowly until a further 0.25 more cysteine residues per monomer have been modified by 60 minutes. Together, the results of the DTNB modification of both WT and Ser52Cys CSUs suggest that Cys52 is considerably more reactive than Cys47 at pH 8.2. The increased reactivity of this residue may be due to the fact that it is solvent exposed making it readily accessible for DTNB modification or may be negatively charged at the experimental pH of 8.2, which would agree with our hypothesis that the Cys52 sulfhydryl group may have an unusually low pK_a (< 6.0).

pH-dependent alkylation of the variant CSU was performed using the slower reacting reagent CIAM, from pH 3.93 to 9.01 in order to determine the pK_a of Cys52. The results in Figure 4.16 indicate that alkylation of the native variant CSU occurs more extensively with increasing pH, as seen by the decrease in unmodified polypeptide peak and concomitant increase of the alkylated polypeptide peak which is shifted by +57 amu. Digestion of the unmodified and alkylated polypeptide using endopeptidase GluC (Figure 4.14) clearly indicates that the alkylation occurs on the peptide containing the Cys52 residue. Further ESI-MS/MS peptide sequencing of this peptide P(51-60) confirmed the expected amino acid sequence as being AC(IAM)TRTRLSFE, with the alkylation occurring on the Cys52 residue (Figure 4.15). A plot of the intensity ratios of (alkylated polypeptide)/((unmodified polypeptide)+(alkylated polypeptide)) versus experimental pHs yields the curve seen in Figure 4.17. By fitting the data to the equation for a single pK_a we determined that the pK_a of Cys52 in the variant CSU is 5.6 ± 0.1 , which confirms

our hypothesis that Cys52 is present in the active site with a depressed pK_a . Other enzymes have also been reported to possess cysteine groups with unusually low pK_a values. Among these is Cys106 in human DJ-1 which was determined to have a pK_a of 5.4 (173) and Cys283 in the active site of human muscle creatine kinase with a pK_a of 5.6 (174).

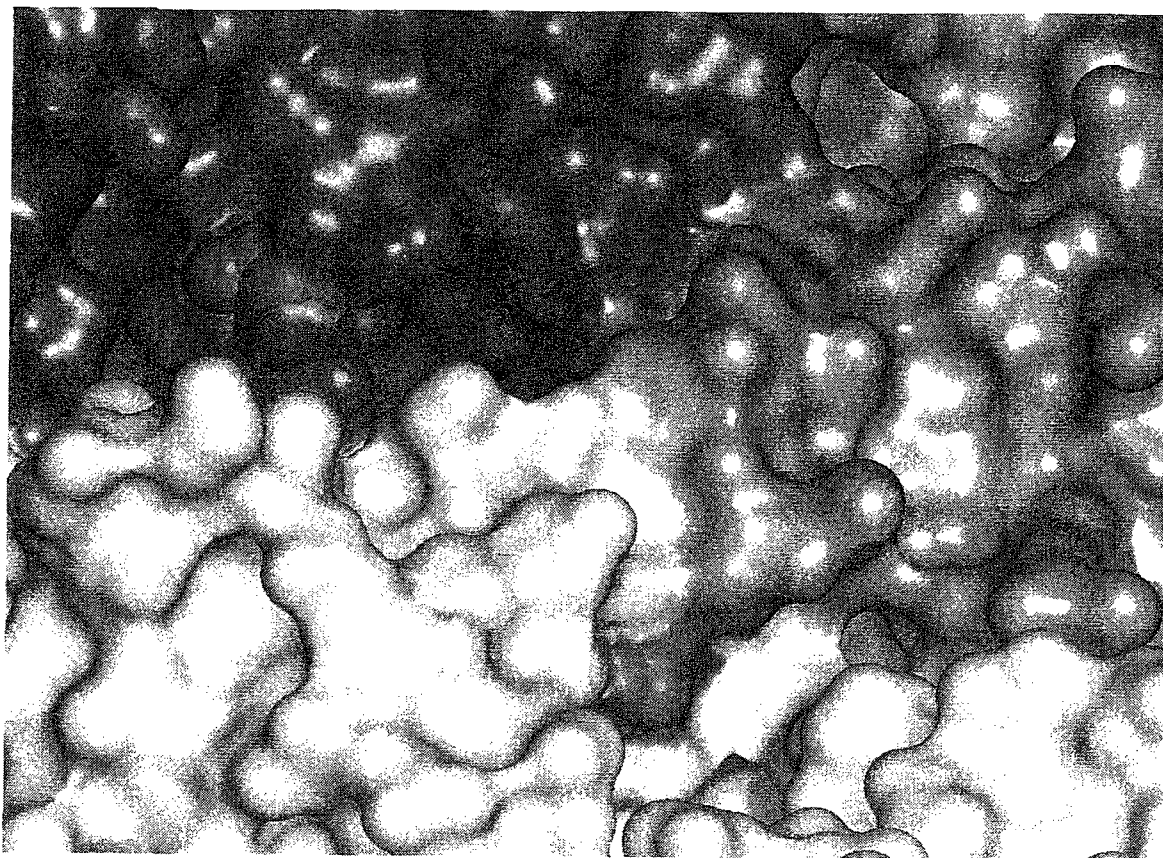


Figure 4.18: Schematic representation of the surface accessibility of Cys47 and Ser(Cys)52 in WT CSU

Each monomer of the CSU is colored in a different shade of gray. Yellow residues represent the side chain Cys47 while red residues represent Ser52. This image illustrates the surface accessibility of the residues at positions 47 and 52, with 52 being more accessible than the buried Cys47. The picture was drawn using PyMol and the coordinates of the crystal structure of the isolated CSU reported by Beernink *et al.* (163) (PDB ID: 3CSU).

The negative charge on the Cys52 thiolate side chain at physiological pH may explain the significantly altered kinetic parameters reported by Turnbull (unpublished). Furthermore, electrostatic repulsion between the thiolate anion and the carbamyl phosphate as well as PALA, which are also negatively charged, as such would alter substrate/PALA binding and catalysis. Moreover, the negative charge of the thiolate might also account for its 11.5°C increase in thermal stability of the Ser52Cys variant relative to the WT trimer.

Since no crystal structure is available for the Ser52Cys variant CSU, the biophysical reasons for the significantly depressed pK_a of the Cys52 residue were rationalized using the crystal structure of the unbound WT CSU (PDB ID: 3CSU) (163).

Several factors, including accessibility, long range electrostatics as well as side-chain entropy, must be taken into consideration when attempting to understand the perturbation of the pK_a of the side chain of an ionizable amino acid residue. Figure 4.18 illustrates the surface of the WT CSU, where Ser(Cys)52 is depicted in red and Cys47 in yellow. The image clearly indicates that Cys47 is buried within the CSU while Ser(Cys)52 is more surface exposed, making this residue accessible to solvent as well as chemical modifying agents, such as DTNB, IAM and CIAM.

Honig and Nicholls (152) have reported that electrostatic interactions operate over long ranges; they suggest that a single charged amino acid 10 – 20 Å away can have a slight effect on the pK_a of a titratable group. Hence, the combined effect of multiple charged residues could conceivably induce a much larger pK_a perturbation. Figure 4.19 illustrates a close-up of the vicinity of Ser(Cys)52 in the active site. This image depicts a single acidic amino acid, Glu50, at a distance of approximately 6 Å from the side chain of

Ser52, whereas five positively charged amino acids are within 3.4 – 8.1 Å; these include Arg54 (7.9 Å), Arg56 (8.1 Å), His134 (5.8 Å), Arg105 (3.4 Å) and Arg296 (7.6 Å). The abundance of basic amino acids in proximity of Ser(Cys)52 may contribute to an overall net positive charge in the vicinity of this residue, hence perturbing the pK_a of Cys52.

Another interesting observation is that Ser(Cys)52 is located at the Ncap position of helix 52-66, an environment which could help promote the deprotonation of a sulfhydryl group and contribute to structural stabilization. Each peptide bond of the peptide backbone contains a dipole moment. Alignment of several dipole moments, such as those found in a helix, produce an electrostatic potential at the C and N termini in the helix; thus the C-terminus possess a partial negative charge, whereas those at the N-terminus possess a partial positive charge. As a result, oppositely charged residues are present at each of the termini in order to neutralize the partial charges originating from the helix dipole (175-179). A cysteine residue positioned at the Ncap of a helix may adopt rotational conformations that place the cysteine thiolate close to the axis of the helix. The residue at the Ncap of a helix is not restricted by the same peptide backbone dihedral angles as for the residues at positions N1 and N2. Two phenomena can occur at the Ncap position giving rise to significantly larger interaction energies; these include both a charge-dipole and hydrogen-bond interaction, where hydrogen bond formation is possible. The hydroxyl moiety of Thr55 located at 3.4Å from Ser52 in the WT CSU, may also form a hydrogen bond with the thiolate of Cys52 in the variant, allowing for increased stabilization. Additionally, the side chain of Cys52 may adopt a conformation which position the thiolate sulphur near the α -helical axis, enabling it to hydrogen bond with the amide nitrogen atoms of both N2 (Arg54) and N3 (Thr55). Hence, maximization

of electrostatic interactions between thiolate and peptide bond dipoles may occur upon placement of the thiolate sulphur atom in center of the helix cylinder, perhaps due to improved geometry (152).

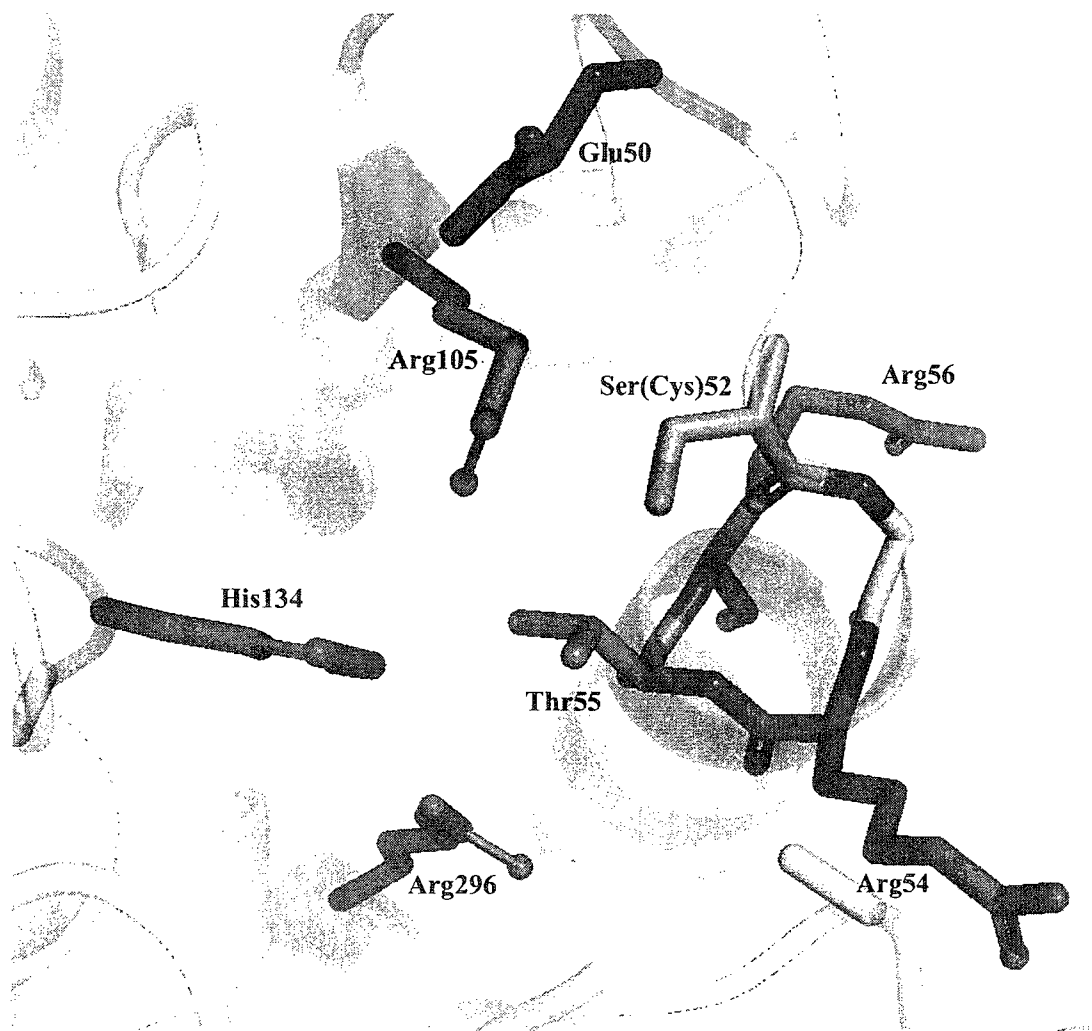


**Figure 4.19: Schematic representation of the location of Ser(Cys)52 on helix 52-66
Within WT CSU**

The green residue represents Ser(Cys)52 at the N-terminus of the yellow helix consisting of residues 52-66. Basic residues are colored in red and the acidic Glu50 is colored in blue. Thr55 is colored in teal and the helix peptide backbone amide groups are colored in blue. This figure was generated using PyMol from the coordinates reported by Beernink *et al.* (163) (PDB ID: 3CSU).

REFERENCES

1. Stryer, L. (1995) *Biochemistry*, 4 ed., W.H. Freeman and Company, New York.
2. Creighton, T. E. (1993) *Proteins: Structure and Molecular Properties*, 2nd edition ed., W.H. Freeman and Company, New York.
3. Rafii, M., McKenzie, J. M., Roberts, S. A., Steiner, G., Ball, R. O., and Pencharz, P. B. (2008) *Am J Physiol Endocrinol Metab* 294, E475-9.
4. Pittard, J. T., and Gibson, F. (1970) *current topics cell regulation* 2, 29-63.
5. Umbarger, H. E. (1978) *Annu Rev Biochem* 47, 532-606.
6. Herrmann, K. M., and Weaver, L. M. (1999) *Annu Rev Plant Physiol Plant Mol Biol* 50, 473-503.
7. Dayan, J., and Sprinson, D. B. (1971) *Biochem J* 108, 1174-1180.
8. Ahmad, S., Wilson, A. T., and Jensen, R. A. (1988) *Eur J Biochem* 176, 69-79.
9. Hudson, G. S., and Davidson, B. E. (1984) *J Mol Biol* 180, 1023-1051.
10. Camakaris, H., and Pittard, J. (1973) *J Bacteriol* 115, 1135-1144.
11. Yanofsky, C. (1988) *J Biol Chem* 263, 609-612.
12. Koch, G. L., Shaw, D. C., and Gibson, F. (1971) *Biochim Biophys Acta* 229, 795-804.
13. Cotton, R. G., and Gibson, F. (1965) *Biochim Biophys Acta* 100, 76-88.
14. Turnbull, J., and Morrison, J. F. (1990) *Biochemistry* 29, 10255-10261.
15. Heyde, E., and Morrison, J. F. (1978) *Biochemistry* 17, 1573-1580.
16. Hudson, G. S., Howlett, G. J., and Davidson, B. E. (1983) *J Biol Chem* 258, 3114-3120.
17. Christendat, D. (1998) in *Chemistry and Biochemistry*, Concordia University, Montreal.
18. Dopheide, T. A. A., Crewther, P., and Davidson, B. E. (1972) *J Biol Chem* 247, 4447-4452.

19. Powell, J. T., and Morrison, J. F. (1978) *Eur J Biochem* 87, 391-400.
20. Coggins, J. R., Abell, C., Evans, L. B., Frederickson, M., Robinson, D. A., Roszak, A. W., and Laphorn, A. P. (2003) *Biochem Soc Trans* 31, 548-552.
21. Haslam, E. (1974) *The Shikimate Pathway*, Wiley, New York.
22. Steinrucken, H. C., and Amrhein, N. (1980) *Biochem Biophys Res Commun* 94, 1207-1212.
23. Herrmann, K. M. (1995) *Plant Physiol* 107, 7-12.
24. Grinter, N. J. (1998) *ChemTech* 28, 33-37.
25. Berry, A., Dodge, T. C., Pepsin, M., and Weyler, W. (2002) *J Ind Microbiol Biotechnol* 28, 127-133.
26. Schmid, J. W., Mauch, K., Reuss, M., Gilles, E. D., and Kremling, A. (2004) *Metab Eng* 6, 364-377.
27. Kramer, M., Bongaerts, J., Bovenberg, R., Kremer, S., Muller, U., Orf, S., Wubboldts, M., and Raeven, L. (2003) *Metab Eng* 5, 277-283.
28. Cabrera-Valladares, N., Martínez, A., Piñero, S., Lagunas-Muñoz, V. H., Tinoco, R., de Anda, R., Vázquez-Duhalt, R., Bolívar, F., and Gosset, G. (2006) *Enzyme and Microbial Technology* 38, 772-779.
29. Seetharam, G., and Saville, B. (2002) *Enzyme and Microbial Technology* 31, 747-753.
30. Ikram, U.-H., and Ali, S. (2002) *Curr Microbiol* 45, 88-93.
31. Bourke, S. L., and Kohn, J. (2003) *Adv Drug Deliv Rev* 55, 447-466.
32. Patnaik, R., Zolandz, R. R., Green, D. A., and Kraynie, D. F. (2008) *Biotechnol Bioeng* 99, 741-752.
33. Rippert, P., Scimemi, C., Dubald, M., and Matringe, M. (2004) *Plant Physiol* 134, 92-100.
34. Sampathkumar, P., and Morrison, J. F. (1982) *Biochim Biophys Acta* 702, 204-211.
35. Hudson, G. S., Wong, V., and Davidson, B. E. (1984) *Biochemistry* 23, 6240-6249.

36. Turnbull, J., Cleland, W. W., and Morrison, J. F. (1991) *Biochemistry* 30, 7777-7782.
37. Vincent, S., Chen, S., Wilson, D. B., and Ganem, B. (2002) *Bioorg Med Chem Lett* 12, 929-931.
38. Christendat, D., and Turnbull, J. (1996) *Biochemistry* 35, 4468-4479.
39. Christendat, D., Saridakis, V. C., and Turnbull, J. L. (1998) *Biochemistry* 37, 15703-15712.
40. Duggleby, R. G., Sneddon, M. K., and Morrison, J. F. (1978) *Biochemistry* 17, 1548-1554.
41. Christopherson, R. I., Heyde, E., and Morrison, J. F. (1983) *Biochemistry* 22, 1650-1656.
42. Chen, S., Vincent, S., Wilson, D. B., and Ganem, B. (2003) *Eur J Biochem* 270, 757-763.
43. Strater, N., Schnappauf, G., Braus, G., and Lipscomb, W. N. (1997) *Structure* 5, 1437-1452.
44. Görisch, H., and Lingens, F. (1974) *Biochemistry* 13, 3790-3794.
45. Andrews, P. R., Smith, G. D., and Young, I. G. (1973) *Biochemistry* 12, 3492-3498.
46. Copley, S. D., and Knowles, J. R. (1987) *J Am Chem Soc* 109, 5008-5013.
47. Andrews, P. R., and Heyde, E. (1979) *J Theor Biol* 78, 393-403.
48. Guilford, W. J., Copley, S. D., and Knowles, J. R. (1987) *J Am Chem Soc* 109, 5013-5019.
49. Sogo, S. G., Widlanski, T. S., Hoare, J. H., Grimshaw, C. E., Bertchold, G. A., and Knowles, J. R. (1984) *J Am Chem Soc* 106, 2701-2703.
50. Andrews, P. R., Cain, E. N., Rizzardo, E., and Smith, G. D. (1977) *Biochemistry* 16, 4848-4852.
51. Bartlett, P. A., Nakagawa, Y., Johnson, C. R., Reich, S. H., and Luis, A. (1988) *J Org Chem* 53, 3195-3210.
52. Delany, J. J., Padykula, R. E., and Bertchold, G. A. (1992) *J Am Chem Soc* 114, 1394-1397.

53. Davidson, M. M., Gould, I. R., and Hillier, I. H. (1996) *J Chem Soc Perkin Trans 2*.
54. Gray, J. V., and Knowles, J. R. (1994) *Biochemistry 33*, 9953-9959.
55. Xue, Y., Lipscomb, W. N., Graf, R., Schnappauf, G., and Braus, G. (1994) *Proc Natl Acad Sci U S A 91*, 10814-10818.
56. Helmstaedt, K., Heinrich, G., Merkl, R., and Braus, G. H. (2004) *Arch Microbiol 181*, 195-203.
57. Xu, H., Yang, C., Chen, L., Kataeva, I. A., Tempel, W., Lee, D., Habel, J. E., Nguyen, D., Pflugrath, J. W., Ferrara, J. D., Arendall, W. B. r., Richardson, J. S., Richardson, D. C., Liu, Z. J., Newton, M. G., Rose, J. B., and Wang, B. C. (2005) *Acta Crystallogr D Biol Crystallogr. 61*, 960-966.
58. Okvist, M., Dey, R., Sasso, S., Grahan, E., Kast, P., and Krenkel, U. (2006) *J Mol Biol 357*, 1483-1499.
59. Lee, A. Y., Stewart, J. D., Clardy, J., and Ganem, B. (1995) *Chem Biol 2*, 195-203.
60. Liu, D. R., Cload, S. T., Pastor, R. M., and Schultz, P. G. (1996) *J Am Chem Soc 118*, 1789-1790.
61. Zhang, S., Kongsaree, P., Clardy, J., Wilson, D. B., and Ganem, B. (1996) *Bioorg Med Chem 4*, 1015-1020.
62. Chook, Y. M., Ke, H., and Lipscomb, W. N. (1993) *Proc Natl Acad Sci U S A 90*, 8600-8603.
63. Vamvaca, K., Butz, M., Walter, K. U., Taylor, S. V., and Hilvert, D. (2005) *Protein Sci 14*, 2103-2114.
64. Zhang, X., Zhang, X., and Bruice, T. C. (2005) *Biochemistry 44*, 10443-10448.
65. Hermes, J. D., Tipton, P. A., Fisher, M. A., O'Leary, M. H., Morrison, J. F., and Cleland, W. W. (1984) *Biochemistry 23*, 6263-6275.
66. Sampathkumar, P., and Morrison, J. (1982) *Biochim Biophys Acta 702*, 212-219.
67. Addadi, L., Jaffe, E. K., and Knowles, J. R. (1983) *Biochemistry 22*, 4494-4501.
68. Christendat, D., and Turnbull, J. L. (1999) *Biochemistry 38*, 4782-4793.

69. Bonvin, J., Aponte, R. A., Marcantonio, M., Singh, S., Christendat, D., and Turnbull, J. L. (2006) *Protein Sci* 15, 1417-1432.
70. Monod, J., Wyman, J., and Changeux, J. P. (1965) *J Mol Biol* 12, 88-118.
71. Koshland, D. E. J., Néméthý, G., and Filmer, D. (1966) *Biochemistry* 5, 365-385.
72. Turnbull, J., Morrison, J. F., and Cleland, W. W. (1991) *Biochemistry* 30, 7783-7788.
73. Christopherson, R. I., and Morrison, J. F. (1985) *Biochemistry* 24, 1116-1121.
74. Christopherson, R. I. (1985) *Arch Biochem Biophys* 240, 646-654.
75. Lutke-Eversloh, T., and Stephanopoulos, G. (2005) *Appl Environ Microbiol* 71, 7224-8.
76. Kenyon, G. L., and Bruce, T. W. (1997) *Methods Enzymol* 47, 407-430.
77. Lundblad, R. L. (1995) in *Techniques in Protein Modification*, CRC Press, London.
78. Gething, M. J., and Davidson, B. E. (1977) *Eur J Biochem* 75, 111-117.
79. Zhang, S., Wilson, D. B., and Ganem, B. (2000) *Biochemistry* 39, 4722-4728.
80. Pohnert, G., Zhang, S., Husain, A., Wilson, D. B., and Ganem, B. (1999) *Biochemistry* 38, 12212-12217.
81. Chook, Y. M., Gray, J. V., Ke, H., and Lipscomb, W. N. (1994) *J Mol Biol* 240, 476-500.
82. Parmentier, L. E., Weiss, P. M., O'Leary, M. H., Schachman, H. K., and Cleland, W. W. (1992) *Biochemistry* 31, 6577-6584.
83. Turnbull, J. L., Waldrop, G. L., and Schachman, H. K. (1992) *Biochemistry* 31, 6562-6569.
84. Weber, K. (1968) *Nature* 218, 1116-1119.
85. Turoverov, K. K., Biktashec, A. G., Khaitlina, S. Y., and Kuznetsova, I. M. (1999) *Biochemistry* 38, 6261-6269.
86. Lipscomb, W. N. (1971) *Cold Spring Harbor Symp. Quant. Biol.* 36, 285-290.

87. Krause, K. L., Volz, K. W., and Lipscomb, W. N. (1985) *Proc Natl Acad Sci* 82, 1643-1647.
88. Ke, H., Lipscomb, W. N., Cho, Y., and Honzatko, R. B. (1988) *J Mol Biol* 204, 725-747.
89. Markby, D. W., Zhou, B. B., and Schachman, H. K. (1991) *Proc Natl Acad Sci* 88, 10568-10572.
90. Gerhart, J. C. (1964) *Brookhaven Symp. Biol.* 17, 222-231.
91. Gerhart, J. C., and Pardee, A. B. (1960) *J Biol Chem* 237, 891-896.
92. Berthell, M. R., Smith, K. E., White, J. S., and Jones, M. E. (1968) *Proc Natl Acad Sci* 60, 1442-1449.
93. Wild, J. R., Loughrey-Chen, S. J., and Corder, T. S. (1989) *Proc Natl Acad Sci* 86, 46-50.
94. Zhou, B. B., and Schachman, H. K. (1993) *Protein Sci* 2, 103-112.
95. Yang, Y. R., Kirschner, M. W., and Schachman, H. K. (1985) *Methods Enzymol* 51, 35-41.
96. Gerhart, J. C., and Schachman, H. K. (1965) *Biochemistry* 4, 1054-1062.
97. Howlett, G. J., Blackburn, M. N., Compton, J. G., and Schachman, H. K. (1989) *J Biol Chem* 264, 2476-2481.
98. Newell, J. O., Markby, D. W., and Schachman, H. K. (1989) *J Biol Chem* 264, 2476-2481.
99. Schachman, H. K. (1988) *J Biol Chem* 263, 18583-18586.
100. Stevens, R. C., and Lipscomb, W. N. (1992) *Proc Natl Acad Sci* 89, 5281-5285.
101. Van Vliet, F., Xi, G., De Staercke, C., de Wannemaeker, B., Jacobs, A., Cherfils, J., Ladjimi, M. M., Herve, G., and Cunin, R. (1991) *Proc Natl Acad Sci* 88, 9180-9183.
102. Roche, O., and Field, M. J. (1999) *Prot Eng* 12, 285-295.
103. Wentz, S. R., and Schachman, H. K. (1987) *Proc Natl Acad Sci* 84, 31-35.
104. Macol, C., Dutta, M., Stec, B., Tsuruta, H., and Kantrowitz, E. R. (1999) *Protein Sci* 8, 1305-1313.

105. Vanaman, T. C., and Stark, G. R. (1970) *J Biol Chem* 254, 3565-3673.
106. Jenness, D. D., and Schachman, H. K. (1983) *J Biol Chem* 258, 3266-3279.
107. Schachman, H. K., Pauza, C. D., Navre, M., Karels, M. J., Wu, L., and Yang, Y. R. (1984) *Proc Natl Acad Sci* 81, 115-119.
108. Xu, W., and Kantrowitz, E. R. (1991) *Biochemistry* 30, 2535-2542.
109. Peterson, C. B., Zhou, B. B., Hsieh, D., Creager, A., and Schachman, H. K. (1994) *Protein Sci* 3, 960-966.
110. Jin, L., Setc, B., Lipscomb, W. N., and Kantrowitz, E. R. (1999) *Proteins* 37, 729-742.
111. Feeney, R. E. (1987) *Int J Pept Protein Res* 29, 145-161.
112. Turk, T., and Macek, P. (1992) *Biochim Biophys Acta* 1119, 5-10.
113. Nagel-Starczynowska, G., and Kaletha, K. (1993) *Biochim Biophys Acta* 1164, 261-267.
114. Liao, T. H., Ho, H. C., and Abe, A. (1991) *Biochim Biophys Acta* 1079, 335-342.
115. Esmann, M., Sar, P. C., Hideg, K., and Marsh, D. (1993) *Anal Biochem* 213, 336-348.
116. Gadda, G., Banejee, A., Dangott, L. J., and Fitzpatrick, P. F. (2000) *J Biol Chem* 275.
117. Davis, D. A., Dorsey, K., Wingfield, P. T., Stahl, S. J., Kaufman, J., Fales, H. M., and Levine, R. L. (1996) *Biochemistry* 35, 2482-2488.
118. Peredo, A. G., Saint-Pierre, C., Adrait, A., Jacquamet, L., Latour, J. M., Michaud-Soret, I., and Forest, E. (1999) *Biochemistry* 38, 8582-8589.
119. Gething, M. J., and Davidson, B. E. (1972) *Eur J Biochem* 30, 352-353.
120. Habeeb, A. F. S. A. (1972) *Methods Enzymol* 25, 457-464.
121. Boja, E. S., and Fales, H. M. (2001) *Anal Chem* 73, 3576-3582.
122. Gurd, F. R. N. (1972) *Methods Enzymol* 25, 424-438.
123. Habeeb, A. F. S. A. (1966) *Anal Biochem* 14, 328.

124. Goldfarb, A. R. (1966) *Biochemistry* 5, 2570-2574.
125. Rieger, C. E., and Turnbull, J. (1996) *Prep Biochem Biotechnol* 26, 67-76.
126. Dudzinski, P. K., and Morrison, J. F. (1976) *Preparative Biochemistry and Biotechnology* 6, 113-121.
127. Dawson, C. M. R., Elliott, C. D., Elliott, H. W., and Jones, M. K. (1986), Oxford Science Publications, Clarendon Press.
128. Turnbull, J. (1988), Australian National University, Canberra.
129. Bartlett, P. A., and Johnson, C. R. (1985) *J Am Chem Soc* 107, 7792-7793.
130. Lindblad, B., Lindstedt, G., Lindstedt, S., and Rundgren, M. (1977) *J Biol Chem* 252, 5073-5084.
131. Craven, D. B., Harvey, M. J., Lowe, C. R., and Dean, P. G. D. (1974) *Eur J Biochem* 41, 329-333.
132. Bhosale, S. B., Rood, J. L., Sneddon, M. K., and Morrison, J. F. (1982) *Biochim Biophys Acta* 717, 6-11.
133. Laemmli, U. K. (1970) *Nature* 227, 680-685.
134. Bradford, M. M. (1976) *Anal Biochem* 72, 248-254.
135. Ellis, K. J., and Morrison, J. F. (1982) *Methods Enzymol* 87, 405-426.
136. Weinglass, A. B., Whitelegge, J. P., Verner, G. E., Faull, K. F., and Kaback, H. R. (2003) *EMBO J* 22, 1497-1477.
137. Riddles, P. W., Blakeley, R. L., and Zerner, B. (1979) *Anal Biochem* 94, 75-81.
138. Riley, M., Abe, T., Arnaud, M. B., Berlyn, M. K., Blattner, F. R., Chaudhuri, R. R., Glasner, J. D., Horiuchi, T., Keseler, I. M., Kosuge, T., Mori, H., Perna, N. T., Plunkett, G. I., Rudd, K. E., Serres, M. H., Thomas, G. H., Thomson, N. R., Wishart, D., and Wanner, B. L. (2006) *Nucleic Acids Res* 34, 1-9.
139. Hoover, T. A., Roof, W. D., Foltermann, K. F., O'Donovan, G. A., Bencini, D. A., and Wild, J. R. (1983) *Proc Natl Acad Sci* 80, 2462-2466.
140. Salleh, H. M., Patel, M. A., and Woodard, R. W. (1996) *Biochemistry* 35, 8942-8947.
141. Britto, P. J., Knipling, L., and Wolff, J. (2002) *J Biol Chem* 277, 29018-29027.

142. Cload, S. T., Liu, D. R., Pastor, R. M., and Schultz, P. G. (1996) *J Am Chem Soc* 118, 1787-1788.
143. Mekhssian, K. (2003), Structure/Function Studies on a Bifunctional Enzyme in Tyrosine Biosynthesis. Concordia University, Montreal, QC, Canada, M. Sc.
144. Sherman, F., Stewart, J. W., and Tsunasawa, S. (1985) *BioEssays* 3, 27-31.
145. Flinta, C., Persson, B., Jornvall, H., and Heijne, G. (1986) *Eur J Biochem* 154, 193-196.
146. Meinnel, T., Mechulam, Y., and Blanquet, S. (1993) *Biochimie* 75, 1061-1075.
147. Lee, A. Y., Karplys, P. A., Ganem, B., and Clardy, J. (1995) *JACS* 117, 3267-3628.
148. Coffee, C. J., Bradshaw, R. A., Goldin, B. R., and Frieden, C. (1971) *Biochemistry* 10, 3516 - 3526.
149. Gasteiger, E., Hooland, C., Gattiker, A., Duvaud, S., Wilkins, M. R., Appel, R. D., and Bairoch, A. (2005) *The Proteomics Protocols Handbook*, Humana Press.
150. Engel, P. C. (1996) *Enzymology*, Bio Scientific Publishers, Oxford, UK.
151. Krekel, F., Samland, A. K., Macheroux, P., Amrhein, N., and Evan, J. N. (2000) *Biochemistry* 39, 12671-12677.
152. Honig, B., and Nicholls, A. (1995) *Science* 268, 1144-1149.
153. Porter, R. W., Modebe, M. O., and Stark, G. R. (1969) *J Biol Chem* 244, 1846-1859.
154. Collins, K. D., and Stark, G. R. (1969) *J Biol Chem* 244, 1869-1877.
155. Rowland, R. L., Perry, W. L., Foreman, E. L., and Friedman, H. L. (1950) *J Am Chem Soc* 72, 2595.
156. Yang, Y. R., Kirschner, M. W., and Schachman, H. K. (1978) *Methods Enzymol* 51, 35-41.
157. Putnam, F. W. (1975) *The Plasma Proteins: Structure, Function and Genetic Control*, Vol. 1, 2 ed., Academic Press, New York.
158. Parry-Smith, D. J., Payne, A. W. R., Michie, A. D., and Attwood, T. K. (1997) *Gene* 211, 45-56.

159. Thompson, J. D., Higgins, D. G., and Gibson, T. (1994) *Nucleic Acids Res* 22, 4673-4680.
160. Cohen, S. L., Padovan, J. C., and Chait, B. T. (2000) *Anal Biochem* 72, 574-579.
161. Keith, R. L., Setiarahardjo, I., Fernando, Q., Aposhian, H. V., and Gandolfi, A. J. (1997) *Toxicology* 116, 67-75.
162. Kelly, S. M., Jess, T. J., and Price, N. C. (2005) *Biochim Biophys Acta* 1751, 119-139.
163. Beernink, P. T., Endrizzi, J. A., Alber, T., and Schachman, H. K. (1999) *Proc Natl Acad Sci* 96, 5388-5393.
164. Endrizzi, J. A., Beernink, P. T., Alber, T., and Schachman, H. K. (2000) *Proc Natl Acad Sci* 97, 5077-5082.
165. Sørensen, S. B., Sørensen, T. L., and Breddam, K. (1991) *FEBS* 294, 195-197.
166. Houmard, J., and Drapeau, G. R. (1972) *Proc Natl Acad Sci* 69, 3506-3509.
167. Drapeau, G. R. (1978) *Can J Biochem* 56, 534-544.
168. Gerhart, J. C., and Holoubek, H. J. (1967) *J Biol Chem* 242, 2886-2892.
169. Graf, R., and Schachman, H. K. (1996) *Proc Natl Acad Sci* 93, 11591-11596.
170. Hirel, P. H., Schmitter, M. J., Dessen, P., Fayat, G., and Blanquet, S. (1989) *Proc Natl Acad Sci* 86, 8247-8251.
171. Wang, X., and Horisberger, J. D. (1996) *Mol Pharmacol* 50, 687-691.
172. Sahlman, L., and Jonsson, B. H. (1992) *Eur J Biochem* 205, 375-381.
173. Witt, A. C., Lakshminarasimhan, M., Remington, B. C., Hasim, S., Pozharski, E., and Wilson, M. A. (2008) *Biochemistry* 47, 7430-7440.
174. Naor, M. M., and Jensen, J. H. (2004) *Proteins* 57, 799-803.
175. Hol, W. G., van Duijnen, P. T., and Berendsen, H. J. (1978) *Nature* 273, 443-446.
176. Aqvist, J., Luecke, H., Quioco, F. A., and Warshel, A. (1991) *Proc Natl Acad Sci* 88.
177. Lockhart, D. J., and Kim, P. S. (1992) *Science* 257, 947-951.

178. Lockhart, D. J., and Kim, P. S. (1993) *Science* 260, 198-202.
179. Sitkoff, D., Lockhart, D. J., Sharp, K. A., and Honig, B. (1994) *Biophys J* 67, 2251-2260.